UiT
THE ARCTIC UNIVERSITY OF NORWAY

Faculty of Science and Technology

Department of Geology

Correlation between changes in paleoceanography, paleoclimate and methane seepage on Vestnesa Ridge, eastern Fram Strait.

Karoline Myrvang

GEO-3900 Master's thesis in Geology
December 2015

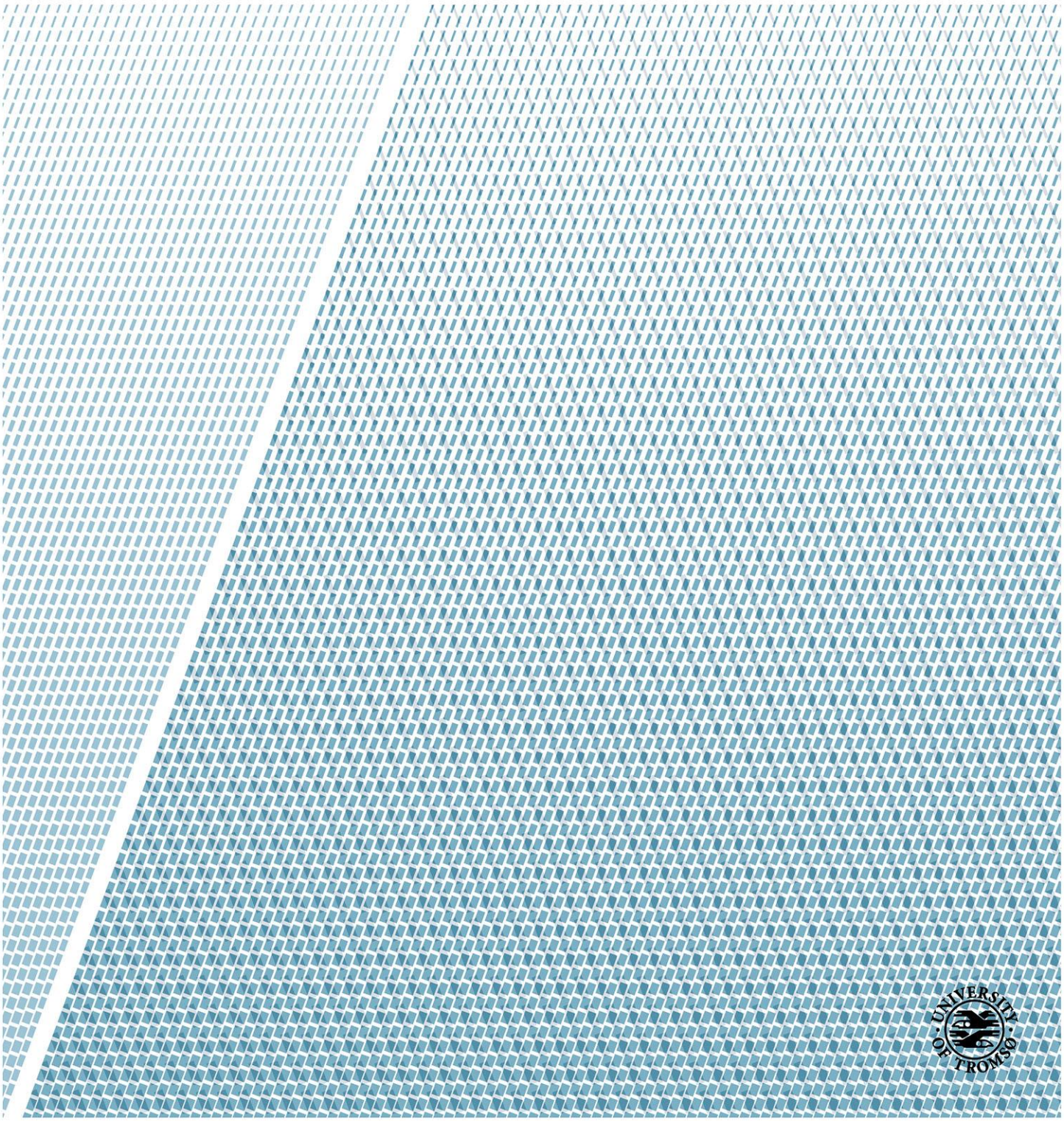

Abstract

Two sediment cores HH14-002 GC and HH12-930 GC from Vestnesa Ridge in the eastern part of Fram Strain have been investigated to reconstruct the paleoclimate and paleoceanographic conditions during the last ~37,000 years, and to study possibly changes in emission of methane from the seabed through time. Core HH14-002 GC was taken from outside a pockmark, while core HH12-930 GC was taken from inside the pockmark.

The two sediment cores HH14-002 GC and HH12-930 GC were divided into six lithological units based on the differences in magnetic susceptibility, lithology, concentration of IRD, grain size distribution and results from stable isotope analysis. HH14-002 GC show a similarity in magnetic susceptibility and lithology to the sediment cores in the study by Jessen et al. (2010), while HH12-930 GC show mainly similarity in lithology.

An age model could be established by correlating the results from HH14-002 GC and HH12-930 GC with Jessen et al. (2010). The age of the cores ranges from 37,829 to 14,070 cal. yr BP, and covers intervals from the mid-Weichselian to early Holocene. Deposition of mass transported sediments in HH14-002 GC and HH12-930 GC indicates that the Svalbard-Barents Sea Ice Sheet reached the shelf break at ~23,820 cal. yr BP, and is a sign of a fully glaciated shelf. After the deglaciation (~20,101 cal. yr BP) and the Heinrich event 1 (~17,652 cal. yr BP) fine-grained laminated sediments were deposited between 14,780 and 14,300 cal. yr BP by turbid meltwater plume. Due to increased bottom currents, parts of the Holocene is missing from HH14-002 GC.

Based on the foraminiferal assemblage distribution, concentration of IRD, stable isotope analysis and the age model the paleoceanographic conditions could be reconstructed. The results indicate influence of Atlantic intermediate water during the upper stage of the mid-Weichselian, and during the LGM, where the productivity was high with presence of seasonal sea-ice in the area. During Heinrich event 1 the water column was stratified and the productivity was low. The influence of Atlantic water was reduced, and the conditions were unstable. During the Bølling/Allerød Interstadials the conditions were slightly improved. The water column was less stratified, however, a layer of melt water was still present in the area. During the Younger Dryas, the surface layer was covered by a low-salinity melt water layer.

Six periods with negative $\delta^{13}C$ values from HH12-930 GC, which was retrieved from a pockmark, are interpreted to be caused by methane seepage. Three of the event can be linked to interstadial periods, and possibly methane seepage was caused by a combination of glacial retreat, increased sea level, eustatic unloading and seismic activity.

Forord

Først og fremst vil jeg takke min veileder Tine L. Rasmussen for muligheten til å skrive denne masteroppgaven. Tusen takk for hjelp, inspirasjon, kunnskap og gode råd. Det har vært en fantastisk reise!

Jeg vil takke CAGE (Centre for Arctic Gas Hydrate, Environment and Climate som støttes av Forskningsrådet gjennom SSF (Senter for fremragende forskning) finansieringsorden bevilgnings nummer 223259).

Jeg vil takke Trine Dahl og Ingvild Hald for all hjelpen på laboratoriet. Og Kamila Sztybor for hjelp med å identifisere forskjellige arter og for alltid å hatt et svar på spørsmål fra en frustrert student.

Takk til Steinar Iversen og Bjørn Runar Olsen for hjelp med å skaffe chirp data, og takk til Matthias Forwick for hjelpen med å skanne sedimentkjernene.

Tusen takk til Ida og Ingrid for fem fantastisk år med mange fine opplevelser og minner, og for støtte og mange klemmer i den siste innspurten av masteren. Dere er best! Jeg vil gjerne takke mine foreldre for oppmuntring og råd. Og min søster for å hatt svar på de rare og matematiske spørsmålene mine.

Og tusen takk til Henrik for tålmodighet, all kjærligheten og ufattelig støttende ord. Du har vært en klippe.

Jeg er evig takknemlig!!

Karoline Myrvang

Tromsø, 21. desember 2015

Table of content

1. Introduction

2. 1 Objectives

The aim of this study is to reconstruct paleoclimate and paleoceanographic conditions of Vestnesa Ridge, and investigate changes in the gas activity related to changes in climate and oceanography during the last 30,000 years.

1. 2 Background

1. 2. 1 The Svalbard archipelago and continental slope

The archipelago Svalbard is located between Norway and the North Pole in the north-western Barents Sea (*Figure 1*). The total area of Svalbard is 62,160 km^2. The archipelago stretches from 74°-81°N, and 10°-35°E, and consist of together seven larger islands; Spitsbergen, Nordaustlandet, Barentsøya, Edgeøya, Kong Karls Land, Prins Karls Forland and Bjørnøya (Ingólfsson, 2004). Approximately 60 % of Svalbard is covered by glaciers, where most of them terminate into the sea. The margin of Svalbard is characterized by a relatively narrow shelf, which is between 60 and 85 km wide, and extends approximately 1000 km in a north-south direction, with a relatively steep slope (up to 5°) (Elverhøi, et al., 1995; Faleide, et al., 1996). Due to dry climate in the central part of Spitsbergen, the glaciers are relatively small, compared to the west and east coast, where large valley glaciers and ice caps are more frequent (Ingólfsson, 2004). The north eastern part of Spitsbergen can be described as a polar desert due to a very dry climate (Ingólfsson, 2004).

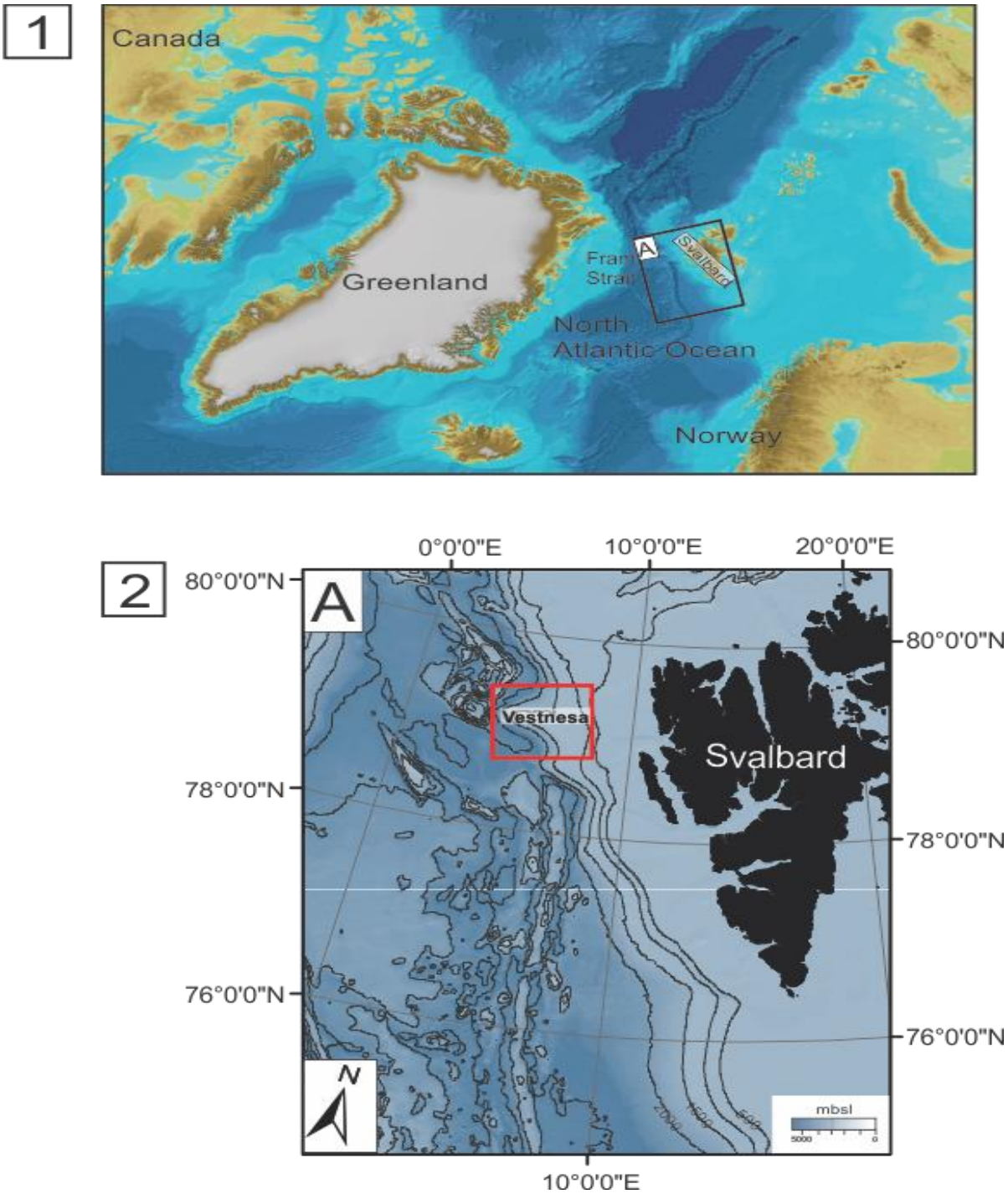

Figure 1: 1: Overview map of the Nordic seas and eastern Arctic Ocean (modified from Jakobsen et al., 2012). 2: Bathymetry of western Svalbard margin. The red box shows the location of the study area.

1. 2. 2 Oceanography

Fram Strait is situated between Svalbard and east Greenland, and is considered to be the most important connection between the Arctic Ocean and the North Atlantic Ocean (*see Figure 1.1*), and a is an ideal place to monitor the interoceanic exchange of heat, salt and volume (Quadfasel, et al., 1978; Quadfasel, et al., 1987). The Fram Strait is the only deep passage between the Arctic Ocean and the Greenland and Norwegian seas that permits exchange of deep water over a sill at about 2500 m (Rudels, et al., 1994). On the western side of the Fram Strait the sea ice is exported from the Arctic Ocean by the East Greenland Current (EGC) into the Greenland Sea (Quadfasel, et al., 1987). The eastern side is however ice-free almost throughout the year (Quadfasel, et al., 1987). The upper layers in the Fram Strait undergoes seasonal variations in temperature and salinity, due to local heating, melting and freezing effects (Quadfasel, et al., 1987). The Barents Sea is dominated by three water masses: coastal water, Arctic water and Atlantic water (Hald, et al., 1989; Loeng, 1991) (*Table 1*).

Names of the water masses		Characteristics of the water masses	
Main water mass		T, °C	S (‰)
Coastal Water	(CW)	>2.0	<34.7
Atlantic Water	(AW)	>3.0	>35.0
Atlantic Intermediate Water	(AIW)	0 – 3	34.7 – 34.9
Arctic Water	(ArW)	<0.0	34.3 – 34.8

Table 1: Name, temperature and salinity of the water masses in the Barents Sea (modified from Loeng, 1991).

Atlantic Water (AW) transports salt and heat to the Arctic Ocean (Manley, 1995). It is transported by the North Atlantic Current (NAC), and continues as the Norwegian Atlantic Current (NwAC) (*Figure 2*) by following the continental slope of the Norwegian margin (*Johannessen, 1986*). The current continues north, where it splits into an easterly and a northern branch (Manley, 1995). One part branches off into the Barents Sea, the other flows northward and follows the slope to the Spitsbergen region (Johannesen, 1986). The northern branch, the West Spitsbergen Current (WSC), transports the Atlantic Water into the Arctic Ocean through the Fram Strait. This inflow is considered to be the major oceanic heat source for the Arctic Ocean (Aagaard & Greisman, 1975; Swift & Aaagard, 1981), and maintain ice-free conditions on the west and north of Spitsbergen to around 80°-82° N (Aagaard, et al., 1978). Towards the north and east in the Barents Sea, there is a general temperature decrease (*Hald et al. 1989*), and heat loss to the atmosphere and to sea ice (Rudels, et al., 2005). The Atlantic Water is submerged below the colder, less saline Arctic Surface Water around 78° N in the Fram Strait (*Johannessen, 1986*), where it becomes an intermediate water mass, which is often referred to as Atlantic Intermediate Water (*e.g Swift, 1986*). This water mass has a temperature between 0° – 3 °C and salinity between 34.7‰ to 34.9‰ (Swift & Aaagard, 1981). The water mass flows along the bathymetry of the western continental slope of Svalbard (*Aagaard, K., 1975*), and splits into three branches at 79.5°N (Manley, 1995). Below these water masses flows cold (-0.9°9 and more saline (>34.91 ‰) water, which is identified as Norwegian Sea Deep Water, and flows northward in the deep West Spitsbergen Current (Aagaard, et al., 1985; Rudels, et al., 2000; Langehaug & Falck, 2012). This is however episodically; it is produced during winter by freezing and brine release in the Barents Sea and Storfjorden (Quadfasel, et al., 1988; Scahuer, 1995). These cold and dense plumes flow down the continental slope, entering the Atlantic Water, and entering the ambient water and the intermediate water as well (Quadfasel, et al., 1988). Ice export has been recognized as an important factor influencing the formation of North Atlantic Deep Water (NADW) (Aagaard & Carmack, 1989; Oppo & Lehman, 1995; Bischof & Darby, 1997). If the ice export increases, the salinity will decrease, and so will the deep water formation (Darby, et al., 2002). Atlantic Water is carried southward in the subsurface Atlantic Return Current, and is transported at the western side of Fram Strait as a part of the East Greenland Current (EGC) (Paquette, et al., 1985).

The Atlantic Water is relatively warm (>3° C) with salinity slightly above 35 ‰ (Coachman & Barnes, 1963). The Atlantic Layer is defined to range in depth from c. 200 m to between 600 m to 800 m with temperatures >3°C (Coachman & Barnes, 1963). The Coastal Water has a temperature similar to the Atlantic Water (<2° C), but a lower salinity (<34.7 ‰) (Loeng, 1991).

Arctic water is characterized by temperature below 0°C and with salinity between 34.3-34.8‰, while the core has a temperature of <-1.5°C and a salinity between 34.4 and 34.7‰ (Loeng, 1991), and dominates the upper part of the water column north of the Polar Front (Pfirman et al., 1994). North of the polar front, sea ice covers the region from fall to early summer (Pfirman et al., 1994), where it eventually retreat towards north and leaves a thin layer of surface water that is warmed by solar radiation (Mosby, 1938; Loeng, 1980; Loeng, 1991). The water mass occupies the upper 150 m of the water column during winter, however, during summer it is covered by 5-20 m thick melt water with low salinity (31.0-34.2‰) (Loeng, 1991).

The Polar Front separates the cold, low-salinity polar waters (Arctic Water) from warmer and more saline waters (Atlantic Water), and constitutes the upper layer of the East Greenland Current (EGC) (Aagaard & Coachman, 1968; Foldvik, et al., 1988). The present position of the Polar Front is south and east of Greenland (Rudiman & McIntyre, 1981). Polar Water has salinity less than 34.4 ‰ and low temperatures (<0°C), however, the summer temperatures can reach 3° to 5°C since the layer is thin and strongly stratified (Swift & Aaagard, 1981).

The input of North Atlantic Deep Water (NADW) is an important mechanism for the global thermohaline circulation (Dickson & Brown, 1994), and is formed when warm, upper-layer water gradually cools with increasing latitude (Böning, et al., 1996).

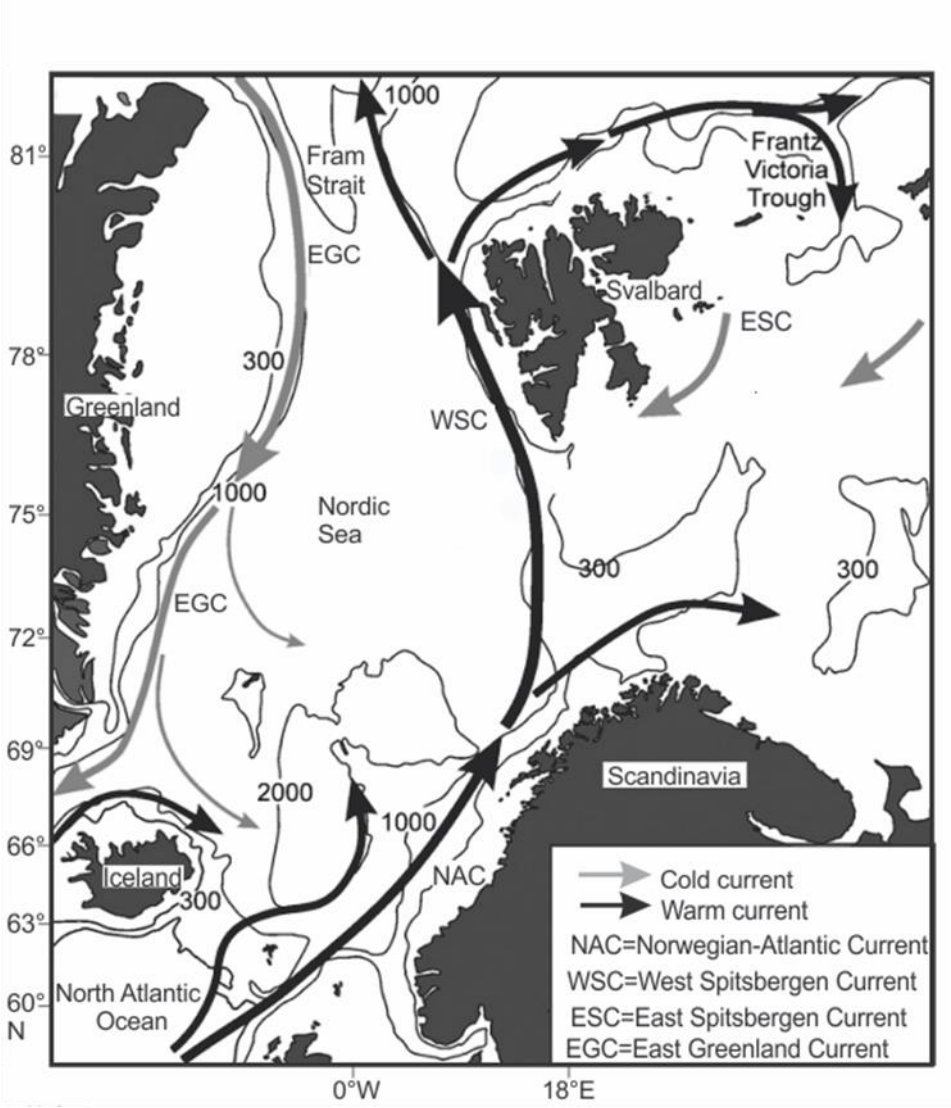

Figure 2: Overview map with the major surface currents in the Nordic Seas and around Svalbard. (Figure modified from Rasmussen et al., 2007).

1. 2. 3 Glacial history of Svalbard and the Barents Sea

The investigation of the growth and retreat and the extent of the Barents Sea Ice Sheet (BSIS) throughout time has increased during the last decades, with focus on the Late Weichselian (Boulton, 1979; Landvik, et al., 1988; Andersen, et al., 1996; Mangerud, et al., 1996; Landvik, et al., 1998; Jessen, et al., 2010).

Results indicate that the Barents Sea has been subject to several glaciations (Sættem, et al., 1992) during the last 2.6 Ma (*Ma=10*^{6}) (Larsen, et al., 1994; Myhre, et al., 1995), with intense erosion of the seafloor (Dimakis, et al., 1998). During the Late Weichselian unlithified glacial sediments together with glaciomarine diamicton were deposited in the Barents Sea (Faleide, et al., 1996). The timing of the onset of the maximum extent of the ice sheet has been debated. According to *Elverhøi et al (1995)* the ice sheet of the western Svalbard and north-western Barents Sea advanced in two steps. The first advance was estimated to occur at approximately 26.9 calendar (cal) ka yr BP (22610±200 ^{14}C yr B P). A decline in δ^{13}C and increased ice rafted debris (IRD) concentration on the western margin indicates the onset of glacial advance to the shelf at around 27 cal. ka yr BP (*Jessen*, et al., 2010). IRD is normally defined as terrigenous, coarse material (> 500 µm, or sometimes >63 µm) randomly distributed in deep – sea sediments (Elverhøi, et al., 1995). They are considered to be too heavy for transportation of ocean current (Ruddiman, 1977; Bond, et al., 1993; Andrews, 2000). The IRD can be transported by sea ice and/or icebergs, or as a result of mass transport deposition. The Barents Sea Ice Sheet increased in size between 27 and 22.5 cal. ka yr BP with establishment of open-water between the Fram Strait and the North Atlantic Ocean, and with an increase in precipitation (Hebbeln, et al., 1994; Andersen, et al., 1996). Around 26 cal. ka yr BP the global sea level had almost reached its minimum (~120 meter), which in time correlates with the ice sheet advance to the shelf break (Peltier & *Fairbanks*, 2006). The second advance occurred at 22.2 cal. ka yr BP (18860±150 14C yr BP), where the ice sheet reached the shelf edge (Elverhøi, et al., 1995; Andersen, et al., 1996; Dowdeswell & Elverhøi, 2002). At the same time the influence of Polar surface Water increased, indicated by decrease in magnetic susceptibility and high percent of the polar foraminifera species *Neogloboquadrina pachyderma (s)* (Jessen, et al., 2010). Jessen et al (2010) proposed that ice sheet reached the shelf break at the beginning of the Last Glacial Maximum (LGM 24 – 20

cal ka BP), and the shelf edge around 23.8 cal. ka years BP, where the entire western shelf of Svalbard was fully glaciated (Figure 3).

During the LGM ice streams drained the Barents Sea Ice Sheet, which was mainly controlled by topography (Landvik, et al., 1998; Ottesen & Dowdeswell, 2009) *(Figure 4*). The ice sheet was thinner over the north-western part of Svalbard, so the ice sheet drained mainly along the major fjords, e. g. Kongsfjorden and Isfjorden (Landvik, et al., 2005). Between 24 and 23.5 cal. ka yr BP mass transport sediments with low magnetic susceptibility (*see 3.2.2*) were deposited on the western Svalbard slope (*Jessen*, et al., 2010), which is taken as a diagnostic signal of a fully glaciated shelf (Laberg & Vorren, 1995; Vorren & Laberg, 1997; King, et al., 1998; Dowdeswell & Elverhøi, 2002). The ice sheet remained on the shelf edge for at least 3.0 ka years (Elverhøi, et al., 1995). *Elverhøi et al (1993)* propose that right after the Barents Sea Ice Sheet reached its maximum the disintegration started due to rising sea level.

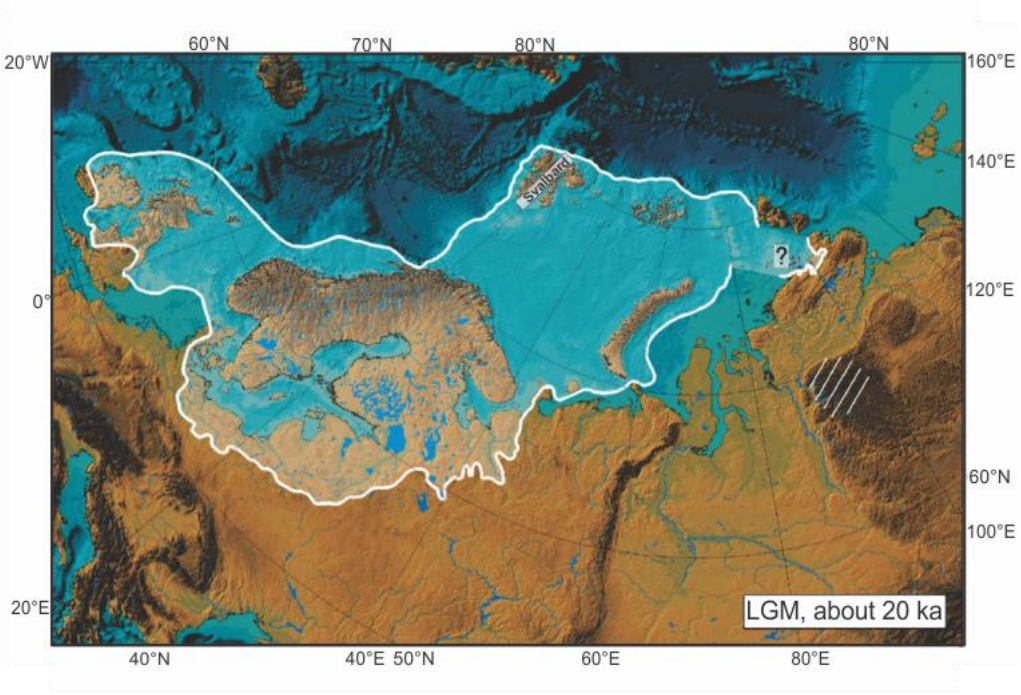

Figure 3: Reconstruction of the Eurasian Ice Sheet limit during the Last Glacial Maximum (LGM) (From Svendsen et al., 2004a).

The eastern and northern Barents Sea margin area were characterized by a relative high sedimentation rate (2-10 cm/ka), high fluxes of planktonic foraminifera and IRD, which could indicate ice-marginal to frequently open water-conditions with drifting icebergs (Nørgaard-Pedersen, et al., 2003). High values of $\delta^{18}O$ (4.5-4.8‰) in the Fram Strait suggest a near surface Atlantic Water mass (*Nørgaard-Pedersen, et al., 2003*). *Nørgaard-Pedersen et al*

(2003) reported decreased $\delta^{18}O$ values from the central Fram Strait-Yermak Plateau-Northern Barents Sea region during the late stage of the LGM (18.5-16 cal. ka yr BP). This decrease reflects an abrupt lowering of regional surface water salinities, which conceivably was caused by a discharge of isotopically light meltwater from the Barents Sea Ice Sheet during the early deglaciation (Jones & Keigwin, 1988; Elverhøi, et al., 1995), and possibly the Arctic Laurentide and the Innutitian Ice Sheet (Darby, et al., 2002).

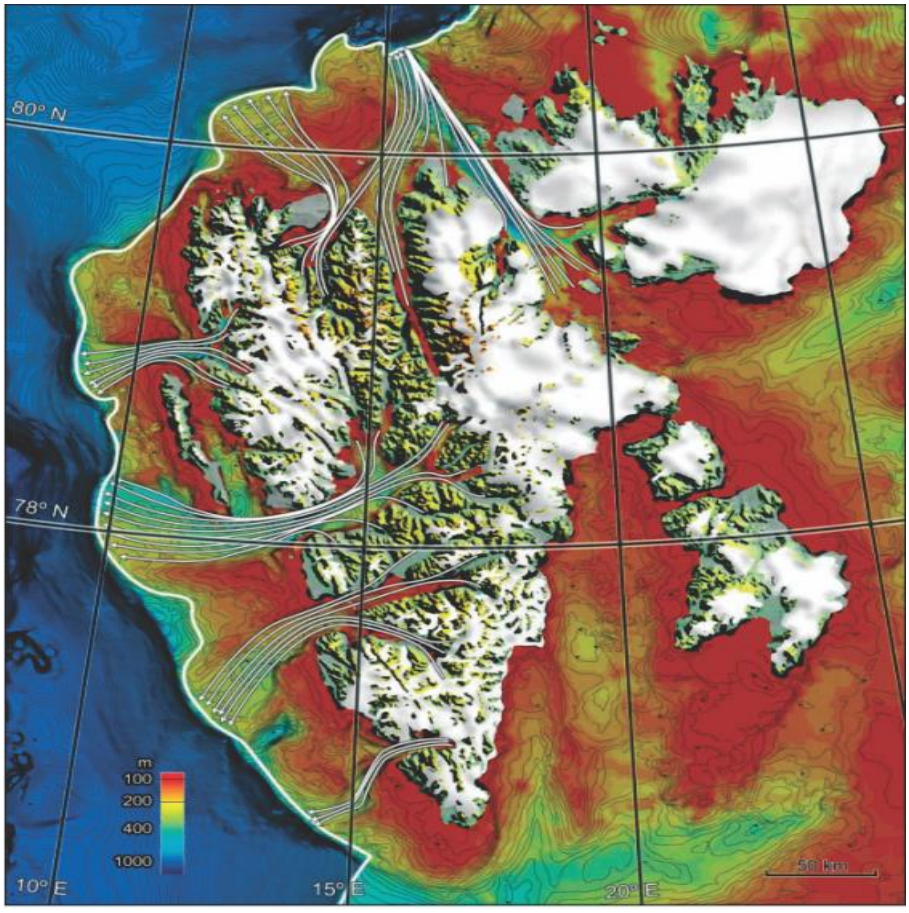

Figure 4: Reconstruction of the ice streams of the Late Weichselian Barents Sea Ice Sheet on the western and northern margin of Svalbard (Figure from Ottesen et al., 2007).

Around 20.5 cal. ka year BP, when the inflow of Atlantic water was reduced and conditions were cold, the deglaciation began on the margin of Svalbard (Jessen, et al., 2010). On the northern and western part of Svalbard there was a constant presence of Atlantic Water at the bottom of the shelf since 15 cal ka BP *(Ślubowska-Woldengen, et al., 2007)*. *Jessen et al (2010)* found a decline in $\delta^{18}O$-values, which is dated to occur 17.4 to 15.7 cal. ka yr BP. This event is found in the Fram Strait and in the Nordic Seas, where the Atlantic Water was reduced and stratified, due to a discharge of cold and relatively fresh water mass

(Rasmussen, et al., 1996a; Rasmussen, et al., 2007; Knies, et al., 1999; Bauch, et al., 2001). This event is correlated in time with the North Atlantic Heinrich Event 1 (Heinrich, 1988; Bond, et al., 1993) and linked to the deglaciation of Svalbard and the Barents Sea (e.g., (Jones & Keigwin, 1988; Elverhøi, et al., 1995; Andersen, et al., 1996). "Heinrich events" are cyclic episodes of icebergs discharge into the North Atlantic, which has been deposited since 130,000 yr BP at a frequency of 6000-10,000 years (Heinrich, 1988). These brief events are also followed by a decrease of foraminiferal fluxes, sea surface cooling, and a distinct decrease in planktic $\delta^{18}O$, which can be an evidence of reduced surface salinities caused by melting of drifting ice (Bond, et al., 1992; Bond, et al., 1993). All these events, together with the influx of ice rafted debris are showed by Bond et al (1993) to coincide with cold stadials, and can be used as a marker for correlations among marine cores (Bond, et al., 1993). Jessen et al (2010) suggest that the meltwater layer was associated with extensive sea ice cover over the Svalbard margin, due to the fact that the low $\delta^{18}O$-values are accompanied by low to moderate concentration of IRD as well as low sedimentation rates. They suggest that the meltwater did not come from the Svalbard-Barents Sea Ice Sheet, but instead most likely came from the southern part of the retreating Fennoscandian Ice Sheet. After this event the flow of Atlantic Water resumed, and sedimentation rates and the concentration of IRD increased west of Svalbard (Jessen, et al., 2010). Prior to these catastrophic events, warmer periods (interstadial) tends to occur (Andersen, et al., 2004). These events, termed Dansgaard – Oeschger events, have been identified from oxygen isotopes from ice cores from Greenland, and shows twenty – four abrupt temperatures changes from the last interglacial, Eemian, to the Holocene. Bond et al (1993) reports that the Dansgaard – Oeschger events lasts for 6000 – 10, 000 years, where a gradual cooling is followed by a sudden warming, which forms a characteristically asymmetrical saw tooth shape.

According to Elverhøi et al (1995) the retreat of the ice sheet also occurred in two steps. The first began at 17.5 cal. ka yr BP (14815±180 ^{14}C yr BP) and the second between 14.8 cal. ka yr BP and 13.9 cal. ka yr BP (13040 and 12485±110 ^{14}C ka yr BP, respectively) where the ice sheet retreated from the inner shelf. Andersen et al (1996) suggest that the early break-up of the ice sheet occurred during the Bølling Interstadial, based on a light peak in $\delta^{18}O$ in slope sediments which is inferred as a meltwater signal. During the early Bølling interstadial the ice sheet retreated rapidly, and laminated sediments from meltwater plumes were

deposited on the Svalbard margin at approximately 14.4 cal ka yr BP (Jessen, et al., 2010). This is interpreted as a sign of rapid retreat of the ice sheet in the Barents Sea (Jessen, et al., 2010). At the onset of Bølling-Allerød Interstadials the sedimentation rate and IRD concentration increased (Jessen, et al., 2010). The sedimentation rate for the Bølling-Allerød is estimated to be high (Jessen, et al., 2010). *Jessen et al (2010)* consider a rise in solar insolation (*Figure 5*) and eustatic sea level to be the possible cause of the increased calving and melting of the ice. On the lower shelf this period is characterized by low accumulation rates of fine –grained and ice –rafted sediments, which was not affected directly by the early phase of the deglaciation, while on the upper slope a relative high amount of coarse sediments were deposited at the same time (Elverhøi, et al., 1995). At this time the inflow of Atlantic Water was increased (Koç, et al., 1993; Hald & Aspeli, 1997), but isolated below a cold and low-saline meltwater layer (Ślubowska, et al., 2005; Ślubowska-Woldengen, et al., 2007). This could indicate a higher rate of iceberg calving, which could have been, according to *Dowdeswell et al (1992)*, kept close to the shelf edge due to strong coastal currents, and thus didn't reach the deeper part of the continental slope *(Elverhøi, et al., 1995)*. The increase of Atlantic Water could, in a combination with increased solar insolation and eustatic sea level, be a cause of the rapid glacial retreat of the Barents Sea (Jessen, et al., 2010). During this period there was extensive sea ice cover, and the productivity was low (Ślubowska, et al., 2005). The concentration of IRD transported from the inner shelves of Svalbard and the Barents Sea increased after the meltwater event (Jessen, et al., 2010). The ice sheet had a minor re-advance on the shelf west of Svalbard around 13.9 cal. ka yr BP (*Calibrated by using Reimer et al., 2013; 12510±90 ^{14}C yr BP)* (Elverhøi, et al., 1995).

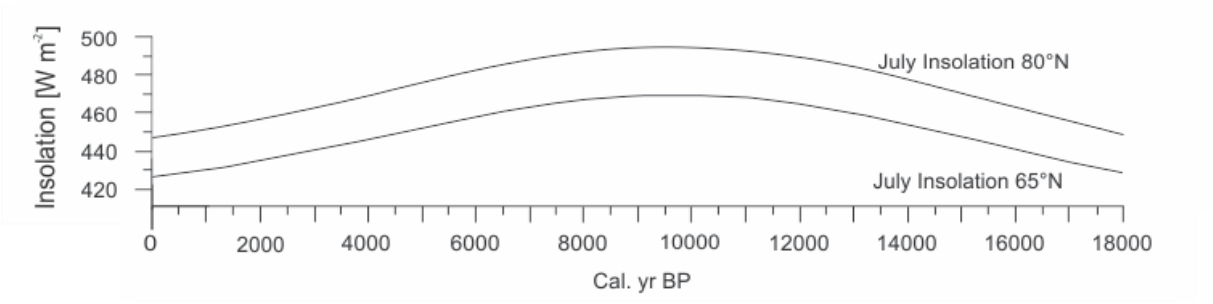

Figure 5: July Solar insolation [Wm^{-2}] at 65°N-80°N (Berger Loutre, 1991), during the last 18 000 cal yr BP (Ślubowska-Woldengen, et al., 2007).

Throughout the Younger Dryas (12.6-11.5 cal. ka yr BP) the bottom waters had decreased temperature and salinity (Ślubowska-Woldengen, et al., 2007). This relatively cold period was characterized by low sedimentation rates, increased ice cover, and low biogenic production which reduced the concentration of foraminifera (Hald & Aspeli, 1997). Moreover, the glaciers advanced on Svalbard (figure 6) and Norway due to rapid climate changes (Vorren & Lysså, 1997; Lehman & Forman, 1992). During the Younger Dryas-Preboreal transition the oxygenation and nutrient depletion of the intermediate water increased (Hald & Aspeli, 1997). The flow of Atlantic Water to the western and northern Svalbard margin was strong during the Early Holocene (10.8-6.8 cal. ka yr BP), and was possibly due to increased solar insolation and wind force that enhanced the flux of Atlantic Water and/or thermohaline circulation (Ślubowska-Woldengen, et al., 2007). The accumulation of hemipelagic mud dominated the slope, and the deposition of ice-rafting material was low (Andersen, et al., 1996). The sea surface temperatures on the continental margin of West Spitsbergen were warmer from 11.2-8.8 cal ka years BP than at present (Hald, et al., 2004), and ice rafting from sea ice and icebergs were reduced (Rasmussen, et al., 2013). The glacier cover on Svalbard was significantly reduced during the Early and Mid-Holocene (8.2 -4 cal. ka years BP) (Svendsen & Mangerud, 1992). Throughout the mid to late Holocene (6.8-1 cal. ka yr BP) the bottom water masses was fresher and colder, and the glacier re-advanced to the present-day conditions (Ślubowska-Woldengen, et al., 2007).

Figure 6: Figure from Mangerud and Landvik (2007) that shows the approximately limit of the Younger Dryas ice sheet, and the extent of the Barents Sea Ice sheet during the LGM (Last Glacial Maximum).

1. 2. 4 Climate

Even though Svalbard is situated far north, the mean temperature during winter is remarkably high, and temperatures above freezing can occur (Hagen, et al., 1993). The Mean Annual Temperature (MAT) is measured to be -6°C on the west coast of Svalbard (Hagen, et al., 1993; Hisdal, 1998). The temperature gets lower and more continental further inland on Svalbard (Hagen, et al., 1993), where the temperature can be as low as -15°C in the mountains (Ingólfsson, 2004).

Relatively warm and saline water transported by the West Spitsbergen Current, a northern branch of the Gulf Stream, and large-scale air circulation is the reason for the mild climate (Hagen, et al., 1993). This also creates areas of open water-conditions during winter (Hagen, et al., 1993). The large-scale air circulation creates a low pressure area near Iceland, and high air pressure area over Greenland, which results in mild air that gets transported towards Svalbard (Hagen, et al., 1993).

Measurements from Isfjord Radio (*Figure 7*) shows that the mean annual temperature rose by 4°–5°C between 1912 and 1920 (Dowdeswell, et al., 1997). Between 1975 and 2000 the mean annual air temperature in Longyearbyen is -5.8°C (Ingólfsson, 2004).

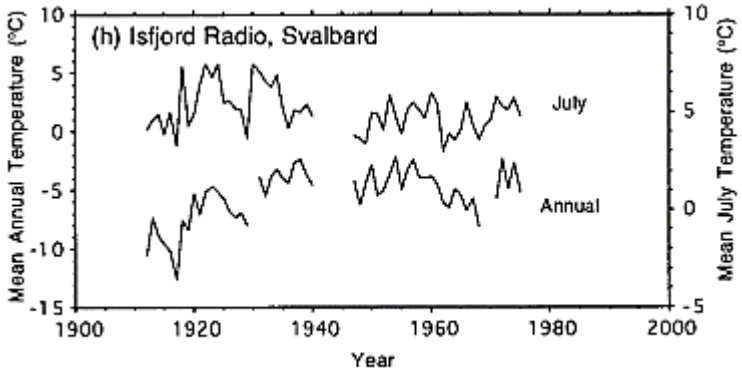

Figure 7: Metrological records from Isfjord Radio, Svalbard (78704°N, 13738°E) in mean July and mean annual temperature (from Dowdeswell et al., 1997).

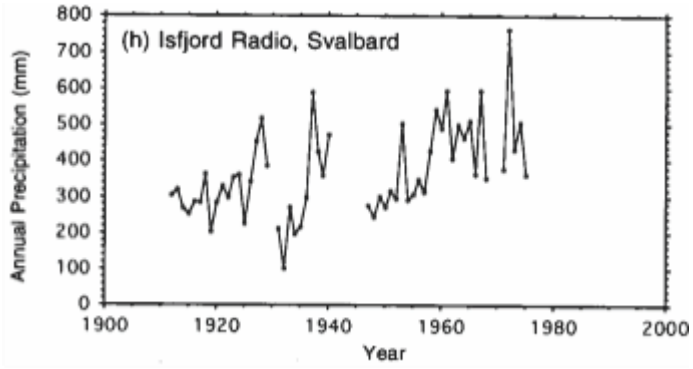

Figure 8: Metrological records of fluctuations in annual precipitation at Isfjord Radio, Svalbard (78704°N, 13738°E) (from Dowdeswell et al., 1997).

In the central Spitsbergen, together with the eastern and western coast of Svalbard the precipitation is 400-600 mm (Figure 8), though near sea level the precipitation is relatively low with 200 mm (Ingólfsson, 2004). Due to the orographic effect, the precipitation is higher on the glaciers, but rarely exceed 2-4 meters of snow (Hagen, et al., 1993).

The ice cover in the Fram Strait today is variable, with permanently and seasonally ice-free areas (Vinje, 1975; Vinje, 1985).

1. 3 Gas hydrates

Gas hydrates, also called gas clathrates, are ice-like substrate which consists of light hydrocarbons, entrapped by a rigid cage of water molecules (Hustoft et al., 2009). Together with water, gas hydrates can be composed with different molecules; methane, which is the most common naturally occurring type of gas hydrate (Kvenvolden and McMenamin, 1980), ethane, propane, normal butane, nitrogen, carbon dioxide and hydrogen sulphide (Sloan, 1998). Gas hydrates can be found in environments with high hydrostatic pressure and low temperature, typical stored in the pore space of the upper most depth zone of sediments at high latitude and on continental margins (Dickens et al., 1995; Haq, 1998; Hustoft et al., 2009; Rajan et al. 2012). The zone where gas hydrates are stable lies between the sediment-water interface and the sub-bottom depth where the geothermal transects the CH_4-hydrate-water equilibrium curve (Figure 9) (Kvenvolden, 1988), and depends on the profile and intercept (bottom water temperature) of the geothermal (Dickens et al., 1995). Due to the restricted conditions, the gas hydrates are confined to the upper few hundred meters of sediments, also called the gas hydrate stability zone (GHSZ) (Hustoft et al., 2009). The occurrence of gas hydrates below the permafrost in the Arctic has been established by petroleum exploration drilling, where marine and seismic studies together with Deep Sea Drilling Project cores have indicated the presence of gas hydrates in the sediment (Kvenvolden and McMenamin, 1980). On seismic data, gas hydrates can be recognized by an anomalous seismic reflector, which is commonly called a bottom-simulating reflector (BSR), where the base mimics the seafloor (Kvenvolden, 1988; Hustoft et al., 2009). The BSR coincides with the predicted transition boundary at the base of the gas hydrate zone (Kvenvolden, 1988). Methane formed during sediment burial is inclined to migrate towards the surface since it is buoyant (Judd and Hovland, 2007). According to Judd and Hovland (2007) low temperature and high pressure conditions favour the formation of gas hydrates that also inhibit migration in deep water. Mud diapirs and gas chimneys, which are associated with gas hydrates (Heggeland, 1996; Bünz et al., 2012) forms in some seabeds due to pressure that builds up in the sediment. As a result, pockmarks may be formed on the seafloor, or lead to seeps with no seabed morphological features (Judd and Hovland, 2007). Pockmarks are depressions in the seabed, which varies in sizes, however, the most common shape is standard circular and elliptical (Hovland and Judd, 1988).

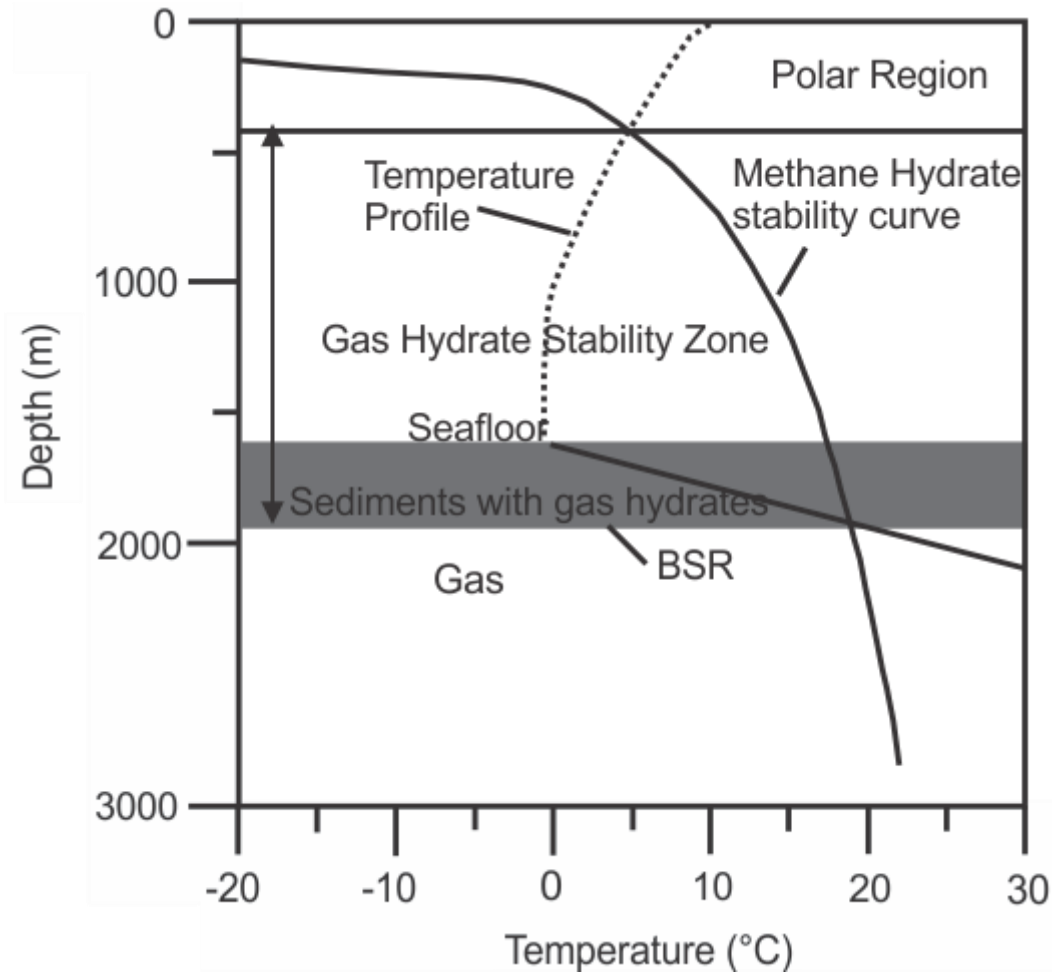

Figure 9: The hydrate stability field in Polar Regions. This example if from offshore Norway, where the geothermal gradient is 50°C/km (Chand & Minshull, 2003). Figure from Chand and Minshull (2003).

The CH_4 originates from free gas, either from below the BSR or by being released from gas hydrate dissociation. Within the sulfate-methane transition zone (SMTZ) (Figure 10), which is typical a zone of few centimeters (Iversen & Jørgersen, 1986; Niewöhner, et al., 1998; Treude, et al., 2005), groups of methanotrophic archaea and sulfate-reducing bacteria can consume up to 90 % of the CH_4 in the sediments, where the overall reaction is $CH_4+SO_4^{2-} \rightarrow HCO_3^-+HS^-+H_2O$ (Barnes & Goldberg, 1976; Borowski, et al., 1996; Boetius, et al., 2000; Hinrichs & Boetius, 2002; Treude, et al., 2003; Reeburgh, 2007). The depth of the SMTZ and the sulfate (SO_4^{2-}) profile can be controlled by the intensity of the upward methane fluxes, if the sediment characteristics and the sulfate diffusion from seawater into the sediment are considered constant (Consolaro, et al., 2015). The precipitation of methane-derived

authigenic carbonate gives rise to negative $\delta^{13}C$ values, and forms the production of bicarbonate from AOM: $CA^{2+}+2HCO_3^- \rightarrow CaCO_3+CO_2+H_2O$ (Kulm & Suess, 1990; Greinert, et al., 2001; Snyder, et al., 2007). DIC derived from the oxidation of CH_4 in the pore space of adjacent sediments are observed to give low $\delta^{13}C$ values in benthic foraminifera tests (Wefer, et al., 1994; Rathburn, et al., 2003; Hill, et al., 2004b; Martin, et al., 2007; Panieri, et al., 2009; Panieri, et al., 2012; Panieri, et al., 2014).

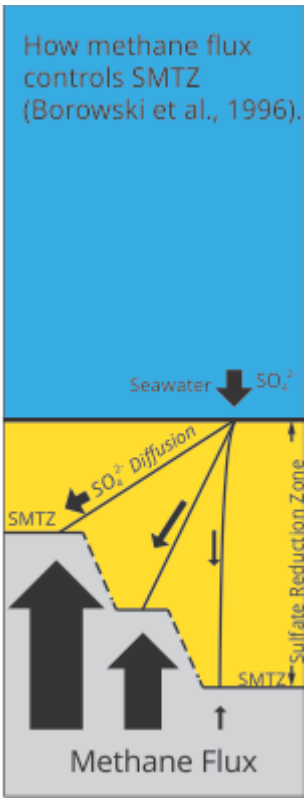

Figure 10: Schematic diagram showing how the SMTZ varies with the methane flux if the flux of sulphate (SO_4^{2-}) from the seawater and the characteristics of the sediments are constant (Consolaro, et al., 2015). Figure modified after Borowski et al (1996) by Consolaro et al (2015.

In recent years there has been more scientific attention regarding the gas hydrate in the Arctic and climate, since the warming of the Arctic occurs at a rate ~2 times faster than at lower latitudes (Graversen, et al., 2008). Methane reservoir are considered an important reservoir for organic carbon (Kvenvolden, 1988), and has a ~25 times higher global warming potential than CO_2 (IPCC, 2007), which could potentially be released and enter the atmosphere and the ocean (Krey, et al., 2009). This can increase acidification and reduce oxygen concentration in the water column (Biastoch, et al., 2011). Gas hydrates also form a potential natural resource (Haq, 1998), and it is estimated that ~104 Gt of carbon is present

in the shallow geosphere at subsurface depth of <200 m (Kvenvolden, 1988), and free gas trapped beneath (Kennett, et al., 2000). In addition, to have an impact on global warming, the gas hydrates are a potential submarine geo-hazard, since changes in pressure and temperature affect their stability, which could lead to slope stability (Kvenvolden, 1993). Gas hydrate prevent sediments compaction, which due to climatic changes makes it an important factor in creating weak layers (McIver, 1982), and can result in methane to be released into the atmosphere and further contribute to climatic changes (Nisbet, 2002; Kennett, et al., 2003). The "Storegga Slide" complex is a submarine slide dated to ~8.2 ka yr BP (Halfidason, et al., 2004), and is considered to be the largest exposed submarine slide in the world (Bugge, 1983). The trigger to this enormous slide is thought to be sediment load and earthquake related to deglaciation (Bryn, et al., 2005). Also, reduced methane gas hydrate stability could have facilitated or contributed to the slope failure (Mienert, et al., 2005). In the study by Mienert et al (2005) they discuss the sensitivity of gas hydrate stability in the Storegga Slide complex to changes in bottom water temperature and sea level since the Last Glacial Maximum (LGM), and if the hydrate stability was a result of post-glacial bottom warming. Methane hydrate provinces are widespread in the Arctic (Biastoch, et al., 2011), and approximately >95 % of the Arctic's gas hydrate reservoir exist in the deep water (Ruppel, 2011). Gas hydrates in ocean sediments are stable when water depths exceed 300 meters and water temperatures approach 0°C (Figure 8) (Kvenvolden, 2000). They are found in outer continental margins in sediments on the slope and rise, where the temperature and bottom water is cold (Kvenvolden, 1998), and the pressure is high (Biastoch, et al., 2011). Recent discoveries suggest that the stability of the gas hydrates at ~400 meter is affected by current ocean warming in the Arctic Ocean (Shakhova, et al., 2010; Ferré, et al., 2012; Berndt, et al., 2014). In regions with presence of gas bubble-plumes a net increase of 1°C at 400 meter water depth in the period 1975 to 2008 was observed (Westbrook, et al., 2009), while the West Spitsbergen Current showed a net increase of 0.8°C between 1997 and 2010 in the Fram Strait (Beszyczynska-Möller, et al., 2012). A possibly increase in methane release activity in the eastern part of Vestnesa Ridge, offshore west of Svalbard, have been detected in 2010 (Bünz, et al., 2012) and in 2012 (Smith, et al., 2014). To reconstruct past marine methane emissions, analyses of carbon isotope ($\delta^{13}C$) of benthic foraminifera is used (Kennett, et al., 2000). In the past, release of methane from methane bearing hydrates in the sediments beneath the sub – seabed have contributed to rapid climate – warming event in

the Quaternary glacial – to – interglacial transitions (Kennett, et al., 2003). Thermal destabilization of methane hydrates are suggested to be linked to episodes of bottom – water warming, and may have driven abrupt decline in $\delta^{13}C$ of oceanic dissolved inorganic carbon (DIC) (Kennett, et al., 2000; de Garidel-Thoron, et al., 2004; Hill, et al., 2004a). Millo et al (2005) reports negative planktic and benthic $\delta^{13}C$ values between 40 and 85 ka in a sediment core from the southwester Greenland Sea. Negative values were observed at peak Dansgaard – Oeschger stadial 22 (85 ka), and matches a major peak in atmospheric CH4 concentration. During this period Atlantic Intermediate water caused a bottom – warming of up to 8°C, which is suggested to be a trigger gas hydrate instability (Millo, et al., 2005). Smith et al (2001) concluded that there could be a parallel to negative $\delta^{13}C$ values and deglaciations and the retreat of ice sheet, and linked the negative values to dissociation of gas hydrates to reduction of ice load and intrusion of warm bottom water.

In a study by Consolaro et al (2015), records of benthonic and planktonic foraminifera from Vestnesa Ridge have been investigated, and shows negative carbon isotope excursions (-4.37‰) for the Bølling-Allerød interstadial and -3.41‰ for the Early Holocene. $\delta^{13}C$ values of the last deglaciation from the Kara Sea have values from -0.5 to 0.3‰ (Lubinski, et al., 2001) and -1 to 0‰ in the northern Barents Sea (Wollenburg, et al., 2001). Surface sample of dead specimens of the benthic foraminifera *Cassidulina neoteretis* from the active Håkon Mosby mud volcano in the Barents Sea shows negative $\delta^{13}C$ values (-1.65 to -2.82‰) (Mackensen, et al., 2006). The negative values in the Bølling-Allerød is interpreted to be due to methane-derived authigenic carbonates (Consolaro, et al., 2015). Authigenic carbonates is the result of the anaerobic methane oxidation coupled with sulphate reduction by consortia of archaea and bacteria (Kulm, 1986; Hovland, et al., 1987; Boetius, et al., 2000; Greinert, et al., 2001). Benthic foraminifera from a methane seeps at Hydrate Ridge, Oregon, exhibits significant shift in $\delta^{13}C$ values, where the values varies from -1.28 to -5.64 ‰, and living benthic foraminifera from the same site are reported to have $\delta^{13}C$ values ranging from -0.4 to -21.2‰ (Hill, et al., 2004b).

Consolaro et al (2015) suggest that a combined effect of rise in sea level, increased seismic activity and high sedimentation load could possibly have led to gas hydrate dissociation on the seabed on Vestnesa Ridge. Deposition of large amount of glacigenic sediments on the upper continental slope occurs during full –glacial conditions when the ice sheet have

reached the continental shelf break (Elverhøi, et al., 1998; Dowdeswel & Siegert, 1999). This does not coincide with the timing of the gas venting documented by *Consolaro et al (2015).* During the deglaciation the sedimentation rate amplified (40-50 cm/ka) (Consolaro, et al., 2015), and from 14.6 to 14.3 cal. ka yr BP the sedimentation rate increased a lot (500 cm/ka) (Jessen, et al., 2010). However, it is not known if a minor sediment load could affect the pore pressure and the stability of the gas hydrate (Consolaro, et al., 2015).

In recent years, there have been reported similar negative foraminiferal $\delta^{13}C$ values interpreted as evidence for methane release in Quaternary records (Kennett, et al., 2000; Smith, et al., 2001; Keigwin, 2002; Millo, et al., 2005; Cook, et al., 2011; Hill, et al., 2012). In a study by *Kennett et al (2000)* they identified four episodes of brief, but still massive release of methane from the continental margin of Santa Barbara Basin during late Quaternary interstadials, indicated by negative δ13C values (*Figure 10*). They inferred it to be resulted by sediment failure due to dissociation of gas hydrate, which is associated with millennial-scale bottom-water changes.

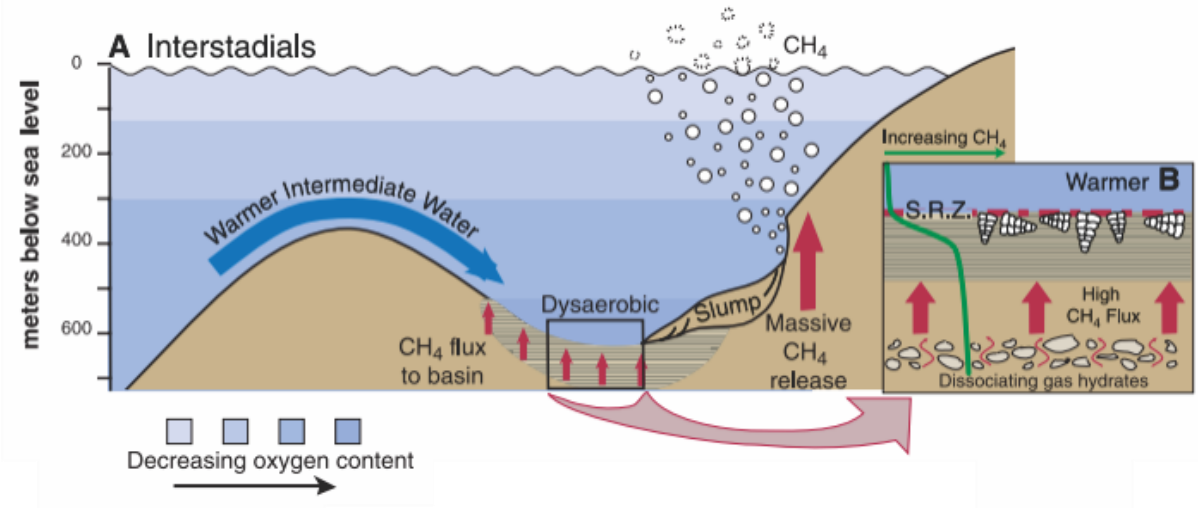

Figure 11: Figure showing stadial-interstadial modes of methane flux (here form Santa Barbara Basin). (A) During interstadial warm intermediate activate methane flux (B) by destabilized the gas hydrates. (Figures modified from Kennett et al., 2000).

Smith et al (2001) documented three excursion of negative $\delta^{13}C$ values from the East Greenland continental shelf caused by release of methane, which occurred during the deglaciation. The mechanism for the expulsion from the seafloor is thought to be from pressure release when the ice sheet retreated. A study by *Panieri et al (2014)* identified five

intervals of events with methane emission from the seafloor during the last 23.5 cal ka yr BP on the Vestnesa Ridge, West Svalbard continental margin. They dated one of the methane emission events to occur during the LGM, the second, which is the largest, pre-dates the Bølling-Allerød Interstadials, the third a few hundred years after the Younger Dryas and the last coincides with the Early Holocene. There is a correlation with regional and global climatic events, and they conclude that the methane emission is a result of one or more geological processes, but no evidence of correlation to increased bottom-water temperature during these events.

1. Study area

2. 1 Vestnesa Ridge

Vestnesa Ridge (*Figure 11.2*) is a SE-NW to E-W bending elongated sediment drift situated at 79° N, offshore western Svalbard in the eastern Fram Strait (*Hustoft et al., 2009*) (Figure11.1). The Fram Strait contains marine sediment records of both ice sheet interactions and bottom water flow, and is the only deep-water connection between the Arctic Ocean to the North Atlantic (Howe, et al., 2008). A CTD record taken at Vestnesa Ridge reveals the present-day oceanographic conditions in the study area (Figure 12). The West Spitsbergen Current transports warm, saline Atlantic Water to the area (Aagaard, et al., 1978). The AW is submerged, and continues as Atlantic Intermediate Water into the Arctic Ocean and in the East Greenland Current (Swift, 1986). Below these water masses flows the cold (-0.9° and more saline (>34.91 ‰) Greenland Sea Intermediate Water (Aagaard, et al., 1985; Rudels, et al., 2000; Langehaug & Falck, 2012). The crest of the Vestnesa Ridge is located at water depth between 1200 and 1300 m (*Bünz et al., 2012*) (Figure 13). Between 500 and 1200 meters water depth the slope of Vestnesa Ridge is approximately 1.5° to 2°, and beyond 1200 m the slope angle is c. 0.5° (Howe, et al., 2008). Vestnesa Ridge contains >2km of sediments of contouritic, downslope and hemipelagic origin (Vogt, et al., 1994; Vogt, et al., 1999). Bottom currents erodes the shelf, and sediments are transported and deposited at the contourite drift (Rebesco, et al., 2013). Investigation of sediment cores from Vestnesa by Howe et al (2008) revealed that the Holocene was dominated by muddy-silty contourites with abundant IRD (Howe, et al., 2008).

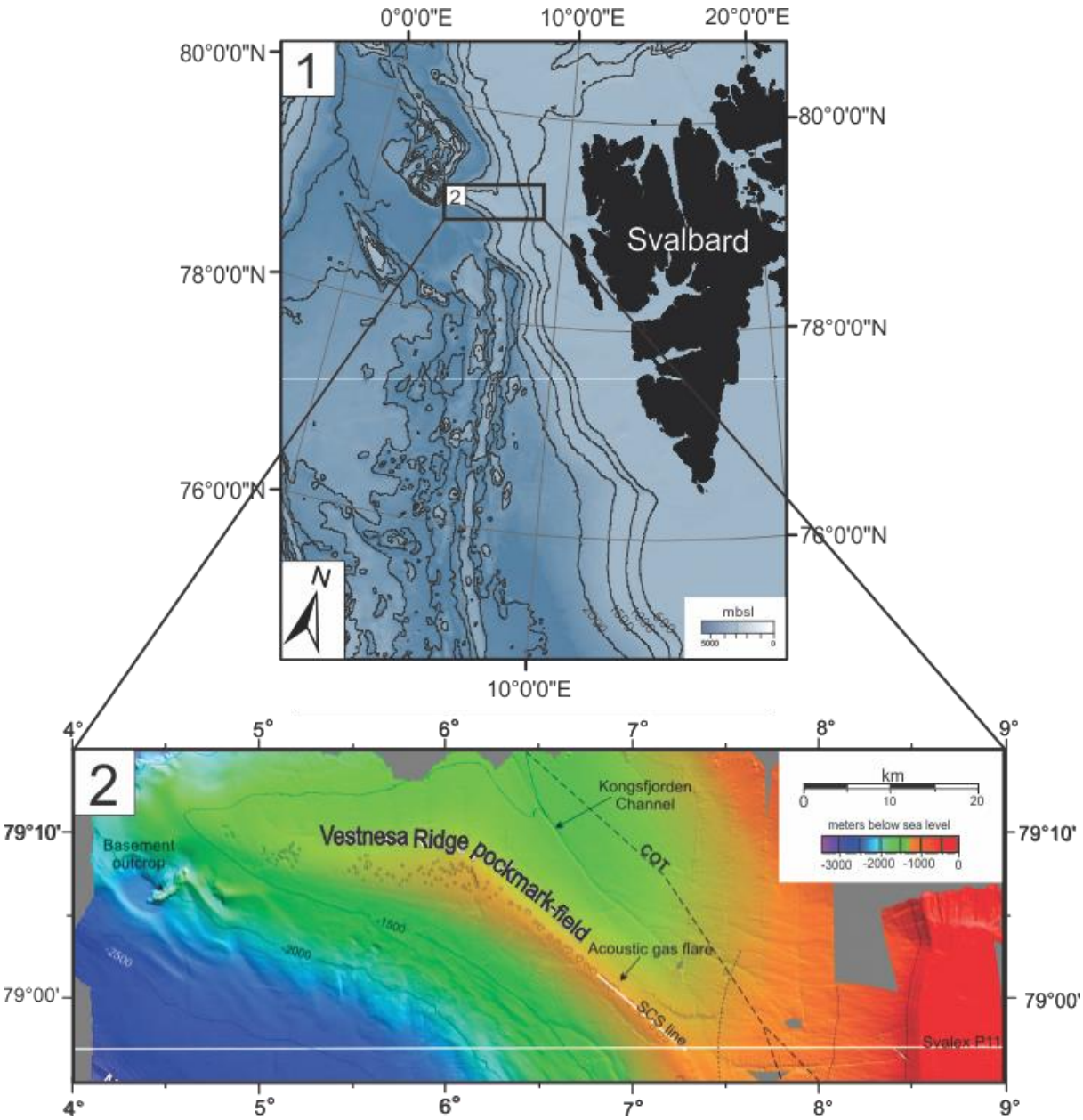

Figure 12: 1: Overview map over study area offshore NW-Svalbard. 2: Bathymetry map over Vestnesa Ridge showing pockmark-field on the crest of the ridge (modified from Hustoft et al (2009)).

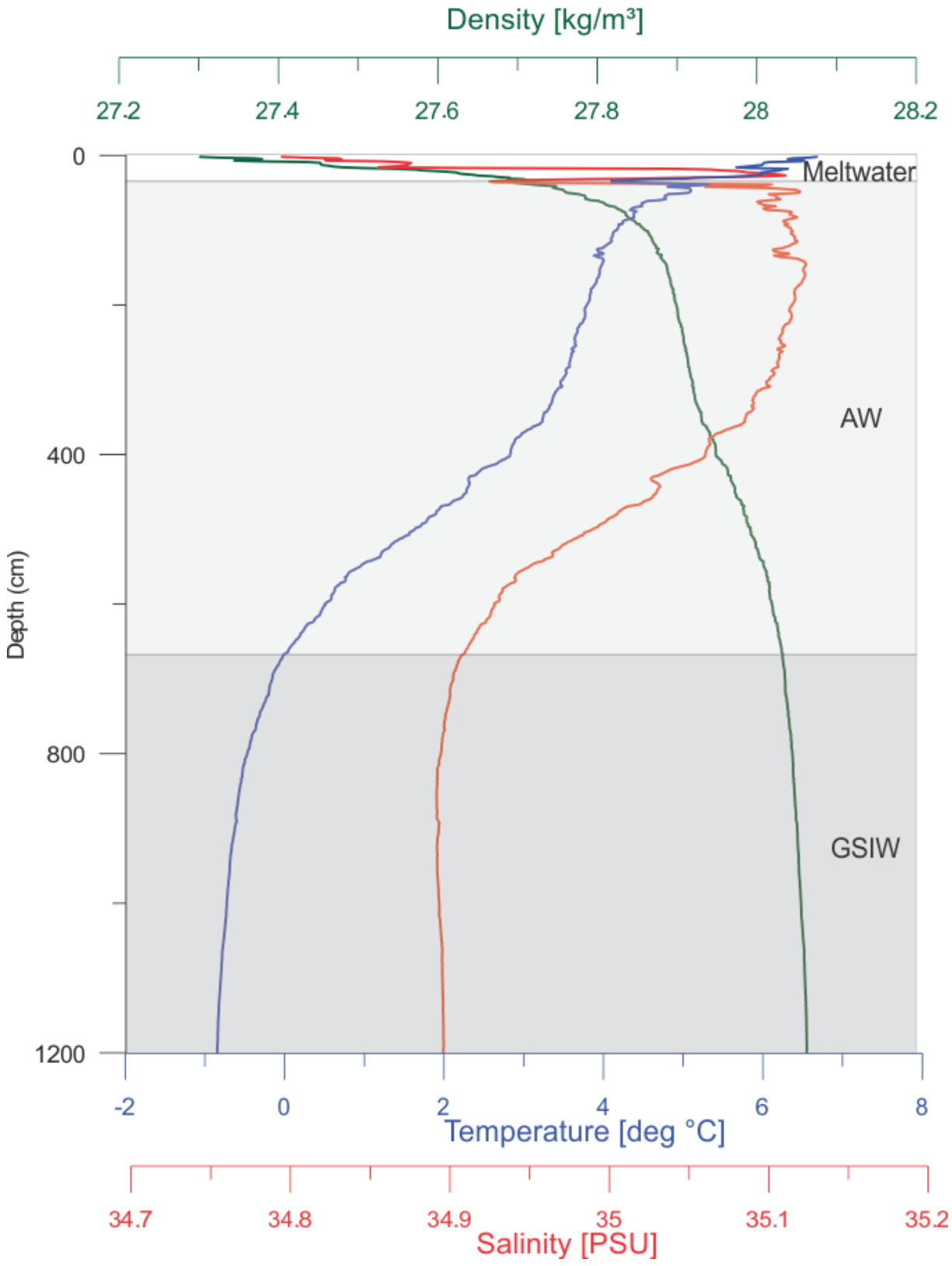

*Figure 13: CTD profiles based on data from measurements during the scientific cruise to the Fram Strait in 2012. The location of the CTD is 79.00.176°N, 006.55.707°E at 1217 m water depth. (*AW=Atlantic Water, GSIW= Greenland Sea Intermediate Water).

Vestnesa Ridge area is known for its gas-hydrate and venting system, and is one of the northernmost documented oceanic gas hydrate provinces, where the crest of Vestnesa Ridge is impaled with fluid flow features (*Hustoft et al. 2009; Bünz et al., 2012*). The gas is thought to be derived from decay of organic matter (Vogt, et al., 1994), however, recent study by Smith et al (2014) suggest that it is a thermogenic source that is supplying methane to the area. According to *Bünz et al (201*2) the seafloor pockmark can vary in size up to 700 m in diameter. *Bünz et al (2012)* documented active pockmarks on Vestnesa Ridge, where methane flares reached up to 800 meters in the water column. However, the reason to what triggers the increase in gas expulsion from the seafloor sediments is unclear according to *Bünz et al., 2012*.

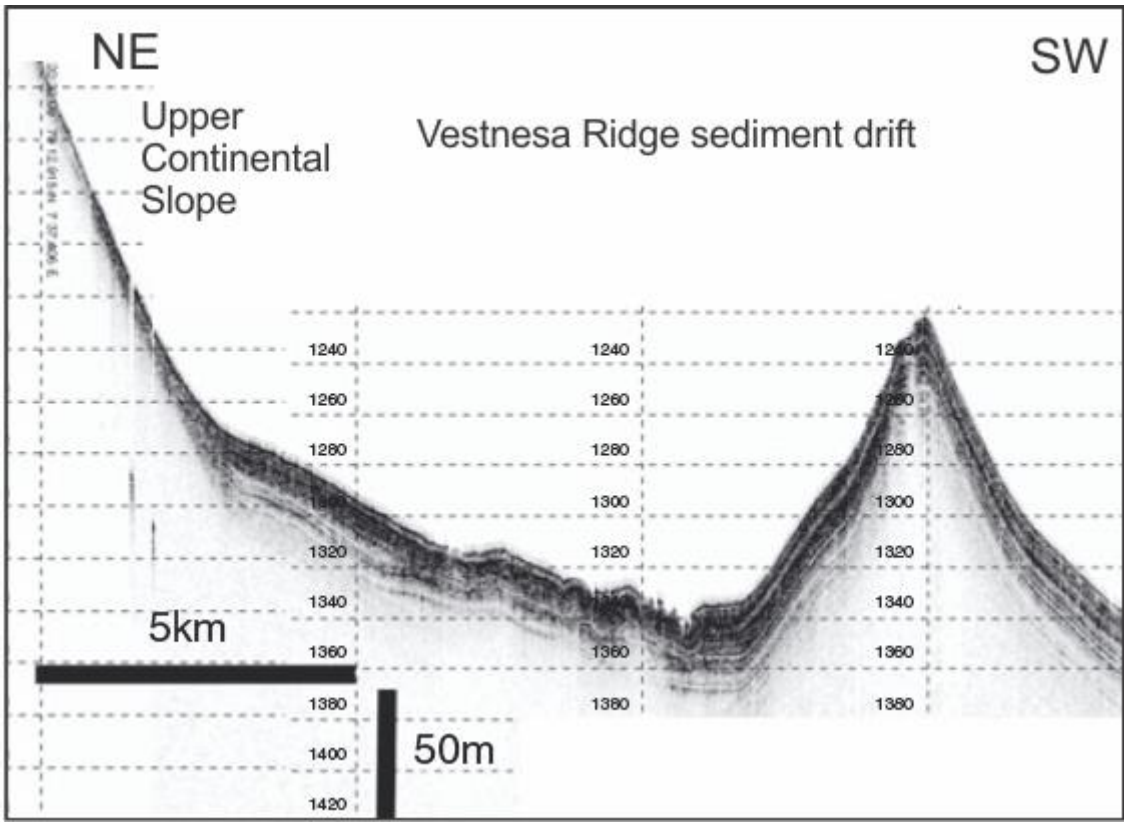

Figure 14: Sub – bottom profile across the Vestnesa Ridge sediment drift, and location compared to the upper continental slope. (Figure modified from Howe et al., 2008).

3. Materials and methods

Two sediment cores were investigated in this study. One of the gravity cores, HH14-002, were collected during a scientific cruise in July, 2014 (Rasmussen et al., 2014) (Figure 15.1), with the research vessel R/V Helmer Hanssen of the University of Tromsø, arranged by CAGE.

The other gravity core, HH12-930, was collected during a teaching cruise in July 2012 (Rasmussen et al., 2014) (Figure 15.2). For further details about the position and times see *Table 1*.

2. 1 Sediment cores

On board on R/V Helmer Hanssen the 6 meter gravity corer consist of a steel barrel with an inner diameter of 11 cm, which is attached to a 1600 kg weight. The gravity corer is attached to a wire, which can be lowered to as deep as 3000 m into the water column. By using gravity the gravity corer can penetrate the sediments. At the bottom, a core catcher is placed to better cut into the sediments and a core cutter to close the system and make sure that the sediments doesn't fall out during the transport to the surface. Vacuum is produced when a valve at the top of the instrument is closed. The core cutter acts also as a knife to cut through the sediment, so it enters the plastic tube inside the gravity core.

When the gravity core is retrieved on board, the plastic tube is pulled out of the steel barrel and divided into preferable 1-meter sections. As a final point, the sections are cleaned, marked and enclosed with plastic caps. The sections were stored in a cooling room (~4 °C) until further investigation.

Station	Date	Time (UTC)	Location	Latitude (N) Longitude (E)	Water depth (m)	Recovery (cm)	Comment
HH14-002GC	22/07-14	0928	Vestnesa, Edge of pockmark 2	79.00.605° 006.54.484°	1211	413	4 sections #4=113 cm
HH12-930GC	27/07-12	-	Vestnesa, pockmark 2,pogophor site	79.00.585° 006.54.461°	1211	538	6 sections, smell of gas in lower parts

Table 2: Information about the gravity cores and the core station location used in this mater thesis. (Rasmussen and Forwick, 2012; Rasmussen, et al., 2014).

3. 2 Chirp data

Sub-bottom chirp profiler are high-resolution frequency-modulated marine sources. The vertical resolution is dependent upon the bandwidth of the source, and can produce real-time sediment profile of the top 30 meter of unconsolidated sediments (Quinn, et al., 1998).

The seismic profiles (Figure 15) was collected during cruises in 2012 and in 2014 by using EdgeTech 3300-HM hull-mounted sub-bottom profile. The pulse mode was 1,5-9,0 kHz during the collection of HH14-002 GC.

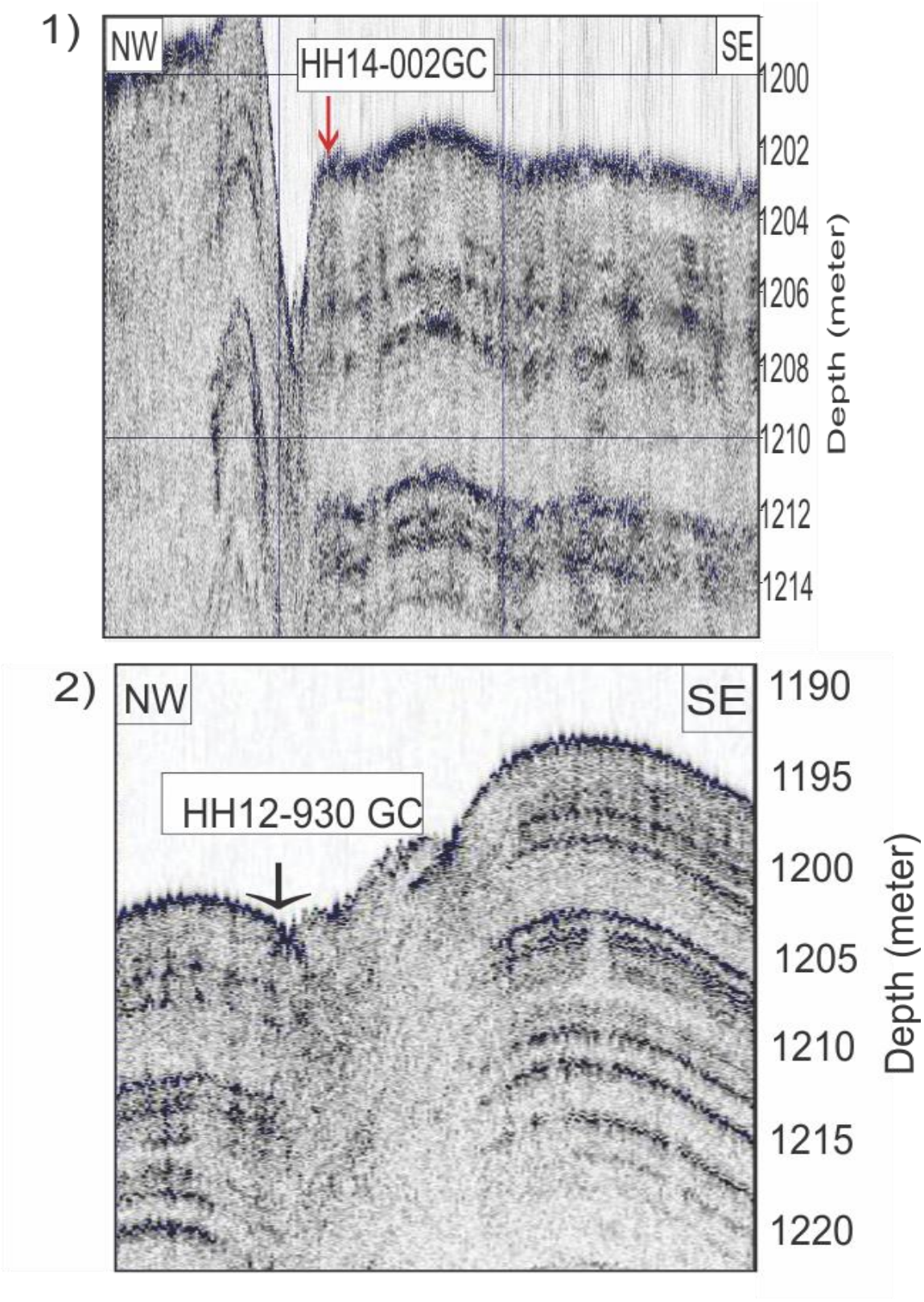

Figure 15: Chirp data showing the coring site of 1) HH14-002 GC and 2) HH12-930 GC.

3. 3 CTD (Conductivity, temperature, depth)

During a scientific cruise in 2012, CTD measurements were collected *(Figure* 12) by using Seabird 911 Plus CTD (?). The instrument is lowered into the water and measures continuously from the surface to the bottom. By doing this, information throughout the entire water column can be received. Temperature and conductivity are measured against the depth, and the conductivity is then calculated into salinity. The CTD was collected from a site close to sediments core HH12-930 GC; *79.00.176°N, 006.55.707°E* at 1217 m water depth. There is a decrease in temperature and salinity with increasing depth, while the density is increasing.

3. 4 Laboratory work

The laboratory work took place at the Department of Geology at UiT, the Arctic University of Tromsø, Norway. Samples analysed for $^{13}C/^{12}C$ and $^{18}O/^{16}O$ were sent to the Geological Mass Spectrometer Laboratory at The University of Bergen, Norway. Radiocarbon dates were analysed at the ^{14}Chrone Centre, Queen's University, Belfast, United Kingdom.

3. 4. 1 Description, opening and logging of the cores

Gravity core HH14-002 GC was split lengthwise into two halves using a circular saw and a knife to separate the two sections. One of the sections was marked as archive, and the other as a work-half. After the sections were labelled and cleaned, they were packed in plastic, duly marked and kept in a cold room (~4°C) until further use. The surface of the work-part section was later cleaned and studied for a lithological log. The other gravity core, HH12-930, was opened in 2012 on board the cruise vessel, carefully wrapped in plastic and sealed and stored in a cold room.

3. 4. 2 Magnetic susceptibility (MS)

The core HH14-002 GC was measured for magnetic susceptibility with a Barrington loop sensor (MS2C) on board on R/V Helmer Hanssen. Because the measurement were done at low resolution (5 cm interval), the magnetic susceptibility was measured again. Both HH14-002 GC and HH12-930 were removed from the cooling room approximately 24 hours before the measurements so that they could obtain room temperature, due to the fact that temperature may influent the result (Weber, et al., 1997). Core HH14-002 and HH12-930 GC the magnetic susceptibility was measured a second time with a hand-held Barrington point sensor (MS2E) every 2 cm. The hand-held point sensor were used since the loop sensor cannot be used on splitted cores.

Magnetic susceptibility measures the ability of the sediment to magnetise. Variations of the magnetic susceptibility in sediment core is controlled by the mineralogy, concentration and grain size distributed in the sediments (Robinson, et al., 1995; Rasmussen, et al., 1996a), which can be ferromagnetic, paramagnetic or antiferromagnetic. Intervals that are relatively low are commonly composed by fine grained sediments, like clay and silt, while high values can be linked to coarser material, preferable in the 63 µm to 1 mm fraction (Rasmussen, et al., 1996a). The magnetic susceptibility is measured by the oscillator circuit in the sensor which produces a pulse of low intensity magnetic field (2 kHz for the point sensor and 0,565 kHz for the loop sensor). Material near the sensor that has magnetic susceptibility will cause the oscillator frequency to change, which is converted into magnetic susceptibility values. The magnetic susceptibility of ocean sediments is dependent on changes in glacial activity, and oceanography; the magnetic susceptibility of the sediments from the North Atlantic and southern Norwegian Sea correlates with the bottom current strength and therefor the intensity of the deep water formation in the Nordic Sea (Rasmussen, et al., 1996a; Rasmussen, et al., 1998; Kissel, et al., 1997; Moros, et al., 2002). However, the correlation is overprinted by changes in sediment provenance, like ice rafting containing material that is non-magnetic or highly magnetic (Andrews, et al., 1995; Grousset, et al., 1993; Robinson, et al., 1995; Stoner, et al., 1996; Pirrung, et al., 2002). Meltwater plumes (Lekens, et al., 2005; Rasmussen, et al., 2007) and mass transportation on glaciated margins (Robinson, et al., 2000; Kuijpers, et al., 2001; Rasmussen, et al., 2007) can significant influence the magnetic susceptibility (Jessen, et al., 2010).

3. 4. 3 Color images

The scanning images of the cores were taken by using Jai L-107CC 3 CCD RBG Line Scan Camera, which is installed on the Avaatech XRF core scanner. The resolution was set to be 70 µm. Before the images were taken, the surface of the two cores, HH14-002 GC and HH12-930 GC, were cleaned and smoothed with a plastic card. The cores have been taken out of the cooling room for more than 24 hours, which reduces reflections on the surface since most the pore water on the surface is evaporated

3. 4. 4 X-ray photography

X-ray photography is a non-destructive technique to imaging technique, that allows physical structures in sediment records to be revealed and analysed (Migeon, et al., 1999).

X-ray photographs was taken at the UiT, the Arctic University of Tromsø with the Geotek X-ray core imaging system *(Figure 14).* This provides information about the internal structures of the cores, such lithological variations, presence of ice-rafted debris, and degree of bioturbation and location of eventual shells. When the X-rays travels through a material, the attenuation depends on the density of the material. Material with high density, like clasts and shells, will appear whiter, while mud, which has low density, will seem darker. This ratio can be adjusted, depending on perforation. The X-ray photo of HH12-002 GC was taken prior to splitting of the core, while the X-ray photos of HH12-930 GC were taken after the splitting.

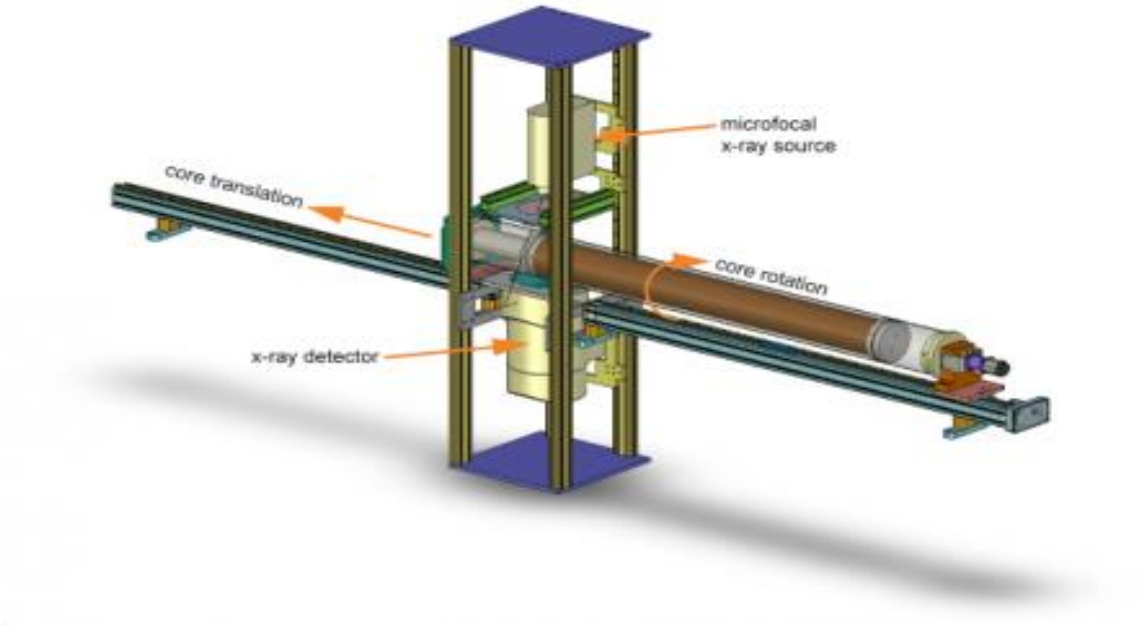

Figure 16: 3D model of the MSCL-XCT (Figure taken from http://www.geotek.co.uk/products/mscl-xct).

3. 4. 5 Sediment sampling

For core HH14-002 GC were first sampled at every 4 cm. Then from 4 cm to 49 approximately every 10 cm were used. From 49 cm to 156 every 4 cm were used. From 163 cm to 412 irregular intervals from 10 cm to 5 cm were used. For HH12-930 GC every 5 cm were sampled. Each sample was cut into 1 cm slices using an osmotic knife to easily cut through the sediment and a spatula. The equipment was cleaned after each sample was taken. The samples were put in labelled and weighed plastic bags. The samples were weighed and samples from HH14-002 GC were kept in a freezer and later dried in a freeze-dryer. The freeze dryer that was used was Christ: Alpha 1 – 4 at the Geology Department Laboratory, UiT, Arctic University of Tromsø. However, due to an unfortunate event the freeze dryer was out of order, so the samples from HH12-930 GC had to be dried in an oven (40°C). After the samples were dried the dry weight were determined. The samples were then wet sieved using a 63 µm, 100 µm and 0, 5 mm size fractions, where the sediments were retrieve from the sieve using distilled water and collected in labelled filter paper. The residue samples were dried in an oven (40°C) until dry, then weighed and put in labelled sample glasses.

Grain sizes over 0.5 mm was counted after weighing by using a binocular microscope (Leica CLS150X – MZ12$_5$). The density of the total 0.5 mm was calculated by dividing the number of grains with the weight (No. IRD pr g).

3. 4. 6 Accelerator Mass Spectrometry (AMS) and radiocarbon dating

3. 4. 6. 1 Principle

Radioactivity is a phenomenon where the decay of unstable atoms emits nuclear particles and radiant energy (Faure & Mensing, 2005). Some isotopes are considered radioactive, like ^{14}C which is therefore the radioactive form of carbon, and are referred as unstable isotopes, while ^{12}C and ^{13}C are stable isotopes.

^{14}C is continually being produced in the atmosphere by nuclear reactions, which is further incorporated into CO_2 molecules due to oxidation (Faure & Mensing, 2005). The CO2 is stored in the global reservoirs; the atmosphere, the hydrosphere, and enter the biosphere through photosynthesis, where plants absorbs the CO_2 (Lowe & Walker, 1997). After the death of the organism, the absorption of atmospheric CO_2 ends, and no replacement will take place, however, the 14C will continue to decay at a controlled rate (Faure & Mensing, 2005). The half-life of ^{14}C is 5,730 years, meaning that half of the original ^{14}C will remain after 5730 years (Bowman, 1990). The radioactive isotope of carbon can hence be used to determine the age of substances containing organic material. This radiometric dating technique is called *radiocarbon dating*, or carbon-14-dating. The method rests on fundamental assumptions; (a) the production of ^{14}C is constant over time, (b) that the ^{14}C:^{12}C ratio in the biosphere and hydrosphere is in equilibrium with the atmosphere, (c) the decay rate of ^{14}C can be established, and (d) it has existed a closed system since the death of the organism (Bowman, 1990).

3. 4. 6. 2 Accelerator Mass Spectrometry (AMS) and 14C dating

Together four samples containing c. 1200 specimens of the planktic foraminiferal species *Neogloboquadrina pachyderma sinistral (s)* (see Table 2) were collected from different intervals in HH14-002 GC. Two samples with 1200 N. pachyderma (s) in each and two

samples containing bivalve shells from HH12-930 GC were collected (see Table 3). Only well – preserved samples with no signs damage were collected, since it could indicate re-deposition. The samples from HH14-002 GC and HH12-930 GC were sent to the 14CHRONO Centre at Queens University in Belfast, United Kingdom, for AMS ^{14}C dating. Based on the results retrieved from Belfast, the sedimentation rate could be calculated from a calibrated radiocarbon dates (see below).

Lab reference	Core	Depth (cm)	Species
UBA-28217	HH14-002GC	215.5	N. pachyderma (s)
UBA-28218	HH14-002GC	259.5	N. pachyderma (s)
UBA-28219	HH14-002GC	275.5	N. pachyderma (s)
UBA-28220	HH14-002GC	323.5	N. pachyderma (s)

Table 2: This table shows the laboratory reference, the name of the core, depth and what kind of species dated. The selected intervals contained large quantities of the planktonic foraminifera Neogloboquadrina pachyderma (sinistral).

Lab reference	Core	Depth (cm)	Species
UBA-30294	HH12-930GC	298	N. pachyderma (s)
UBA-30295	HH12-930GC	320.5	Shell (Vesicomyidae)
UBA-30296	HH12-930GC	433	N. pachyderma (s)
UBA-30297	HH12-930GC	508	Shell fragment

Table 3: Laboratory reference, name of the core, depth and what kind of material was used for dating. In this core not only planktic foraminifera was used, but shell and shell fragments as well.

The principle of accelerator mass spectrometry is based on how the atomic weight is a controlling factor which decides on how great the deflection of a charge particle moving through a magnetic field in a straight path will be; the lighter the weight, the superior amounts of deflection (Linick, et al., 1989). If the particles travels by very high speed, however, and are subject to high voltage difference, the mass spectrometers can discriminate between ^{14}C and ^{14}N, which has a similar weight, and detect a very small number of ^{14}C atoms in the a sample (Linick, et al., 1989).

^{14}N, a non-radioactive isotope of nitrogen, has a very similar weight to ^{14}C, complicates the measurement of ^{14}C, since 78% of the atmosphere consists of nitrogen (Linick, et al., 1989). However, due to the fact that nitrogen does not form negative ions, the AMS-instrument is able to eliminate most of the ^{14}N (Linick, et al., 1989).

3. 4. 7.3 Calibration and marine reservoir effects

To calibrate the ^{14}C dates retrieved from the ^{14}C accelerator mass spectrometry, the program Calib 7.0.4 (Stuvier & Reimer, 1993) was used. The program makes the conversion from radiocarbon age to calibrated calendar years (cal. yr. BP) by calculating the probability distribution of the sample's true age. The calibration data set was set to "Marine13.14C" (Reimer, et al., 2013), which is a "global" marine calibration data set, and used since the samples were of marine origin. The marine reservoir age (ΔR) was set to be 0, since core HH14 – 002 GC is collected from the deep sea. The σ2 dating uncertainty was used, where the mean calibrated age was calculated, and is presented as calibrated calendar years before present (cal yr BP).

3. 4. 8. Stable isotopes

For the stable isotope analysis, the planktic foraminifer Neogloboquadrina pachyderma (s) and the benthic foraminifera Cassidulina neoteretis were used. From 0 – 412 cm 64 samples were examined using a binocular microscope (Leica CLS150X – MZ12s). Only undamaged foraminifera with no contaminations was used. Not all off the samples contained sufficient material to be analysed. All of the measurements of stable oxygen and carbon were

analysed using a Finnigan MAT 253 mass spectrometer with a Kiel IV device at the Geological Mass Spectrometer (GMS) laboratory at the University in Bergen. The precision for $\delta^{18}O$ was ±0.06‰ and ±0.03‰ for $\delta^{13}C$. All the isotope values are presented per mill (‰).

3. 4. 8. 1 Principle

Changes in isotopes can be measured and interpreted to improve the understanding of geological, biological, hydrological and atmospheric processes on Earth (Faure & Mensing, 2005).

The isotopic composition of carbon and oxygen in carbonate fossils are dependent on the ambient temperature and/or the isotopic composition of carbon and oxygen sources (Poole, 1994). This is a result of chemical reactions such as condensation of water, evaporation, and physical processes like diffusion (Faure & Mensing, 2005).

Geochemical analysis of the test calcified by foraminifera have increased the last decades (Katz, et al., 2010). By assuming that the isotopic composition is only a function of the temperature and the isotopic composition of the ambient water (Poole, 1994), the oxygen and carbon isotopic composition of fossil benthic and planktic foraminifera can be used to reconstruct paleoclimate and paleoceanographic conditions, together with ocean paleocirculation patterns, ice-volume, sea-level and the carbon cycle, and how these record varies through time (Katz, et al., 2010). Foraminiferal species precipitate their test in isotopic disequilibrium, and one of the controlling factors are the vital effect (Poole, 1994). Vital effect is manifested by disequilibrium isotopic composition and in almost all cases gives rise to depletions in the heavy isotope (Gossman, 1987). In microfossils variation in carbon isotope content is caused fractionation as a result of different vital effect (Jansen, 1989). The benthic species Cassidulina neoteretis is in equilibrium with the ambient water in terms of oxygen isotope composition (Poole, 1994). *Neogloboquadrina pachyderma (s)* has been reported to be in disequilibrium with the ambient water, which results in vital effect (Kozdon, et al., 2009). The results are expressed as δ (‰ vs. PDB).

Benthic foraminifera provides information on the conditions in and on the seafloor, such as for example the food and oxygen availability, since they are abundant in the upper 1 cm of sediment (Katz, et al., 2010). Planktic foraminifera can be found in the surface waters, and reflects water temperature, as well as food availability (Katz, et al., 2010).

3. 4. 8. 2 Oxygen isotope

Oxygen is the most abundant chemical element in the Earth's crust, and consists of three stable isotope: ${}^{16}_{8}O$, ${}^{17}_{8}O$, and ${}^{18}_{8}O$ (Faure & Mensing, 2005). The isotopes have different masses, which affects the mass of the element they bond with, like H_2O. Water molecules consist of either the heavy or the light isotope, where the light water molecules have a higher velocity in gas than the heavy molecules (Faure & Mensing, 2005).

During the last decades the use of stable oxygen isotope ratios ($^{18}O/^{16}O$) has become a standard too indicate the paleotemperature (Urey, 1947; McCrea, 1950; Epstein, et al., 1953). The foraminifera tests, which is made up of calcium carbonate, record the seawater (δ_w), and therefor reflects (1) the global ice volume and (2) region/local river-water input (3) evaporation/precipitation for shelf and surface waters (Katz, et al., 2010). Isotopic analyses are expressed in terms of the PDB standard (Epstein, et al., 1953), and its isotopic composition corresponds to the SMOW (Standard Mean Ocean Water) scale (Craig, 1965).

According to Zeebe (1999) the $\delta^{18}O$ of the foraminiferal calcite decreases with increasing pH, or CO_3^{2-}.

During the calcifying of the tests a temperature-dependent fractionation occurs, were the "light" H_2O^{16} evaporates easily, which produces ^{16}O-enriched precipitation (Katz, et al., 2010). The precipitation falls like snow, which leads to the glacial ice and river runoff to be enhanced with ^{16}O-molecules during glacial periods (Katz, et al., 2010), while the oceans is rich in the heavier ^{18}O-molecule. However, during interglacial periods, the ^{16}O-enriched precipitation returns to the ocean via snow melt (Katz, et al., 2010). These variations, and the fluctuations in ice-sheet size, have an effect on the mean ocean value (δ_w), which in turn changes the $\delta^{18}O_{calcite}$ value, however, a temperature increase of 1°C can cause a ~0.23‰ decrease in the measured $\delta^{18}O_{calcite}$ (Katz, et al., 2010). The $\delta^{18}O$ value of ice sheets is estimated to be -35 to -40 ‰, while the mean $\delta^{18}O$ ocean value is 0‰ (Katz, et al., 2010). Approximately 3 % of the world's ocean was removed during the last glacial maximum when the global sea level was lowered by ~120±5 m, which caused a δ_w value that was 1.2‰ higher than present (Katz, et al., 2010). A shift to heavier isotopic values in marine records mainly reflects an increase in storage of $H_2{}^{16}O$, which implies a significant increase in volumes of continental land ice (Lowe & Walker, 1997).

The polar species *Neogloboquadrina pachyderma (s)* inhabit the subsurface ocean layers, and during reproduction it settles below the pycnocline (Simstich, et al., 2003). In these cold deep subsurface waters the N. pachyderma (s) wraps its initial test with a secondary crust made of calcite (Simstich, et al., 2003), which is in the upper 50 meter north of the Fram Strait (Bauch, et al., 1997). The isotopic signal which the foraminifera has accumulated throughout its life, reflects the whole depth range it inhabited (Simstich, et al., 2003), which is preserved in the sediment after its death.

3. 4. 8. 3 Carbon isotope

Carbon has two naturally occurring stable isotopes: ^{13}C and ^{12}C (Walther, 2009), which are incorporated into carbon dioxide (CO_2) molecules in the atmosphere due to oxidation (Lowe & Walker, 1997). CO_2 is exchanged between the atmosphere and the ocean (Smetacek, 1999), and is a part of photosynthesis, which lead to the surface waters to be enriched in ^{12}C than the deep waters. Foraminifera builds its test by extracting $CaCO_3$ from the sea water (Armstrong & Braiser, 2005). The carbon isotopic ratio $^{13}C/^{12}C$ is expressed as $\delta^{13}C$, and is a function of temperature and isotopic composition of the dissolved inorganic carbon (DIC) in seawater (Urey, 1947; Graham, et al., 1981; Gossman, 1987; McCorkle & Keigwin, 1990), and is generally reported relative to PDB (Peedee formation belemnite from South Carolina) (Walther, 2009). Broecker (1982) suggested that carbon isotopes could provide a proxy for changing CO_2 throughout the ice ages. They revealed that the $\delta^{13}C$ in benthic and planktonic foraminifera has varied throughout the last 130,000 years and can, together with the $\delta^{18}O$ record, show changes in ventilation of the ocean and past productivity. The $\delta^{13}C$-values in the upper water masses tends to be greatest during glacial phases and least during interglacial stages (Armstrong & Braiser, 2005), while the $^{13}C/^{12}C$ ratio in carbon dissolved in the deep ocean is lower during glaciations (Shackelton, 1977). Measurements of carbon isotopes from deep-sea sediments can be used to obtain the history of the mean ^{13}C content of dissolved CO_2 in the ocean (Shackleton, 1987), provide information on the history of the carbon cycle, paleoproductivity (Armstrong & Braiser, 2005) and deep water formation and ventilation of the ocean (Berger & Vincent, 1986). Analysis of δ13C in planktonic foraminifera can show prior changes in productivity in the upper layers of the oceans, also the fluctuation of ^{12}C in surface waters (Shackleton & Pisias, 1985).

Bacterial decay of organic matter beneath the sediment –water interface releases ^{12}C – enriched CO_2 back to the pore water (Armstrong & Braiser, 2005), which could influence the infaunal foraminifera taxa (McCorkle & Keigwin, 1990). Cassidulina neoteretis is reported to have a test 1.5‰ lighter than the equilibrium (Poole, 1994). Cassidulina neoteretis is an infaunal species, so the carbon isotopes composition can be affected by the oxidation of organic matter within the sediments which can be local (Poole, 1994)

3. 4. 8. 4 Stable isotope ($\delta^{18}O$ and $\delta^{13}C$) analyse

For the stable isotope analyses two species of foraminifera were used; the planktic foraminiferal species *N. pachyderma (s)* and the benthic foraminiferal species *Cassidulina neoteretis*. Approximately 30 specimens of *N. pachyderma (s)* and 30-50 of *C. neoteretis* were picked for the stable isotope analysis. The two species were picked in the size fraction ≥100 µm, and only undamaged foraminifera with no signs of contamination were collected. The samples were analysed at the Geological Mass Spectrometer Laboratory at the University of Bergen, using a ThermoFinnigan MAT253 IRMS mass spectrometer with a Kiel III device. The precision for $\delta^{18}O$ was ±0.06 ‰ and ± 0.03 ‰ for $\delta^{13}C$ (relative to the PDB standard).

For both core HH12-930 GC and for HH14-002 GC samples with sufficient number of specimens were analysed. For both cores all samples were carefully examined to look for *N. pachyderma (s)* and *C. neoteretis* in a microscope (Leica CLS 150X-$MZ12_5$).

3. 4. 9 Foraminifera distribution analysis

For foraminifera picking and counting from core HH14-002 GC the size fraction ≥100 µm was used. To pick and identified the foraminifera a binocular microscope (Leica CLS150X – MZ12s) was used. Each sample was evenly distributed over a picking tray with 45 identical squares, with a collecting tray placed underneath to retrieve the picked and counted foraminifera. The picking tray and collecting tray was cleaned after each sample. For the samples that were considered too large to fit the picking tray, a sampler splitter was used to split the sample evenly 50/50.

Since the samples contains both planktic and benthic foraminifera a minimum 300 specimens of each was picked, counted and identified to species level and percentages calculated. At least 300 specimens are required for statistical reliability (Knudsen, 1998). However, in some of the samples the amount of foraminifera were too low for quantification. Approximately 600 specimens of planktic and benthic foraminifera were counted and identified in a total of 64 samples. Samples containing less than 80 individuals, is considered to be uncertain, and thus not representative and will be removed from the results.

4. Foraminifera

Foraminifera are single celled organisms, that either live amongst the marine plankton or on the seafloor. Foraminifera can be found in mostly every marine environments; from fresh water to the deep sea, and from the tropical to the Arctic areas. They are adapted to tolerate different salinities and temperatures, and can be found in saltmarshes, shallow brackish water in estuaries, on the seafloor on the continental shelf or in the deep ocean (Armstrong & Braiser, 2005). Their tests are composed of either calcite, aragonite (secreted minerals), agglutinated or organic matter (tectin) (*Armstrong and Brasier, 2005*). Calcareous species are well preserved in most oceanic sediments, however, due to high levels of carbonate undersaturation of bottom waters, the carbonate tends to be dissolved at abyssal depths (Corliss, 1985). Because foraminifera are easy to study, abundant and diverse, they are an important for the study of the biostratigraphy and as well global correlation and, paleoenvironments and climatic reconstruction (Armstrong & Braiser, 2005).

4. 1 Dominating species

4. 1. 1 Planktic foraminifer

Planktic foraminifera lives in the surface layer of the open ocean. Controlling factors for the species relative abundance are salinity, temperature and seawater chemistry (Schiebel & Hemleben, 2005). The quantity of the species vary with season, water masses and water depth (Schiebel & Hemleben, 2005). The coiling direction of the species *Neogloboquadrina pachyderma* can be used as an indicator of sea-surface temperature (Ericson, 1959; Bandy, 1960). Additionally, the narrow temperature range of planktic foraminifera have become useful as a tool to reconstruct the paleotemperature, in particularly the sea surface temperature (Hutson, 1980; Pflaumann, et al., 1996; Waelbroeck, et al., 1998; Pflaumann, et al., 2003).

4. 1. 1. 1 Neogloboquadrina pachyderma (*Ehrenberg, 1861*)

The most abundant planktic species in both H14-002 GC is the left coiled *Neogloboquadrina pachyderma (sinistral).* This polar species makes an important proxy for determine temperature, salinity, sea ice and nutrient conditions in the past (Kohfeld & Fairbanks, 1996), and could reflect polar surface water and glacial conditions (Bauch, et al., 2001). It reflects /records ambient water properties at varying depths below the thermocline from ca. 25 m to 250 m water depth (Simstich, et al., 2003). *Neogloboquadrina pachyderma (sinistral)* is the dominant planktic species found in surface samples north of the Arctic Front in the Greenland, Iceland and Norwegian Sea (Pflaumann et al., 1996). In these areas it is most abundant in sea surface temperature (SST) <5°C and during summer <8°C (Pflaumann, et al., 1996). Moreover*, Neogloboquadrina pachyderma (sinistral)* could indicate temperatures below 5 – 6 °C (Jansen, et al., 1983).

4. 1. 2 Benthic foraminifera

Benthic foraminifera live either within the top 200 – 10 mm (infaunal) or on the seafloor (epifaunal). The abundance of the species are controlled by temperature, salinities (Mackensen, et al., 1985; Mackensen, et al., 1995) food supply and oxygen (Gooday, 1994; Gooday & Rathburn, 1999). Their tests are composed of different material, however, calcareous tests are the most abundant (Armstrong & Braiser, 2005). After death, they are incorporated in the sediment and therefor becomes a part of the geological record. The study of benthic foraminifera is an important tool in Quaternary stratigraphy and reconstruction of paleoenivronmetnal, palaeoceanography and paleoproductivity (Hald & Vorren, 1987; Gooday, 1994; Kaiho, 1994; Gooday & Rathburn, 1999; Sejrup, et al., 2004; Rasmussen, et al., 2007; Rasmussen & Thomsen, 2015).

4. 1. 2. 1 Cassidulina neoteretis (Seidenkrantz, 1995)

Cassidulina neoteretis is a shallow infaunal species (Mackensen & Hald, 1988; Wollenburg & Mackensen, 1998; Husum & Hald, 2004a), and lives in areas of fine grained, organic-rich, terrigenous mud (Mackensen, et al., 1985). It is found in arctic and Antarctic to subarctic water masses, and is mainly a deep-sea species (Seidenkrantz, 1995). It thrives in cold water conditions and can be an indicator of glaciomarine paleoenvironments (Mackensen & Hald, 1988), and high salinities, where it is rarely found at salinities <32‰ (Steinsund, et al., 1994). Recent distribution of *Cassidulina neoteretis* is restricted to areas influenced by chilled Atlantic water (Mackensen & Hald, 1988), commonly flowing as a subsurface current (cf. Jennings & Helgadottir, 1994). On the continental slope of the Norwegian slope, *Cassidulina neoteretis* dominates the benthic foraminifera assemblage where the bottom water has a temperature c. – 1°C and with salinities ~34.92‰ (Mackensen & Hald, 1988). *Cassidulina neoteretis* is frequently accompanied by high abundance of planktic foraminifera (Polyak & Mikhailov, 1996), and associated to phytoplankton blooms (Gooday & Lambshead, 1989) and to productive area (Mackensen, et al., 1985).

4. 1. 2. 2 Cassidulina reniforme (Nørvangi, 1945)

Cassidulina reniforme is the most common calcareous foraminifera on the Arctic shelves (Polyak, et al., 2002). It is an infaunal species, which occupy the upper few mm's of the sediment (Hald & Korsun, 1997), and requires a silty muddy substrate (Mackensen, et al., 1985) of Arctic waters at depth that is normally shallower than 100 meters (Mudie, et al., 1984). It prefers high salinity (Steinsund, et al., 1994) and low temperatures (<2°C) and seasonal sea-ice cover (Polyak, et al., 2002). *Cassidulina reniforme* is an opportunistic species, and frequently dominates foraminiferal assemblage in environments that are stressed/unstable (Osterman & Nelson, 1989). It is typical of areas with little or no influx of temperate water (Holtedahl & Bjerkli, 1982), and prefers cold Intermediate Waters (Hald & Korsun, 1997), such as the homohaline Greenland Sea Intermediate Water (Hald & Vorren, 1987). *Cassidulina reniforme* is frequent in glaciomarine environments (Sejrup, et al., 1981; Vilks, et al., 1989), with varying and/or reduced salinity (Hald & Vorren, 1987), and proximal

to the glaciers (Mackensen & Hald, 1988). Due to its small size, *Cassidulina reniforme* can be subject to redisposition in sandy muds downslope (Mudie, et al., 1984).

4. 1. 2. 3 Melonis barleeanum (Williamson, 1858)

Melonis barleeanum is an infaunal foraminifer (Jennings, et al., 2004) that lives in fine-grained sediments rich in organic matter, which can be an indicator of high surface productivity (Caralp, 1989). It is considered to be highly adaptable to change in food availability and/or altering environmental conditions, also it can adjust from infaunal to epifaunal if needed (Linke & Lutze, 1993). In the Barents Sea it appears to be restricted to the chilled Atlantic water, and prefer temperatures around 4°C (Hald & Steinsund, 1992), and is restricted to low salinity (Steinsund, et al., 1994). *Melonis barleeanum* is considered to indicate increased influx of chilled Atlantic – derived water to the Arctic Ocean (Polyak & Solheim, 1994; Polyak & Mikhailov, 1996), and can be an indicator of influx of organic matter to the sea floor (Jennings, et al., 2004). Some hypotheses relate *Melonis barleeanum* to bottom currents (Murray, 1984), and others linked it to high sedimentation rate (Mackensen, et al., 1985). Together with *Islandiella norcrossi* it indicates inflow of Atlantic Water that changed the bottom water conditions towards increased salinities and probably higher temperatures (Ślubowska, et al., 2005).

4. 1. 2. 4 Islandiella norcrossi (Cushman, 1933)

Islandiella norcrossi is an arctic species (Jennings, et al., 2004) found on the Arctic shelf and slope, and which thrives in cold water (Mudie, et al., 1984). It is a dominate species from 660 to 1200 meter in the Norwegian – Greenland Sea (Belanger & Streeter, 1980). It reflects increased flux of organic matter (Jennings, et al., 2004), increased productivity and presence of seasonal sea – ice cover (Steinsund, et al., 1994). It prefers relatively high and stable bottom water salinities (Korsun & Hald, 1998), and relatively low temperatures and not too reduced salinities (Steinsund, et al., 1994). It could be an indicator of increased inflow of Arctic Water (Wilson, et al., 2011). In the modern environment, *Islandiella norcrossi* is abundant in distal glaciomarine sediments with ice rafted debris and marine mud (Korsun & Hald, 1998). The species is observed in the Central Deep of the Barents Sea that is filled with

winter bottom water and characterized by relatively low sedimentation rates (Steinsund, et al., 1994).

4. 1. 2. 5 Elphidium excavatum forma (f) clavatum (Cushman, 1944)

Elphidium excavatum forma (f) clavatum is possibly the most important species in the Quaternary record of the Arctic shelf (Vilks, 1981). In the Barents Sea it is abundant in areas of sea – ice cover and/or influence of nearby glaciers, and is confined to Arctic Water with winter sea-ice cover (Steinsund, et al., 1994). It prefers reduced salinity (30-34‰), relatively low temperatures (<1°C) (Miller, et al., 1982; Steinsund, et al., 1994) and can be found in areas with high turbidity, like proximal to glaciers (Steinsund, et al., 1994). It is thought to be a glaciomarine indicator (Hald & Korsun, 1997; Korsun & Hald, 1998). The species is considered an opportunist, since it is found in areas with relatively low number of foraminifer's pr. gram sediment (Steinsund, et al., 1994). In the northern part of the Barents Sea it is abundant in cold bottom waters where the temperatures are lower than 2°C (Sejrup, et al., 2004).

4. 1. 2. 6 Stainforthia loeblichi (Feyling-Hanssen, 1954)

Stainforthia loeblichi is an infaunal species, which prefers fine-grained mud (Steinsund, et al., 1994). It is found in cold waters (~0°C), and areas covered by seasonal sea-ice (Steinsund, et al., 1994). This Arctic species is considered to be opportunistic and taking advantage of pulses of high productivity (Gustafsson & Nordberg, 2001).
Stainforthia loeblichi has a similar distribution pattern of N. labradorica (see 4. 1. 2. 8) (Polyak, et al., 2002).

4. 1. 2. 7 Cibicides lobatulus (Walker & Jacob, 1798)

Cibicides lobatulus is an epifaunal species, which is found attached to exposed solid surface like rocks and algae, and prefers salinities >32‰ (Steinsund, et al., 1994). It is associated

with strong bottom current (Hald & Vorren, 1984; Husum & Hald, 2004b), which prevents sedimentation of fine grained material (Klitgaard Kristensen & Sejrup, 1996), and is also related to warm, saline Atlantic Water (Mackensen, et al., 1985).

4. 1. 2. 8 Nonionellina labradorica (Dawson, 1860)

Nonionellina labradorica is a deep infaunal species associated with buried organic matter (Corliss, 1991; Hunt & Corliss, 1993). It prefers slightly sandy sediments, low temperatures (<1°C) and reduced salinities (33-34‰) (Steinsund, et al., 1994). It is found in glaciomarine environments distal to glaciers (Korsun & Hald, 2000), but also in deep basins with relatively warm bottom water and low oxygen (Mudie & Aksu, 1984; Williamson, et al., 1984). This Arctic species has its maximum concentration along the oceanic polar front (Steinsund, et al., 1994), and is associated to Atlantic Water in arctic fjords (Hald & Korsun, 1997). It is also found on the slopes of banks in areas with high organic production (Steinsund, et al., 1994). Near the surface sediment, *Nonionellina labradorica* feeds on fresh phytodetritus (Jennings, et al., 2004), and may reflect increased nutrient supply (Korsun & Hald, 1998).
(Hald & Steinsund, 1992)

4. 1. 2. 9 Oridorsalis umbonatus (Reuss, 1851)

Oridorsalis umbonatus occupies the uppermost centimeter (0 – 4 cm) of the sediment (Rathbum & Corliss, 1994; Schmiedl, et al., 1997). It is can occur as an epifaunal and infaunal species (Rathbum & Corliss, 1994), and prefers temperatures below ~4°C (Rathmann & Kuhnert, 2008). It is common up to 1200 meter in recent sediments (Jansen, et al., 1983), and as well a common deep – sea benthic foraminifera in the present Norwegian/Greenland Sea and Arctic Ocean (Belanger & Streeter, 1980; Sejrup, et al., 1981). The species can tolerate low food supplies and prefers well – oxygenated pore waters (Mackensen, et al., 1985). It has been reported to dominate periods with an ice-covered sea surface (Jansen, et al., 1983). It correlate with low organic carbon content (Mackensen, et al., 1985), and can be adapted to conditions with reduced surface productivity (Jansen, et al., 1983).

4. 2 Sub – dominating species

4. 2. 1 Planktic species

4. 2. 1. 1 Neogloboquadrina pachyderma (Ehrenberg, 1861)

*Neogloboquadrina pachyderma (dextra*l) is a planktonic foraminifera that resemble the sinistral *Neogloboquadrina pachyderma*, but preferable coils its test dextral. It has been suggested that the coiling direction is a genetic trait, and that *Neogloboquadrina pachyderma (dextral)* and *Neogloboquadrina pachyderma (sinistral)* should be considered two different species (Darling, et al., 2006). Darling et al (2006) propose a new name for the *dextral Neogloboquadrina pachyderma* to be *N. incompta.* It is a temperate species that prefers temperatures around 12°C (Schmidt, et al., 2004).

4. 2. 1. 2 Globigerinita glutinata (Egger, 1893)

Globigerinita glutinata is a near-surface dwelling species (Shackleton & Vincent, 1978) which is found near areas of upwelling and in transitional waters (Bé & Tolderlund, 1971).

4. 2. 1. 3 Turborotalita quinqueloba (Natland, 1938)

Turborotalita quinqueloba is a subpolar species (Bauch, 1994), which indicates the advance of the Arctic Front (dividing the Arctic and Atlantic waters), or Polar Front (dividing polar and Arctic waters) (Johannessen, et al., 1994). Recent, it is found as far north as in the Nansen Basin, where is lives in the upper 500 of the water column and occupies the deeper layers of the Atlantic Intermediate Water (Carsten & Wefer, 1992).

4. 2. 2 Benthic species

4. 2. 2. 1 Epistominella exigua (Brady, 1884)

Epistominella exigua is a benthic foraminifera with calcareous tests. The benthic specie is considered an opportunist and is adapted to pulsed nutrient supply, and is relatively abundant in the Northeast Atlantic (Gooday, 1993). It correlates with high seasonal primary production (Sun, et al., 2006), and is largely controlled by the presence of organic material on the seafloor.

4. 2. 2. 2 Triloculina tricarinata (d'Orbigny, 1826)

Triloculina tricarinata is a benthic foraminifera. This miliolid species is found in fine sandy mud (Wang & Chappell, 2001), and in depth below 2400 meter in the central North Atlantic (Hermelin & Scott, 1985).

4. 2. 2. 3 Quinqueloculina lamarckiana (d'Orbigny, 1839)

Quinqueloculina lamarckiana is a deep – water species (Cann, et al., 2000). The species is found at approximately 300 m to 1000 m depth, and prefers temperatures around 3.9°C to 6.7°C, and salinities ranging from 34.3 ‰ to 34.5‰ (Bandy & Arnal, 1957).

4. 2. 2. 4 Buccella spp.

This group prefers temperatures around 0 – 1 °C and salinities from 33 ‰ to 34 ‰, and is frequent around areas with seasonally sea ice formation (Steinsund, et al., 1994).

4. 2. 2. 5 Pyrgo williamsoni (Silvestri, 1923)

Pyrgo williamsoni is a benthic foraminifera with porcelacous test, which requires a full marine environment to thrive (Schoning, 2002). It is an epifaunal species and is found in the deep – sea areas in the Norwegian Sea (Corliss & Chen, 1988)

In addition, five other species were identified, but due to the relatively low abundance per samples in the sediments core, they will not be included in the results. These species includes Buccella frigida (Cushman, 1921), Lagena elongata (Dunikowski, 1879), Elphidium spp, Pullenia bulloides (d'Orbigny, 1846) and Stainforthia spp.

5. Results

The most important results from HH14-002 GC and HH12-930 GC will be presented and described in this chapter. The two sediment cores are divided into lithological units (14 – 1 to 14 – 6 for HH14 – 002 GC, and 12 -1 to 12 – 6 for HH12 – 930 GC), based on x – ray photography, grain size distribution, and variation in magnetic susceptibility (Figure 15 to 18 and figure 22 to 25).

In chapter 5. 1. 7 the results from the stable isotope analysis in HH14 – 002 GC will be presented, and divided into the same units as the lithological units (14 – 1 to 14 – 6).

The results from the foraminiferal distribution pattern in core HH14 – 002 GC will be presented in chapter 5. 1. 8, where the foraminiferal units are defined.

5. 1 HH14-002 GC

Core HH14 – 002 GC has been described by visual inspection and measured for magnetic susceptibility (Figure 17) and x-ray photography (Figure 18) and color photography (Figure 15). Based on these data a lithological log has been made (Figure 17 and 18). Data of percent grain size distribution and concentration of clasts over 0.5 mm (Figure 18) will presented with the color photography and the lithology. Foraminifera distribution pattern are resented in 5. 1. 7. Fine-grained sediments dominate the lithology, with abundance of coarser material, most likely ice rafted debris. The color of the sediments throughout the core varies (See figure 17 and figure 18). By studying the x-rays photography of core HH14-002 GC it is possible to detect subsurface features as clasts, laminations/layering and shells. Three intervals with relatively high amount of IRD occurs in the core. The values of the magnetic susceptibility vary throughout the core, where the highest values are 48 (10-5) SI, and the lowest values are c. 10 (10-5) SI.

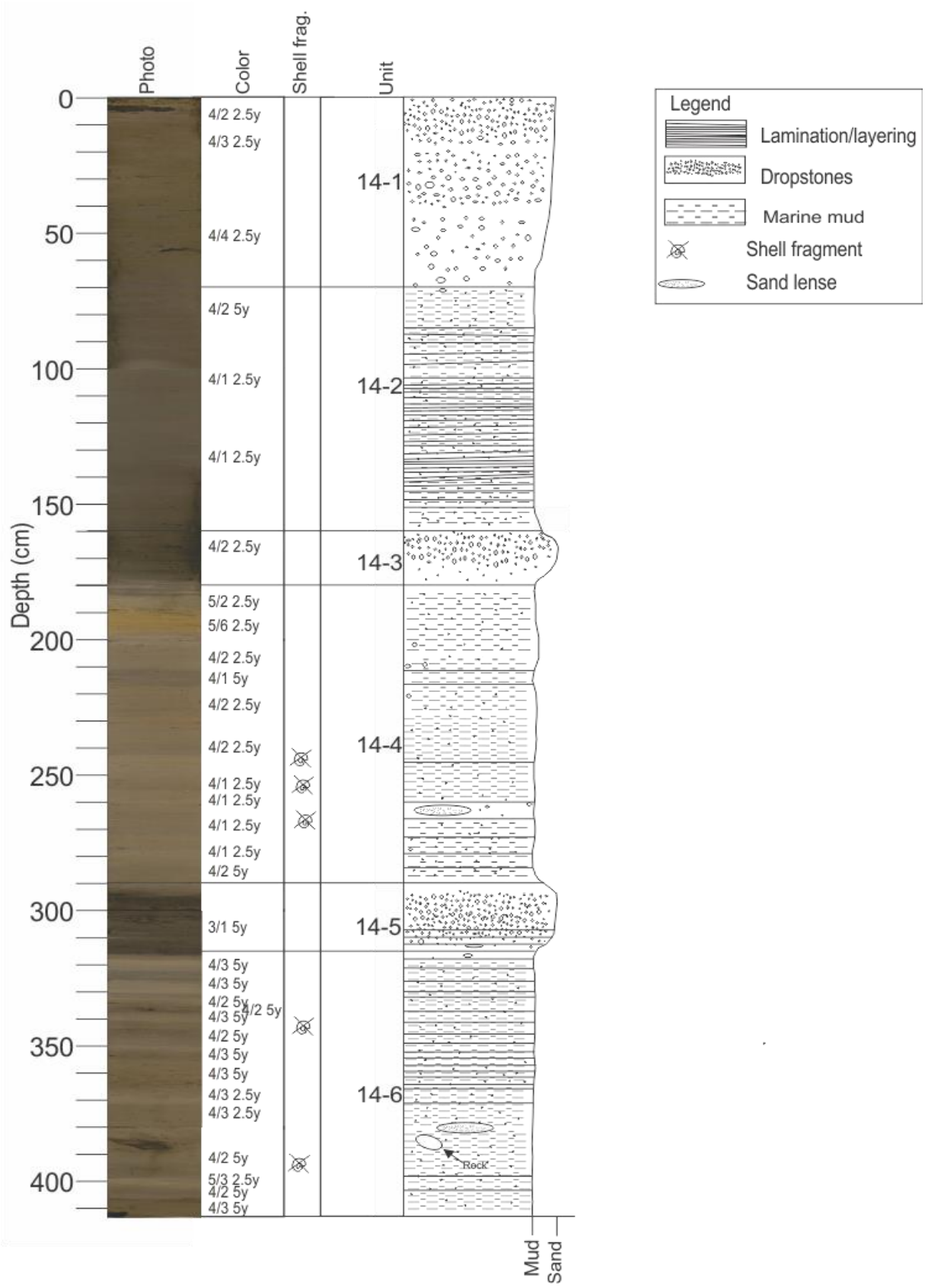

Figure 17: The figure shows core image and a lithological log of the core, together with the different units plotted against depth (cm). The color of the sediments are indicated. The position where shell fragments were observed is also indicated.

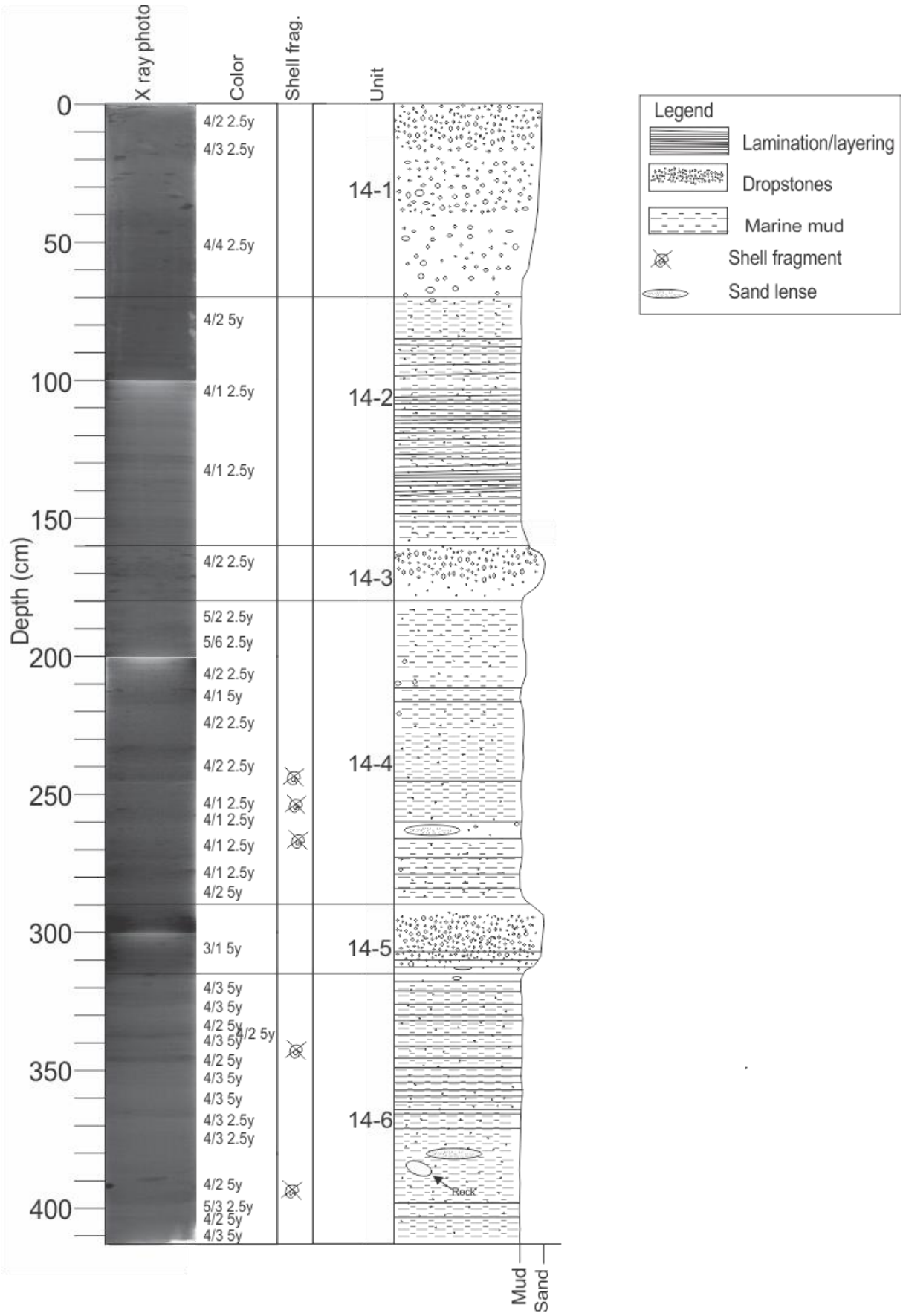

Figure 18: X – ray photograph, lithological log, color of the sediments and the six different units plotted against depth (cm). Clasts and layers with higher density is appears as darker. In the lower part of the core a clast were observed. It is not so visible on the x – ray photograph. This could be due to the position of the core when the x – ray photograph was taken.

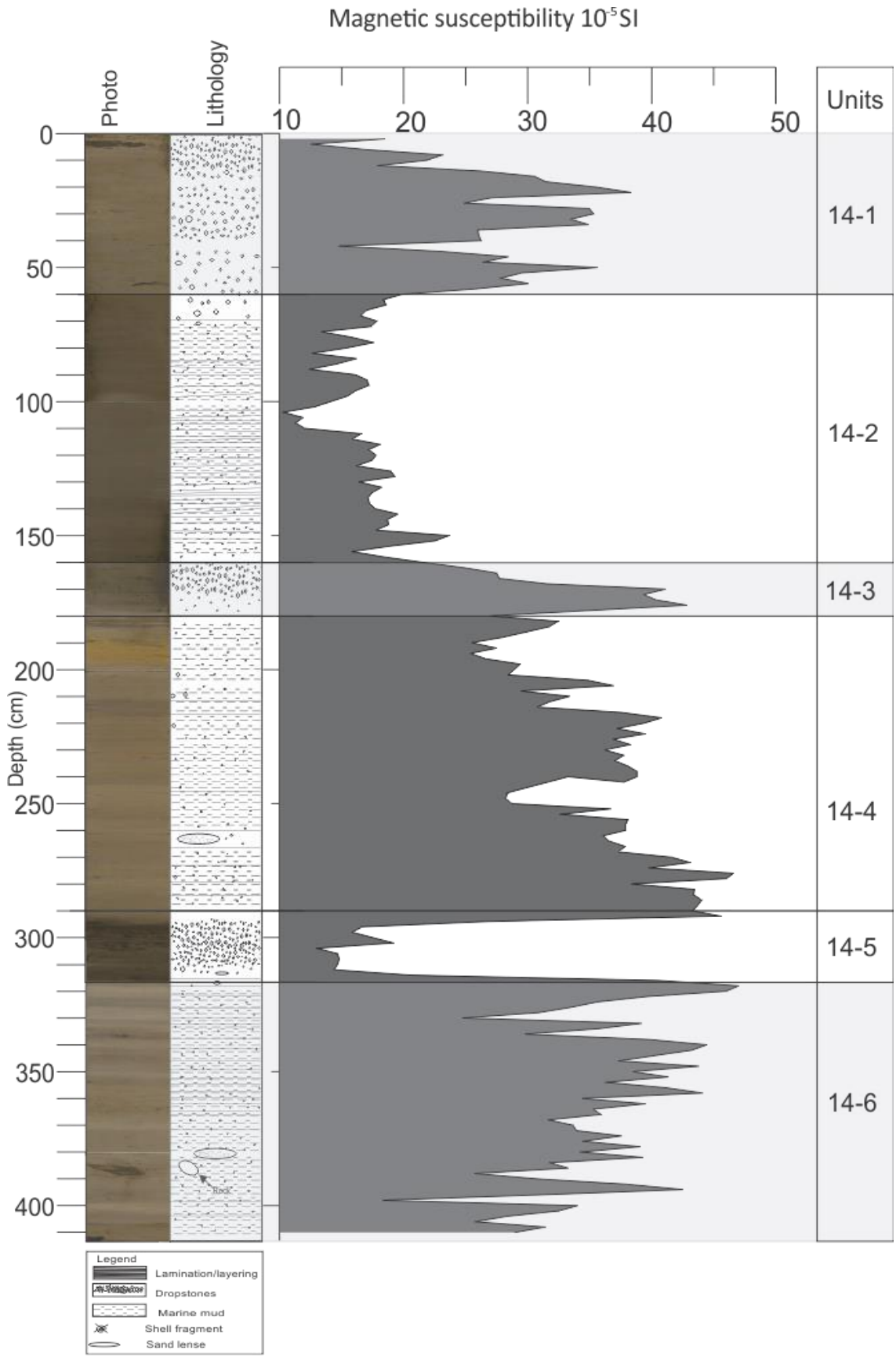

Figure 19: The photo of the core together with the magnetic susceptibility. The lithology of the core is also indicated, but simplified.

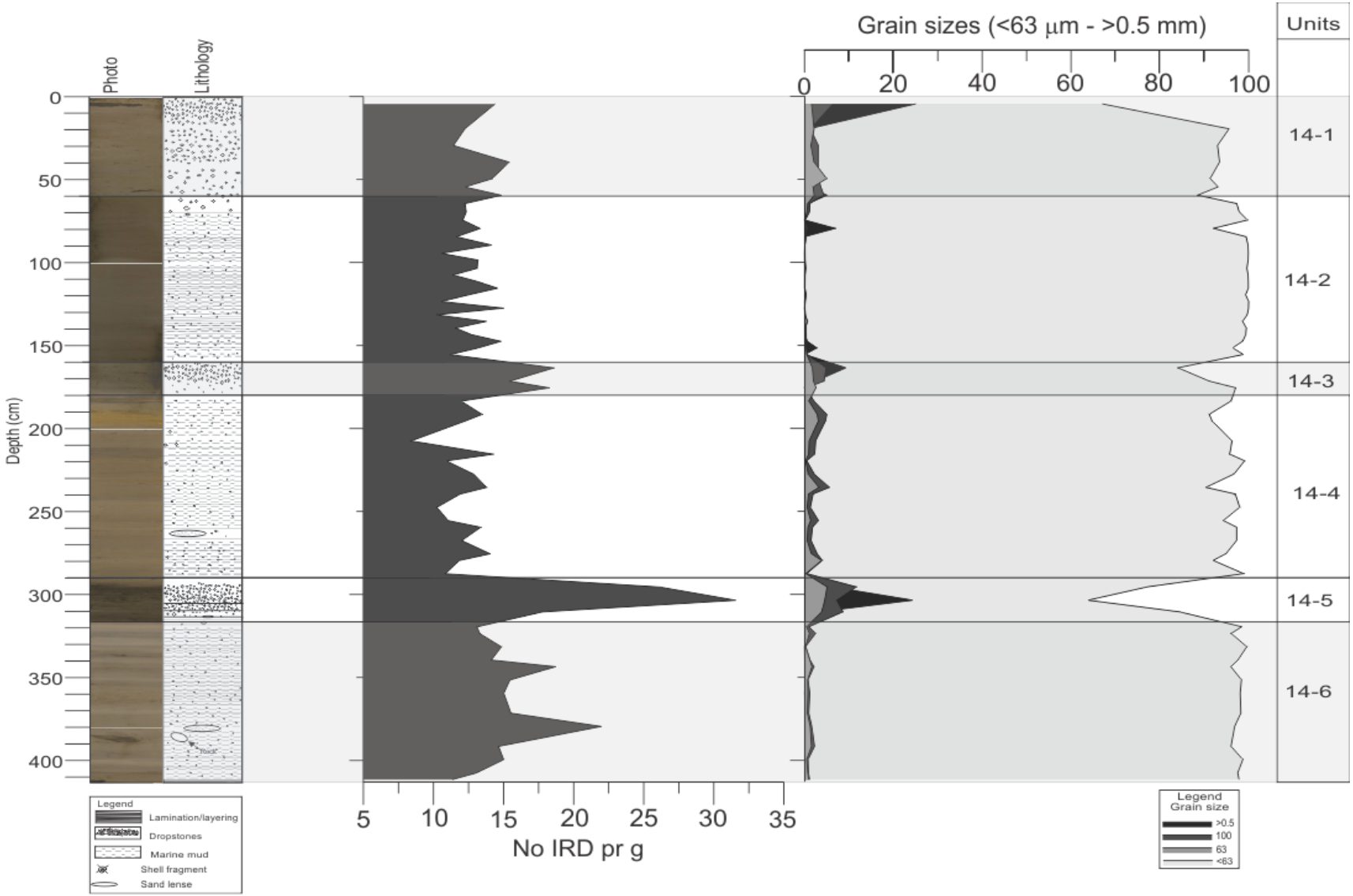

Figure 20: The lithology and photography of the core, together with number of IRD per gram and the grain sizes. The different units are indicated.

5. 1. 1 Unit 14 – 1:

The uppermost unit (14 – 1) (0 – 70 cm down – core) is rather massive in the upper 35 cm and consist of dropstones (Figure 20). Mud is dominant in this unit (68 – 99 %) with sand (5 – 15 %), where the amount of dropstones decreases with depth, and layering increases. The dropstones are visible on the x – ray photograph (Figure 18), and so are the layering in the lowermost part of the unit. From 0 cm – 8 cm the color of the sediment is dark greyish brown (4/2 2.5y), and from 8 cm – 70 cm the color is olive brown (4/3 2.5y) (Figure 17). The magnetic susceptibility varies, but is moderately high (Figure 19).

5. 1. 2 Unit 14 – 2:

Unit 14 – 2 (70 – 160 cm) is relatively homogenous; it contains relatively little dropstones, except in the upper and lower part. In this interval laminated is found, which is clearly visible on the x – ray photography (Figure 18). The unit consist of relatively high amounts of mud (92 – 100 %), and little sand (4 %). The color at the upper part of this unit is olive grey (4/2 5y) and shifts to dark grey (4/1 2.5y) at the lower part (Figure 17). The magnetic susceptibility decreases, and stays low throughout the unit (Figure 19).

5. 1. 3 Unit 14 – 3:

In unit 14 - 3 (160 – 180 cm) there is a drop in the mud-content (from c. 98 to 84 %), and both the concentration of sand and dropstones increases (Figure 20). On the x – ray photography the dropstones are highly visible (Figure 17). The color is uniform; dark greyish brown (4/2 2.5y) (Figure 17). The magnetic susceptibility – values starts to increase at 160cm, and then drops at approximately 180 cm (Figure 19).

5. 1. 4 Unit 14 – 4:

Unit 14 - 4 (180 – 290 cm) contains relatively little dropstones (Figure 20), however, some dropstones can be observed on the x – ray photography (Figure 16), together with layering throughout the whole unit. The unit consist of high amounts of mud (85 – 98 %), with varied concentrations of sand (2 – 10 %) (Figure 20). From 240 cm to 270 cm shell fragments were observed visually. The color in this unit varies (Figure 17 and 18). From 180 cm the magnetic

susceptibility – values increase, and shows several episodes of high and low values (Figure 19). At the transition to unit 5 at 290 cm the values decreases rapidly (Figure 19).

5. 1. 5 Unit 14 – 5:

Unit 14 – 5 (290 – 315 cm) contains high amounts of dropstones, which is visible on the x – ray photography (Figure 18). At this relatively short unit (280 – 312 cm) there is a drop in the mud concentration (to c. 65 %), and an increase in sand (30 %) (Figure 20). The color of this unit is very dark grey (3/4 5y) (Figure 17 and 18), and clearly visible on the x – ray photography as a relatively darker part of the core, which could imply higher density (Figure 18). At 290 cm the magnetic susceptibility – values drop from 45 (10-5) SI to 17 (10-5) SI, and continues to drop for c. 20 cm (Figure 19).

5. 1. 6 Unit 14 – 6:

The lowermost unit 14 – 6 (312 – 413 cm), contains some dropstones and a clast at ca 385 cm (Figure 17 and 18), which can be observed on the x – ray photography in the upper part of the unit (Figure 19). The unit has a relatively high concentration of mud (95 – 98 %) (Figure 20). Above the clast at 385 cm a sand lenses was observed. The amount of sand drops as well (<7 %). Layering in the upper and in the lower part can be observed on the x – ray photography (Figure 18). The middle part is somewhat massive. In the upper and lower part of this unit, shell fragments were visually observed. The upper part of this unit is dominated by olive (4/3 5y) - olive grey (4/2 5y) sediments, which shifts to olive brown (4/3 5 y) at 372 cm (Figure 18). From 372 cm the color of the sediments are olive grey (4/2 5y), and then changes to light olive brown (5/3 2.5y) at 398 cm (Figure 18). Toward the bottom of the core the color shifts from olive grey (4/2 5y) to olive (4/3 5y) (Figure 18). In the upper part of the unit the magnetic susceptibility – values increases, and reaches the highest values (47 (10-5) SI) throughout the core at 319 cm (Figure 19). From 319 to 330 the values decreases more or less gradually.

5. 1. 7 Foraminiferal assemblage units in HH14 – 002 GC

In the 64 (>100 µm size - fraction) samples that were analyzed, 28 different foraminifera species were identified. The planktic foraminifera (Figure 21) and the nine most dominate benthic species will be presented (Figure 22), together with the planktic, benthic flux and concentration (Figure 21 and 22, respectively). The five sub – dominated species will be presented (Figure 23), but nearly discussed later. The species that dominates the different units will be emphasized. In all of the units the planktic assemblages are dominated by *Neogloboquadrina pachyderma (s)*, while the benthic faunas are dominated by *Cassidulina neoteretis*, and other. The result from the foraminifera distribution analysis is divided into six different faunal units (14 – A to 14 – F), which are close to the boundaries of the lithological units (unit 14 – 1 to 14 – 6), and will be presented from the bottom of the core (412 cm) to the top (0 cm).

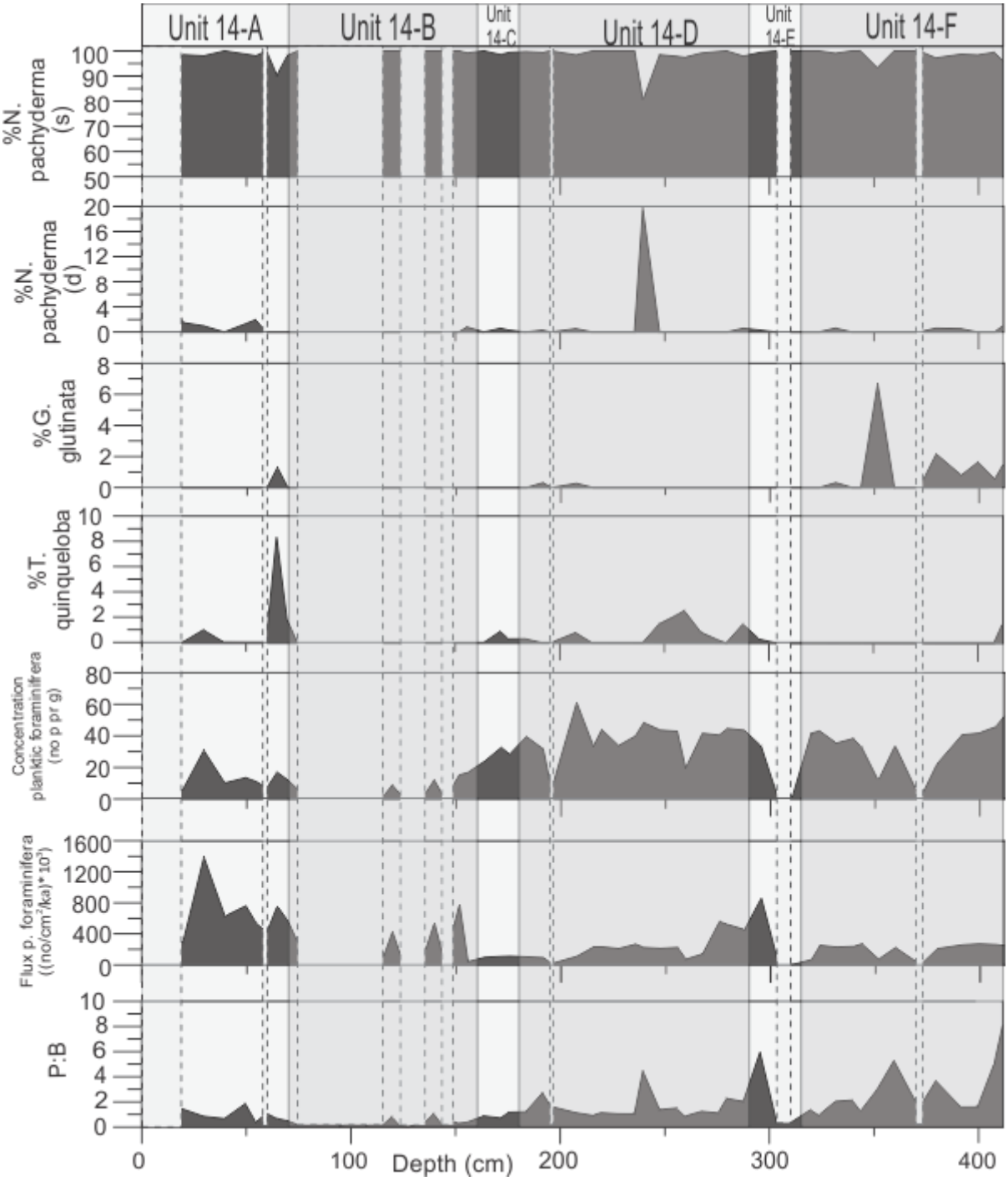

*Figure 21: Distribution (%) of the planktic species plotted against depth (cm), together with the planktic flux of foraminifera ((number of planktic foraminifera/cm²/ka)*10³), concentration of planktic foraminifer and P:B ratio. The different faunal units are indicated on the figure. The dashed lines indicates samples in the core which contains less than 80 foraminifera, and is there for considered as a non – representative sample.*

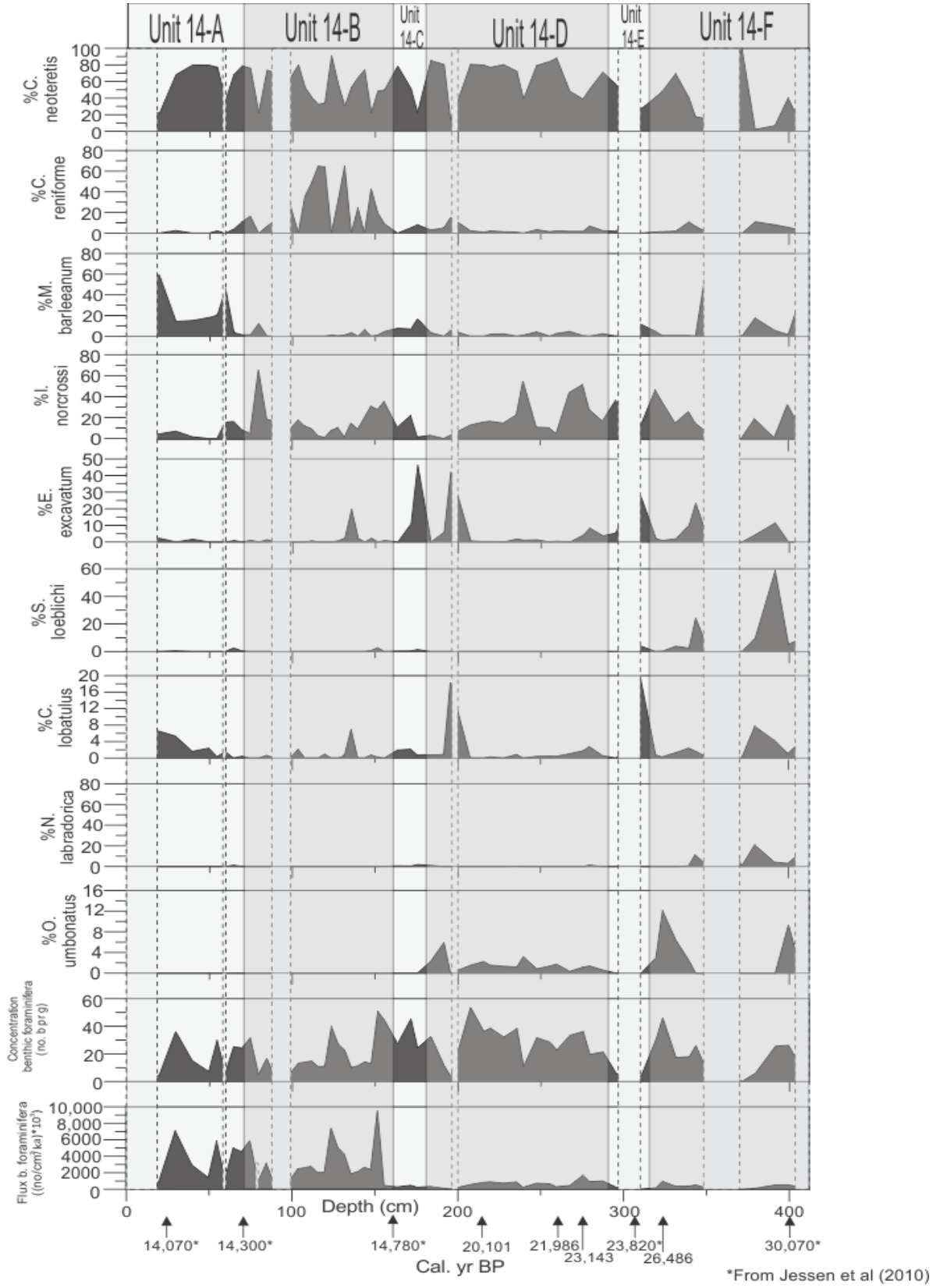

*Figure 22: Distribution (%) of the dominating benthic species, together with the flux of benthic foraminifera ((number of benthic foraminifera/cm²/ka)*10³), and the concentration of benthic foraminifera plotted against depth (cm). The different faunal units are indicated on the figure. The dashed lines indicates samples in the core which contains less than 80 foraminifera, and is there for considered as a non - representative sample.*

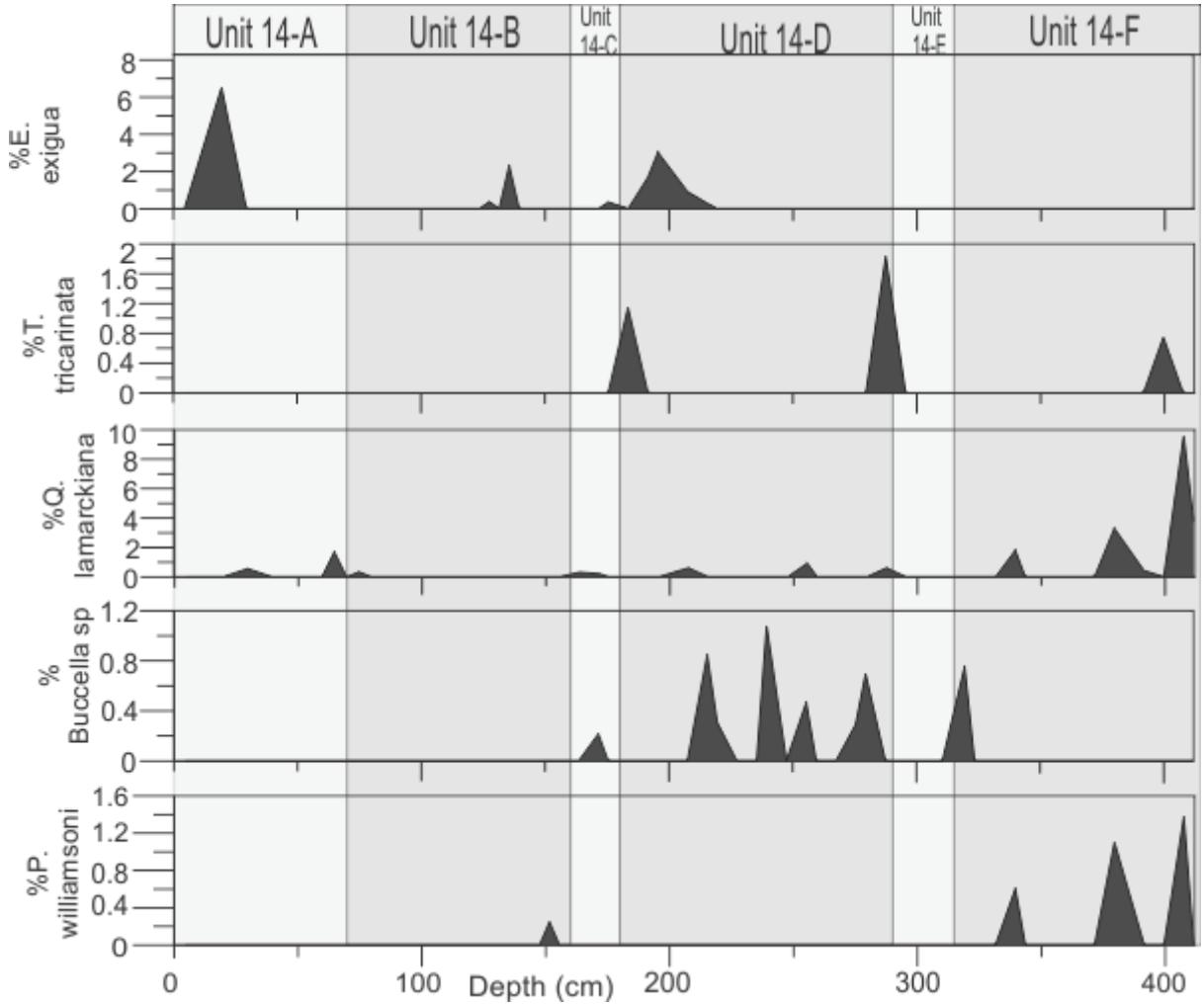

Figure 23: The sub – dominating species constitute for an insignificant part of the total fauna. The different units are indicated.

Unit 14 – F (412 – 318 cm)

The dominant planktic species in the lowermost unit (14 – F) is dominated by *Neogloboquadrina pachyderma (s)* (Figure 21). This planktic species constitutes between 98 % and 80% of the planktic fauna. *Cassidulina neoteretis* accounts for between 100 % and 2 % of the total benthic assemblage in this unit (Figure 22), and is clearly the dominating benthic species. In addition, other species that peak in this zone is *Melonis barleeanum*, *Islandiella norcrossi*, *Elphidium excavatum f. clavatum* and *Stainforthia loeblichi* (Figure 22). The diversity of the arctic species *Cassidulina reniforme* remain low, but stable throughout this unit. Other species that has minor peaks in this zone is *Nonionellina labradorica*, *Oridorsalis umbonatus* and *Cibicides lobatulus*. The benthic flux of foraminifera is low (Figure 22). The planktic flux is moderate, and the P:B ratio is relatively high (Figure 21).

Unit 14 – E (315 – 290 cm)

In the relatively short unit 14 – E there is a decrease in the planktic and benthic flux (Figure 21 and 22, respectively). The benthic assemblage is dominated by *Cassidulina reniforme*, *Melonis barleeanum*, *Islandiella norcrossi* and *Elphidium excavatum f. clavatum* (Figure 22). The percent of *Cassidulina neoteretis* decreases. The benthic flux decreases (Figure 22). The amount of benthic species decreases at the end when the planktic species *Neogloboquadrina pachyderma (s)* and the planktic flux and P:B ratio increases (Figure 21).

Unit 14 – D (290 – 180 cm)

In in this unit *Neogloboquadrina pachyderma (s)* dominates the planktic fauna (Figure 21). The planktic flux and P:B ratio decreases at the after 290 cm (Figure 21). At 245 cm *Neogloboquadrina pachyderma (s)* decreases, and the subpolar species *Neogloboquadrina pachyderma (d)* dominates 20 % of the planktic fauna (Figure 21). *Cassidulina neoteretis* dominates benthic fauna (Figure 22). Other species that inhabits the benthic fauna, especially in the beginning, is Islandiella norcrossi (up to 60 %) and *E. excavatum f. clavatum* together with Cibicides lobatulus (Figure 22). The diversity of *Cassidulina reniforme* and *Melonis barleeanum* stays low, but stable throughout the unit (Figure 22).

Unit 14 – C (180 – 160 cm)

Neogloboquadrina pachyderma (s) dominates the planktic fauna (Figure 21). Both the planktic and benthic fluxes decreases, and the P:B ratio is moderate (Figure 21 and 22, respectively). *Elphidium excavatum* f. *clavatum* reaches its highest value, and occupies 50 % of the fauna at the beginning of this unit (Figure 21). *Cassidulina neoteretis* increases when *Elphidium excavatum* f. *clavatum* decreases (Figure 22). Other species that occupies the assemblage is *Islandiella norcrossi* and *Melonis barleeanum* (Figure 22). *Cibicides lobatulus* and *Nonionellina labradorica* have stays relatively low in this unit, but remains stable throughout the unit.

Unit 14 – B (160 – 70 cm)

The planktic flux decline (Figure 21), while the benthic increases, but are varying (Figure 22). The P:B ratio is at its lowest in this unit (Figure 21). *Neogloboquadrina pachyderma (s)* is the dominating planktic species (Figure 21). The abundance of *Cassidulina neoteretis* varies (Figure 22). There is an increase in *Cassidulina reniforme*, which dominates up to 60 % of the benthic fauna (Figure 22). Towards the upper and lower part the diversity of *Cassidulina*

reniforme decreases, and Islandiella norcrossi increases. *Cassidulina reniforme* has a peak at the beginning of the unit, together with *Cibicides lobatulus*.

Unit 14 – A (70 – 0 cm)

The flux of planktic and benthic foraminifera increases in the middle of the unit (Figure 21 and 22, respectively), and decreases towards the uppermost part of the core. The P:B ratio is moderate (Figure 21). *Neogloboquadrina pachyderma (s)* is the dominating planktic species (Figure 21). *Cassidulina neoteretis* dominates the benthic, but decreases after 20 cm (Figure 22). *Melonis barleeanum* increases towards the top of the core (Figure 22). *Islandiella norcrossi* increases at the beginning and at the middle part of the unit. There is a small increase of *Cibicides lobatulus* at the top of the core.

5. 1. 8 Stable isotope analysis

The stable isotope analysis consist of together four results; two $\delta^{18}C$ and two $\delta^{13}C$ (Figure 24). The measurements from *N. pachyderma (s)* will be referred as planktic, and measurements from *C. neoteretis* as benthic. The uppermost part of the measurements are missing due to no or too little material in the samples. The stable isotope results are divided into the same units as the lithological units (Figure 17, 18, 19 and 20).

The measurements of the stable isotopes in unit 14 – 1 starts at 19 cm (planktic) and 29 cm (benthic) (Figure 24). From the start point to approximately 60 cm the oxygen values stays moderate (4.2 – 3.9 ‰ and 5. 2 – 5 ‰). The carbon isotope fluctuates a bit at this interval; the planktic values for varies from c. -0.18 ‰ to 0.15‰, while the benthic values goes from 0.2 ‰ to 0.38 ‰.

At unit 14 – 2 (Figure 24) the oxygen isotopes values for benthic stays relatively high from 70 cm to 160 cm, and moderate for the planktic in the same interval. For the carbon isotopes there is a slightly drop (from 0.38 ‰ to -0.1 ‰) in the benthic from 70 cm to 135 cm, and increases from 135 cm to 160 cm, while the planktic remains negative from 80 cm to 160 cm, except from a minor increase with values just over 0 ‰.

In unit 14 – 3 1(160 cm to 180 cm) (Figure 24) the stable isotopes values of both planktic and benthic makes a drop towards negative values.

In unit 14 – 4 (180 cm to 290 cm) (Figure 24) both the benthic and planktic oxygen isotopes values increases for. For the planktic the values fluctuates from 4.75 ‰ to 4.48 ‰, while the values for benthic varies from 5.57 ‰ to 5.38 ‰. For the carbon isotope the benthic values decreases after 180, and then increases after 200 cm where the values varies between (-1.2 ‰ to -0.6 ‰). The planktic carbon isotope increases after 180cm and stays relatively high until a decrease towards unit 14 – 5.

In unit 14- 5 (290 cm – 315 cm) both the planktic and benthic oxygen and the carbon isotope values decreases (Figure 24).

Towards unit 14 – 6 (Figure 24) the planktic and benthic carbon isotope increases, until 295 cm where the planktic values decreases. The planktic oxygen isotope values oscillates and varies between 4.6 ‰ to 3.6 ‰, whereas the benthic oxygen isotope decreases from 5.4 ‰ to 4.7 ‰ towards the bottom of the core.

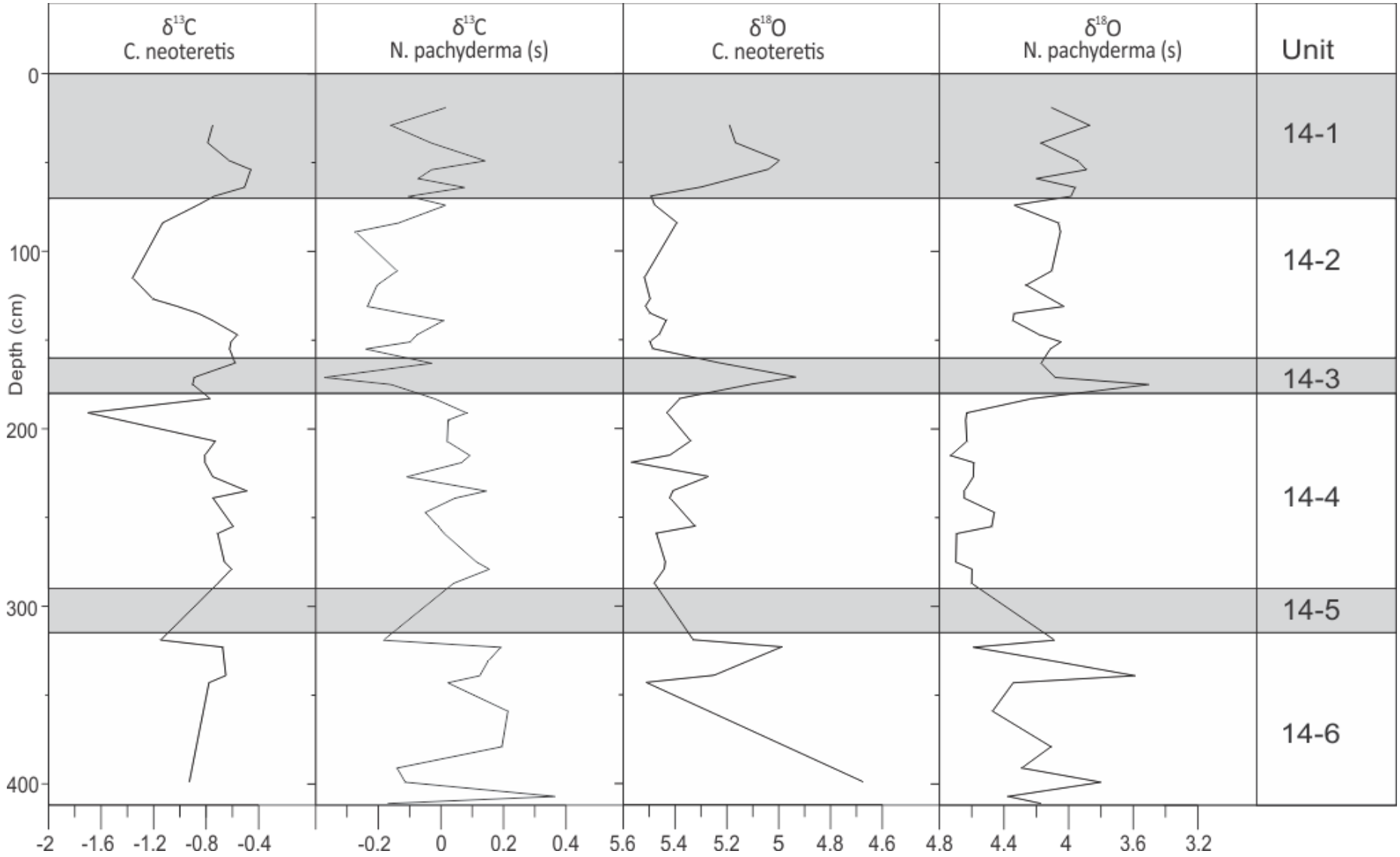

Figure 24: The benthic (C. neoteretis) and planktic (N. pachyderma (s)) carbon and oxygen isotope record plotted against depth (cm), and divided into units. The values of the benthic and planktic oxygen isotope is presented as reverse.

5. 2 HH12-930 GC

Sediment core HH12-930 GC was retrieved from within a pockmark, Vestnesa Ridge. The core has been visually studied to determine the color of the sediments using a "Munsell soil color charts" (Figure 25 and 26). It was taken x – ray photo (Figure 26) and a color photography (Figure 25) of the core, and measured for magnetic susceptibility every 2 cm (Figure 27). Grain size distribution were carried out for every 5 cm, same with counting clasts <0.5 mm (Figure 28) and stable isotope analysis, which will be presented in chapter 5. 2. 7. The lithology is presented in a lithological log (Figure 25 and 27), and is mainly the same as in HH14 – 002 GC; fine grained sediments, with coarser material, however, in this core a layer containing high abundance of shell was observed. The shell layer can be observed on the x – ray photography as white due to lower density compared to clasts, which appears as darker. Clasts appears frequently in the upper 170 cm of the core, and less frequently in the middle and lower part. The core contains as well layer of varying colors, especially in the lower part of the core, which is visible on the color photography, and can be studied on the x – ray photography due to density differences. The magnetic susceptibility flocculates throughout the core, where the peaks could be linked interglacial periods (Rasmussen, et al., 1996a). Throughout the core the magnetic susceptibility is low compared to HH14 – 002 GC, except from the upper part of the core (0 – 50 cm). The magnetic susceptibility has somewhat similar pattern to the magnetic susceptibility from HH14 – 002 GC, and parts of the core can possibly be correlated to Jessen et al (2010). Most of the parts of the magnetic susceptibility seems to be disturbed for unknown reasons. The core was divided into together six units, where the upper unit is named 12 – 1 and the lowermost unit 12 – 6. The units are based on lithological differences, which could reflect different sedimentological environment. The six units will be presented separately, where the lithology, x – ray photography, color and the magnetic susceptibility will be described.

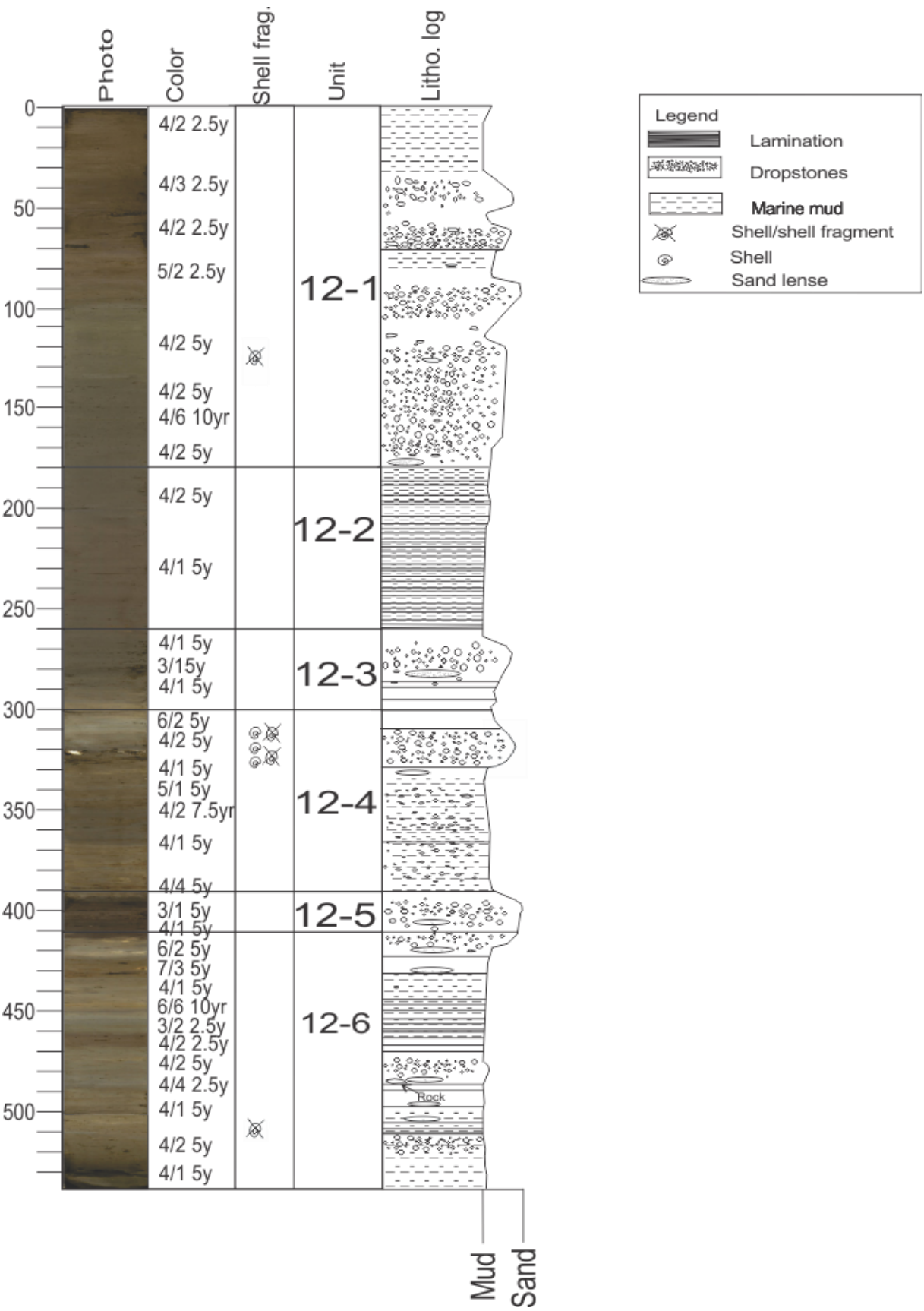

Figure 25: The figure shows the image of the core HH12-930 GC with the lithological log and the six different units. The color of the sediments are indicated. This core contained whole shells and shell fragments.

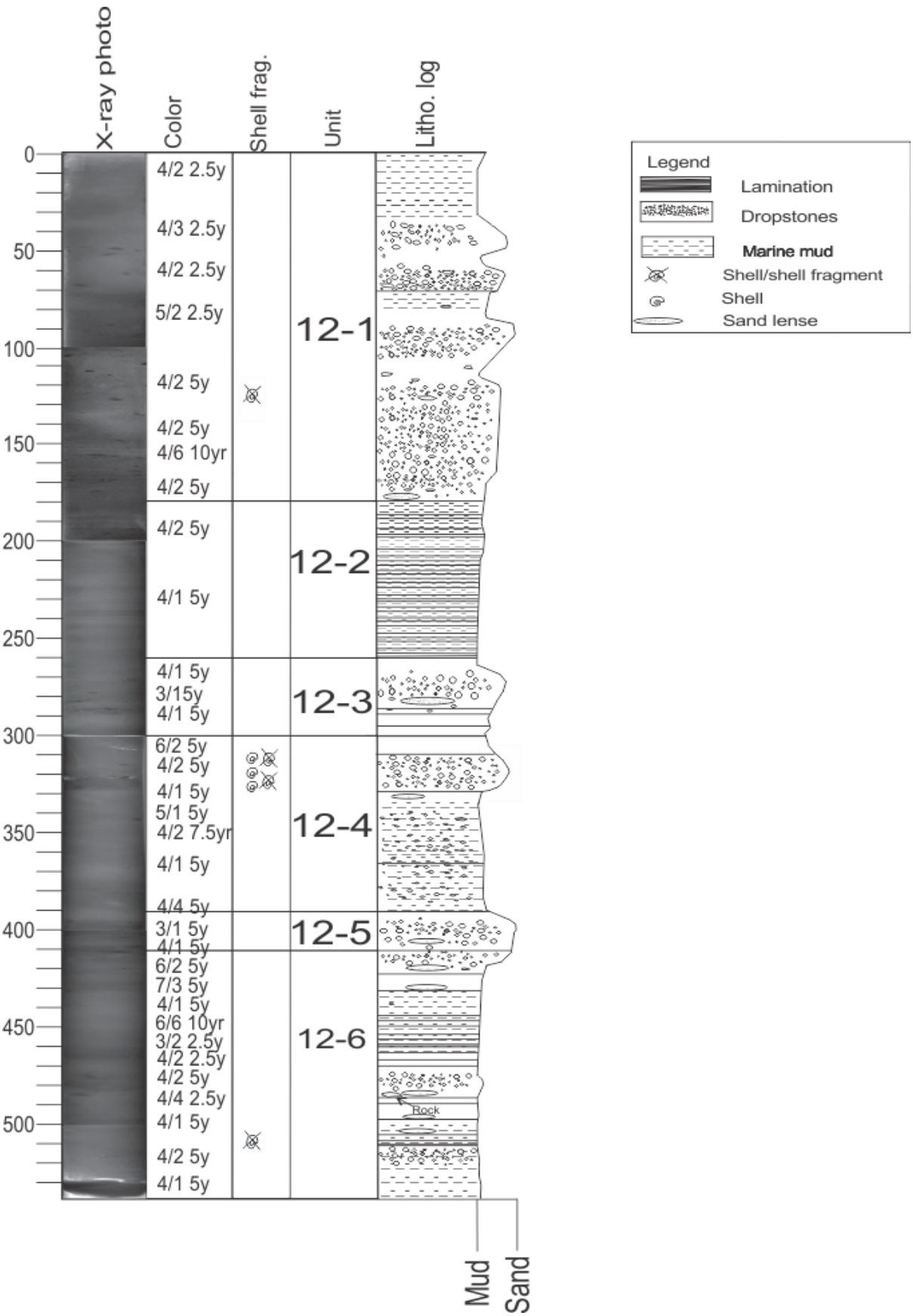

Figure 26: X – ray photo, lithological log, color of the sediments and the six different units found in HH12-930 GC plotted against depth (cm). Clasts and layers with higher density is appears as darker, while the shells is whiter.

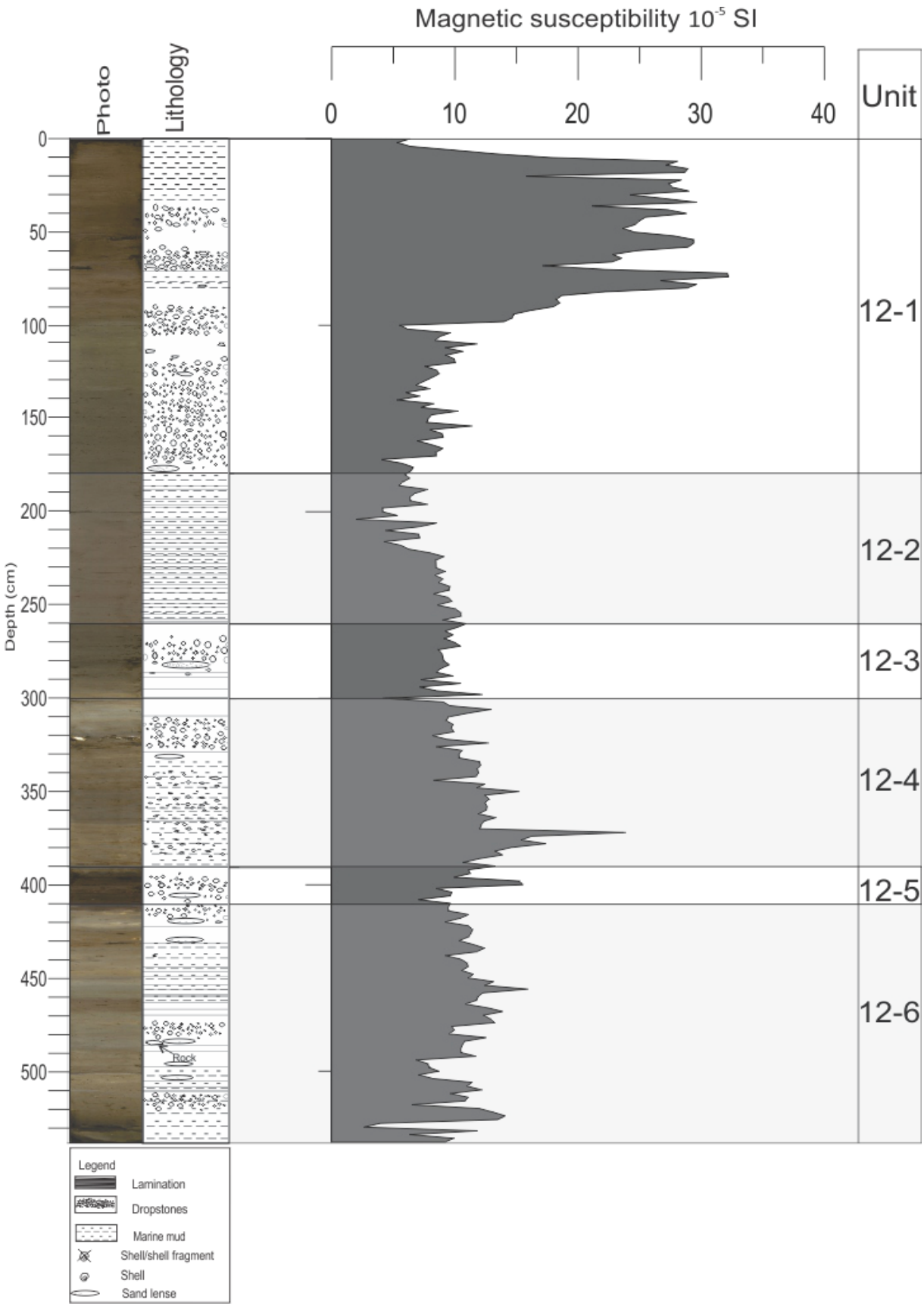

Figure 27: The photo of the core HH12-930 GC together with the magnetic susceptibility. The magnetic susceptibility shows some disturbance after 180 cm. A simplified version lithology of the core is also indicated.

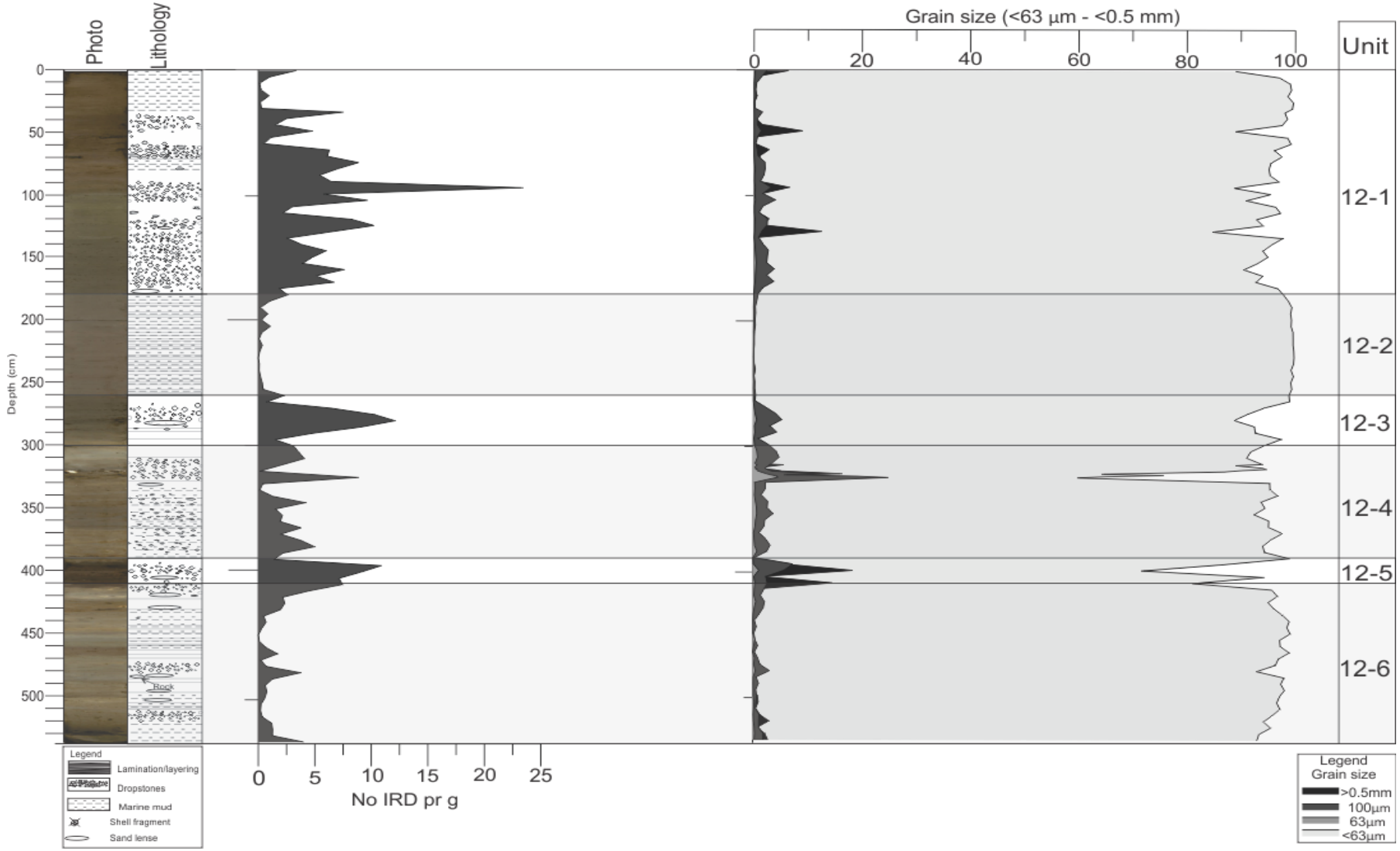

Figure 28: A photo of the core and a simplified version of the lithology and the core, together with number of IRD per gram and the grain sizes plotted against depth (cm). The six different are indicated on the figure.

5. 2. 1 Unit 12 - 1

Unit 12 – 1 consist of the upper 180 cm of the core. In this unit there is high abundance of material coarser than 0.5 mm. These are visible on the x – ray photo (Figure 26). Intervals with sand occurs as well. However, mud is the dominant (97 – 85 %) grain size in this unit (Figure 28). Layering and lamination is spares in the upper part (Figure 25 and 26). In the uppermost part of the unit the color is dark greyish brown (4/2 2.5y) and shifts to olive brown (4/3 2.5y) at 40 cm. At 60 cm the color is again dark greyish brown (4/2 2.5y), which shifts to greyish brown (5/2 2.5y) at 80 cm, and further to olive grey (4/2 5y). At 160 cm the color is dark yellowish brown (4/6 10yr), and shifts to olive grey (4/2 5y) again at 170 cm (Figure 25 and 26). The magnetic susceptibility flocculates in this unit. From 3 cm to 90 cm the values reaches its maximum throughout the core, and varies between 16 (10^{-5} SI) and 32 (10^{-5} SI). After 90 cm the values decreases. From 100 cm to 180 cm the values flocculates again, but the values are lower (4 (10^{-5} SI) to 12 (10^{-5} SI)) (Figure 27).

5. 2. 2 Unit 12 – 2

In unit 12 – 2 lamination/layering increases, and is visible on x- ray photography (Figure 26). The lamination/layering continues from 180 cm to 280 cm. The dominant grain size in this unit is mainly mud (98 – 100 %), but coarser material is present in the upper part (Figure 28), and can be observed on the x – ray photography on the lowest part of the unit (Figure 26). The whole unit consist of dark grey (4/2 5y) sediments (Figure 25 and 26). The magnetic susceptibility values varies and is relatively low from 180 cm to 220 cm (2 (10^{-5} SI) to 8 (10^{-5} SI)). From 220 cm to 260 cm the values increases (8 (10^{-5} SI) to 12 (10^{-5} SI)), and is more stable (Figure 27).

5. 2. 3 Unit 12 – 3

Unit 12 – 3 consist of coarser material (> 0.5 mm) in the upper part and lamination/layering in the lower part (Figure 25 and 26). There is also a lenses with sand in the middle part. Mud is dominant grain size, but the amount has decrease (88 %). The amounts coarse sediments (> 0.5 mm) has increased, together with the quantities of sand (Figure 28). The color shifts from dark grey (4/1 5y) to very dark grey (3/1 5y) (Figure 25 and 26). The magnetic susceptibility varies, and the values shifts between 8 (10^{-5} SI) and 12 (10^{-5} SI), and is mainly the same as in the lower part of 12 – 2 (Figure 27).

5. 2. 4 Unit 12 – 4

The lithology of unit 12 – 4 (300 cm – 390 cm) varies; intervals with high abundance of coarser sediments (>0.5 mm), sand lenses and lamination/layering occurs (Figure 25 and 26). There is a drop in mud content (60 %) at 330 cm, and where the abundance of sand and grain size coarser than 0.5 mm increases (Figure 28). In this unit a 20 cm thick layer with shells and shell fragments was observed. By study one of the shells, it is assumed that the species is *"Vesicomyidae"*, but since the shells were missing important parts to be completely identified, it is just an assumption. The color of the sediments in this unit varies compared to the units above (Figure 25 and 26). At the top of this unit (300 cm) the color is light olive grey (6/2 5y), and shifts to olive grey (4/2 5y) at around 315 cm. From 315 the color changes to dark grey (4/1 5y). This interval contains shell and shell fragment, and can be observed in the x-ray photo (Figure 26). From 340 cm to 355 cm the color shifts from grey (5/1 5y) to brown (4/2 5y), and to dark grey (4/1 5y). From 380 cm to 390 cm the color is olive (4/4 5y) (Figure 25 and 26). The value of the magnetic susceptibility is varying between 4 (10^{-5} SI) and 24 (10^{-5} SI) (Figure 27). There are some small peak throughout the unit, where the highest peak is located at 375 cm.

5. 2. 5 Unit 12 – 5

Unit 12 – 5 is 20 cm thick (390 cm – 410 cm), and consist of an interval with high abundance of coarse material (>0.5 mm) (Figure 28). The mud content has dropped down, which varies between 72 % and 84 %. The units contains a lenses with sand. The color shifts from very dark grey (3/1 5y) to dark grey (4/1 5y) in this unit (Figure 25 and 26). The values of the magnetic susceptibility consist of a peak (15 (10^{-5} SI)) in the middle of this unit, and then decreases (8 (10^{-5} SI)) toward 410 cm (Figure 27).

5. 2. 6 Unit 12 – 6

The lowermost unit (410 cm – 538 cm) consist of varied lithological features; intervals with moderate abundance of coarser material (>0.5 mm), and especially in the upper part, there are occurrence of lamination/layering and zones with sand lenses (Figure 28). At ca 485 cm a clast can be found, which is visible on the x – ray photography (Figure 26). Above and below

this clast, sand lenses were observed (Figure 25 and 26). In this unit the mud content has increased (93 % to 97 %). The color is particularly diverse in this unit (Figure 24 and 26). Between 411 cm to 430 the color changes from light olive grey (6/2 5y) to pale yellow (7/3 5y). From 430 cm to 467 cm the color changes from dark grey (4/1 5y) to brownish yellow (6/6 10yr), and further to darker color; very dark greyish brown to dark greyish brown (4/2 2.5y). From 467 cm to 487 cm the color is olive grey (4/2 5y)/olive brown (4/4 2.5y). Towards the bottom of the core the color shifts between dark grey (4/1 5y) to olive grey (4/2 5y), and towards dark grey (4/1 5y) again. In this unit the values of the magnetic susceptibility is variable, but moderate - low (3 (10^{-5} SI) to 14 (10^{-5} SI) (Figure 27).

5. 2. 7 Stable isotope analysis

The stable analysis is based on measurements of N. pachyderma (s) and C. neoteretis. The results consist of four results; planktic and benthic oxygen isotope ($\delta^{18}O$) and planktic and benthic carbon isotopes ($\delta^{13}C$) (Figure 29). The stable isotopes are divided into the same units as seen the lithological units (Figure 25, 26, 27 and 28). The lowermost part of unit 12 – 6 lack the benthic isotope measurements due to insufficient material.

In unit 12 – 1 (0 cm – 180 cm) the planktic and benthic $\delta^{18}O$ values are low to moderate, and varies between 3.75 – 3.0 ‰ and 4.8 – 4.4 ‰ (Figure 29). The oxygen values increases after ca 100 cm (Figure 27). The benthic $\delta^{13}C$ values stays between 0.0 – -0.5 ‰ from 0 to 100 cm and then drops to -2.1‰ after 123 cm (figure 27). The values increases to -1.0‰ after 130 cm (Figure 29). The planktic $\delta^{13}C$ values varies between 1.8 to -1.8 ‰ and stays relatively unaltered throughout the unit (Figure 27).

The planktic and benthic $\delta^{18}O$ increases in Unit 12 – 2 (180 – 260 cm), and varies between 4.1 – 4.8 ‰ and 5.3 – 5.4 ‰, respectively (Figure 29). The planktic $\delta^{13}C$ values relatively unchanged (~0.0 – -1.9 ‰) (Figure 29). The benthic $\delta^{13}C$ values decreases towards -2 ‰ in the lower part of the unit (Figure 29).

In unit 12 – 3 (260 – 300 cm), both the planktic and benthic $\delta^{18}O$ values decreases to a minimum (2.0‰ and 4.6 ‰, respectively) (Figure 29). The planktic $\delta^{13}C$ values stays unaltered, and the benthic $\delta^{13}C$ values varies between -1.0 and -2.0 ‰ (Figure 29).

The planktic and benthic $\delta^{18}O$ values increase from 3.6 to 4.75 ‰ and 5.3 to 5.6 ‰, respectively, towards unit 12 – 4 (300 – 390 cm) (Figure 29). The planktic $\delta^{13}C$ values makes a decrease to -3.47 ‰ at ca 353 cm, however, the values stays relatively unchanged throughout the unit (Figure 29). The benthic $\delta^{13}C$ values flocculates, and ranges between -1.0 to -3.5 ‰ (Figure 29). The minimum benthic $\delta^{13}C$ value throughout the unit occurs at 353 cm (3.5 ‰) and at 368 cm (-2.57 ‰) (Figure 29).

In the relatively short unit 12 – 5 (390 – 410 cm) the planktic $\delta^{18}O$ and benthic values makes a slightly increase of 0.2 ‰, while the benthic $\delta^{18}O$ values remains stable at 5.5 ‰. The benthic $\delta^{13}C$ values increases to moderate values (-1.4 ‰), and the planktic $\delta^{13}C$ values decreases to -2.42 ‰ at 388 cm, and to -2.26 ‰ at 403 cm (Figure 29). Toward the upper part of unit 12—6 the values declines to -6.08 ‰ (413 cm) (Figure 29).

In unit (12 – 6; 410 – 538 cm) the planktic $\delta^{18}O$ values increases to high values (4.0 – 4.75 ‰) (Figure 27). The benthic $\delta^{18}O$ makes s drop after 400 cm, and decreases to 4.8 ‰ (Figure 29). The benthic $\delta^{13}C$ values varies between -1.0 and -3.5 ‰ (Figure 29). In the upper part of this unit the planktic $\delta^{13}C$ values reaches -6.08 ‰ (413 cm). The values makes a drop from -0.07 ‰ (458 cm) to -4.07 ‰ at 463 cm (Figure 29). The values increases, and then declines drastically at 488 cm (-3.64 ‰), and continuous to decrease to a minimum value at 518 cm (-10.44 ‰) and at 528 cm (-11.34 ‰) (Figure 29).

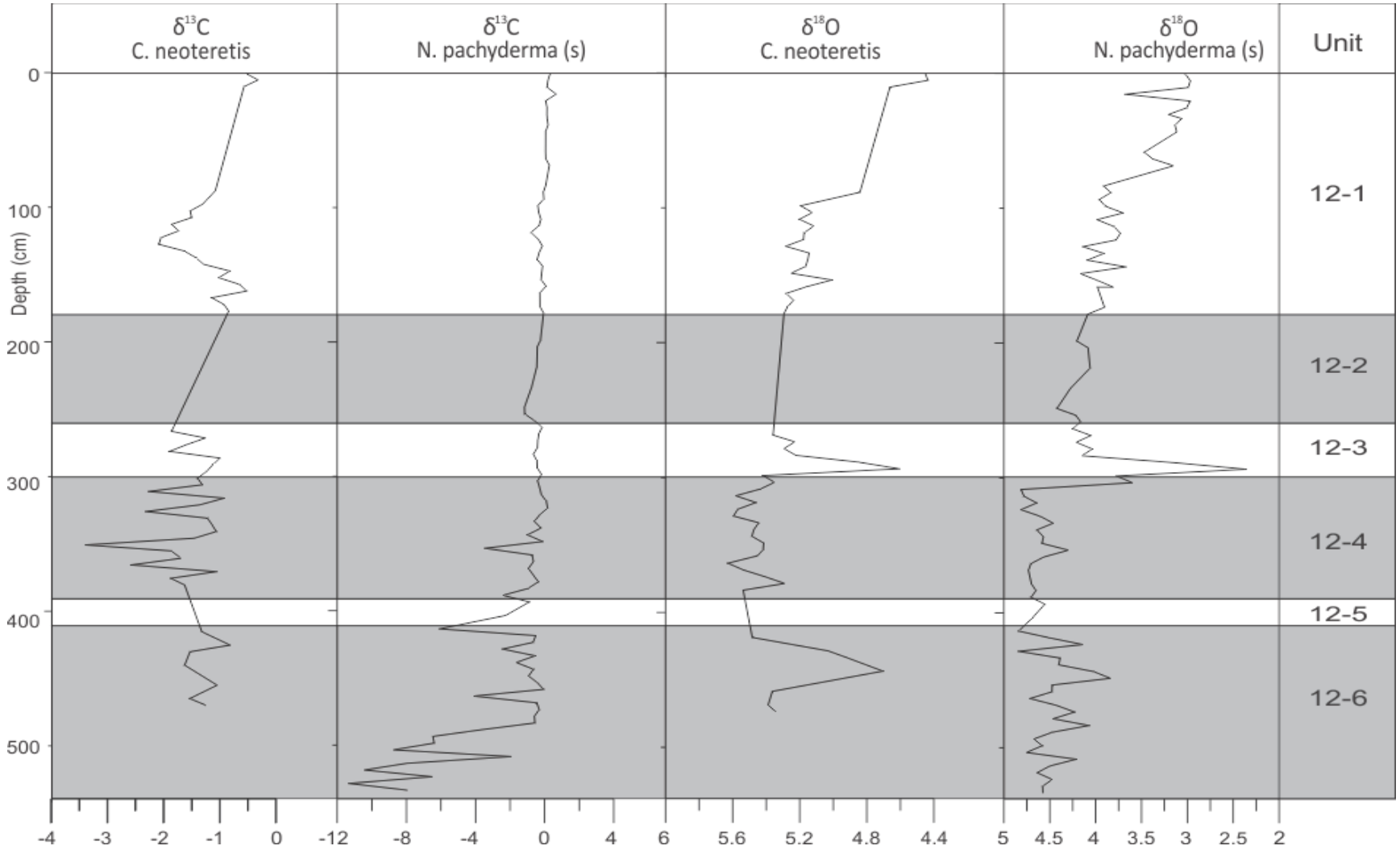

Figure 29: Stable isotope for sediment core HH12 – 930 GC. The planktic $\delta^{13}C$ value stays relatively uniform from 0 to 488 cm when the values drops to -3.64 ‰ and continuous to decline towards -11.34 ‰. The planktic and benthic $\delta^{18}O$ values seem to be slightly increasing toward the bottom of the core, except in unit 14 – 3, were the values drops to a minimum.

6. Chronology and establishment of an age model

6. 1 HH14-002 GC

The chronology of HH14 – 002 GC is based on four AMS radiocarbon dates from the planktic foraminifera *N. pachyderma (s).* The four samples was send to the 14CHRONO Centre at Queens University in Belfast for AMS ^{14}C dating. The dating are based on the mean values of the σ2 range. The four dating range from 215 cm to 323 cm in the core, leaving the upper part and some of the lower part of the core with no radiocarbon age (Figure 30). This was because there was not sufficient material to be dated in these intervals.

6. 1. 1 Radiocarbon dates

The radiocarbon dates were converted to calibrated ages using Calib 7.0.4 (Stuvier & Reimer, 1993), and the calibrating data set that was used was Marine13 (Reimer, et al., 2013). ΔR was set to be zero. The calibrated dates ranges from 20,101 cal. yr BP to 26,486 cal. yr BP (Table 4).

Core	Lab ref.	Depth (cm)	Species	^{14}C uncalibrated yr	Cal. yr BP 2σ range	Cal. yr BP 2σ mean
HH14-002GC	UBA-28217	215.5	*N. pachyderma (s)*	17,059±77	19,857-20,344	20,101
HH14-002GC	UBA-28218	259.5	*N. pachyderma (s)*	18,533±103	21,677-22,294	21,986
HH14-002GC	UBA-28219	275.5	*N. pachyderma (s)*	19,590±85	22,856-23,430	23,143
HH14-002GC	UBA-28220	323.5	*N. pachyderma (s)*	22,635±111	26,111-26,861	26,486

Table 4: The laboratory reference, together with the ^{14}C dates and the calibrated ages.

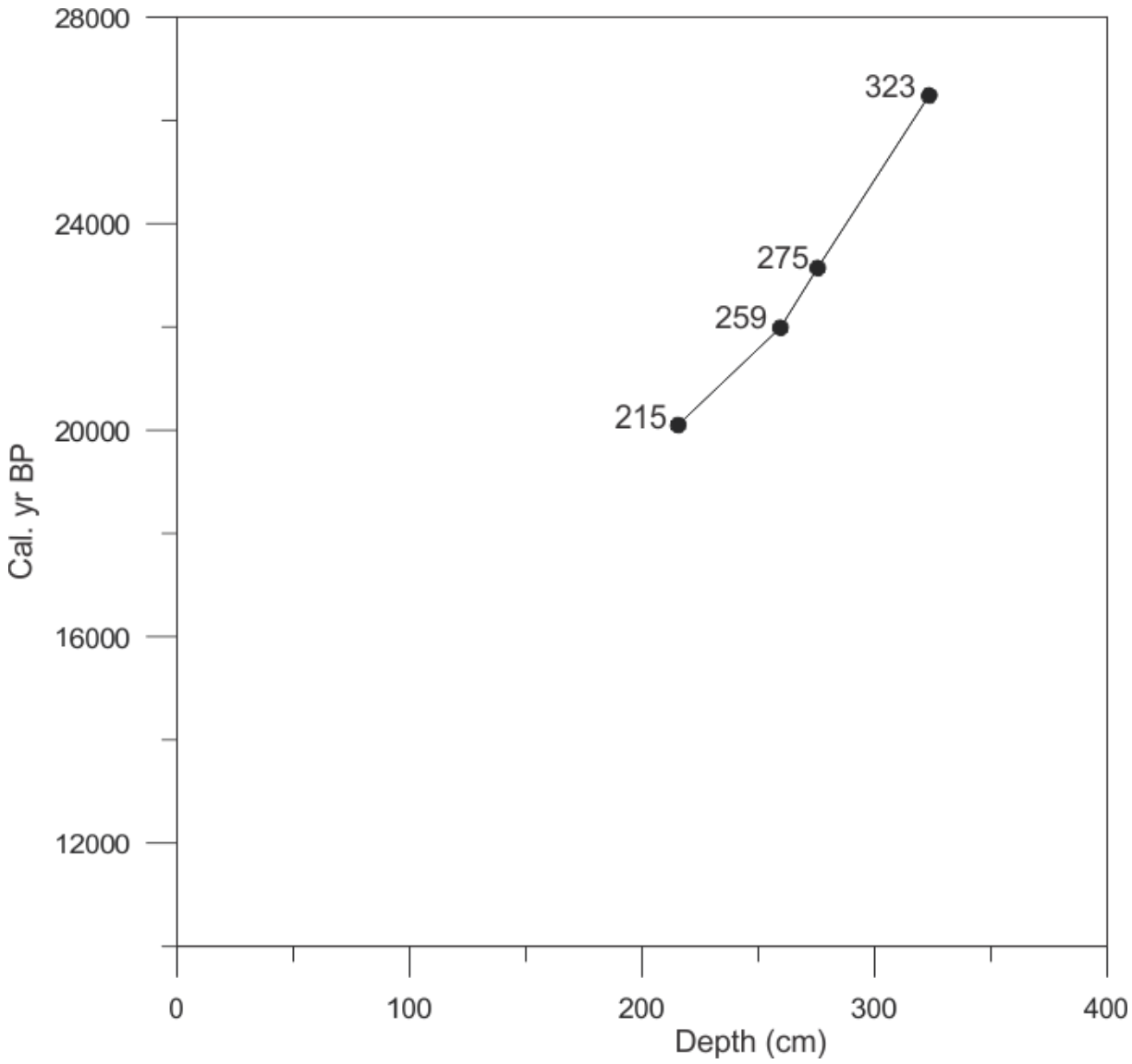

Figure 30: Calibrated radiocarbon dates plotted against depth. The sampling depth is shown by black dots.

6. 1. 2 Sedimentation rate

The linear sedimentation rate in Fram Strait is estimated by Hebbeln and Wefer (1997) to be 2.4 – 3.0 cm/ka during glaciations and 1.2 – 1.3 cm/ka for interglacial periods. The controlling factor for variations in the sedimentation rate in the Fram Strait is the intensity of ice rafted debris, bottom topography and bottom currents (Gard, 1987).

The linear sedimentation rate was calculated by assuming that the sedimentation rate has been constant between the radiocarbon dates. Four radiocarbon dates establish together three linear sedimentation rate (Table 5). The linear sedimentation rates are presented as cm/ka (10^3) against depth (cm).

Core	Depth (cm)	Species	^{14}C cal year BP	Cal. yr BP 2 σ mean	Sedimentation rate (cm/ka)
HH14-002GC	215.5	*N. pachyderma (s)*	17,059±77	20,101	23.34 cm/ka (between 259.5 and 215.5)
HH14-002GC	259.5	*N. pachyderma (s)*	18,533±103	21,986	13.83 cm/ka (between 275.5 and 259.5)
HH14-002GC	275.5	*N. pachyderma (s)*	19,590±85	23,143	14.36 cm/ka (between 275.5 and 323.5)
HH14-002GC	323.5	*N. pachyderma (s)*	22,635±111	26,486	

Table 5: Table showing form which depth the dating were sampled, ^{14}C years, calibrated calendar years and the linear sedimentation rate.

The sedimentation rate covers the three lowermost units in the core (unit 14 – 4 to unit 14 – 6), so the sedimentation rate for upper part of the core is unknown. Between the upper radiocarbon dates the sedimentation rate is estimated to be 23.34 cm/ka. The two samples were taken from 215 cm and 259 cm, where the samples were dated to 20101 cal. yr BP and 21986 cal. yr BP, respectively. For the middle the sedimentation rate were estimated by material sampled from 259 cm and 275 cm, where the samples from 275 cm were dated to

23143 cal. yr BP. This part covers an age span of 1157 years. The sedimentation rate decreases in this interval down to 13.82 cm/ka. In the lower part the sedimentation rate is estimated by using the age from 275 cm and from 323 cm, which was dated to 26486 cal. yr BP. The sedimentation rate was estimated to be 14.358 cm/ka in the lower part. The average sedimentation rate for this core is calculated to be 17.1726 cm/ka.

6. 2 HH12-930 GC

In HH12 – 930 GC the chronology is based on two samples contain *N. pachyderma (s),* one contain shell fragment of unidentified species and one with a shell which is believed to be of the species *Vesicomyidae*. The samples were sent to 14CHRONO Centre at Queens University in Belfast for AMS 14C dating. The dating range from 298 cm to 508 cm in the core (Figure 31). The dating are also based on the mean value of the σ2 range. The upper part of the core contains no dating due to lack of material.

6. 1. 1 Radiocarbon dates

The dating were calibrated ages using Calib 7.0.4 (Stuvier & Reimer, 1993), and the calibrating data set that was used was Marine13 (Reimer, et al., 2013). ΔR was set to be zero. The dating will be presented as cal. yr BP (calibrated calendar years before present). The four dating range from 18429 cal. yr BP to 37829 cal. yr BP (see Table 6).

Core	Lab ref.	Depth (cm)	Species	^{14}C cal year BP	Cal. yr BP 2σ range	Cal. yr BP 2σ mean
HH12-930GC	UBA-30294	298	*N. pachyderma (s)*	15,572±68	18,235-18,623	18,429
HH12-930GC	UBA-30295	320.5	Shell *(Vesicomyidae)*	18,254±86	21,351-21,881	21,616
HH12-930GC	UBA-30296	433	*N. pachyderma (s)*	25,022±180	28,214-29,056	28,635
HH12-930GC	UBA-30297	508	Shell fragment	34,074±554	36,427-39,231	37,829

Table 6: Laboratory references, species of the samples material together with the ^{14}C age and the mean calibrated calendar dates.

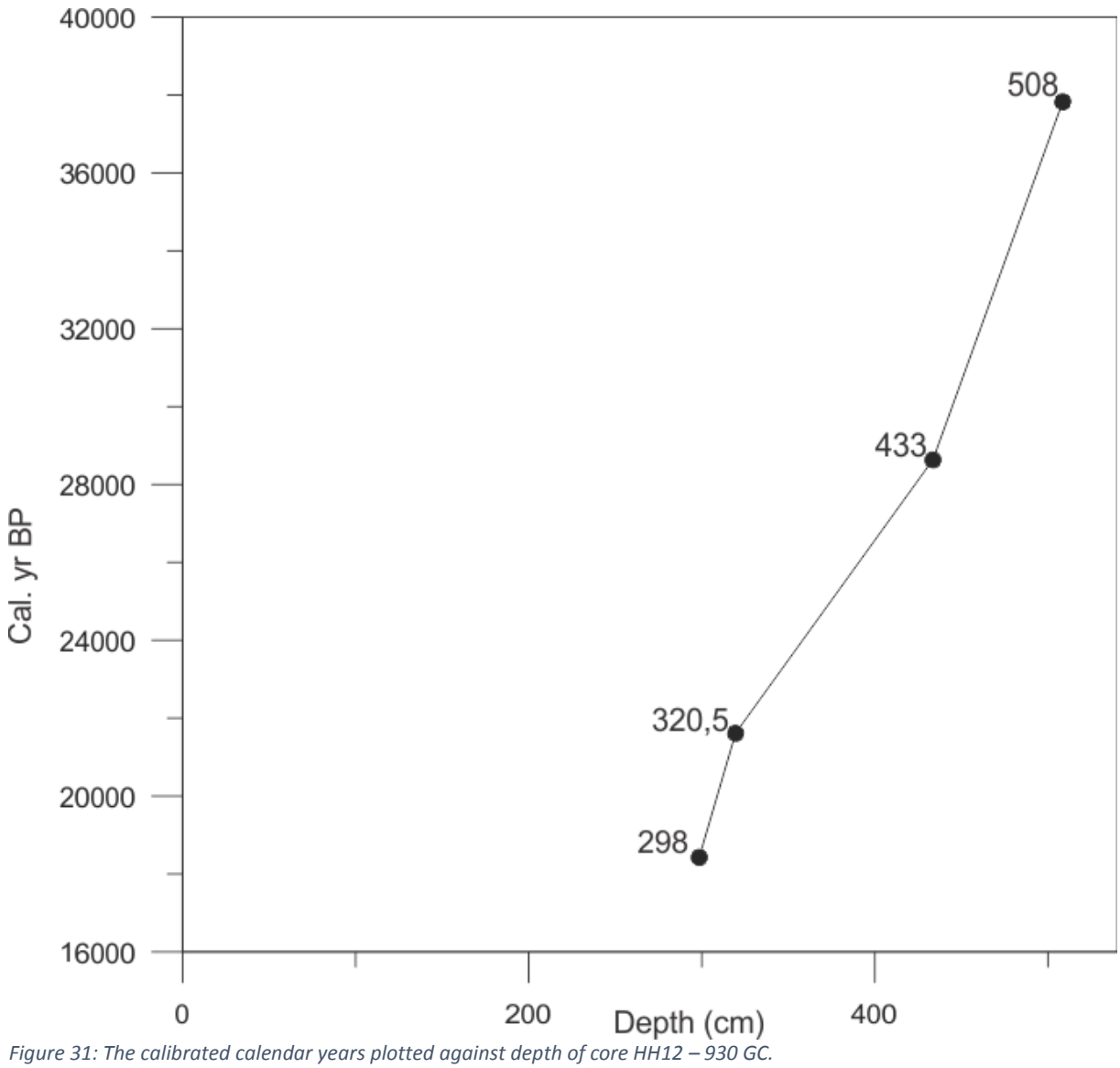

Figure 31: The calibrated calendar years plotted against depth of core HH12 – 930 GC.

6. 1. 2 Sedimentation rate

To estimate the sedimentation rate, it is assumed that the sedimentation rate has been constant between the radiocarbon dates. The depth and the age between two intervals was used to calculate the sedimentation rate, which is the same procedure as for HH14 – 002 GC (see 6. 1. 2). Together three sedimentation rates for core HH12 – 930 GC was calculated (Table 7).

Core	Depth (cm)	Species	^{14}C cal year BP	Cal. yr BP 2 σ mean	Sedimentation rate (cm/ka)
HH12-930GC	298	*N. pachyderma (s)*	15,572±68	18,429	7.06 cm/ka (between 298 and 320.5)
HH12-930GC	320.5	Shell *(Vesicomyidae)*	18,254±86	21,616	16.03 cm/ka (between 320.5 and 433)
HH12-930GC	433	*N. pachyderma (s)*	25,022±180	28,635	8.16 cm/ka (between 433 and 508)
HH12-930GC	508	Shell fragment	34,074±554	37,829	

Table 7: The depth, ^{14}C age, calibrated calendar age and the calculated sedimentation rate for HH12 – 930 GC.

The sedimentation rate is estimated to be 7.06 cm/ka between 298 cm and 320.5, and increases to 16.03 cm/ka at 320.5 cm to 433 cm. Between 433 cm and 508 cm the sedimentation rate decreases down to 8.16 cm/ka (See table 7).

The four radiocarbon dates covers together the lowermost part of unit 12 – 3, upperpart of unit 12 – 4 and upper and lower part of unit 12 – 6. The sedimentation rate and the age of unit 12 – 1 and unit 12 – 2 is unknown. The sedimentation rate between 298 cm and 320.5 cm is estimated to be 7.06 cm/ka, and increases between 320.5 and 433 to 16.03 cm/ka. Between 433 cm and 508 cm the sedimentation rate decreases to 8.16 cm/ka. The average sedimentation rate for core HH12 – 930 GC is calculated to be 10.42 cm/ka.

6. 3 Correlation and age model

A study by Jessen et al (2010) demonstrate that sediments core from the Western Svalbard slope can be used for correlation and as a chronological tool. The sediment core varies from water depth between 630 m to 1880 m, and are collected between 76° to 80°N (Figure 29a). All of the cores in Jessen et al (2010) showed clear similarities in lithology and magnetic susceptibility (MS), and penetrated into mass transported material and laminated, fine grained sediments. Both of these layers show low magnetic susceptibility values (Figure 32). A stacked MS – chronology provides eight absolute dating extending from 8355 to 27,500 cal yr BP (Figure 32) (Jessen, et al., 2010). Two of the ages used in HH14-002 GC were estimated by using linear regression and all of the calibrated ^{14}C ages from the core.

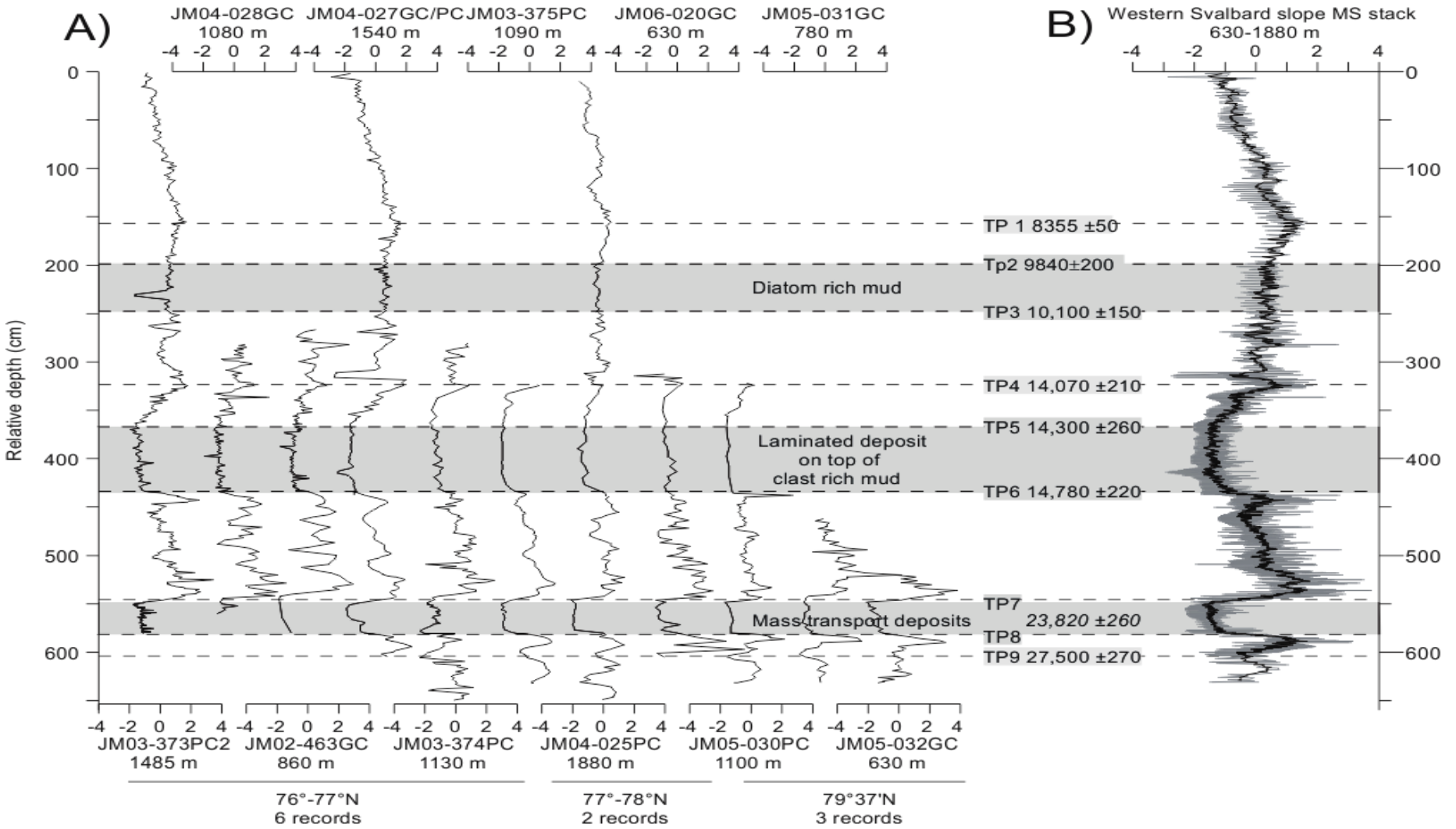

Figure 32: A) Eleven sediments cores collected from the western Svalbard slope. B) Stacked magnetic susceptibility based on the eleven sediment cores. The ages are indicated in calibrated years BP. (TP=Tie-Point). (Both figure A) and B) are from Jessen et al (2010)).

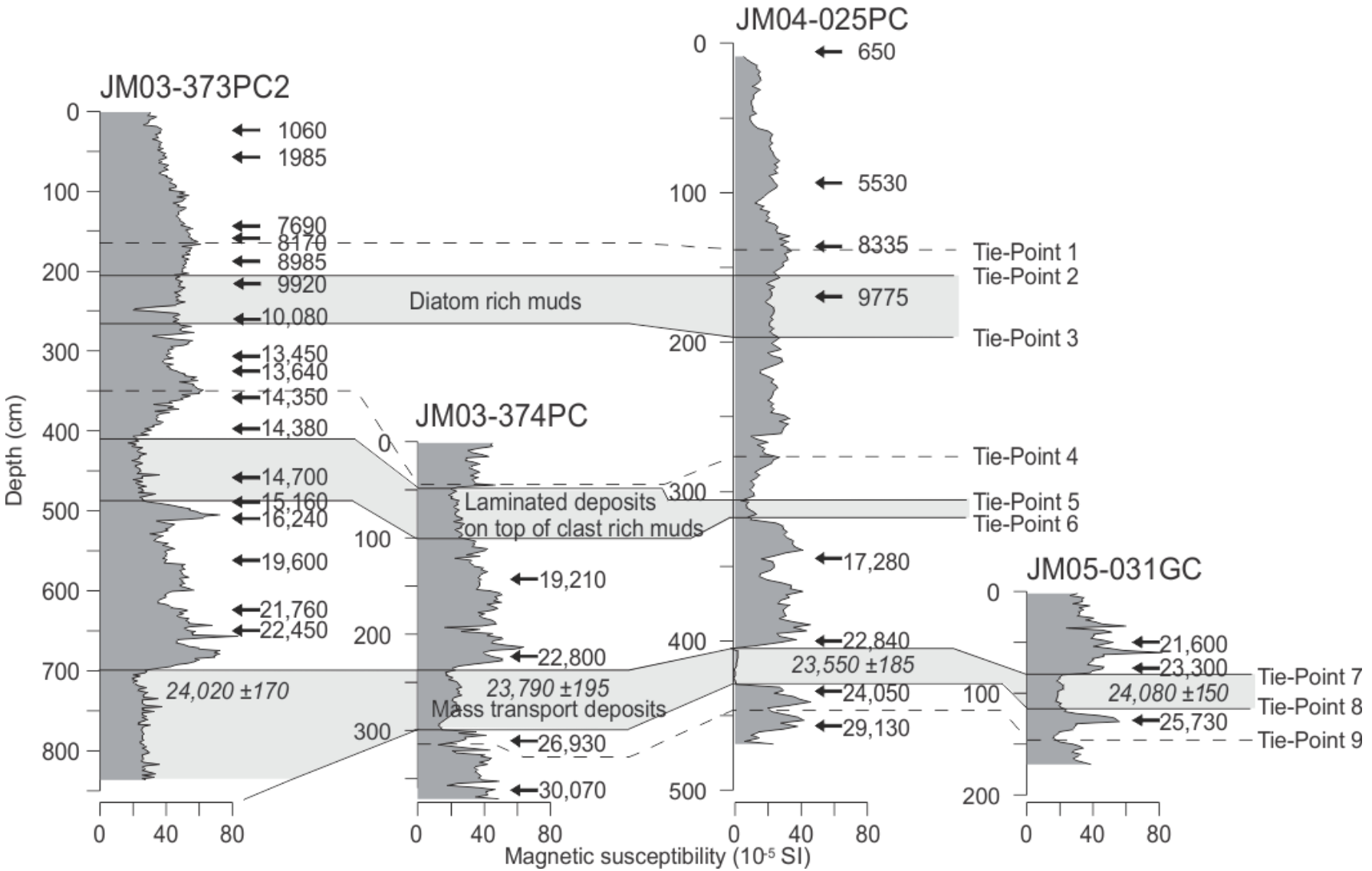

Figure 33: Four of the sediment cores from the western Svalbard slope (76°24 to 79°37'N) from Jessen et al (2010). All of the four cores contained laminated sediments (between tie-pint 5 and 6) and mass transported deposits (between tie-point 7 and 6) which shows relatively low magnetic susceptibility. Figure from Jessen et al (2010).

The cores HH14 – 002 GC and HH12 – 930 are taken offshore western Svalbard (Figure 12 and 15). The two sediment cores HH14 – 002 GC and HH12 – 930 GC show similarities in lithology and grain size distributions (Figures 17, 20 and figures 25 and 28, respectively) and similarities to the lithology and magnetic susceptibility patterns published by Jessen et al. (2010).

The magnetic susceptibility in HH12 – 930 GC (Figure 27) is disturbed for unknown reasons (see discussion below), however the upper part of HH12 – 930 GC shows a similar pattern as in the upper part of HH14 – 002 GC. Unit 14 – 1 and 12 – 1 both contains mud rich in clast (Figures 18 and 28, respectively), and the magnetic susceptibility in the upper part of unit 12 – 1 (Figure 27) shows a similar pattern to the pattern seen in the magnetic susceptibility of unit 14 – 1 (Figure 19). The thickness of this layer in HH14 – 002 GC is 70 cm (Figure 17 and 18), while in HH12 – 930 GC the layer is 180 cm thick (Figure 24 and 25). In unit 14 – 2 and unit 12 – 2 fine – grained, laminated sediments can be observed (Figures 17, 18 and figures 25 and 26, respectively). The thickness of the laminated layers in unit 14 – 2 and 12 -2 varies between 91 cm to 80 cm, respectively.

The laminated layers are younger than 20,101 years in core HH14-002 and located 55 cm above this date, and younger than 18,429 years in core HH12-930 and located 38 cm above this date. The laminated layers probably correlate closely in time with the laminated layers found in cores from the western Svalbard margin by Jessen et al. (2010) and with similar age as the tie – points 5 – 6 (14,300 and 14,780 cal yr BP, respectively). In core HH14-002 GC the magnetic susceptibility values are also low as in the records from Jessen et al. (2010) (Figure 19).

Below both of the laminated layers in unit 14 – 2 and 12 – 2 deposits with high abundance of coarse material are observed. This layer (unit 14 – 3) is 20 cm thick in HH14 – 002 GC (Figure 15). The coarse material is visible on the x – ray photo (Figure 18) and by its dark color in otherwise light-colored sediments (Figure 17). In HH12 – 930 GC the layer (unit 12 – 3) is 40 cm thick (Figure 25). On the x – ray photo (Figure 26) the coarse material is clearly visible in the upper part of this unit and as in in HH14-002GC it stands out by its darker color (Figure 25). Both units 14 – 4 (Figure 17 and 18) and 12 – 4 (Figure 25 and 26) show layering. The grain sizes in HH14-002 GC and HH12-930 GC (Figure 18 and 28, respectively) and the color of the sediments (Figure 17 and 25, respectively) varies. In unit 14 – 5 (Figure 20) and unit 12 – 5 (Figure 28) the abundance of coarse material increases,

and the amount of mud drops. In HH14 – 002 GC the magnetic susceptibility decreases in this unit (Figure 19). The coarse layers show obvious similarities to the coarse layers found in Jessen et al. (2010), both in lithology, color and magnetic susceptibility values (core HH14-002, only). Also the layers are framed by dates of 23,143 years in core HH14-002 right above the coarse layer and by 28,635 years in core HH12-930 23 cm below the layer and thus probably correlate in time with Jessen et al. (2010), who dated the layer to 24,000 years.

In unit 14 – 6 and unit 12 – 6 the amount of mud increases (Figure 19 and 28, respectively), and in both cores a clast deposited below a sand lense can be observed at 385 cm in HH14 – 002 GC (Figure 17 and 18) and at 485 cm in HH12 – 930 GC (Figure 25 and 26). This clast could potentially have been deposited simultaneously, however, due to lack of absolute dating this correlation is rather uncertain.

By comparing the lithology, grain sizes and parts of the magnetic susceptibility a correlation between the units in HH14 – 002 GC and HH12 – 930 GC is possible and further a correlation to the stack of Jessen et al. (2010) (Figure 35).

The magnetic susceptibility in HH14 – 002 GC (Figure 19) shows some of the same patter as seen in the stacked magnetic susceptibility (Figure 32). The layer in unit 14 – 5 is possibly the similar layer observed in Jessen et al (2010), which is indicated in figure 32 in between TP7 and TP8, and given an age of 23,820±260 cal yr BP (Jessen, et al., 2010). The two dating in HH14 – 002 GC gives unit 14 – 5 an age between 23,143 and 26,486 cal yr BP, which is in good agreement with TP7 and TP8 in Jessen et al (2010) (Figure 32), which has calculated an average age of the mass transported deposition to be 23,820 ±260 cal yr BP. Jessen et al (2010) also describe fine – grained, laminated sediments with low magnetic susceptibility, which is found between TP5 (14,300 ±260) and TP6 (14,700±220) (see Figure 29). This layer is deposited on top of clast rich mud (Jessen, et al., 2010). A layer similar to the laminated, fine – grains sediments in Jessen et al (2010) can be found in unit 14 – 2, which also shows laminated layers (Figure 17 and 18) and a drop in magnetic susceptibility (Figure 17). This layer contains high amount of mud (Figure 20). The laminated layer is deposited on top of mud rich in clasts (unit 14 – 3) (Figures 17 and 18). Due to the similar lithology and magnetic susceptibility correlation between unit 14 – 2 and the laminated layer in Jessen et al (2010) is possible (Figure 32b). This gives unit 14 – 2 an age of 14,300±260 cal yr BP (TP5) in the upper part (70 cm) (Figure 32 and 33) and the lower part of the unit (160 cm) an age of

14,780±220 cal yr BP (Figure 33).The upper part of the magnetic susceptibility of HH14 – 002 GC (Figure 19) shows some of the same pattern as in TP4 in the stacked magnetic susceptibility (Figure 32) in Jessen et al (2010). By correlating TP4 with the similar pattern in the magnetic susceptibility in unit 14 – 1 gives an age of 14,070 ±210 cal yr BP at ca 22 cm (Figure 33).

By correlating the similar pattern in the magnetic susceptibility in core JM03 – 374PC2 in Jessen et al (2010) (Figure 32) with the lower part of 14 – 6 (Figures 15 and 16), the age at ca 400 cm in HH14 – 002 GC could be 30,070 cal yr BP (Figure 33).

By combining the similar lithology and magnetic susceptibility, correlation between Jessen et al (2010) and HH14 – 002 GC can be possible, and further an age model for HH14 – 002 GC can be established. Together five absolute age control point (TP4 – 8) from Jessen et al (2010) can be correlated to HH14 – 002 GC (Figure 34).

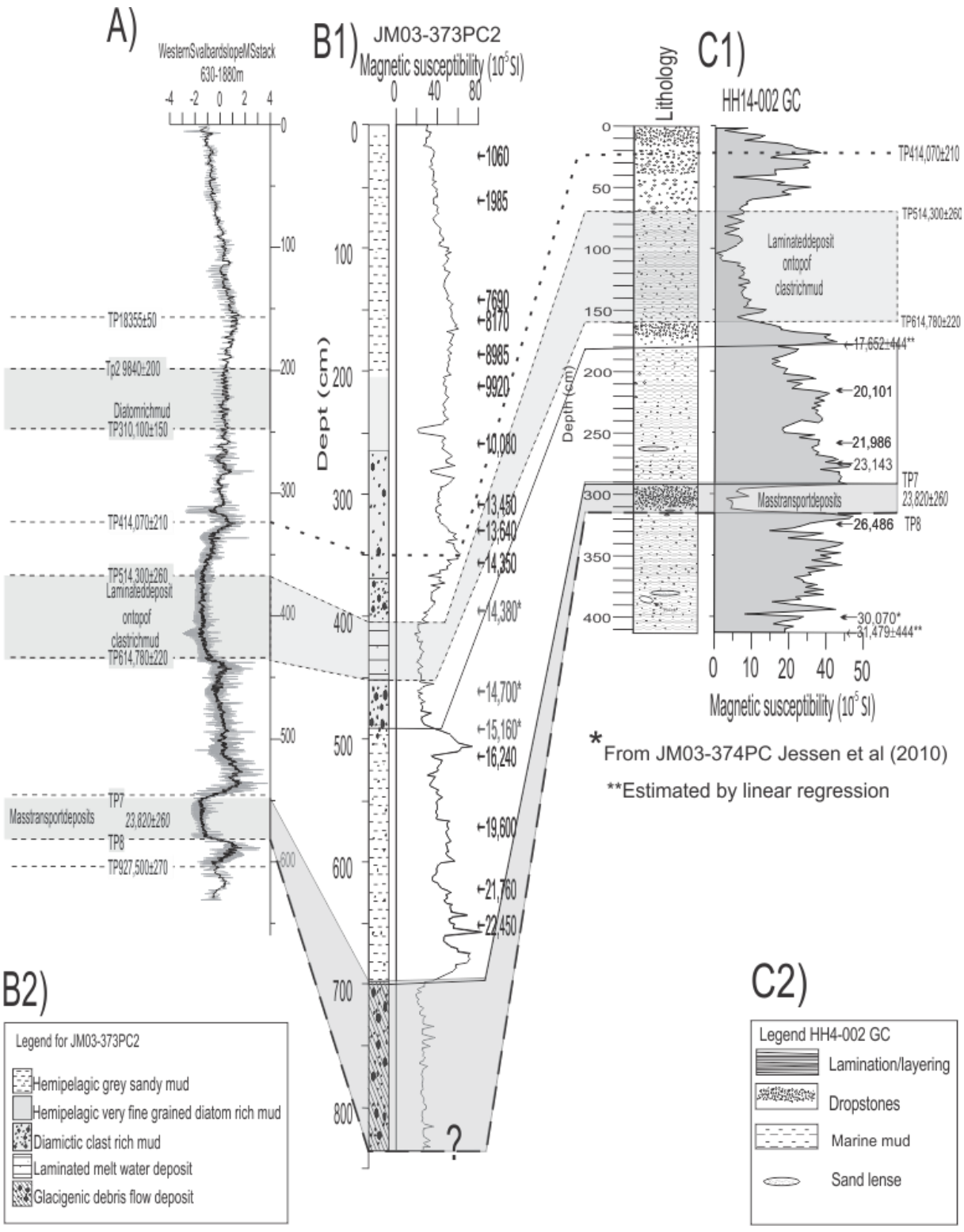

Figure 34: The figure shows correlation between A) stacked magnetic susceptibility from sediment core from the western Svalbard slope, B) the lithology and magnetic susceptibility of JM03-373PC2 and the legend of the lithology of JM03-373PC2, C) the magnetic susceptibility and lithology of HH14 – 002 GC. All the ages is indicates as cal yr BP. Figure 31A and B are from Jessen et al (2010). (dating from a core in Jessen et al (2010)).*

The correlating between HH14 – 002 GC, stacked magnetic susceptibility and lithology from Jessen et al (2010) (Figure 34) can be used to further correlate with HH12 – 930 GC). The two distinct layers, the mass transported deposition and the laminated layer, in Jessen et al (2010) (Figure 31 and 32) which is observed in HH14 – 002 GC (Figure 31C) can also be found in HH12 – 930 GC (Figures 25, 26 and 27). By further correlating the results from figure 31 with HH12 – 930 GC (Figure 34) it can provide an age model for HH12 – 930 GC.

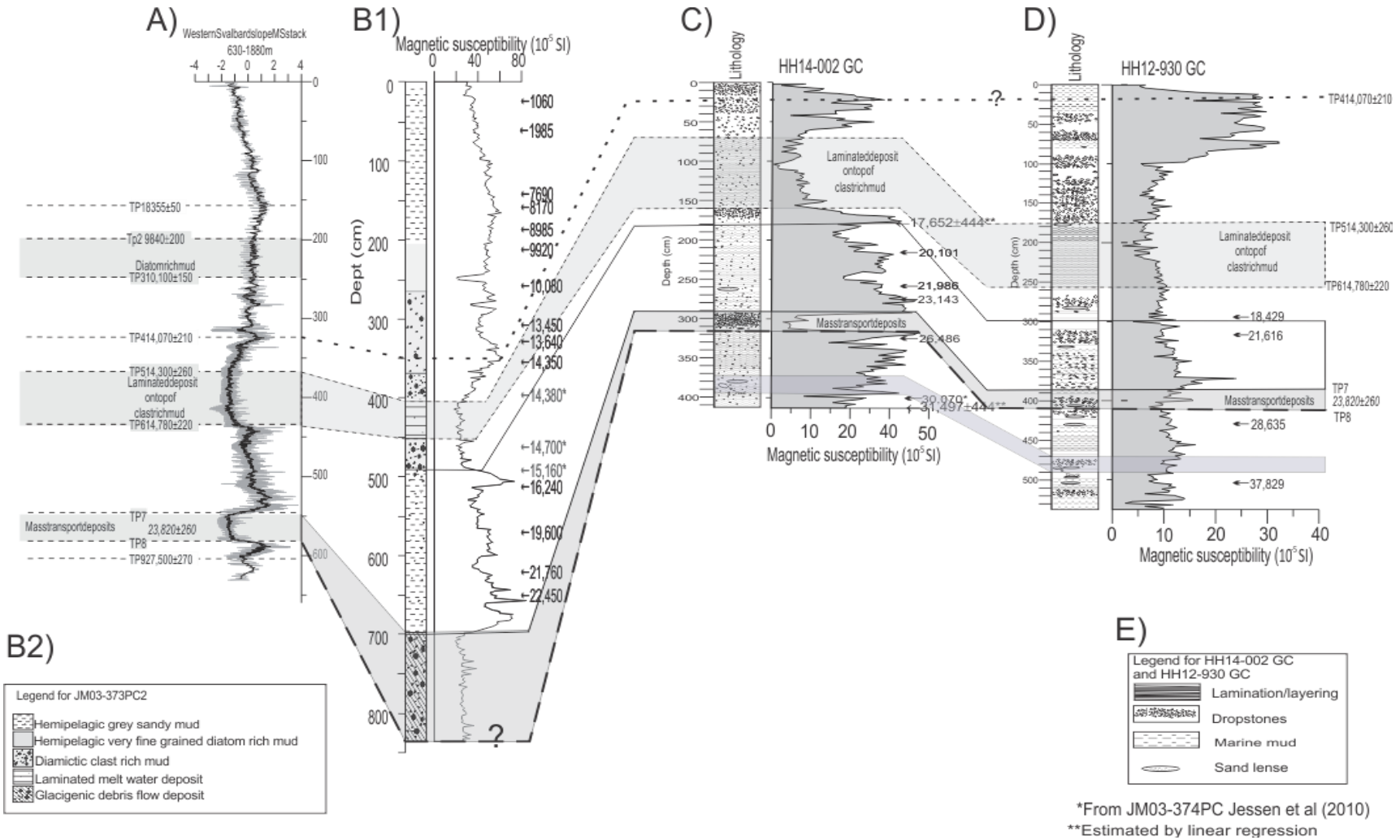

Figure 35: The figure shows correlation between A) stacked magnetic susceptibility from the western Svalbard, B) lithology and magnetic susceptibility from JM03 – 373PC2, C) HH14 – 002 GC and D) HH12 – 930 GC. B2) illustrate the legend for JM03-373PC2 and E) the legend for HH14 – 002 GC and HH12 – 930 GC. At ca 400 cm (HH14 – 002 GC) the dating showing 30,070 cal yr BP is from core JM09 – 373PC (Jessen, et al., 2010). In the lower part of HH14 – 002 GC and HH12 – 930 GC layers containing clast and sand lenses have been correlated. All the ages is indicated as cal yr BP. (Figure A, B1 and B2 are from Jessen et al (2010).)

By combining the dating from HH14 – 002 GC and HH12 – 930 GC and the dating from Jessen et al (2010) (Figure 35) a "new" sedimentation for each of the cores can be calculated. The linear sedimentation rate was calculated by assuming that the sedimentation rate has been constant between the radiocarbon dates. The depth and the age (Figure 36) between two intervals was used to calculate the sedimentation rate (Table 8 and 9).

Core/ref	Age (cal. yr BP)	Depth (cm)	Sedimentation rate (cm/ka)
Jessen et al (2010)	14070	24.5	
Jessen et al (2010)	14300	69.5	195.65
Jessen et al (2010)	14780	159.5	187.5
Linear regression	17,652	180	7.31
HH14 – 002 GC	20101	215.5	14.49
HH14 – 002 GC	21986	259.5	23.34
HH14 – 002 GC	23145	275.5	13.81
Jessen et al (2010)	23820	307.5	47.41
HH14 – 002 GC	26486	323.5	6.00
Jessen et al (2010)	30070	399.5	21.2
Linear regression	31,479	412	8.87

Table 8: Sedimentation rate for HH14 – 002 GC with dating from Jessen et al (2010). The sedimentation rate is based on the depth between two dating.

Core/ref	Age (cal. yr BP)	Depth (cm)	Sedimentation rate (cm/ka)
Jessen et al (2010)	14070	55.5	
Jessen et al (2010)	14300	178.5	534.78
Jessen et al (2010)	14780	258.5	166.6
HH12 – 930 GC	18429	298.5	10.96
HH12 – 930 GC	21616	319.5	6.59
Jessen et al (2010)	23820	398.5	35.8
HH12 – 930 GC	28635	433.5	7.27
HH12 – 930 GC	37829	508.5	8.16

Table 9: Sedimentation rate for HH12 – 930 GC with dating from Jessen et al (2010).

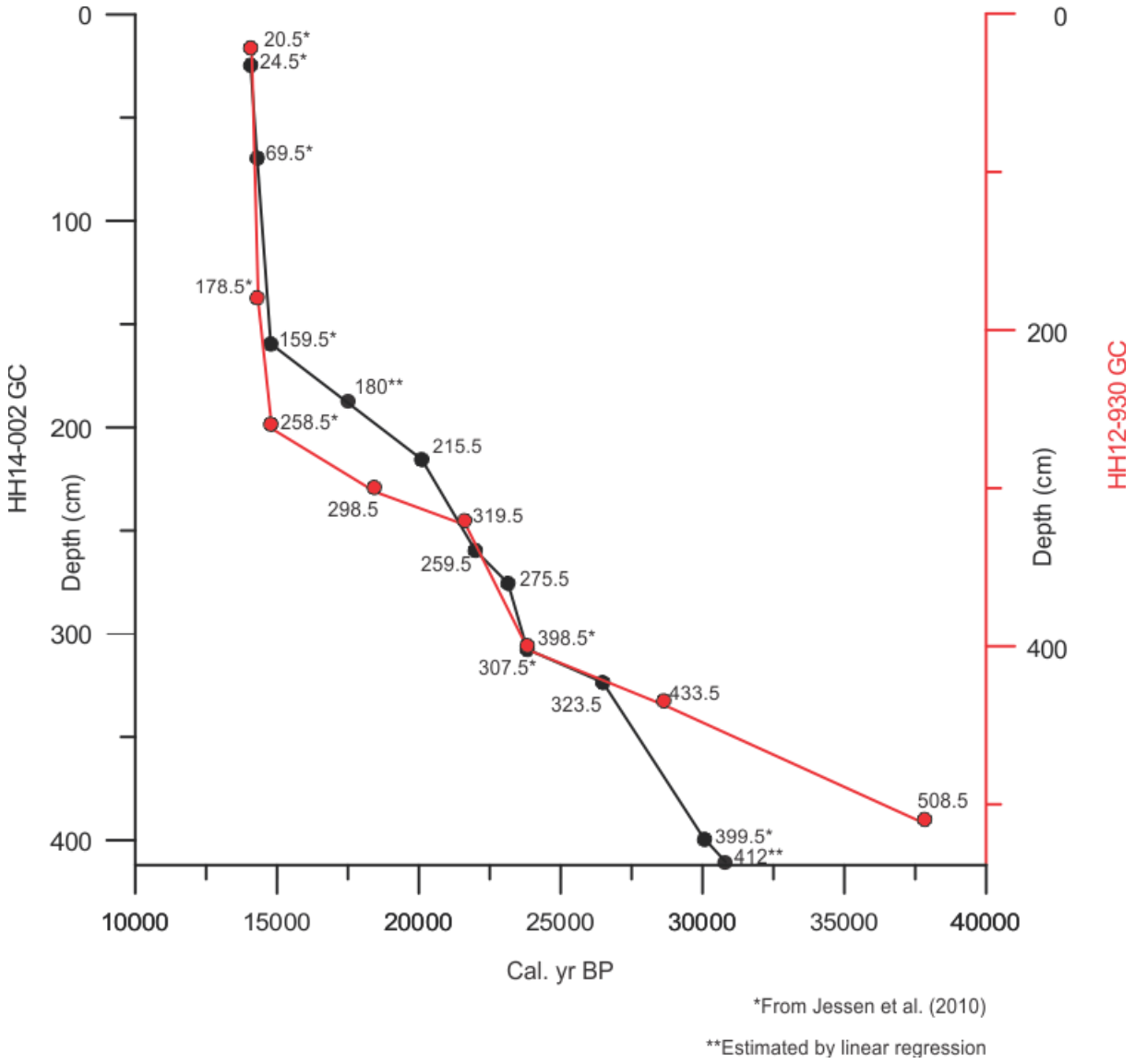

*Figure 36: Graph show the dates from HH14 – 002 GC and HH12 – 930 GC plotted against depth. The dating are marked on the graph with the depth. Dating marked * are from correlated from Jessen et al (2010).*

7. Interpretation

The interpretation will be based on the results from HH14 – 002 GC and HH12 – 930 GC, which include grain size distribution, number of IRD per gram (Figures 20 and 28, respectively) and magnetic susceptibility (Figures 19 and 27, respectively), together with the stable isotope analysis (Figure 24 and 29, respectively) and the relative abundance of planktic (Figure 21) and benthic (Figure 22) foraminifera from HH14 – 002 GC. However, due to disturbed signal of magnetic susceptibility below 180 cm in HH12 – 930 GC (Figure 27), it will not be given so much emphasis in the interpretation.

Both of the cores have been correlated with Jessen et al (2010) to establish an age model together with the calibrated ^{14}C ages (Figure 35). Based on this the two cores can be divided into seven different time intervals: the Middle Weichselian (>37,829 – 30,070 cal yr BP); the LGM (Last Glacial Maximum) (30,070 – 20,101 cal yr BP); Heinrich Event 2 (23,820 cal yr BP); Early deglaciation (20,101 cal yr BP); Heinrich Event 1 (c. 18,429 – 14,780 cal yr BP); Bølling/Allerød Interstadial (14,780 -<14,070 cal yr BP); Early Holocene (<14,070 cal yr BP). HH14-002 GC and HH12-930 GC contain both a muddy layer rich in clasts (Figure 37 and 38, respectively), laminated sediments (Figures 37 and 38, respectively) with high sedimentation rate (Table 8 and 9, respectively), possibly Heinrich Event 1 (Figures 37 and 38, respectively) and mass transported sediments (Figure 37 and 38, respectively), which correlated with Jessen et al (2010) (Figures 32 and 33). However, the intervals “Middle Weichselian” and “Early Holocene” applies only for HH12 – 930 GC.

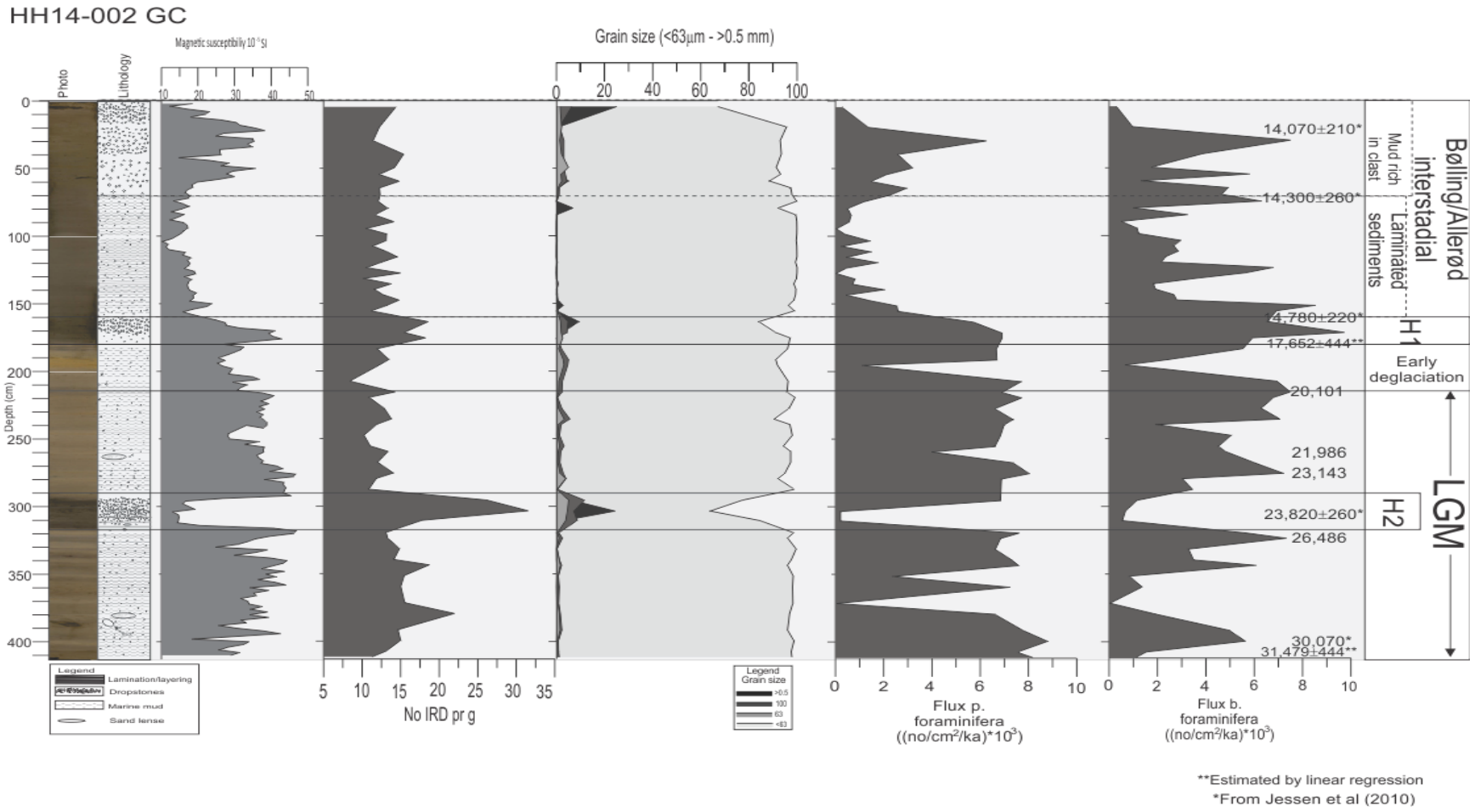

Figure 37: Proxy data for HH14 – 002 GC. The image to the left shows color of the sediments. The dark color seem to be related to coarse – grained material, and increased IRD. The benthic flux increases during the Bølling/Allerød, and stays low during Heinrich Event 1 and 2. It appears that the flux of planktic foraminifera increases after Heinrich Event 1 and 2. During the Heinrich Event 2 the magnetic susceptibility is extremely low, while the value is high during the rest of the LGM. All ages are presented as cal. yr BP. LGM = Last Glacial Maximum, H2 = Heinrich Event 2, H1 = Heinrich Event 1.

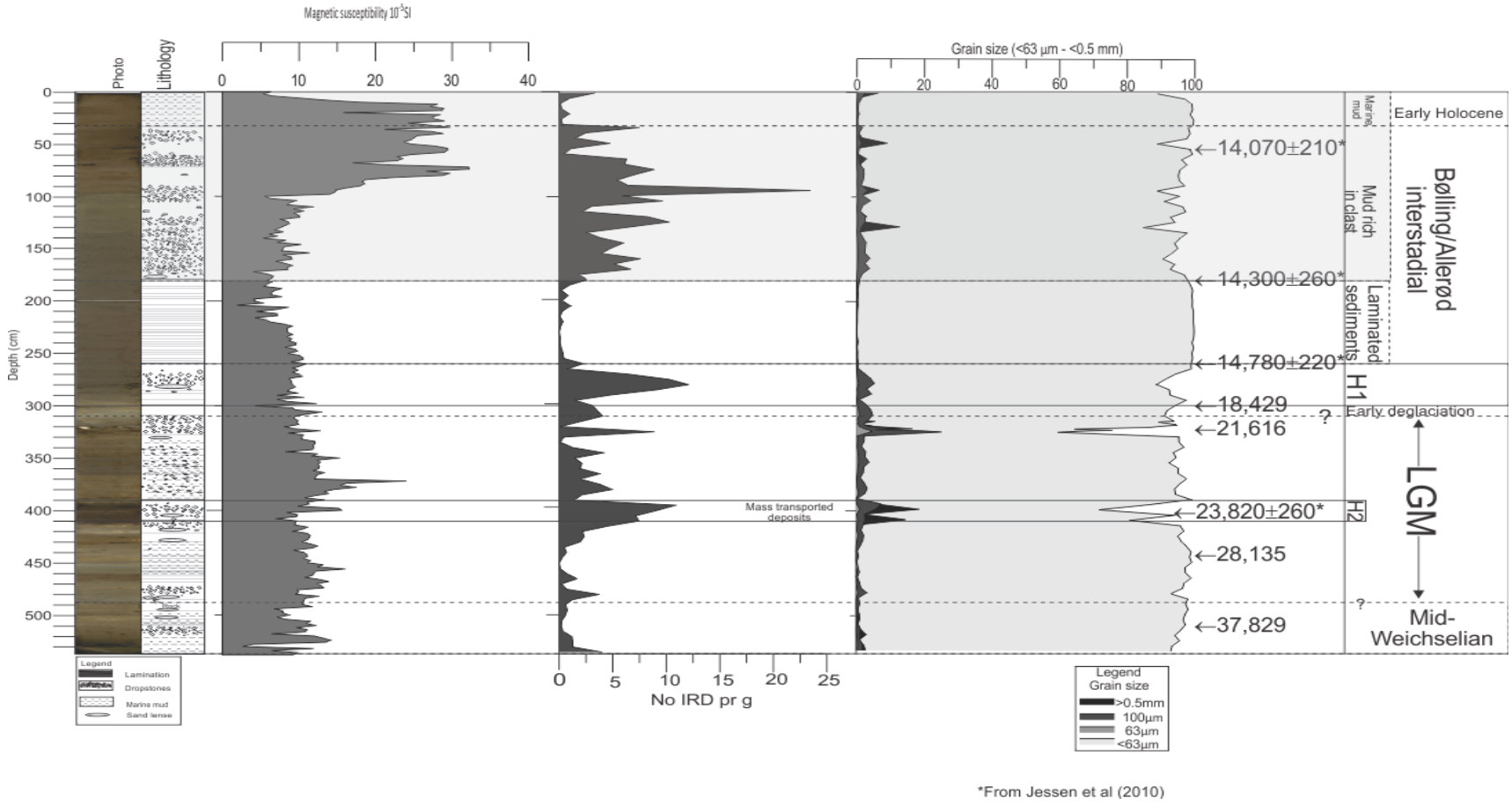

Figure 38: Proxy data for HH12 – 930 GC. The magnetic susceptibility in this core appears to be disturbed, as it does not show the distinct drop at Heinrich Event 2. The boundary between the Mid – Weichselian and the LGM is unclear, however, it is correlated with a similar layer found in HH14 – 002 GC found just above 30,070 cal yr BP. The boundary between the early deglaciation and Heinrich Event 1 is uncertain, but is estimated to be at a peak in IRD as seen in HH14 – 002 GC. All ages are presented as cal. yr BP. LGM = Last Glacial Maximum, H2 = Heinrich Event 2, H1 = Heinrich Event 1

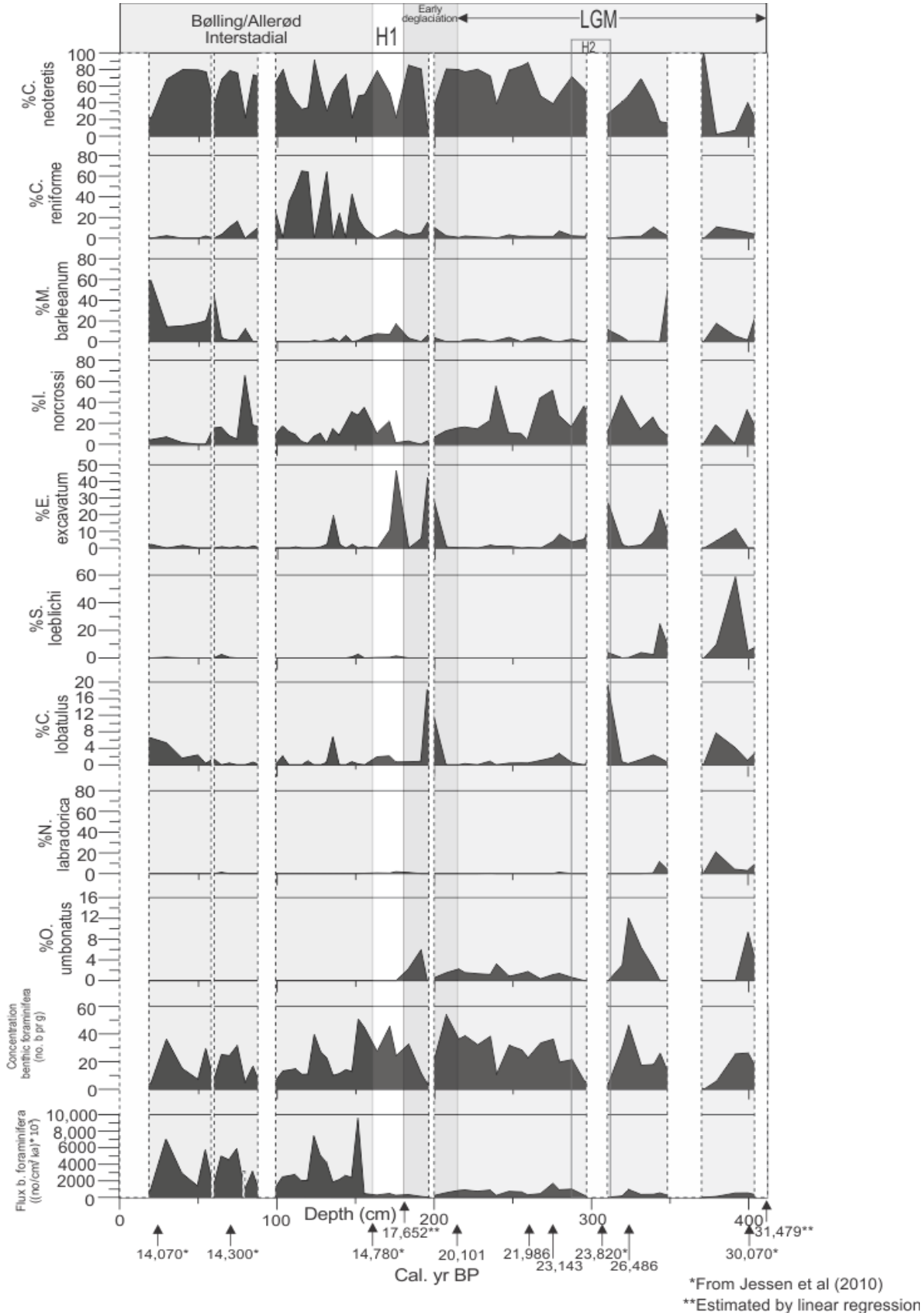

Figure 39: The dashed lines indicates samples in the core which contains less than 80 foraminifera, and is there for considered as a non - representative sample, and therefore not taken into account. The Heinrich Event 2 contained few foraminifera, compared to Heinrich Event 1. During the rest of the LGM after Heinrich Event 2 C. neoteretis is dominating. All ages are presented as cal. yr BP. LGM = Last Glacial Maximum, H2 = Heinrich Event 2, H1 = Heinrich Event 1

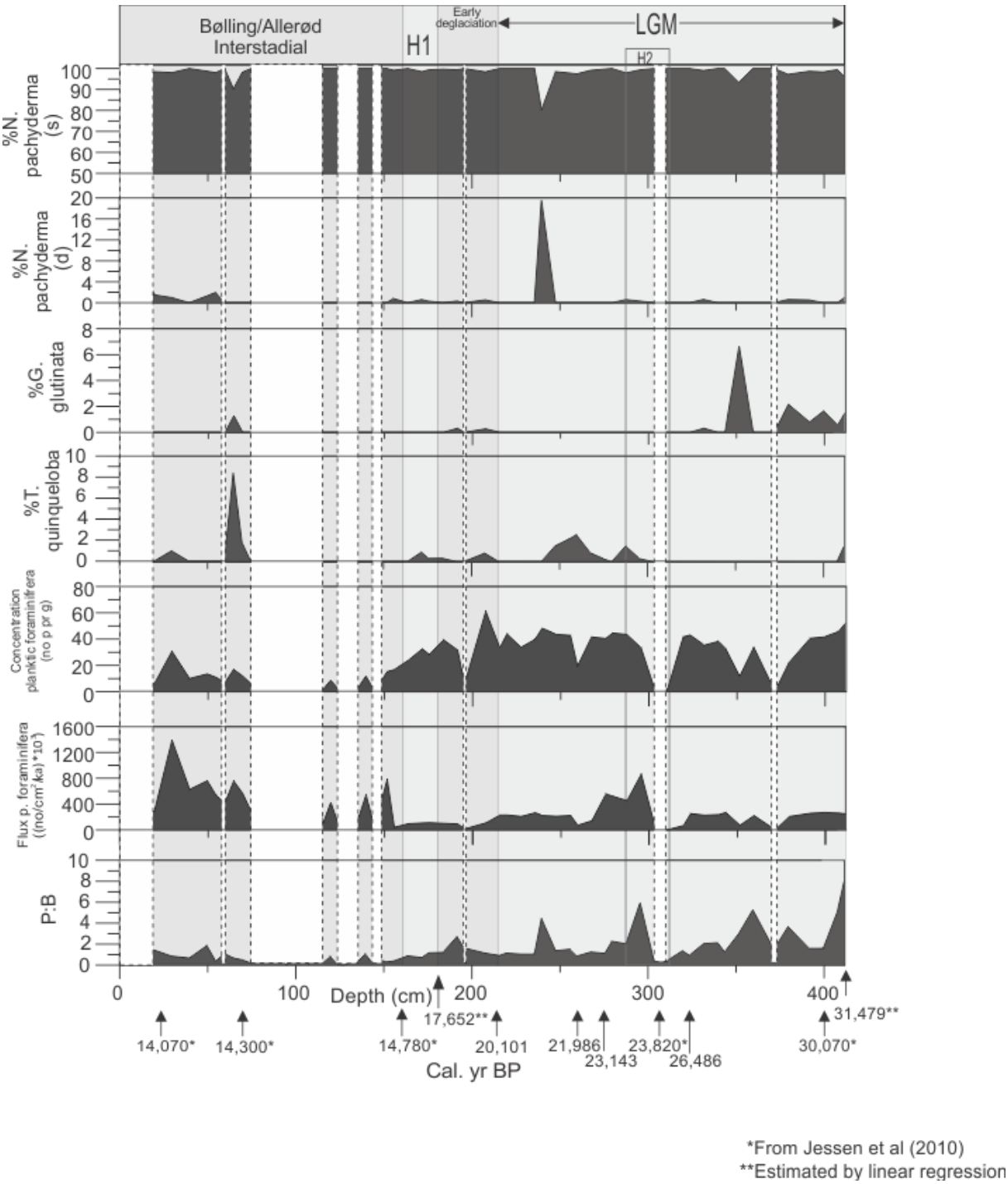

Figure 40: The dashed lines indicates samples in the core which contains less than 80 foraminifera, and is there for considered as a non - representative sample. The uppermost part of the core contained very few foraminifera. N. pachyderma (s) is the dominating planktic species throughout the whole core. The P:B ratio is calculated by the concentration of planktic foraminifera divided by the concentration of benthic foraminifera. All ages are presented as cal. yr BP. LGM = Last Glacial Maximum, H2 = Heinrich Event 2, H1 = Heinrich Event 1.

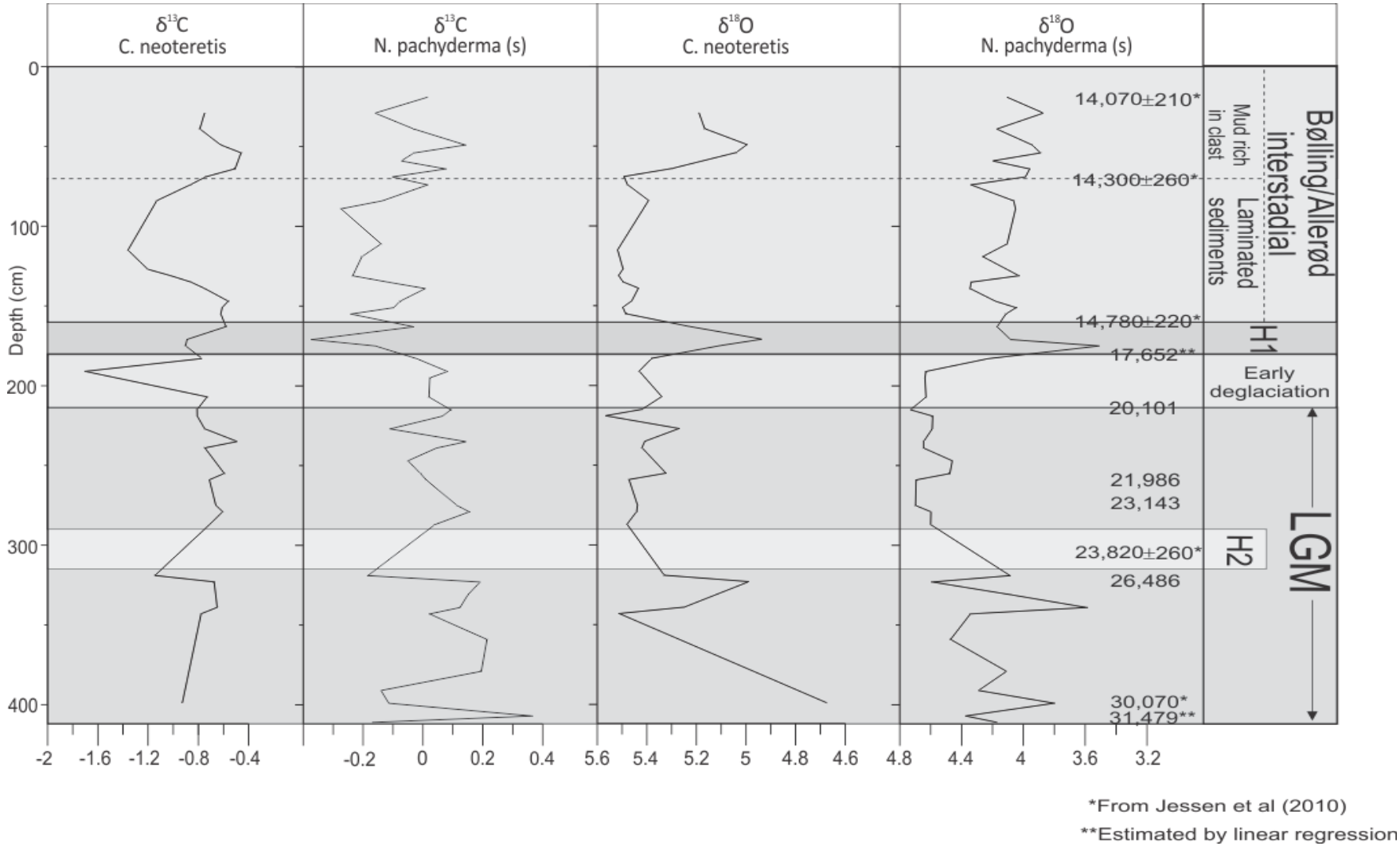

Figure 41: Figure showing stable isotope analysis for sediment core HH14 – 002 GC. The planktic and benthic $\delta^{18}O$ values stays relatively high after 23,820 cal yr BP. Heinrich Event 1 differs from Heinrich Event 2 by low isotopic values, while the Bølling/Allerød Interstadials is characterized by moderate isotope values. The benthic $\delta^{18}O$ value in the bottom of the core is low. All ages are presented as cal. yr BP. LGM = Last Glacial Maximum, H2 = Heinrich Event 2, H1 = Heinrich Event 1.

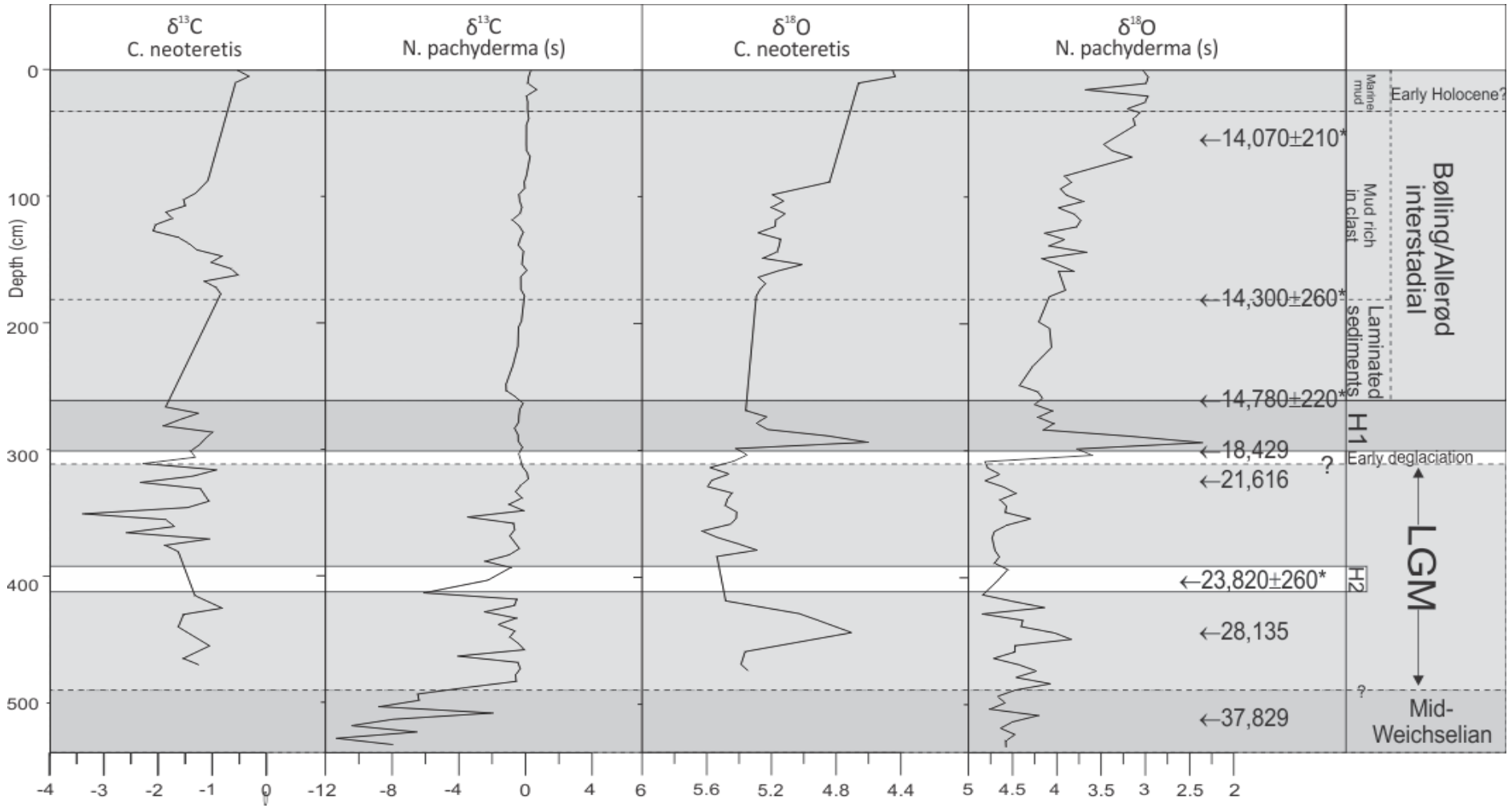

Figure 42: Stable isotope analysis for sediment core HH12 – 930 GC. The $\delta^{13}C$ (carbon) and $\delta^{18}O$ (oxygen) isotope are divided into intervals based on the different values that appears down – core. The Mid- Weichselian is characterized by extreme low planktic carbon values. The Last Glacial Maximum (LGM) is characterized by high oxygen values, while. Heinrich Event 1 (H1) appears to have low benthic and planktic oxygen values. After H1 the oxygen values seems to have a decline upward in the core.

7. 1 Mid – Weichselian (> 37,829 cal yr BP – 30,070 cal yr BP)

This interval is found in HH12 – 930 GC (Figure 38). The x – ray photo (Figure 26) shows relatively homogenous sediments with IRD in the lower part, which could indicate a glacial environment. The high content could imply presence of high concentration of icebergs with sediments in the area. The content of IRD decreases towards 37,829 cal yr BP (Figure 38). The low to moderate content of IRD further up (Figure 38) could reflect that the temperature in the ocean was relatively warm, which would imply that the icebergs would have melted before reaching the area (Jessen, 2015). It could also imply that there was little ice rafting, due to little calving or that the iceberg contained only small amounts of sediments. This again could indicate a shift from slightly warmer conditions (interstadials) periods to more glacial conditions, and probably mark the OIS (oxygen isotope stage) 3/2 boundary (35 ka). The content of mud decreases towards the lower part (Figure 35). The sedimentation rate for HH12 – 930 GC between 37,829 cal yr BP and 28,635 cal yr BP is estimated to be 8.16 cm/ka (Table 9). The sediments have very varying colors; from very dark greyish brown to brownish yellow (Figure 25 and 26), which could indicate imprints of

Compared to HH14-002 GC, HH12-930 GC seems to have a lower content of IRD (Figure 37 and 38, respectively) after 37,070 cal. yr BP and into the LGM.

7. 2 > 30,070 – 20,101 cal yr BP (The last glacial maximum)

This interval is represented by unit 14 – 6 to parts of unit 14 – 4 (412 cm to 215) (Figures 17, 18, 19 and 20), and by unit the upper part of 12 – 6 to unit 12 - 4 (490 cm to 310 cm). In HH14 – 002 GC five ages covers this interval; 30,070 cal yr BP (from Jessen et al., 2010), 26,486 cal yr BP, 23,143 cal yr BP, 21,986 cal yr BP and 20,101 cal yr BP (Figure 37). In HH12 – 930 GC the age is between 28,135 cal yr BP and 21,616 cal yr BP (Figure 38). The oldest ages in HH14 – 002 GC are 30,070 cal yr BP, which is situated below a layer containing a clast and sand lenses, and 31,479 cal yr BP at 412 cm (Figure 37). Similar layer containing a clast and a sand lenses is found at 485 cm in HH12-930 GC (Figure 38). The layer in HH12 – 930 GC is younger than 37,829 cal yr and older than 28,635 cal yr (Figure 38). The layers in HH14-002 GC and HH12-930 GC contains high content of IRD (Figure 37 and 38, respectively).

Major meltwater events can be identified by low $\delta^{13}C$ and $\delta^{18}O$ values (Duplessy, et al., 1988; Stein, et al., 1994a; Stein, et al., 1994b), indicated by the low planktic and benthic $\delta^{18}O$ and planktic $\delta^{13}C$ values and is observed HH14 – 002 GC (Figure 41). The low planktic $\delta^{18}O$ could indicate the presence of meltwater, and the low planktic $\delta^{13}C$ could indicate that the ventilation in the surface water was decreased as also suggested by Spielhagen and Erlenkeuser (1994). The low isotope values could correspond in time with Heinrich Event 3, which occurred approximately 27,000 ^{14}C yr BP (between 30,085 and 32,539 cal yr BP) (Bond, et al., 1993). The relative abundance of *N. pachyderma (s)* is high, which indicates glacial conditions and polar surface water (Bauch, et al., 2001). *C. neoteretis* could indicate the presence of chilled Atlantic water (Figure 39), probably flowing as a subsurface current (cf. Jennings & Helgadottir, 1994), with high salinity indicated by the presence of *C. reniforme* (Steinsund, et al., 1994). The presence of *I. norcrossi* indicates that the productivity was relatively high (Steinsund, et al., 1994). From 30,070 cal yr BP to 26,486 cal yr BP there is a high flux of planktic foraminifera (Figure 40), and an increase in the relative abundance of *N. pachyderma (s)* (Figure 40), which indicates glacial conditions and polar surface waters (Bauch, et al., 2001), and also an increase in sea – ice cover (Carsten & Wefer, 1992).

Throughout the LGM the $\delta^{18}O$ values in both HH14-002 GC (Figure 41) and HH12-930 (Figure 42) GC is relatively high. Negative planktic $\delta^{13}C$ value is identified in HH12-930 GC during the first stages of LGM, and one at base of Heinrich Event 2, and at the upper part of LGM both benthic and planktic $\delta^{13}C$ are observed (Figure 42). These negative $\delta^{13}C$ values are interpreted to represent low flux of methane, similar to the interpretation of Consolaro et al (2015).

The rest of the interval in HH14 – 002 GC is characterized by a layers with moderate to high abundance of coarser material or ice rafted detritus (IRD) (Figure 37) which is visible on the x – ray photo (Figure 18). This is increase in IRD is also observed in in HH12-930 GC (Figure 38). Both of these coarse grained layers can be correlated with Jessen et al (2010) (Figure 32 and 33) and give it an age of 23,820 cal. yr BP (Figure 36). The increase in the concentration of

IRD could imply more glacial environment (Bond & Lotti, 1995; Voelker et al, 2002). With a more interstadial environment the iceberg would cause the icebergs to melt due to warmer surface water before being deposited in the area (Jessen, 2015). This interval shows also areas with sand lenses (37) and layered sediments are observed (Figure 37), which according to Andersen et al (1996) could indicate semi – permanent bottom currents. The magnetic susceptibility in HH14-002 GC varies, and has a distinct drop at 315 – 290 cm (Figure 37), which corresponds to unit 14 – 5 (Figure 15, 16, 17, 18). This is according to Kuijpers et al (2001) characteristic for sediments mixed by mass flow processes. This distinct drop in magnetic susceptibility and sudden increase of coarse sediments could be interpreted to have been caused by the deposition of mass transported sediments, and intense ice rafting (Jessen, et al., 2010; Chauhan, et al., 2015; Jessen & Rasmussen, 2015). This event correspond in time with Heinrich Event 2 in the North Atlantic (Bond, et al., 1993; Jessen, et al., 2010; Rasmussen & Thomsen, 2013; Zamelczyk, et al., 2014)

After 23,820 cal yr BP the planktic $\delta^{18}O$ shows high values (4.7 – 4.4 ‰) in HH14-002 GC (Figure 37) probably related to an increase in salinity and temperature in the surface water, and possibly inflow of warm, saline Atlantic water as suggested by Spielhagen and Erlenkeuser (1994). The increase in $\delta^{13}C$ could indicate more ventilated surface water, and that there was limited ice – cover (Spielhagen & Erlenkeuser, 1994)

C. neoteretis peaks throughout this interval (Figure 39), which could indicate the presence of Atlantic Water, flowing as a subsurface current (cf. Jennings & Helgadottir, 1994) and low bottom temperature (-1°C) (Mackensen & Hald, 1988). *C. reniforme* and *E. excavatum f. clavatum* peaks occasionally in this interval (Figure 39), which is typical for the high Arctic glacially influenced environment (Ślubowska-Woldengen, et al., 2007). At 350 cm there is an increase of *M. barleeanum* (Figure 39), which could indicate bottom water current (Murray, 1984), and increased sedimentation rate (Mackensen, et al., 1985) and increase of chilled Atlantic water (Polyak & Solheim, 1994; Polyak & Mikhailov, 1996). The higher relative abundance of *I. norcrossi* (Figure 39) indicates increased flux of organic matter (Jennings, et al., 2004), higher productivity and the presence of seasonal sea – ice

cover (Steinsund, et al., 1994). *M. barleeanum* and *I. norcrossi* together indicate that the bottom water has changed towards increased salinities and higher temperature, due to increased inflow of Atlantic water (Ślubowska, et al., 2005).

The flux of benthic and planktic foraminifer's decreases (Figure 39 and 40, respectively), which could indicate a more unstable environment. This is indicated by the increase of *E. excavatum f. clavatum* and *C. reniforme* (Figure 34). *E. excavatum f. clavatum* is found in areas with high turbidity with low salinities and temperatures (Steinsund, et al., 1994). It is also considered an opportunist, which is found in areas with low number of foraminifera per gram sediments (Steinsund, et al., 1994). C. reniforme is also considered an opportunist, and is adapted to stressed and unstable environments (Osterman & Nelson, 1989). There is an increase of C. lobatulus, which is associated with strong bottom current (Hald & Vorren, 1984; Husum & Hald, 2004b).

From 23,820 cal yr BP to 20,101 cal yr BP the magnetic susceptibility in HH14-002 GC varies, but decreases slightly after 23,643 cal yr BP (Figure 37). This could, together with increase in relative abundance of *N. pachyderma (s)* (Figure 40) indicate an inflow of Polar surface water and a weakened current strength (Jessen, et al., 2010). The high abundance of *N. pachyderma (s)* could indicate glacial conditions until a slightly increase in the subpolar species *N. pachyderma (d)* at 240 cm (Figure 40). N. pachyderma (d) prefers temperatures around 10-12°C (Schmidt, et al., 2004), and indicates warmer surface waters. The abundance of *C. neoteretis* is relatively high and stable (Figure 39), which indicate that the area is influenced by chilled Atlantic water (Mackensen & Hald, 1988), perhaps as a subsurface current (Jennings, et al., 2004). The abundance of *I. norcrossi* (Figure 39) could indicate that seasonal sea – ice cover was present, a higher productivity (Steinsund, et al., 1994), and that the salinities were relatively high and stable (Korsun & Hald, 1998).High planktic $\delta^{18}O$ values (Figure 41) could indicate an inflow of warm, saline Atlantic water (Spielhagen & Erlenkeuser, 1994).

The number of IRD per g stays in HH14-002 GC moderate (Figure 37), which could indicate some degree of calving of the ice sheet. The sedimentation rate for this interval is estimated

to be between 23.34 cm/ka to 13.81 cm/ka (Table 8). In this interval the color of the sediments is mostly dark grey to dark greyish brown (Figure 17 and 18).

7. 3 Early deglaciation (20,101 cal yr BP)

At 20,101 cal yr BP there is an increase in mud in both of the cores (Figure 15 and 22). The content of IRD declines, but an increase in gran sizes between 63 and 100 µm is observed (Figure 34 and 35). This could indicate moderate fluxes of sea ice/and or iceberg, since sand – sized sediments are too heavy for current transportation (e.g., Ruddiman, 1977; Bond et al., 1993; Andrews, 200). The stable isotope values decreases slightly after 20,101 cal yr BP, which could indicate a minor influence of meltwater (Spielhagen & Erlenkeuser, 1994). There is a small decrease of *N. pachyderma (s)* (Figure 40), which is still the dominating planktic species, meaning that the conditions was still cold, and that polar surface water persisted in the area (Bauch et al., 2001). It is possible that *N. pachyderma (s)* calcified below the meltwater layer, and thus did not recorded low values in the planktic $\delta^{18}O$. The flux of planktic foraminifera is moderate (Figure 40), and the benthic flux decreases (Figure 39). The benthic foraminifera fauna is dominated by *E. excavatum f. clavatum* together with *C. reniforme* in the early stage of the deglaciation (Figure 39), which indicates a more stressed and a typical glaciomarine environment (Hald & Korsun, 1997).

The stable isotope values decreases in HH14-002 GC (Figure 41), and the concentration of IRD increases towards 17,652 cal yr BP, implying an increase in meltwater, and fluxes of sea ice/icebergs. In HH12-930 GC a decline in benthic $\delta^{13}C$ values is observed between 21,616 and 18,429 cal. yr BP (Figure 42). This is could indicate higher fluxes of methane close to the seafloor, causing low rates of AOM.

7. 4 Heinrich Event 1 (18,429 – 14,780 cal yr BP)

The age of Heinrich Event 1 inHH14-002 GC is estimated by linear regression to be 17,652 ±444 cal years BP (Figure 37). In this interval the magnetic susceptibility in HH14 – 002 GC increases (Figure 37). There is a clear decline in both planktic and benthic $\delta^{18}O$ values in HH14-002 GC and HH12-930 GC (Figure 41 and 42, respectively) and a decrease in planktic

$\delta^{13}C$ in HH14-002 GC (Figure 39), indicating presence of low – saline waters, caused by icebergs and sea ice (Spielhagen & Erlenkeuser, 1994). This is typical for Heinrich Event 1 on the Svalbard margin (Rasmussen, et al., 2007; Jessen, et al., 2010; Zamelczyk, et al., 2014). Low planktic $\delta^{13}C$ values could imply decreased ventilation of the surface water, and possibly the presence of seasonally sea ice (Spielhagen & Erlenkeuser, 1994). The low planktic and benthic $\delta^{18}O$ observed together with the decline in $\delta^{13}C$ values GC in HH14-002 GC and HH12-930 GC (Figure 41 and 42, respectively), could indicate a stratification of the water column (Bond, et al., 1993). The input of IRD in HH14-002 GC increases and the amount of mud declines (Figure 37). The P:B ratio decreases, and so does the planktic and benthic flux (Figure 40 and 39, respectively). This low ratio could be due to dissolution of planktic foraminifera (Berger, 1968; Berger, 1973; Berger, 1979; Malmgren, 1983), however, most likely it could reflect a low planktic production rate (Rasmussen et al., 1996a). Polar regions with extensive winter sea ice cover and unstable conditions could be indicated by low P:B ratios and low planktic production (Vilks, 1969; Vilks, 1970; Vilks, 1975; Vilks, 1989; Gibson, 1989; Scott, et al., 1989a; Scott, et al., 1989b; Scott & Vilks, 1991)**.** The abundance of *C. neoteretis* decreases in this interval, which could imply a reduction of the inflow of Atlantic water. An increase in *E. excavatum f. clavatum* could indicate fluctuating bottom conditions, and as suggested by Rasmussen et al (1996a) that the vertical circulation was reduced, with irregular deep-water renewal. This interval correspond in time to the deglaciation and Heinrich Event 1, which has an age of 17,400 cal yr BP – 15,700 cal yr BP according to Jessen et al (2010).

7. 5 Bølling/Allerød Interstadial (14,780 – 14,070 cal yr BP)

From 14,780 cal yr BP to 14,350 cal yr BP there is an increase in mud (<63 µm), and the grain sizes >63 µm drops to a minimum in HH14-002 GC and HH12-930 GC (Figure 37 and 38, respectively). The magnetic susceptibility in HH14 – 002 GC is low (Figure 37). The color of the sediments are olive – brown, which could indicate an interstadial period (Rasmussen, et al., 2013). Low magnetic susceptibility is characteristic for stadials (Rasmussen et al., 1996).

In the Nordic Sea, low magnetic susceptibility values could indicate reduced bottom current strength of the overflow waters during glaciations (Rasmussen, et al., 1996a; Moros, et al., 1997; Ballini, et al., 2006). However, the Bølling/Allerød Interstadials have abnormal low values compared to other interstadials (Rasmussen et al., 1996a). In this interval between 90 and 120 cm laminated sediments were deposited within less than 500 years (Figure 37 and 38). The sedimentation rate was particularly high, and is estimated to be between 195.65 – 187.5 cm/ka (Table 8). This layer can possibly be interpreted to be deposited by turbid meltwater (Elverhøi et al., 1993; Jessen et al., 2010). *N. pachyderma (s)* dominates the planktic fauna, and the flux of planktic foraminifera increases (Figure 40), indicating cold conditions and polar surface waters (Bauch et al., 2001), and high planktic productivity. The P:B ratio and the concentration of planktic foraminifera are moderate (Figure 40). The concentration of benthic foraminifera is low (Figure 39), and the fauna is dominated by the opportunist species *E. excavatum f. clavatum* (Figure 39), which indicates a more stressed environment with high turbidity (Steinsund, et al., 1994), low salinities and temperature (Miller, et al., 1982; Steinsund, et al., 1994). The decrease of *C. neoteretis* could indicate that the inflow of Atlantic water was reduced (cf. Jennings & Helgadottir, 1994). The benthic and planktic $\delta^{18}O$ values increases compared to values observed during Heinrich Event 1, but are lower than during the LGM (Figure 39 and 40). The planktic and benthic $\delta^{13}C$ values in HH14-002 GC is low (Figure 41), and could indicate decreased ventilation (Spielhagen & Erlenkeuser, 1994). In HH12-930 GC the benthic $\delta^{13}C$ values is decreases down to -2.32 ‰ (Figure 42). The negative $\delta^{13}C$ values could indicate that the methane flux was high, and low rates of AOM (Consolaro, et al., 2015). The low amount of IRD (Figure 37), the relatively low isotope values (Figure 41) and the decrease in *C. neoteretis* (Figure 39) could possibly imply that the surface water was cold and covered with low – saline waters, but not perennial sea – ice, indicated by high fluxes of planktic foraminifera.

After 14,300 cal yr BP the number of IRD per g decreases in HH14-002 GC and HH12-930 GC (Figure 37 and 38, respectively). The magnetic susceptibility increases in both HH14-002 GC and HH12-930 GC (Figure 37 and 38, respectively), and this is also observed in HH12 – 930 GC (Figure 35). The color of the sediment inHH14-002 GC is olive brown (Figure 17 and 18).

This could indicate higher flux of iceberg and/or presence of sea – ice, also indicated by low $\delta^{18}O$ values in both HH14-002 GC and HH12-930 GC (Figure 41 and 42, respectively). Between 14,300 and 14,070 cal. yr BP negative $\delta^{13}C$ values down to -2.32 ‰ is observed in HH12-930 GC (Figure 42). The negative values could be due to high methane flux, and a shallow SMTZ. The methane is released to the bottom waters, where it is oxidized by methanotrophic aerobic microbes in the water column (Niemann, et al., 2006). The relative abundance of *C. neoteretis* increases (Figure 39). Together with *M. barleeanum* and *C. lobatulus* (Figure 39) it could indicate strong inflow of Atlantic water and increased food supply (cf. Rasmussen, et al., 2007). *N. pachyderma (s)* decrease at 14,300 cal yr BP, while *T. quinqueloba* increases (Figure 35). An increase of *T. quinqueloba* have been reported in samples from the Nordic Sea coeval in time with the Bølling/Allerød warming (Koç-Karpuz & Jansen, 1992).

After 14,070 cal. yr BP the IRD concentration increased in HH12-930 GC (Figure 38), and the planktic and benthic $\delta^{18}O$ values decreased (Figure 42), which could correspond to the Younger Dryas stadial (12,600-11,500 cal. yr BP). Higher abundance of marine mud in HH12-930 GC (Figure 38) could represent the early part of Holocene.

8. Discussion

In this chapter the interpretation of HH14 – 002 GC and HH12 – 930 GC will be discussed. Core HH14-002 GC was taken at the rim of a pockmark in normal marine sediments unaffected by gas seepage. This record will be discussed in terms of only paleoceanography. Core HH12-930 GC taken from inside the pockmark show signs of being affected by gas seepage, and will be discussed in terms of paleoceanography and effects of gas leakage on the proxy data. The destruction of the magnetic susceptibility signal will be discussed below. The chapter will be divided into three parts: 1) the glacial history of the area, where the results regarding the lithology, magnetic susceptibility, isotope analysis, grain sizes and the age of the sediments of both cores will be interpreted. The interpretation will be discussed and compared to other studies to check whether correlation are possible. 2) Paleoceanography, where the results from the foraminiferal assemblage analysis from HH14-002 GC will be discussed. The paleoceanography will be linked up to the glacial history and the correlation in the first part. 3) Gas seepage. In this part the results from the isotopic analysis from HH12 – 930 GC will be interpreted and discussed, and compares with the interpretation in part 1) and 2) to see if there is a link between the timing of the gas emission and paleoceanographic development in the area.

7. 1 The glacial history of Vestnesa Ridge

7. 1. 1 Middle Weichselian and possibly Heinrich Event 3

Glacial periods in the North Atlantic are characterized by a major increase in delivery of ice – rafted and terrigenous debris, which has been documented by several studies (Ruddiman & McIntyre, 1976; Fillon, et al., 1981; Alm, 1993; Heinrich, 1988; Heinrich, et al., 1989). Throughout the Middle Weichselian periods of extensive iceberg production occurred and ice-rafted material was found in the north-eastern part of the Norwegian-Greenland Sea (Andersen, et al., 1996). During Isotope stage 3 (59-27 ka) Andersen et al. (1996) reports presence of hemipelagic mud with ice-rafted material, turbidites and hemipelagic sediments, where the main source of IRD was the eastern Svalbard-Barents Sea area. In core HH12-930

GC the sediments deposited before 37,829 cal yr BP (Figure 38) consist of marine mud with occurrence of IRD, which could correspond to the hemipelagic mud with ice – rafted debris described by Andersen et al (1996). Ice-rafted material could reflect advance of the ice sheet at 30 ka, however the finding of shell fragments in glacially reworked sediments dated between 40 and 22 (Elverhøi, et al., 1993), suggests that the Barents Sea was ice – free during that period (Andersen, et al., 1996). It is proposed that the Fennoscandian Ice Sheet (Mangerud, 1991) and the Svalbard Ice Sheet (Landvik, et al., 1992; Mangerud & Svendsen, 1992) did not exist or were limited in size (Andersen, et al., 1996) during most of Isotope stage 3. The mid- Weichselian glaciation (65-60 ka) (Figure 43), which correspond to marine isotope stage 4 (MIS), was followed by a deglaciation that started around 50 ka, which is indicated by the finding of raised beaches on Svalbard (Mangerud, et al., 1998). The relative sea level was estimated to be 65 to 55 meter lower than today between 45 and 35 ka (Lambeck, et al., 2002). Nørgaard-Perdersen et al (1998) interpreted the middle OIS 3 to represent an interglacial or interstadial period. The south-eastern part of the Barents Sea shelf was ice free not much later than 42.7 cal yr BP (39.2 ^{14}C yr BP) (Polyak, et al., 2000). The decrease in IRD in HH12-930 GC (Figure 38) could correspond to this deglaciation in time. This could imply that there was an increased influx of warm Atlantic water, perhaps as a subsurface current, and which resulted in melting of the icebergs before they reached the area (Jessen, 2015). The IRD could have been transported by sea ice, or possibly by the result of mass wasting. Turbidites have been mentioned as a source to ice – rafted and terrigenous material in the North Atlantic during the Isotope Stage 3 (Ruddiman & McIntyre, 1976; Fillon, et al., 1981; Alam, et al., 1983; Heinrich, 1988; Heinrich, et al., 1989), which was also the case along the western Svalbard margin (Andersen, et al., 1996).

Prior to 30,070 cal yr BP the color of the sediments varies in HH14 -002 GC (Figure 17 and 18) and HH12- 930 GC (Figure 25 and 26). There is a shift between olive grey and olive brown sediments, which could indicate minor fluctuations in the climate. Rasmussen et al (2013) reports shifting colors in a sediment core from the north – west slope of Svalbard. The reddish – grey, referred as “pink layers”, corresponds to warm, interstadial periods, while greenish – grey layers corresponds to cold, stadials (Figure 41). The “pink layers” is fine –

grained sediments from Devonian Red Beds. During warming, these sediments are transported in suspension by meltwater from the adjacent ice sheet (Rasmussen & Thomsen, 2013). Rasmussen and Thomsen (2013) correlate these changes in color to the Greenland interstadials and stadials, which are sudden fluctuations in temperature. In HH14 -002 GC a layer containing light olive brown sediments at ca 400 cm, with relatively low content of IRD is observed (Figure 37). The planktic oxygen and carbon isotope are relatively high (Figure 41), which could imply a warmer climate and good ventilation in the water column (Spielhagen & Erlenkeuser, 1994). In HH14 – 002 GC the planktic $\delta^{13}C$ and the planktic and benthic $\delta^{18}O$ values decreases after 30,070 cal yr BP (Figure 41). A layer with high abundance of IRD, a distinct clast and a sand lense is found in both HH14-002 GC at 385 cm (Figure 37) and in HH12-930 GC at 485 cm (Figure 38), which in time could possibly be linked to Heinrich Event 3 (Figure 44) (Heinrich, 1988; Bond, et al., 1992). Vidal et al. 1997 suggest that Heinrich Event 3 has an age of ca 31 cal ka yr BP (28.2 ^{14}C ka yr BP). This can also correspond to the Heinrich Event 3 seen in Rasmussen and Thomsen (2013) (Figure 45). The age of Heinrich Event 3 in the North Atlantic is not well dated, but an age of 27,000 ^{14}C yr BP is preferred (between 30,085 and 32,539 cal yr BP) (Bond, et al., 1993). The increase in IRD in both of the HH14-002 GC and HH12-930 GC (Figure 37 and 38, respectively), together with a decrease in planktic $\delta^{13}C$, and a slightly decline in benthic $\delta^{18}O$ could possibly correspond in time with the event seen in Rasmussen and Thomsen (2013) (Figure 46). Andersen et al (1996) suggest that it could be a certain temporal relationship between clast-rich diamictons deposited on the western Svalbard slope and the IRD – rich sediments, Heinrich layers, deposited in the North Atlantic (Heinrich, 1988; Bond, et al., 1993). The clast-rich diamictons differs from the Heinrich layer (Figure 44) in that they lack the specific limestone and dolomite grains derived from sources in eastern Canada (Bond, et al., 1992), and were not deposited within a few hundred years, as suggested for the Heinrich layers (Lehman, 1993). Instead, they were deposited over a period of 2000 – 5000 years, which could imply that the Svalbard-Barents Sea Ice Sheet disintegrated more frequently than the Laurentide Ice Sheet (Andersen, et al., 1996), and did not collapse through surges as suggested for the Laurentide Ice Sheet (Bond, et al., 1992).

The warming period in MIS 3 could have led to high inflow of meltwater, which cooled the surface water, which could explain the low planktic and benthic $\delta^{18}O$. It is suggested that the onset of Heinrich Event 3 was rather abrupt, (Gwiazda, et al., 1996) and to occur at ca 31 cal ka yr BP (28.2 ^{14}C ka yr BP) (Vidal, et al., 1997).

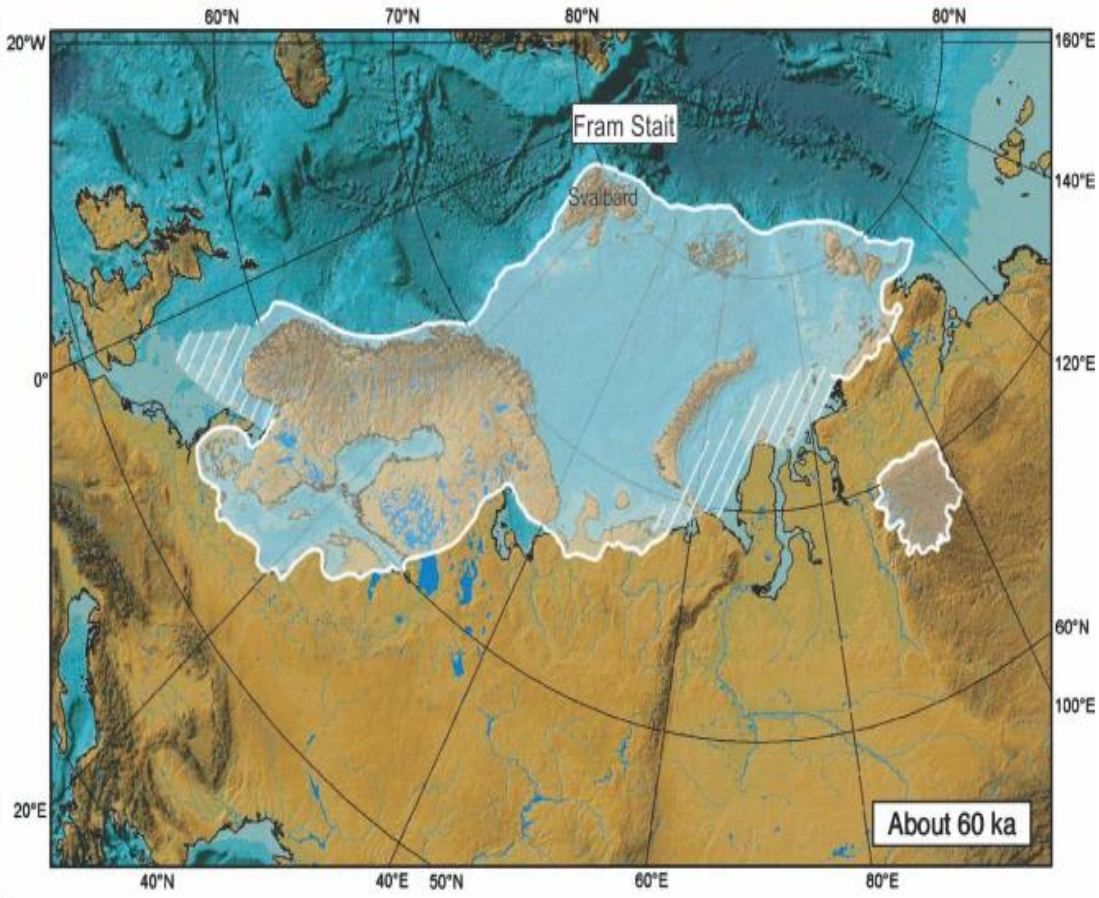

Figure 43: Reconstruction of the ice sheet limit and extend of the Eurasian ice sheet during the Middle Weichselian glacial maximum (60 – 50 ka). The north – western Barents Sea shelf was affected by a major glaciation during the Middle Weichselian (Svendsen, et al., 2004a), where the ice front terminated near the western and northern shelf margins (Mangerud, et al., 1998). Core HH12 – 930 GC (Figure 35) could represent the deglaciation which followed after this glaciation.

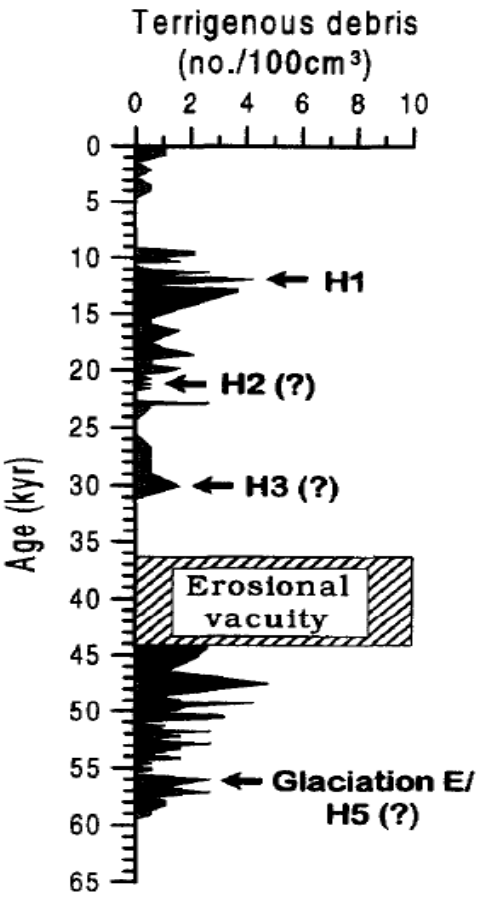

Figure 44: H1, H2, H3 and H5 represent the IRD – rich sediments deposited during Heinrich Events. Numbers of terrigenous grains (>2 mm/100 cm³) from a sediment core from the western Svalbard lower slope plotted against ^{14}C age. Figure from Andersen et al (1996).

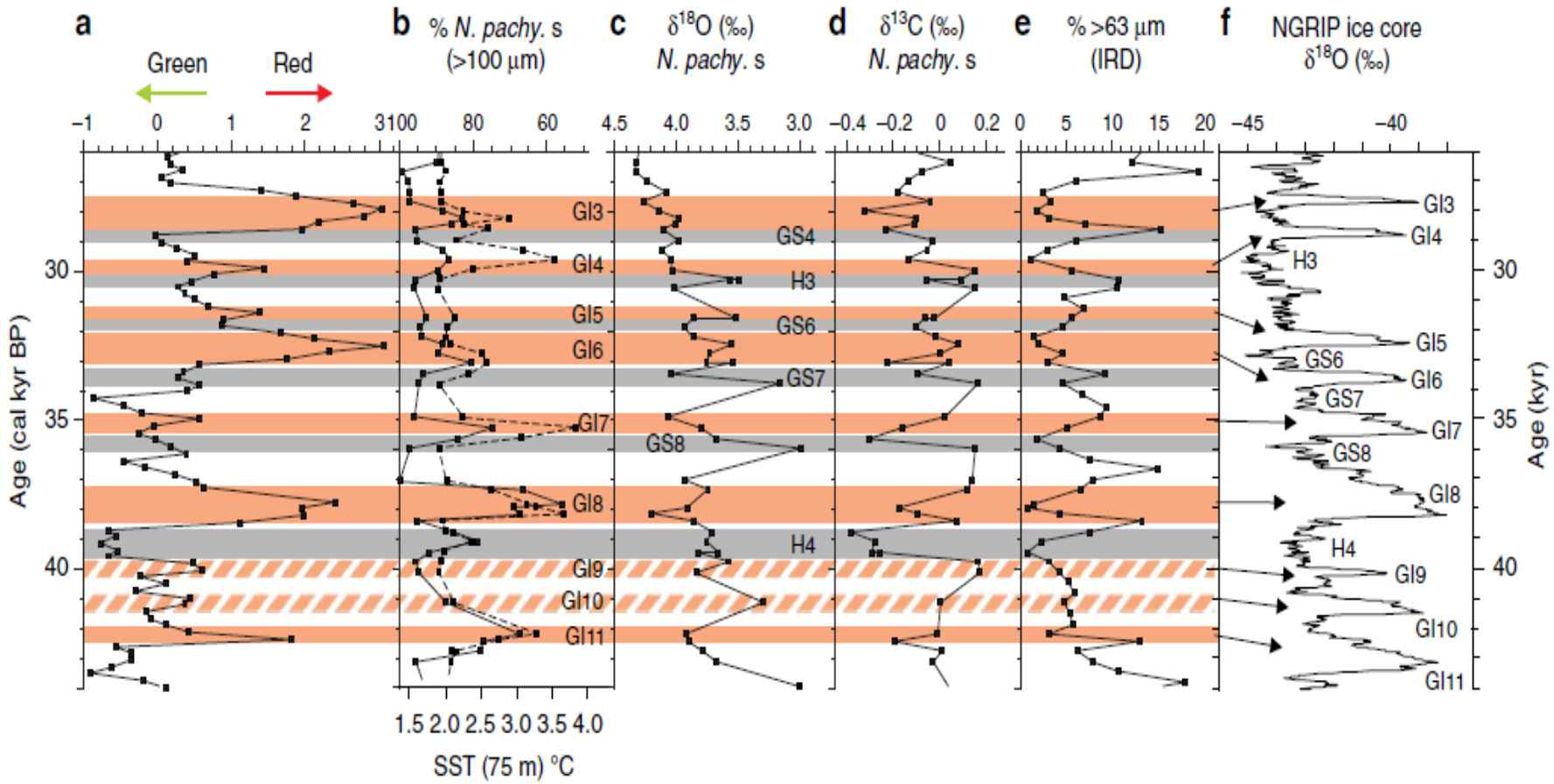

Figure 45: Figure from Rasmussen and Thomsen (2013) which shoes the Greenland interstadial events 11 – 13 in sediment core JM05 – 31GC from the northwest of Svalbard versus the NGRIP ice core. A) Spectrophotometer data showing the red – green color of the sediments in JM05 – 31GC. B) The subsurface temperatures (SST) (dashed line) and the relatively abundance of planktic foraminifera N. pachyderma (s) (>100µm) (solid line). C) Planktic $\delta^{18}O$ values measured from N. pachyderma (s). D) Planktic $\delta^{18}O$ values measured from N. pachyderma (s). E) The weight of grains >63 µm. F) $\delta^{18}O$ values measured on NGRIP ice core on the GICC05 timescale 2,000 years (data from Svensson et al (2008)). GI=Greenland Interstadial, H=Heinrich Event (Rasmussen & Thomsen, 2013).

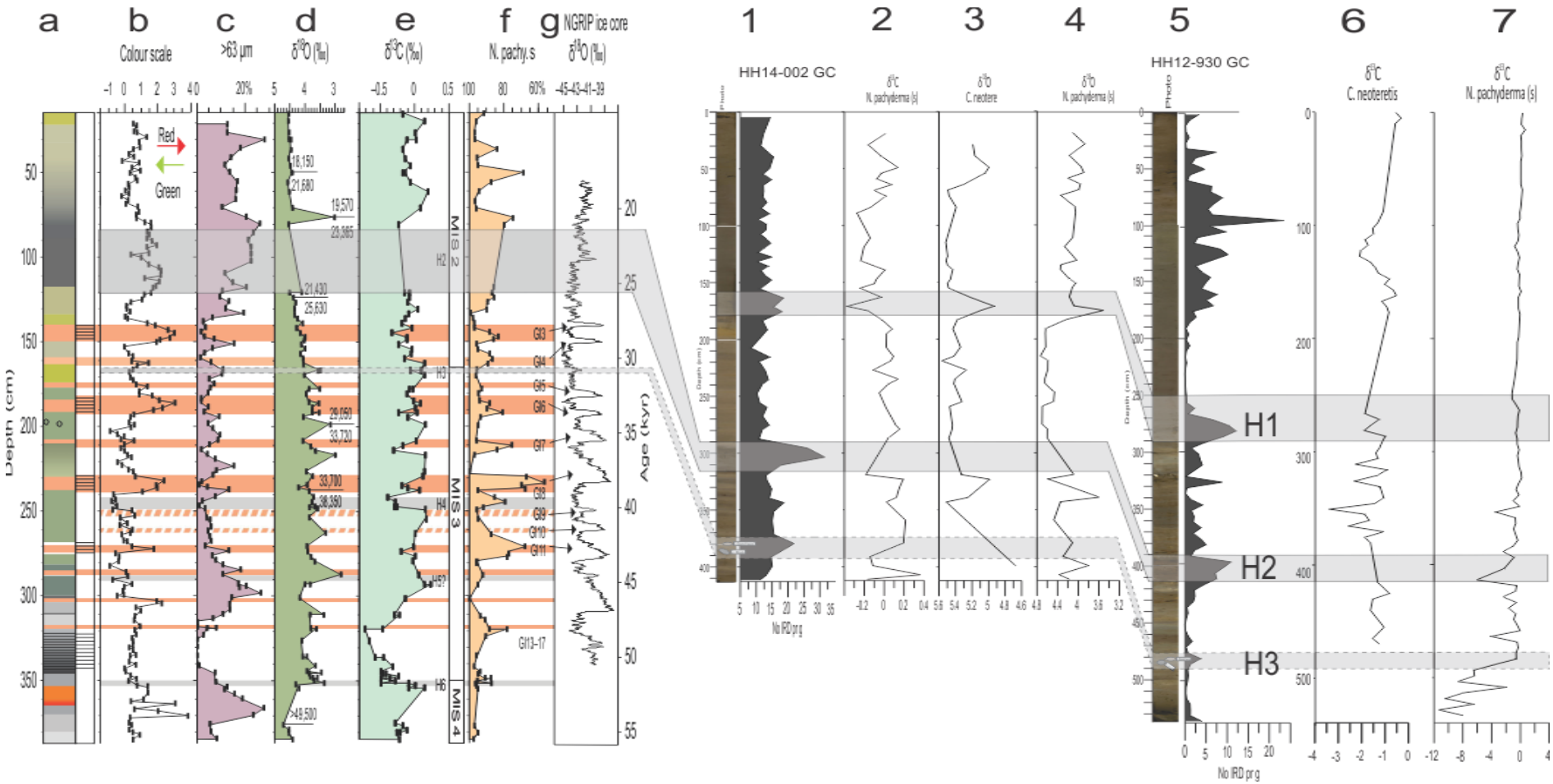

Figure 46: Figure from Rasmussen and Thomsen (2013).1 A) Lithology log showing color variations. B) The subsurface temperatures (SST) (dashed line) and the relatively abundance of planktic foraminifera N. pachyderma (s) (>100µm) (solid line). C) The weight of grains >63 µm. D) Planktic $\delta^{18}O$ values measured from N. pachyderma (s). E) Planktic $\delta^{13}C$ values measured from N. pachyderma (s). F) The relatively abundance of planktic foraminifera N. pachyderma (s) (>100µm) G) $\delta^{18}O$ values measured on NGRIP ice core on the GICC05 timescale 2,000 years (data from Svensson et al (2008)). GI=Greenland Interstadial, H=Heinrich Event (Rasmussen & Thomsen, 2013). 1) Sediment core HH14 – 002 GC with number of IRD per gram. 2) Planktic $\delta^{13}C$ values measured from N. pachyderma (s). 3) Benthic $\delta^{18}O$ measured from C. neoteretis in HH14-002 GC. 4) Planktic $\delta^{18}O$ measured from N. pachyderma (s) in HH14-002 GC. 5) Sediment core HH12 – 930 GC and number of IRD per gram. 6) Benthic $\delta^{13}C$ from C. neoteretis in HH12-930 GC. 7) Planktic $\delta^{18}O$ measured from N. pachyderma (s) inHH12-930 GC. Possibly H1, H2 and H3 (Heinrich Event) are indicated in the figure. H2 and H1 will be discussed further in chapter 7. 1. 2 and 7. 2. 2, respectively.

7. 1. 2 The LGM and Heinrich Event 2

According to Andersen et al (1996), Landvik et al (1998) and Siegert and Dowdeswell (2002) the Svalbard-Barents Sea Ice Sheet Started to grow at ca 32,000 cal yr BP, which is related to a drop in global sea level (Elverhøi, et al., 1993). Open-water conditions acted as moisture supply to the growing ice sheet (Hebbeln, et al., 1994). In core HH14-002 GC and HH12-930 GC laminated sediments with a grey to olive grey color are observed. During stadials the magnetic susceptibility is considered to measure high values (Rasmussen, et al., 1996a). This is in good agreement with the magnetic susceptibility in HH14 – 002 GC, which is relatively high until 26,486 cal yr BP (Figure 37). The amount of IRD in the lowest part of core HH14 – 002 GC (Figure 37) could correspond to first period of the LGM. According to Elverhøi et al (1995) the first period of the Last Glacial Maximum (LGM) is characterized by low influx of icebergs and low accumulation rate.

Jessen et al (2010) noted a decline in $\delta^{13}C$ values and increase in IRD at the western Svalbard margin at 27,000 cal yr BP, which was interpreted to correlate with the onset of glacial advance to the shelf, which is in accordance with earlier reconstructions (Elverhøi, et al., 1995; Andersen, et al., 1996; Mangerud, et al., 1998; Vogt, et al., 2001). An increase in IRD (Figure 34) followed by a decrease in $\delta^{13}C$ values (-1.5‰) seen below 26,486 cal yr BP in HH14 – 002 GC (Figure 41) and a decline in planktic $\delta^{13}C$ HH12-930 GC below 28,135 cal yr BP (Figure 42) could possibly correspond to this event in time, and imply an ice sheet advance. This increase in IRD is also observed in HH12 – 930 GC (Figure 38). The sea level had reached its minimum at 26,000 cal yr BP, which is agreement with the ice sheet advance (Peltier & Fairbanks, 2006). Between 30,070 cal yr BP and 23,820 cal yr BP the sedimentation rate varied between 21 cm/ka to 6 cm/ka in HH14 – 002 GC (Table 8), and between 28,135 cal yr BP and 23,820 cal yr BP the sedimentation rate for HH12 – 930 GC is estimated to be 7.72 cm/ka (Table 9). In HH14 – 002 GC (Figure 37) the concentration of IRD is moderate, and in HH12 – 930 C (Figure 38) the content is low. Low sedimentation rates and low IRD concentrations have been observed between 30,000 and 24,000 cal yr BP on the slope of Svalbard (Andersen, et al., 1996; Mangerud, et al., 1998; Jessen, et al., 2010). After 26,486 cal yr BP the amount of IRD decreased in HH14-002 GC (Figure 37). During cold stages the rate of terrigenous input to the ocean tends to be low due to the lack of meltwater and extensive ice (Gard, 1987). According to Jessen et al (2010) the low IRD concentration could

be a due to a cold based, thin ice (Elverhøi, et al., 1998) which was a result of the final ice advance to the shelf break (Andersen, et al., 1996). Cold based ice transport much less debris (Elverhøi, et al., 1998). Jessen et al (2010) suggest that the ice sheet reached the western Svalbard shelf break at ca 24,000 cal yr BP. At this point the depositional environment changed and erosion of the western banks ended (Andersen, et al., 1996). Hebbeln et al (1994) suggest that during an advection of warm Atlantic water which entered the Norwegian – Greenland Sea, the Svalbard – Barents Sea Ice Sheet expanded to the shelf edge, and started to break up after reaching its maximum position. Glacigenic sediments being bulldozed to the upper slope can result in excess pore pressure in the underlying sediments (Laberg & Vorren, 1995; Elverhøi, et al., 1997; Elverhøi, et al., 2002). The upper slope becomes unstable within a few centuries after glacial peak, which can result in mass wasting (Dimakis, et al., 2000). A distinct unsorted layer with high content of IRD and dark color is observed in HH12 – 930 GC (Figure 38) and HH14 – 002 GC (Figure 37), which in addition showed low magnetic susceptibility (Figure 37). Rasmussen et al (2007) observed a similar unsorted layer with low magnetic susceptibility with an age of 22,267 cal yr BP, interpreted as a debris flow in a sediment core from the southwestern Svalbard slope. Intervals with low magnetic susceptibility correlates with Heinrich events and stadials (Rasmussen, et al., 1996a). The turbidite corresponding to Heinrich Event 2 (Figure 47) have been correlated with Jessen et al (2010), which gives it an age of 23,820 cal yr BP (Figures 36). Andersen et al (1996) suggest also a debris flow to be deposited during peak glacial-period. Jessen et al (2010) found mass transported sediments in all of the sediment cores in the study indicating that they were deposited simultaneously at 23,820±260 cal yr BP, and that presence of the mass transported deposit is taken as a sign of a fully glaciated western Svalbard shelf (Laberg & Vorren, 1995; Vorren & Laberg, 1997; King, et al., 1998; Dowdeswell & Elverhøi, 2002; Jessen, et al., 2010). The age by Jessen et al (2010) is 2400 cal years earlier than earlier reconstructions (Elverhøi, et al., 1995; Landvik, et al., 1998; Dowdeswell & Elverhøi, 2002), however, in good agreement with the indication by Andersen et al (1996), which proposed that the shelf was fully glaciated before 22,600 cal yr BP.

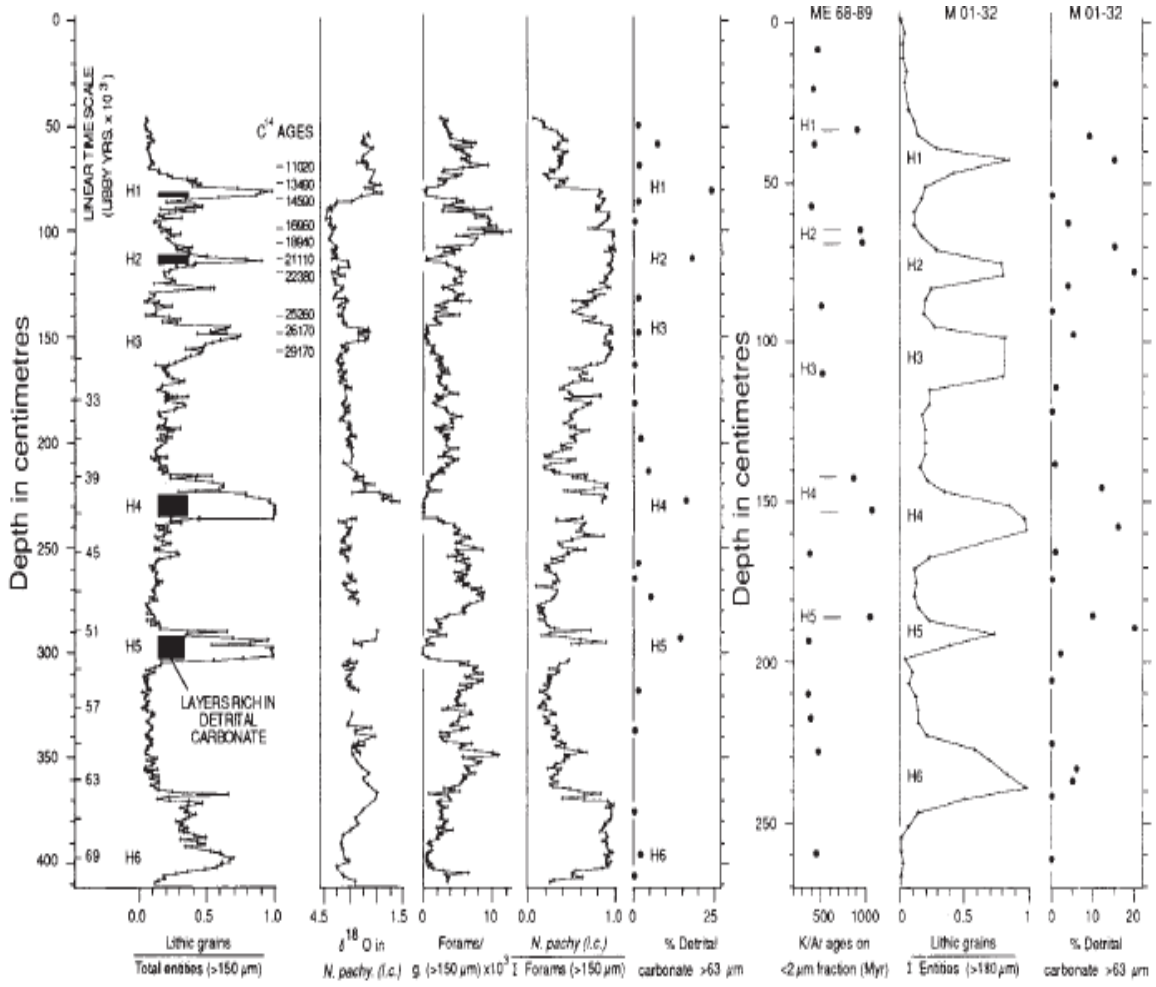

Figure 47: Figure from Bond et al (1992) showing summary of radiometric, planktic $\delta^{18}O$, foraminifera and lithic measurements in cores from DSDP site 609 (50°N and 24°W see Broecker et al (1992)). H = Heinrich events, and ages are in ^{14}C yr BP. Low foraminifera concentration occurs in material >150 μm in the Heinrich layers in the cores (Bond, et al., 1992).

7. 1. 3 Early deglaciation and Heinrich Event 1

Vogt et al (2001) proposed that the ice sheet started to retreat at ca 19,100 cal yr BP. Other studies suggest that the initial retreat of the Svalbard – Barents Sea Ice Sheet started 17,700 cal yr BP (Elverhøi, et al., 1995; Andersen, et al., 1996; Landvik, et al., 1998; Mangerud, et al., 1998). Knies et al (1998) suggest that the beginning of the last deglaciation began 18,325 cal yr BP. Rasmussen et al (2007) observed hemipelagic sedimentation in Storfjordrenna with an age of 19,430±150 cal yr BP. The glacier retreated from the shelf break before 20,000 cal yr BP, based on the onset of the hemipelagic sediments in the Storfjordrenna (Rasmussen, et al., 2007). Jessen et al (2010) suggest glacial retreat at 20,500±500 cal yr BP, based on IRD in sediment cores from the western Svalbard slope. An age of 20,101 cal yr BP in HH14 – 002 GC of 20,101 could correspond in time with the early stage of deglaciation (Figure 37) mention by Jessen et al (2010). At 20,101 cal yr BP a peak in IRD is observed (Figure 37). In HH12 – 930 GC the early deglaciation occurred between 21,616 and 18,429 cal yr BP (Figure 38). Moderate magnetic susceptibility values are observed in HH14 – 002 GC, which could indicate a transition from glacial to more interstadials environments. Low magnetic susceptibility are also associated with fine – grained sediments, mainly clay and silt (Rasmussen, et al., 1996a), however, the content of IRD is moderate, with a minimum value after 20,101 cal yr BP in HH14-002 GC (Figure 37). The amount of gran sizes between 63 – 100 µm is increasing in this interval (Figure 37). Outside the north-eastern Svalbard high IRD concentrations are observed shortly after 20,000 cal yr BP (Knies, et al., 1999; Kleiber, et al., 2000; Knies, et al., 2001). Elverhøi et al (1995) reports an event of meltwater production that lasted until 15,016 cal yr BP (13,000 ^{14}C yr BP), indicated by δ^{18}O values from the western Svalbard slope, at the same time as the Svalbard – Barents Sea Ice Sheet retreated from the shelf break west of Isfjorden. High amounts of coarse material mark this period on the upper slope, indicating increased rates of iceberg calving. Low δ^{18}O values interpreted as a meltwater signal in slope sediments are

also reported by Andersen et al (1996). On the lower slope the early disintegration of the ice sheet is marked by low $\delta^{18}O$ values and low accumulation rates of fine-grained and ice-rafted sediments, meaning that the lower slope had not been affected by the early phase of deglaciation (Elverhøi, et al., 1995). The boundary between the LGM and the deglaciation in HH14 – 002 GC is marked by a peak in IRD (Figure 37), which is also observed in HH12 – 930 GC (Figure 38), and a slight drop in benthic and planktic $\delta^{18}O$ values in both cores (Figure 41 and 42, respectively), which can be interpreted as a minor meltwater signal, and could correspond to a meltwater event suggested by Elverhøi et al (1995) and Andersen et al (1996). At the onset of deglaciations and glaciations increased sedimentation rates due to increased input of terrigenous material by meltwater and from eroding glacial ice occur (Gard, 1987). Jessen et al (2010) observed a decrease in IRD concentration from 20,000 to 15,500 cal yr BP, and suggest a reduction in accumulation of snow could have caused a glacial retreat and low IRD concentration. This could also be the reason for the decrease in number of IRD per gram observed in HH14 – 002 GC after 20,101 cal yr BP (Figure 37) and in HH12 – 930 GC between 21,616 and 18,429 cal yr BP (Figure 38). Solar insolation and global sea level was at its minimum prior to the retreat (Peltier & Fairbanks, 2006). On the Norwegian slope laminated sediments were deposited by meltwater plumes. The sediment – laden meltwater plumes originated from a rapidly retreating ice stream (Hjelstuen, et al., 2004; Lekens, et al., 2005). Jessen et al (2010) suggest that this melting of ice could have been linked to increased summer insolation (Laskar, et al., 2004), and rise in eustatic sea level (McCabe, et al., 2005), together with an increase in inflow of Atlantic water at lower latitudes (Rasmussen, et al., 1996a). The North Atlantic Ocean responded dramatically to orbital induced insolation changes during the last glacial/interglacial transition Broecker et al. (1985). At the onset of the deglaciation the insolation increased further. Together with increased heat flux from the increased flow of West Spitsbergen Current, and lead to the glacier to retreat, which released pulses of meltwater (Broecker, et al., 1985)

The stable isotope values continuous to drop in in HH12 – 930 GC after 18,429 cal. yr BP (Figure 38) and in HH14 – 002 GC after 17,652 cal yr BP (Figure 41), and is accompanied by relatively high concentrations of IRD (Figure 38 and 37, respectively). This meltwater

event can correspond to the regional Heinrich Event 1 (Heinrich, 1988; Bond, et al., 1993). This event will be further discussed in chapter 7. 2. 2.

7. 1. 3 Bølling/Allerød Interstadial and early Holocene

At the onset of Bølling Interstadial the Svalbard – Barents Sea Ice Sheet retreated rapidly (Vorren & Kristoffersen, 1986; Mangerud, et al., 1992; Elverhøi, et al., 1995; Polyak, et al., 1995; Polyak & Mikhailov, 1996; Landvik, et al., 1998; Lubinski, et al., 2001). The Bølling Interstadial is characterized by high sedimentation rates from turbid meltwater plumes origin from the Svalbard – Barents Sea Ice Sheet (Elverhøi, et al., 1995; Andersen, et al., 1996; Svendsen, et al., 1996; Birgel & Hass, 2004). In Storfjorden high sedimentation rates are reported from ca 14,332 to 13,911 cal yr BP (12,640 to 12,430 ^{14}C yr BP), which resulted in deposition of laminated fine clays (Rasmussen, et al., 2007). The δ^{13}C and δ^{18}O had a minor increase in HH14-002 GC at the transition from Heinrich Event 1 and Bølling/Allerød Interstadials (Figure 37), but was still low compared to the LGM (Figure 37), which could imply that the surface water was still affected by melt water and iceberg calving as suggested by Jessen et al (2010). The magnetic susceptibility is low 14,780 to 14,300 cal yr BP in HH14 – 002 GC (Figure 34), and in HH12 – 930 GC (Figure 38). Fine-grained laminated mud have been reported to be deposited on the western Svalbard slope and Yermak Plateau between 76°13’ an 81°13’N (Elverhøi, et al., 1995; Birgel & Hass, 2004; Rasmussen, et al., 2007; Jessen, et al., 2010). These laminated sediments is interpreted to be deposited by cold turbid meltwater, and is suggested to originate from the southern Barents Sea (Elverhøi, et al., 1993). It is suggested that the decaying ice sheet released meltwater plumes with large amounts of fine-grained sediments (Figure 46), which was transported by the West Spitsbergen Current (Andersen, et al., 1996). Between 14,780 to 14,300 cal yr BP laminated sediments and a high concentration of fine-grained material and low magnetic susceptibility have been observed in in HH14 – 002 GC (Figure 37) and in HH12 – 930 GC (Figure 38). The

sedimentation rates is estimated to be 187.5 cm/ka for HH14 – 002 GC from 14,780 to 14,300 cal yr BP (Table 8), and 166.6 cm/ka for HH12 – 930 GC (Table 9), which is considered to be high. Low values can be linked to glacial intervals, however, the Bølling/Allerød Interstadials can show lower values in magnetic susceptibility compared to other interglacial intervals (Rasmussen, et al., 1996a). The laminated sediments in HH14 – 002 GC and HH12 – 930 GC is suggested to be deposited by cold turbid meltwater as suggested by Elverhøi et al. (1995), and represent a rapid retreat of the Svalbard – Barents Sea Ice Sheet, same as seen in the study by Jessen et al (2010) (Figure 30). Jessen et al (2010) suggest an increase in insolation and eustatic sea level caused the Svalbard – Barents Sea Ice Sheet to be melting and calve. Increased inflow of Atlantic water flowing as a subsurface current could also have had an impact (Jessen, et al., 2010).

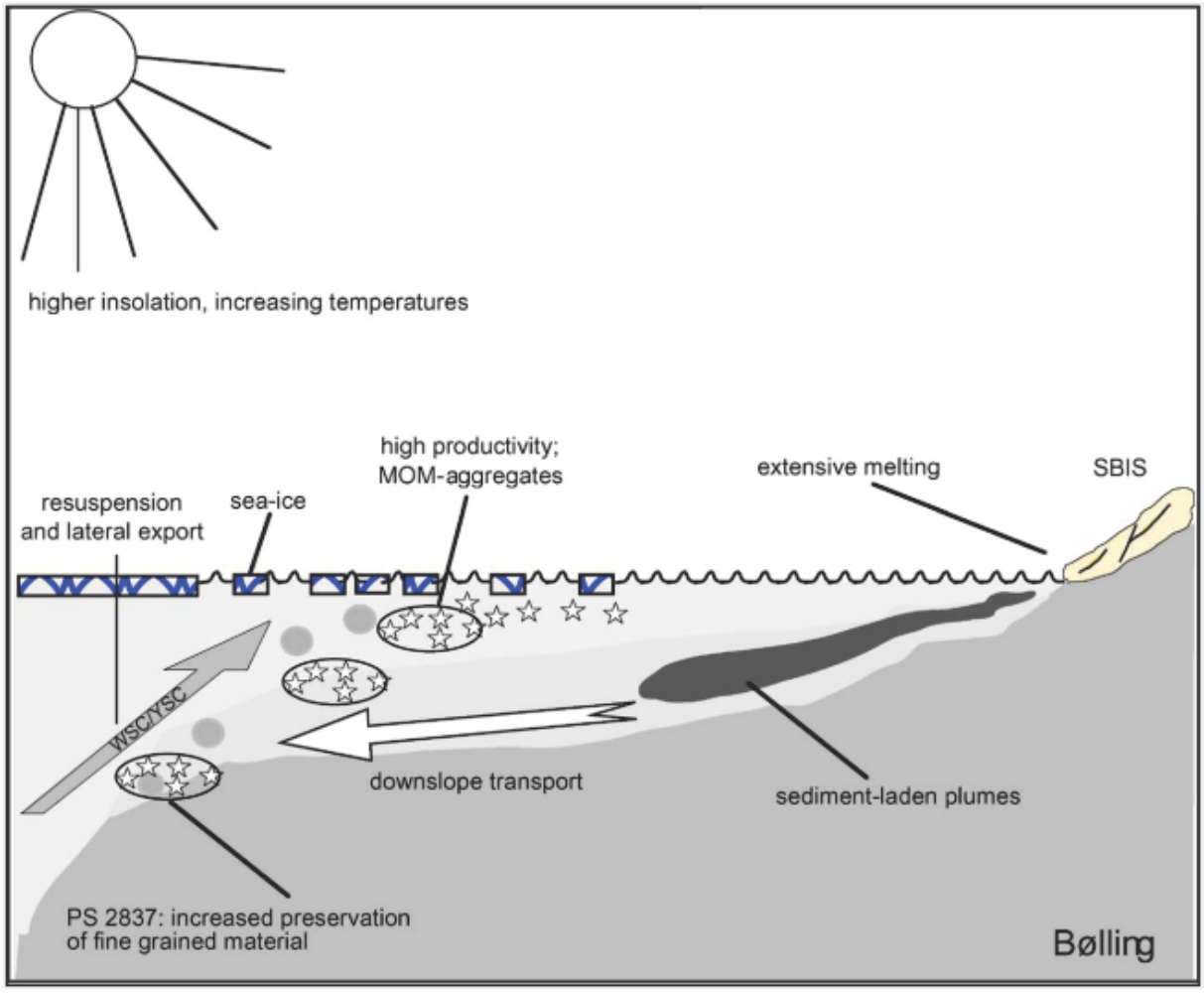

Figure 46: Modified figure From Birgel and Hass (2004) showing the environment during the Bølling Interstadial on the western Svalbard and the western Yermak slope. High amounts of sediments were released in the bottom waters by a sediments – laden meltwater plume from the disintegrating Svalbard – Barents Sea Ice Sheet. MOM = Marine organic matter, which were transported northward by the West Spitsbergen Current (Birgel & Hass, 2004).

After 14,070 cal. yr BP, the concentration of IRD decreases in HH12-930 after a period of high values (Figure 38). The sudden increase of IRD could possibly represent Younger Dryas stadial (12,600-11,500 cal. yr BP) (Ślubowska-Woldengen, et al., 2007), which is observed in records from the North Atlantic and represent a distinct cold event (Koç, et al., 1993; Koç, et al., 1996). However, on the western (Ślubowska-Woldengen, et al., 2007) and northern (Koç, et al., 2002) the IRD concentration was low which indicates low fluxes of icebergs. The Svalbard-Barents Sea Ice Sheet retreated into the fjord during the Younger Dryas (Elverhøi, et al., 1995; Bondevik, et al., 1995; Polyak, et al., 1995; Landvik, et al., 1998; Svendsen, et al.,

1996; Svendsen, et al., 2004b). After this event the IRD concentration decreased and the deposition of hemipelagic sediments dominates in HH12-930 GC (Figure 38), which is characteristic for the early part of Holocene (Andersen, et al., 1996). The summer insolation at 80°N during the early Holocene was 8% higher than compared to day (Berger, 1978). Sediments of early Holocene are characterized by high abundance of diatoms, and is first described in the Fram Strait by Stabell (1986). This diatom maxima have also been observed in cores from the Skagerrak/Norwegian Sea (Stabell, 1986). Jessen et al (2010) describes the Early Holocene sediments to be hemipelagic fine – grained, structureless and with high abundance of diatoms, where IRD is absent (Figure 32, 33 and 34B1). This layer is dated to be deposited 10,100±150 cal yr BP to 9840±200 cal yr BP (Jessen, et al., 2010) (Figure 32 and 33). After 9840±200 cal yr BP IRD occurs in very low concentrations, and hemipelagic grey sandy mud is dominant (Jessen, et al., 2010). These sediments seems to be absent in HH14 – 002 GC (Figure 37), however, could occur in HH12 – 930 GC (Figure 38).

Core HH12 – 930 GC is retrieved from a pockmark, which could possibly act as a sediment trap. The upper 30 cm in HH12 – 930 GC contains relatively homogenous marine mud (Figure 38), which could correspond to the Early Holocene sediments described by Jessen et al (2010), however, the uppermost part of the core lacked datable material and an age could not be obtained. The correlation between HH12 – 930 GC and the records from Jessen et al (2010) is uncertain due to the disturbed magnetic susceptibility (Figure 38). The reason for the disruption in the magnetic susceptibility could be due to diagenetic processes, which occurs in gas hydrate provinces (Paull, et al., 1994). It is suggested that a stronger bottom current during the early part of Holocene could have eroded the fine – grained sediments, leaving the coarser material, like IRD, behind to form a lag deposit (Andersen, et al., 1996). This could be the reasons for the lack of Early Holocene in HH14 – 002 GC and possible parts of the Holocene in HH12-930 GC.

Today, the East Greenland Current has a maximum velocity of 9cm/s in the upper 200 meter of the water column over the deep part of the continental slope, and the

northward flowing West Spitsbergen Current has a maximum speed of 24 cm/ka over the upper continental slope (Fahrbach, et al., 2001) (See figure 49).

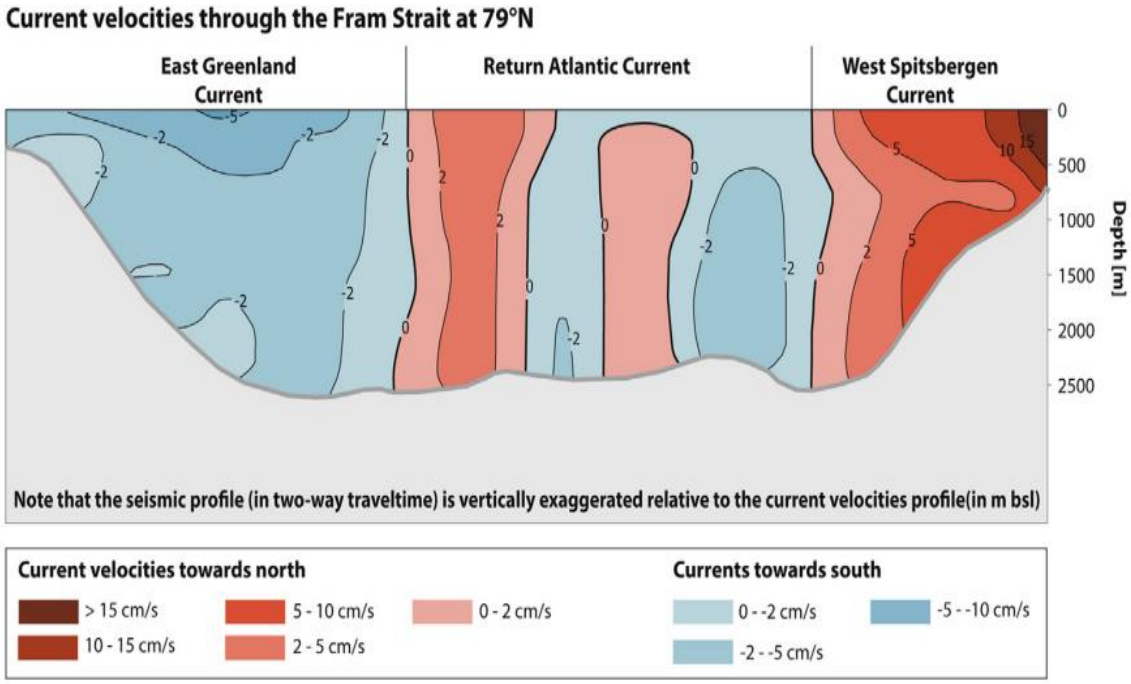

Figure 49: Figure taken from Gebhardt et al (2014) showing an oceanographic profile at 79°N and how the velocities varies with depth and increases towards east (Gebhardt, et al., 2014).

Active erosion episodes occurred on the Nova Scotia continental rise during the Holocene, which resulted in very low sedimentation rates (5.5 cm/ka) (Faugères & Stow, 1993). Contourites are able to transport grain sizes ranging from clay to sand, and very strong currents may scour the sea bed and result in gravel – lag contourites (Faugères & Stow, 1993). During the Early Holocene there was an increased thermohaline circulation in the Arctic Ocean (Ślubowska-Woldengen, et al., 2007), which possibly could have caused an erosion of the sediments on Vestnesa Ridge.

7. 2 Paleoceanography the last ~30,000 cal yr BP

7. 2. 1 Influence of Atlantic water during the LGM

The high planktic $\delta^{18}O$ values in HH12-930 GC gives an indication that the area might been influenced by Atlantic water before 37,829 cal. yr BP, and for a period after (Figure 41). The middle part of IOS 3 is characterized by open water conditions during summer (Nørgaard-Pedersen, et al., 1998). During two short periods between 31.1 – 26.5 cal. yr BP and 23 – 17.4 cal. yr BP relatively warm water entered the Norwegian/Greenland Sea from the North Atlantic and served as a source of moisture for the Svalbard – Barents Sea Ice Sheet build – up during the late Weichselian (Hebbeln, et al., 1994). The inflow of Atlantic water was strong, indicated by an estimated SST (sea surface temperature) of ca 1.6 – 3.0 °C. However, the SST may be overestimated, and a deeper calcifying of *N. pachyderma (s)* may indicate that the Atlantic water flowed as a subsurface water – mass (Nørgaard-Pedersen, et al., 2003). Studies from the Svalbard margin and Fram Strait have reported that the LGM was a period with high concentration of planktic foraminifera and high productivity (Hebbeln, et al., 1994; Dokken & Hald, 1996; Lloyd, et al., 1996; Hald, et al., 2001; Nørgaard-Pedersen, et al., 2003). During stadials the P:B ratio is relatively high (Rasmussen, et al., 1996a), which is varies between 8 to 1 in HH14 – 002 GC (Figure 40). From 30,070 the high abundance of N. pachyderma (s) (Figure 40) indicates that the environment was glacial with cold surface water. The increased abundance of both planktic and benthic foraminifera could indicate seasonally ice – free conditions since the production of zooplankton requires open water conditions and requires nutrient and insolation (Smith, 1995). This is also suggested by Knies et al (1999). It is proposed that the waters of the eastern part of the Fram Strait was seasonally ice – free during most of the LGM, and that the open water conditions were important for the build – up of the Barents Sea Ice sheet as it provided as a moisture source (Hebbeln, et al., 1994; Dokken & Hald, 1996).

Nørgaard – Pedersen et al (2003) reports high planktic $\delta^{18}O$ values during the LGM in the Fram Strait, which together with stable paleotemperature estimates indicate a homogenous near surface water mass. High sedimentation rate (2 – 10 cm/ka) and planktic flux and an increase in IRD could indicate that the area was characterized repeatedly by seasonally open – water conditions, relatively high biogenic productivity and abundant drifting icebergs (Figure 50) (Nørgaard-Pedersen, et al., 2003). High $\delta^{18}O$ values in HH12-930 GC are observed

throughout the LGM (Figure 42). This could possibly indicate influence of warm Atlantic water (Spielhagen & Erlenkeuser, 1994). However, a low salinity surface layer could have been present during the LGM, but too thin (<50 m) to leave any traces in the proxies (Nørgaard-Pedersen, et al., 1998). High fluxes of planktic foraminifera indicate increased nutrient supply induced by upwelling of Atlantic water (Knies, et al., 1999). After Heinrich Event 2 (23,820 cal yr BP) high flux in planktic foraminifera is observed in HH14 – 002 GC (Figure 36). High productivity seems to coincide with or follow immediately after Heinrich Events (Dokken & Hald, 1996). An increased concentration of IRD in the period between 30,070 to 26,486 cal yr BP is seen in HH14 – 002 GC (Figure 37). According to Knies et al (1999) the release of IRD can also occur in area with polynyas, areas of open water in sea ice, which is caused by upwelling of warm water. If the area was completely covered by sea – ice *N. pachyderma (s)* would disappear (Kohfeld, et al., 1996). Knies et al (1999) suggest that coastal polynya was kept open by katabatic winds blowing from the ice sheet. According to Pflaumann et al (2003) and Sarntheim et al (2003) water beyond 78°N in the Fram Strait was covered in perennial sea ice, while the area south of 78°N there was established an open – water conditions.

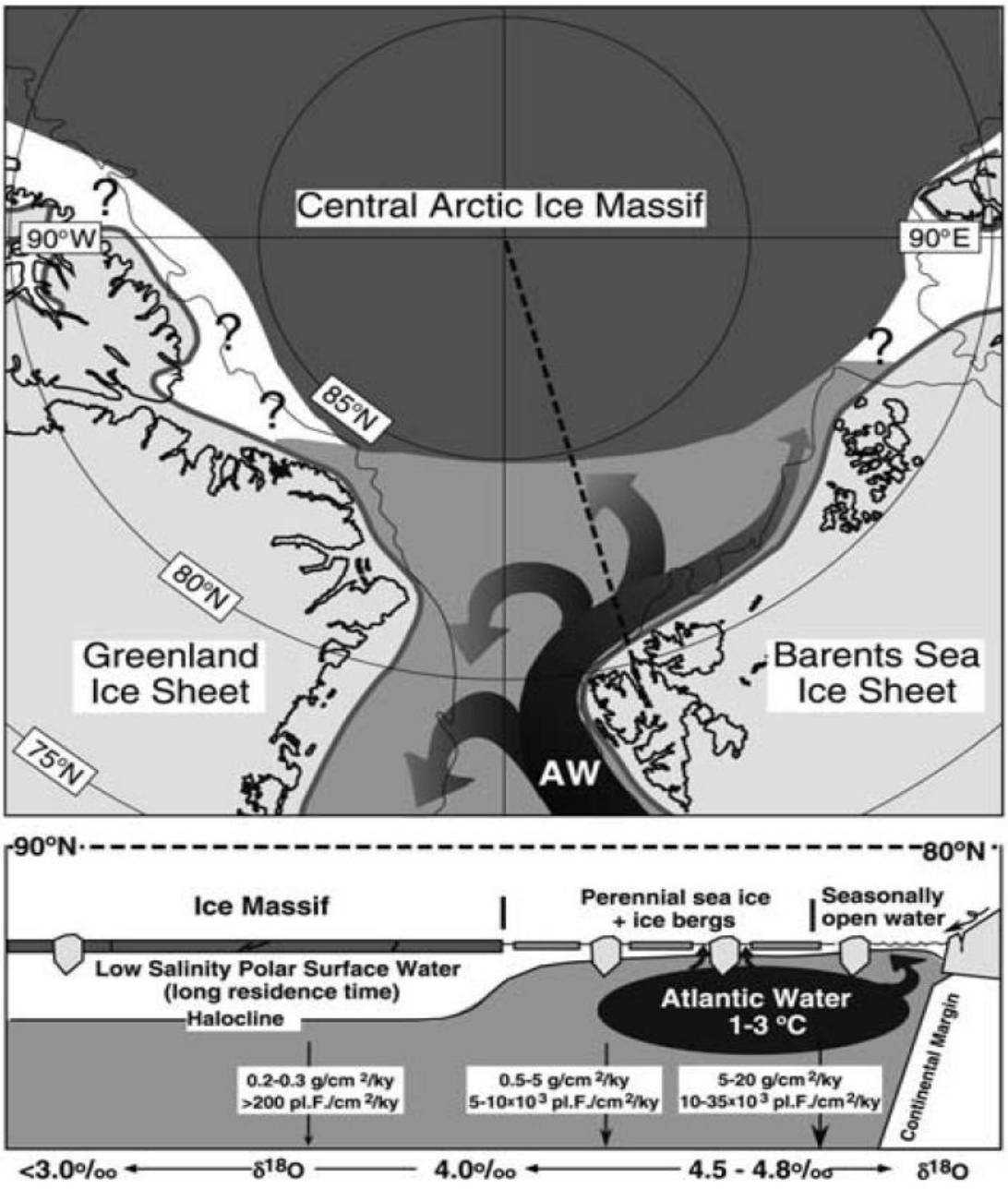

Figure 50: Figure from Nørgaard – Pedersen et al (2003) showing the sea ice and ice berg conditions in the Fram Strait during the LGM. Sedimentation rates, planktic $\delta^{18}O$ values, planktic foraminifera flux and mean SST values of the Atlantic Water mass are indicated (Nørgaard-Pedersen et al., 2003).

7. 2. 2 Early deglaciation and Heinrich Event 1

The paleocirculation was affected by the retreating Barents Sea Ice Sheet, and the Fennoscandian Ice Sheet, which resulted in isostatic rebound in the Barents Sea region (Forman, et al., 1996; Svendsen, et al., 1999; Siegert & Dowdeswell, 2002). Number of IRD per gram varies from 10 to 17 in HH14 – 002 GC (Figure 37). At 20,101 cal yr BP the IRD peaks (Figure 37). Jessen et al (2010) observes two IRD peak in sediment cores from the western Svalbard slope between 20,500 and 20,000 cal yr BP, and between 21,200 and 19,800 cal yr BP. It is suggested to indicate glacial retreat (Siegert & Dowdeswell, 2002), and is also observed in the north – eastern part of Svalbard after 20,000 cal yr BP (Knies, et al., 1999; Kleiber, et al., 2000; Knies, et al., 2001). Reduced precipitation due to increasing sea ice cover over the Arctic Ocean caused by a weakening of the warm Atlantic water inflow (Müller, et al., 2009) and the advance of the Svalbard – Barents Sea Ice Sheet to the shelf edge (Andersen, et al., 1996), could have triggered the retreat (Gildor & Tziperman, 2001). During a high peak of IRD after 17,652 cal yr BP the amount of mud decreases (Figure 37), and the planktic and benthic $\delta^{18}O$ and the planktic $\delta^{13}C$ values decreases in HH14-002 GC and HH12-930 GC (Figure 41 and 42, respectively). This could indicate stratification and a decrease in ventilation due to higher fluxes of icebergs and presence of sea ice (Spielhagen & Erlenkeuser, 1994) that melted over the area. With sea-ice covered area the exchange with the atmosphere tends to be effectively inhibited, and allows metabolic CO_2 from residual bacterial respiration to accumulate in the water, and the $\delta^{13}C$ values decreases (Spielhagen & Erlenkeuser, 1994), which could explain the low $\delta^{13}C$ values in HH14-002 GC (Figure 39). This cold and fresh surface water mass causing stratification could have reduced the inflow of Atlantic water, and correlate to the regional feature Heinrich Event 1 in time (Heinrich, 1988; Bond, et al., 1993), which is observed in the Nordic Sea and Fram Strait (Rasmussen, et al., 1996a; Rasmussen, et al., 2007; Knies, et al., 1999; Bauch, et al., 2001; Jessen, et al., 2010). The event is thought to be related to the deglaciation of Svalbard and

the Barents Sea (Jones & Keigwin, 1988; Elverhøi, et al., 1995; Andersen, et al., 1996). According to Bond et al (1993) Heinrich Event 1 is interpreted to be very cold, with low planktic $\delta^{18}O$ values and high abundance of IRD, which is observed in HH14-002 GC (Figure 37 and 41) and HH12-930 (38 and 42). Rasmussen et al (2007) link low $\delta^{18}O$ values and high abundance of IRD as an indicator of accelerated retreat of the ice sheet, and other studies from Svalbard and the Fram Strait have similar results, indicating abundance of iceberg and presence of cold meltwater at the surface (Hald, et al., 1996; Dokken & Hald, 1996; Andersen, et al., 1996; Svendsen, et al., 1996; Lloyd, et al., 1996; Knies, et al., 1999; Nørgaard-Pedersen, et al., 2003; Birgel & Hass, 2004). Lekens et al (2005) and Jessen et al (2010) suggest that the meltwater originated from retreat of the Fennoscandian Ice Sheet. The Heinrich Event 1 is suggested to begin at 17,400 cal yr BP and Rasmussen et al (2007) has set the transition from LGM to Heinrich Event 1 to 18,062 cal yr BP to 17,765 cal yr BP (15,500 – 15,000 ^{14}C yr BP). This is in agreement with the age in HH14 – 022GC estimated by linear regression to be 17,652±444 cal yr BP. Ślubowska – Woldeng et al (2007) reports higher fluxes of IRD in the time interval 17,500 – 14,500 cal yr BP, and *E. excavatum f. clavatum* and *C. reniforme* to be dominated benthic species in this interval. Both of these species is observed in HH14 – 002 GC and indicates an arctic glaciomarine environment (Hald & Korsun, 1997). A decrease in the relative abundance of *C. neoteretis* (Figure 39) could indicate a reduction in the inflow of Atlantic water, and an increase of *E. excavatum f. clavatum* (Figure 39) could indicating sea – ice cover, decreased salinities and reduced temperatures (Steinsund, et al., 1994). The conditions were cold and polar, and peaks of *E. excavatum f. clavatum* indicates low – saline water (Rasmussen, et al., 2007). *O. umbonatus* disappears from the fauna (Figure 39). A decrease in benthic (Figure 39) and planktic (Figure 40) foraminifera could indicate low productivity, and low P:B ratio (Figure 40) could indicate extensive winter sea ice and unstable conditions (Vilks, 1969; Vilks, 1970; Vilks, 1975; Vilks, 1989; Gibson, 1989; Scott, et al., 1989a; Scott, et al., 1989b; Scott & Vilks, 1991)**.** Together with relatively low flux of benthic and planktic foraminifera (Figure 39 and 40, respectively) it could indicate stressed conditions with cold bottom waters and low salinity (Ślubowska-Woldengen, et al., 2007). The surface and bottom productivity is suggested by Rasmussen et

al (2007) to be decoupled during this event, and that the nutrient was mainly recycled in the upper part of the water column, which is indicated by high accumulation rate of planktic foraminifera and low for benthic foraminifera. According to Dokken and Hald (1996) there could be a chronological correlation between high productive zones, Heinrich Event and warming of surface waters in the North Atlantic. High productivity zones occurs after the Heinrich Event, where the increase of IRD is associated with high productivity zones (Dokken & Hald, 1996).

7. 2. 3 Bølling/Allerød Interstadial and possibly early Holocene

After this Heinrich Event 1 and during the early stage of Bølling/Allerød Interstadial (14,780 - <14,070) laminated sediments were deposited from turbid meltwater plume originating from the Svalbard – Barents Sea Ice Sheet (Elverhøi, et al., 1995; Andersen, et al., 1996; Svendsen, et al., 1996; Birgel & Hass, 2004). At the core site the abundance of IRD decreased and the concentration of mud increased in HH14-002 GC and HH12-930 GC (Figure 37 and 38, respectively), indicating less icebergs and sea ice. Together with a minor increase in $\delta^{18}O$ and $\delta^{13}C$ values in HH14-002 GC (Figure 37), it could indicate a reduction in the influence of surface meltwater and a slightly increased ventilation (Rasmussen, et al., 2007). However, the $\delta^{18}O$ and $\delta^{13}C$ values was lower than during the LGM (Figure 37), which could that a less homogenous near surface water mass (Nørgaard-Pedersen, et al., 2003), and less stratified than compared to Heinrich Event 1 (Rasmussen, et al., 2007). Aagaard – Sørensen et al (2014) reports low $\delta^{13}C$ values which indicates that the water column was stratified caused by sea ice and melt water. Declined $\delta^{13}C$ values are also reported in other studies further south in the Fram Strait (77°N) (Ebbesen, et al., 2007) and at 75°N in the Barents Sea (Sarntheim, et al., 2003). According to Morris (1988) low $\delta^{18}O$ values can represent rapid deglaciation periods, which is accompanied by low planktonic carbon isotope values.

The relatively high abundance of *I. norcrossi* is reported in HH14 – 002 GC at the onset of the Bølling/Allerød (Figure 39) could imply that the area was influenced by seasonally sea ice (Steinsund, et al., 1994). The P:B ratio is low (Figure 40), and occasionally close to 1, which is normal in interstadial (Rasmussen, et al., 1996a). The planktic assemblage is dominated by *N. pachyderma (s)* (Figure 40), indicating a cold surface conditions, which is also documented on the SW Svalbard margin by Rasmussen et al (2007). Aagaard – Sørensen et al (2014) reported low faunal fluxes and high abundance of *N. pachyderma (s)* from the eastern Fram Strait, which together with low $CaCO_3$ could indicate that there was polar conditions in the area with reduced productivity (Johannessen, et al., 1994). Aagaard – Sørensen et al (2014) documented cold summer conditions (average 2°C), in the area during Bølling/Allerød, and the $sSST_{Mg/Ca}$ (3.5 °C) suggest that *N. pachyderma (s)* calcified in chilled Atlantic Water. Earlier studies have reported a strong meridional advection of Atlantic water in the Eastern

Fram Strait (Birgel & Hass, 2004; Ślubowska, et al., 2005; Rasmussen, et al., 2007). On the SW Svalbard shelf the temperatures increased, but remained lower than during Heinrich Event 1, due to heat loss to the atmosphere and outpouring of meltwater (Rasmussen, et al., 2007). Several studies has interpreted that Atlantic water was present after the start of Bølling Interstadial (Polyak & Solheim, 1994; Lubinski, et al., 1996; Koç, et al., 2002; Wollenburg, et al., 2004; Ślubowska, et al., 2005). The dominating benthic dominated by *C. neoteretis* and *C. reniforme* during the early Bølling/Allerød (figure 39) indicates that there was inflow of warm and saline Atlantic water in the area, flowing as a subsurface current under cold and fresh polar water (Mackensen & Hald, 1988; Jennings & Helgadottir, 1994; Rasmussen, et al., 1996b; Rytter, et al., 2002; Jennings, et al., 2004), and possibly a more unstable environment (Osterman & Nelson, 1989). Rasmussen et al (2007) reports that the benthic fauna was dominated by *C. reniforme* and *C. neoteretis* after 14,332 cal yr BP (12,450 ^{14}C yr BP). Ślubowska – Woldengen et al (2007) also reported this particular fauna from the western Svalbard shelf during Bølling – Allerød (14,500 – 12,600 cal yr BP).

In the eastern part of the Norwegian Sea increased inflow of Atlantic water occurred during the Bølling – Allerød Interstadial (Hald & Vorren, 1987; Klitgaard-Kristensen, et al., 2001; Rasmussen, et al., 2002). This is in contrast to the cold surface waters in the western and northern Svalbard margin (Ślubowska-Woldengen, et al., 2007). The surface waters were cold in the southwestern Barents Sea and the northern Norway indicated by the lack of planktic foraminifera (Hald & Aspeli, 1997).

The increased abundance of both benthic and planktic foraminifera after 14,300 cal yr BP (Figure 39 and 40, respectively) could indicate seasonally ice – free conditions since the production of zooplankton requires open water conditions and requires nutrient and insolation (Smith, 1995), which is also been suggested by Knies et al (1999). The increase in coarse material after 14,300 cal yr BP in HH14-002 GC and HH12-930 GC (Figure 37 and 38, respectively) could indicate increased fluxes of iceberg and/or sea – ice. This is supported by a decrease in planktic and benthic δ^{18}O values in HH12-930 GC (Figure 42). The low values of δ^{13}C (Figure 42) indicates stratification caused by sea ice and melt water as suggested by Spielhagen and Erlenkeuser (1994), and could possibly explain the moderate values of IRD

observed in HH14 – 002 GC after 14,300 cal yr BP (Figure 37). After 14,300 cal yr BP *T. quinqueloba* increases for a short period (Figure 40). An increase of *T. quinqueloba* have been reported in samples from the Nordic Sea to coeval in time with the Bølling/Allerød warming (Koç-Karpuz & Jansen, 1992). The conditions were glacial wit polar surface water indicated by the high abundance of *N. pachyderma (s)* (Figure 39). Together with *C. neoteretis* and *M. barleeanum* (Figure 39) it is suggested that there was influence of Atlantic water, flowing as a subsurface current under a layer with cold and low – saline meltwater (Mackensen & Hald, 1988; Polyak & Solheim, 1994; Steinsund, et al., 1994; Jennings & Helgadottir, 1994; Rasmussen, et al., 1996a; Rasmussen, et al., 1996b; Rytter, et al., 2002; Jennings, et al., 2004). This is supported by the declined benthic and planktic $\delta^{18}O$ values (Figure 38).

The age of the uppermost part of HH14-002 GC and HH12-930 GC s unknown. However, the interval after 14,070 cal. yr BP could correspond to the upper part of Bølling – Allerød Interstadial, and possibly towards the Allerød/Younger Dryas stadial – boundary based on the peak in IRD. Rasmussen et al (2007) describes the similar benthic fauna found in HH14 – 002 GC after 14,070 cal yr BP in a sediment core (JM02 – 460) from the southwestern slope of Svalbard. This is below the Younger Dryas stade boundary, which is marked by a peak in *E. excavatum f. clavatum* and a decrease in both benthic and planktic $\delta^{18}O$ values on the shelf (Rasmussen, et al., 2007). The lack of *N. pachyderma (*s) suggest that polar surface water was presence, and the decrease in *M. Barleeanum, C. lobatulus* and C. neoteretis propose a reduction in the influence of Atlantic water (Rasmussen, et al., 2007). Ślubowska – Woldengen et al (2007) reports high abundance of *N. labradorica* in the Younger Dryas stadial. In HH14 – 002 GC there is no increase in *E. excavatum f. clavatum* or *N. labradorica*, however, it rather shows an increase in *M. barleeanum, C. neoteretis* and *C. lobatulus*, which indicates a relatively strong influence of Atlantic water and that food supply increased (Rasmussen, et al., 2007). By assuming the fauna found after 14,070 cal yr BP in HH14 – 002 GC (Figure 39) could be the similar fauna found in Rasmussen et al (2007), the upper part of HH14 – 002 GC could correspond to Bølling/Allerød Interstadial, possibly just above the boundary to Younger Dryas. This implies that the Younger Dryas and the Holocene <11,316

cal yr BP (10,000 ^{14}C yr BP) is missing from HH14 – 002 GC. Gard (1987) reported that Holocene was absent from a cores taken from the north-western continental slope of Svalbard. The low δ^{18}O values in HH12-930 GC (Figure 42) is interpreted as a result of reduced salinity. This could correspond the Younger Dryas (12,600-11,500 cal. yr BP), and could possibly be a result of a shift in the prevailing water masses there was a freshening of bottom water that occurred around 13,400 cal. yr BP (Ślubowska-Woldengen, et al., 2007).

7. 3 Gas seepage

The results from the stable isotope analysis from HH12 – 930 GC, shows a drastic decline in the planktic δ^{13}C values during the Middle—Weichselian (~37,829 cal. yr BP) which values as low as -11.34 ‰ at 528 cm and -10.44 ‰ at 518 cm (Figure 42). During the early stages of the LGM (>28,135 cal. yr BP) the values drops down to -4.09 ‰ at 463 cm, and to -6.08 ‰at the lower part of the Heinrich Event 2 (413 cm) (Figure 42). Low planktic δ^{13}C values (-3.47 ‰), occurs at the upper part of the LGM (between 23,820 to <21,616 cal. yr BP) at 353 cm (Figure 42). During the LGM in HH14-002 GC the planktic δ^{13}C values varies between -0.2 and 0.38 ‰, and the minimum value observed is -0.39 ‰, so compared to HH14-002 GC (Figure 41) the values in HH12-930 GC (Figure 42) are considered low. Other studies of "normal" marine sediments have reported values between -0.5 to 1 ‰ (Volkmann & Mensch, 2001; Nørgaard-Pedersen, et al., 2003; Sarntheim, et al., 2003; Jessen, et al., 2010).

In core HH12-930 GC the benthic δ^{13}C values decreases to -3.38 ‰ at 353 cm, and stays relatively low in the upper part of the LGM (between 23,820 to <21,616 cal. yr BP (Figure 42). At the boundary to the early deglaciation the benthic δ^{13}C values decreases again (-2.72 ‰). During the lower part of Bølling/Allerød Interstadial (between 14,300 to 14,070 cal. yr BP) the benthic δ^{13}C values decreases to -2.32 ‰ (Figure 42). Compared to the minimum benthic δ^{13}C value observed in HH12-002 GC during the late stage of LGM (minimum -0.8 ‰), and a minimum value of -1.7 ‰ throughout the core during the early deglaciation, and the Bølling/Allerød Interstadial (minimum -1.38 ‰), the values observed in

HH12-930 GC are considered low values. The benthic $\delta^{13}C$ values range from -1 to 0 ‰ during the deglaciation in the northern Barents Sea (Wollenburg, et al., 2001), and from -0.5 to 0.3 ‰ in the Kara Sea (Lubinski, et al., 2001). In the southwestern Barents Sea Aagaard-Sørensen et al. (2010) reports values from ca. 0 to 1.5 ‰.

The planktic oxygen values throughout the Middle-Weichselian and LGM have high values (5.6 and 4.6 ‰) (Figure 42), which could indicate inflow of warm, saline Atlantic water, and open water. With sea-ice covered areas the exchange to the atmosphere tends to be effectively suppressed, and allows metabolic CO_2 from residual bacterial respiration to accumulate, and thus the $\delta^{13}C$ values declines (Spielhagen & Erlenkeuser, 1994). According to Stott et al (2002) in particular benthic foraminifera can be influenced by pore water with DIC shifts associated with changes in productivity in surface water, and re-mineralization at the sea floor and in the sediment, and record $\delta^{13}C$ values to be as low as -2.5 ‰ (Stott, et al., 2002). This could possibly explain the low benthic $\delta^{13}C$ values (-1.89 ‰) observed in in HH12-930 GC during the Heinrich Event 1 (Figure 42) and HH14-002 GC during the early deglaciation (Figure 41). Also riverine dissolved inorganic carbon (DIC) can affect the $\delta^{13}C$ values in the surface waters of the Arctic Ocean, and ranges from -5 to -10 ‰ (Spielhagen & Erlenkeuser, 1994). The lack of evidence of sea-ice cover in the area, and since the area is known as a gas-hydrate province (Hustoft, et al., 2009; Bünz, et al., 2012; Smith, et al., 2014), the other event with low benthic and planktic $\delta^{13}C$ values are interpreted to most likely be affected by processes that involves CH_4. These processes are the precipitation of methane-derived authigenic carbonate derived from the production of bicarbonate of AOM by the consumption of methane by methanotrophic archaea and sulfate-reducing bacteria (see chapter 1. 3 for further references). Since most of the CH_4 is consumed by methanotrophic archaea in the sediments, and in the water column, it is not expected that live planktic foraminifera will record the signal from CH_4 (Dickens, 2001; Reeburgh, 2007). Since the foraminifera has not been cleaned for authigenic carbonate overgrowth, some of the negative values can occurred due to enrichment in elements like Mg, which is typical for methane-derived authigenic carbonate (Torres, et al., 2003; Torres, et al., 2010). Consolaro et al (2015) observed that the $\delta^{13}C$ values of C. neoteretis from the Vestnesa Ridge, obtained

after submitting specimens to a thorough cleaning procedure were still significantly low compared to uncleaned specimens.

The negative signal seen in the planktic $\delta^{13}C$ values (-11.34 ‰) during the mid-Weichselian (Figure 42) is thus most likely due to enrichment in methane-derived authigenic carbonate, since it is not expected that the CH_4 reach far enough in the water column to be recorded by planktic foraminifera. Consolaro et al (2015) interpreted the finding of both benthic and planktic foraminifera with negative $\delta^{13}C$ values in samples dated to the Bølling/Allerød Interstadial (CIEI) to be due to secondary carbonate precipitation after they were buried (Figure 50). Live benthic foraminifera may be capable of recording negative $\delta^{13}C$ composition of methane-influenced DIC in the bottom and pore waters (Sen Gupta, et al., 1997; Rathburn, et al., 2000; Hill, et al., 2003; Rathburn, et al., 2003; Martin, et al., 2004). It is possible that all the negative values of *N. pachyderma (s*) found in HH12-930 GC resulted from methane-derived authigenic carbonate precipitation, which have oversaturated the pore water in respect to carbonate minerals. Meaning that all of the methane is oxidized by AOM since the methane flux is low (Borowski, et al., 1996). This can furthermore be the case for the low planktic $\delta^{13}C$ value (-6.08 ‰) just below the boundary to Heinrich Event 2 (~23,820 cal. yr BP) (Figure 42), and for the benthic and planktic $\delta^{13}C$ value (-3.38 and -3.47 ‰, respectively) seen at 353 cm in the upper stages of the LGM, between 23,820 to 21,616 cal. yr BP (Figure 42).

At the boundary to the Early Deglaciation (after 21,616 cal. yr BP) and during the Bølling/Allerød Interstadial (14,300-14,070 cal. yr BP) (Figure 42) the case could be different. In these event only benthic foraminifera show negative $\delta^{13}C$ values (-2.27 and -2.32 ‰, respectively). Consolaro et al (2015) found only benthic foraminifera with low values in the Early Holocene (CIEII), and interpreted it to be because of high flux of methane, leading to lower rates of AOM since the oxidation is less efficient (Figure 51). This causes methane to be released into the bottom water, where is further oxidized by methanotrophic aerobic microbes in the water column (Niemann, et al., 2006).

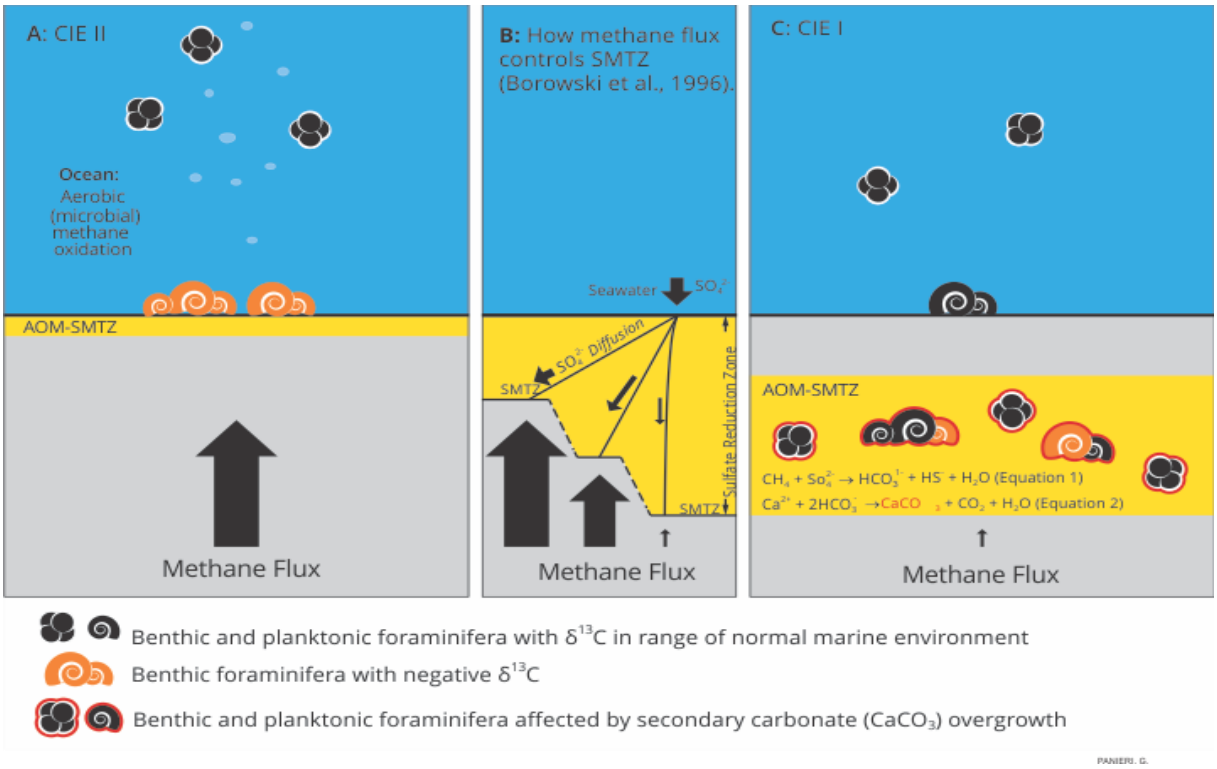

Figure 51: Schematic diagram showing two methane release event observed by Consolaro et al (2015). A) Figure representing event CIE II during the Early Holocene where only benthic foraminifera exhibit negative $\delta^{13}C$ values. B) Figure showing how the SMTZ is controlled by the methane flux if the flux of sulphate (SO_4^{2-}) from the seawater and the characteristics of the sediments are constant (Consolaro, et al., 2015). C) Figure showing CIE I, which represent an event during Bølling/Allerød where both benthic and planktic foraminifera showed negative $\delta^{13}C$ values. Figure from Consolaro et al (2015).

Due to the lack of data of the pore water, which is used to measure methane flux toward the sea floor (Borowski, et al., 1996), it is difficult to tell if the negative $\delta^{13}C$ values are due methane-derived authigenic carbonate where the methane flux is low, or because of higher methane flux, which could possibly lead to a release of methane into the bottom waters.

In the mid-Weichselian (>37,829 - >28,135 cal. yr BP) there is observed negative planktic $\delta^{13}C$ values (down to -11.34 ‰), which could be due to secondary carbonate precipitation after burial. Low $\delta^{13}C$ value are observed in the southwestern Greenland Sea and further correlated with Dansgaard-Oeschger (DO) events by Millo et al (2005). Minor pulses (up to -2 ‰) were observed near DO interstadial 9 (~40.7 ka), which is suggested to be due to thermal destabilization and DIC derived from the oxidation of methane (Rathburn, et al., 2003; Hill, et al., 2004b). Millo et al (2005) correlated negative $\delta^{13}C$ value with the an atmospheric CH_4 record from the Greenland Ice Sheet Project 2 (GISP2) from Blunier and Brook (2001), and found major $\delta^{13}C$ minima during event that matches atmospheric CH_4 maxima (Blunier & Brook, 2001) during MIS 5.2, 5.1 and 3. Comparing the planktic and benthic $\delta^{13}C$ value to the GISP2 (Greenland Ice Sheet Project 2) and GRIP (Greenland Ice Core Project) from Blunier and Brook (2001) (Figure 52), there is a CH_4 peak between 35 and 40 ka, which possibly could correspond to the low $\delta^{13}C$ value seen in the upper part of mid-Weichselian in HH12-930 GC (Figure 42). This event correspond to GIS8 seen in Rasmussen and Thomsen (2013) (Figure 45 and 46). According to Kennett et al (2003) during interstadial warmings destabilization of methane hydrates may have contributed to increase atmospheric CH_4. This interval is interpreted to represent a deglaciation, where the south-eastern part Barents Sea shelf was ice free (Polyak, et al., 2000), and there was possibly an inflow of warm Atlantic Intermediate water. Shallow depths are more sensitive to temperature changes than to increased sea level (Vanneste, 2000; Mienert, et al., 2001; Vogt & Jung, 2002; Jung & Vogt, 2004). The relative sea level was estimated to be 65 to 55 meter lower than today between 45 and 35 ka (Lambeck, et al., 2002). In deeper part of the ocean, sea level rise and increased pressure is a more dominant factor which affects the position of the base of the hydrate stability zone (Mienert, et al., 2005). Millo et al (2005) suggest that a cessation of the deep-water convection in the Greenland Sea, thermal

instability of gas hydrates and northward advection of warm intermediate water caused highly negative $\delta^{13}C$ values. Other studies have reported low $\delta^{13}C$ value interpreted as methane release in Quaternary records (Kennett, et al., 2000; Smith, et al., 2001; Keigwin, 2002; Cook, et al., 2011; Hill, et al., 2012).

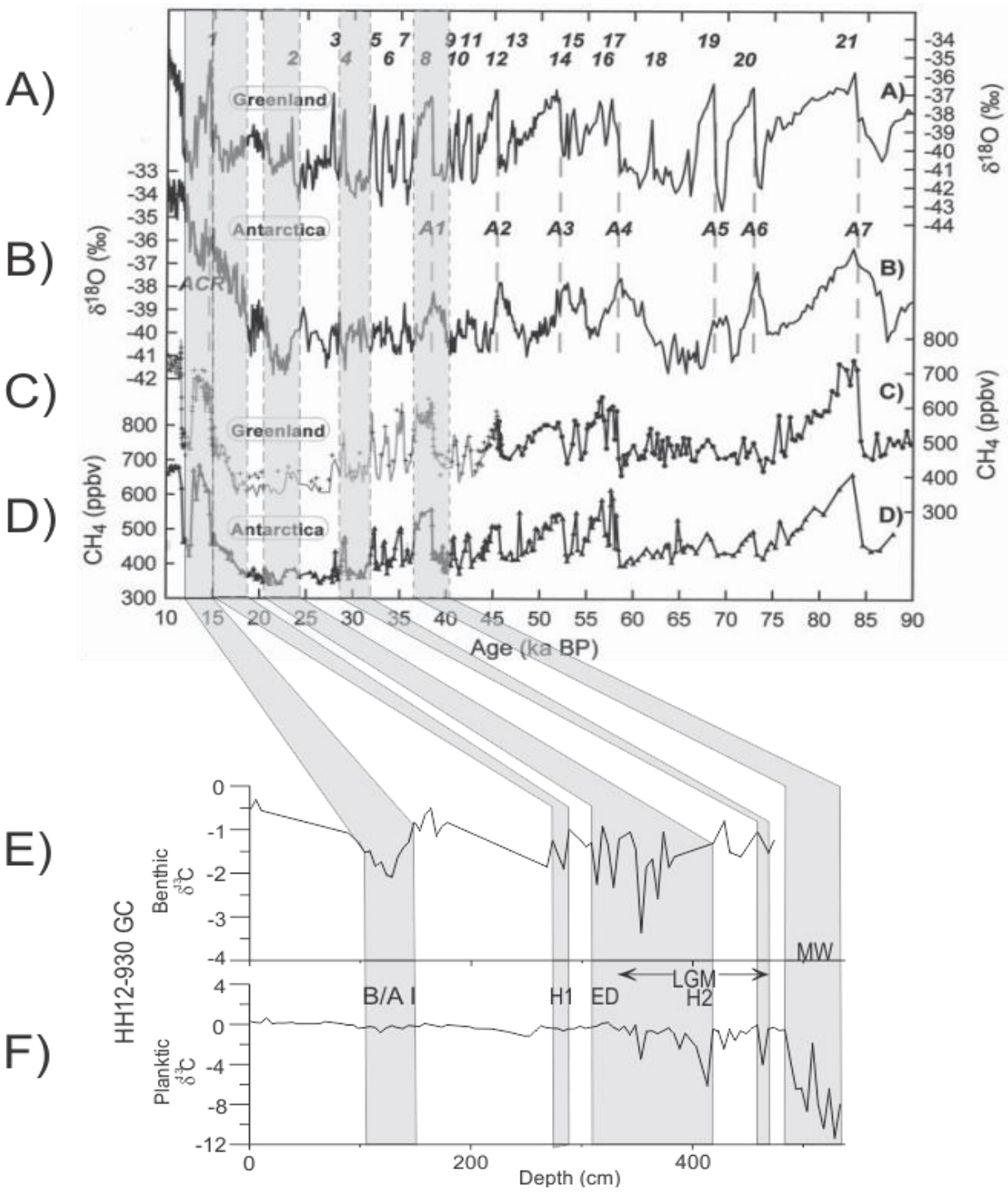

Figure 52: Figure from Blunier and Brook (2001) showing the isotopic and CH_4 from Greenland and Antarctica on the GISP2 time scale. A) Oxygen isotope from GISP2, Greenland. B) Oxygen isotope from Byrd station, Antarctica. C) CH_4 from GISP2 and GRIP. D) CH_4 from Byrd station. Dashed line indicates the onset of major D-O event (Blunier & Brook, 2001). E) Benthic $\delta^{13}C$ graph from HH12-930 GC, showing negative values during B/A I, ED and upper stage of LGM. F) Planktic δ13C graph from HH12-930 GC. The negative values are confined to the upper and lower stage of LGM, H2 and MW. A1 to A7 indicates major warming events in Antarctica.(B/A I= Bølling/Allerød Interstadials, H1=Heinrich Event 1, ED= Early deglaciation, H2=Heinrich Event 2, LGM=Last Glacial Maximum and MW= Mid-Weichselian)

It is suggested that a combined effect of loading of glacigenic sediments and shelf ice glaciations during periods of climatic changes leads to overpressure and further generation an initiation of focused fluid flow, and possibly to gas emission and reactivation of chimney structures (Hustoft, et al., 2009a; Plaza-Faverola, et al., 2011). Gas chimneys represent a pre-existing zones of weakness and may act as a pathway for fluid flow. Gas hydrate may fill there fractures in deep water (Kim, et al., 2011). It is not known where the source of the methane emission is located (Bünz, et al., 2012; Smith, et al., 2014). The deposition of mass-transported sediments during Heinrich Event 2 could possibly have led to pore pressure build-up, which could have led to more unstable gas hydrate. On the study site this specific layer is about 25 cm thick in HH12-930 GC (Figure 38). Most likely the deposition of glacigenic sediment had minor effect on the sediments and the gas hydrate on the study site during the LGM, where both benthic and planktic $\delta^{13}C$ values are negative (-3.38 and -3.47 ‰, respectively) (Figure 42), due to the distance and the water depth and the relative low sediment loading on the slope outside trough-mouth-fans (Laberg & Vorren, 1995; Hjelstuen, et al., 1996). However, together with increased seismicity it could possibly be a factor.

The negative planktic $\delta^{13}C$ values (-4.09 ‰) observed during the lower part of LGM (<37,829 and >28,135 cal. yr BP) (Figure 42) shows relatively moderate values correlated to the atmospheric CH4 in figure 51, compared to mid-Weichselian. The correlation with atmospheric CH_4, which could possibly be linked to regional event, is speculation, due to the uncertain age model at this interval. The Svalbard-Barents Sea Ice Sheet started to grow around 32,000 cal. yr BP (Andersen, et al., 1996; Landvik, et al., 1998; Siegert & Dowdeswell, 2002). The linear sedimentation rate at that point in HH12-930 GC is estimated to be 8.16 cm/ka (Table 9). This is a relatively low sedimentation rate compared to the Bølling/Allerød Interstadial, where the linear sedimentation rate is estimated to be 166 cm/ka (Table 9). It seems unlikely that during the early stage of LGM the low $\delta^{13}C$ values could have been caused by sediment load. This is due to the low sedimentation rate and as Consolaro et al (2015) suggested, the study area is deep water and distal to the shelf edge. The glacial

growth is related to a fall in global sea level (Elverhøi, et al., 1993). Cook et al (2011) suggest that a cold and deep (1476 meter water depth) coring site requires a warming of 6—16°C and a sea level drop of 300 to 1000 meters to cause sufficient release of pressure to destabilise gas hydrate.

At ~23,820 cal yr BP negative planktic $\delta^{13}C$ values down to -6.08 ‰ is observed just at the base of the Heinrich Event 2-boundary (Figure 42). The atmospheric CH_4 values seems to have a minor increase during this event (Figure 52). However, the low carbon signal in HH12-930 GC is possibly a local event since the planktic foraminifera are not expected to record a methane signal in the water column (Dickens, 2001; Reeburgh, 2007), and probably recorded the low $\delta^{13}C$ values from secondary crust after burial. The deposition of glacigenic sediments during Heinrich Event 2 was taken as a sign of a fully glaciated shelf (Laberg & Vorren, 1995; Vorren & Laberg, 1997; King, et al., 1998; Dowdeswell & Elverhøi, 2002; Jessen, et al., 2010). Major loading of glacigenic sediments can lead to excess pore pressure in the underlying sediments (Laberg & Vorren, 1995; Elverhøi, et al., 1997; Elverhøi, et al., 2002), however, it is difficult to tell if the deposition of mass transport sediments was large enough to cause gas hydrate dissociation. It seems like the dissociation occurred on an early stage of the event or possibly prior to it. After Heinrich Event 2 both planktic and benthic $\delta^{13}C$ values declines (Figure 42). The low values could have been due to low methane fluxes, similar to the scenario seen in Consolaro et al (2015), but different timing (Figure 51). This event occurred after the deposition of mass transported sediments during peak glaciation (Andersen, et al., 1996). After the glacial peak the Svalbard-Barents Sea Ice Sheet started to disintegrate, and Hebbeln et al (1994) suggest that at this point warm Atlantic water entered the Norwegian-Greenland Sea. This could lead to the suggestion that the combination of inflow of Atlantic water, and with the early stage of ice sheet collapse could have caused a methane release.

During the Early Deglaciation (<21,616-18,429 cal. yr BP) the benthic $\delta^{13}C$ values are low (-2.27 ‰) (Figure 42). Smith et al (2011) documented negative $\delta^{13}C$ values from the East Greenland continental shelf caused by methane release during the deglaciation, and

concluded that there could be a parallel to negative $\delta^{13}C$ values and deglaciation and the retreat of the ice sheet. They link the low carbon isotope to dissociation of gas hydrates to reduction of ice load and intrusion of warm bottom water. The retreat of the glacier lead to isostatic rebound, and possibly increased sedimentation rates (Landvik, et al., 1998; Forman, et al., 2004; Bungum, et al., 2005), which would have triggered other processes, like lithospheric stress changes resulting in increased seismicity (Consolaro, et al., 2015). All these factors could have caused the methane release and contributed to the low $\delta^{13}C$ values seen in the Early Deglaciation. Consolaro et al (2015) observed low $\delta^{13}C$ values during the Bølling/Allerød Interstadial and Early Holocene interpreted to be due to either low methane flux which leads to a deeper SMTZ, or a shallower SMTZ due to higher methane flux, respectively (Figure 51). These events occurred during a period when the deep convection was strong (McManus, et al., 2004; Ezat, et al., 2014), and during an increase in sea level and in the concentration of atmospheric CH_4 (Consolaro, et al., 2015). Figure 52 show a correlation in increase in atmospheric CH_4 with the negative $\delta^{13}C$ values observed during Bølling/Allerød Interstadial in HH12-930 GC (Figure 42). Prior to this event laminated sediments were deposited (Figure 38), and the sedimentation rate increased drastically (Table 9), which could have led to increased pore pressure and further activating gas migration through the gas chimneys (Hustoft, et al., 2009a; Plaza-Faverola, et al., 2011). The high sedimentation rate together with seismic activity due to isostatic rebound could have triggered gas hydrate destabilization. Consolaro et al (2015) speculate that during a rapid deglaciation, increased sea-level and sediment loading, and seismic activity could have led to methane emission on the Vestnesa Ridge.

8. Summary and conclusion

Two sediment cores HH14-002 GC and HH12-930 GC from Vestnesa Ridge in the eastern part of Fram Strait have been analysed in order to reconstruct the glacial history and paleoceanographic development between the mid-Weichselian and early Holocene in the area, and to investigate if there is a correlation between methane seepage and climate change. Core HH14-002 GC was taken from outside a pockmark of active gas seepage, while core HH12-930 was taken from inside the pockmark.

- The sediment cores shows a clear similarity in magnetic susceptibility (mainly core HH14-002 GC), lithology and age with the sediment cores in the study by Jessen et al (2010), and show that a close correlation is possibly.
- Possible interstadial conditions in the study areas during the upper part of the mid-Weichselian (>37,829 cal. yr BP). The Svalbard-Barents Sea Ice Sheet advanced to the shelf between 28,135 and 26,486 cal. yr BP indicated by a decline in $\delta^{13}C$ values. At 23,820 cal. yr BP the ice sheet reached the shelf break that led to the deposition of mass transported sediments, and is taken as sign that the shelf was fully glaciated. The early stage of the deglaciation indicated by a peak in IRD occurred around 20,101 cal. yr BP. Low $\delta^{18}O$ values correlates in time with Heinrich event 1, which occurred around 17,652 cal. yr BP, and can be related to the deglaciation. The deposition of laminated sediments between 14,780 and 14,300 cal. yr BP corresponds to the Bølling/Allerød Interstadials. Parts of the Holocene is missing from HH14-002 GC due to erosion by increased bottom current.
- High $\delta^{18}O$ values could indicate the presence of Atlantic water during the upper part of mid-Weichselian (>37,829 cal. yr BP). The LGM (31,479-20,101 cal. yr BP) was characterized by influence of Atlantic water, possibly under a low-saline surface layer. The productivity was high before and after Heinrich event 2 (~23,820 cal. yr BP) indicated by relative high abundance of N. *pachyderma* (s) and high P:B ratio. Relative high concentration of IRD indicate presence of drifting icebergs in the area.

During Heinrich event 1 the ventilation was reduced, and the water column was stratified, as indicated by a decline in $\delta^{18}O$ and $\delta^{13}C$ values. A reduction in percentage of *C. neoteretis* could imply a reduction of the inflow of Atlantic water, and low flux in planktic and benthic foraminifera low productivity and decreased P:B ratio indicates unstable conditions. The high relative abundance of *I. norcrossi* indicates the area was influenced by seasonal sea ice during the Bølling/Allerød Interstadial (14,700-17,070 cal. yr BP). A slightly increase in $\delta^{18}O$ and $\delta^{13}C$ values indicate that the water column was less stratified compared to Heinrich event 1. Low fluxes of *N. pachyderma (s)* indicate reduced productivity. *C. neoteretis* and *C. reniforme* indicates an influence of Atlantic intermediate water, flowing as a subsurface current. A decline in $\delta^{18}O$ values in HH12-930 GC could represent the Younger Dryas, and increased content of marine mud could indicate that HH12-930 GC contains parts of the Holocene.

- Together six periods with negative $\delta^{13}C$ values from core HH12-930 GC retrieved from inside a pockmark have been interpreted to be caused by methane seepage. Three of the events of negative $\delta^{13}C$ values, and thus possible events with methane seepage have, been linked to interstadial periods. The results of more interstadial conditions, glacial retreat and increased sea level could have caused eustatic unloading and seismic activity, which resulted in increase in methane seepage.

References

Aagaard, K., 1975. Oceanography of the Arctic Seas.. Reviews of Geophysics and Space Physics (Special issue; U. S. National Report to IUGG), Volume 13 (3), pp. 614-615,659-660.

Aagaard, K. & Carmack, E. C., 1989. The role of sea ice and other fresh water in the Arctic circulation.. Journal of Geophysics Research, Volume 94, pp. 14,485-14,498.

Aagaard, K. & Coachman, L. K., 1968. The East Greenland Current north of Denmark Strait: Part II.. Arctic, Volume 21.4, pp. 267-290.

Aagaard, K., Foldvik, A. & Hillman, S. R., 1978. The West Spitsbergen Current: Disposition and Water Mass Transformation.. Journal of Geophysical Research, Volume 92.C4, pp. 3778-3784.

Aagaard, K. & Greisman, P., 1975. Towards new mass and heat budgets in the Arctic Ocean.. Journal of Geophysical Research., Volume 80, pp. 3821-3827.

Aagaard, k., Swift, J. H. & Carmack, E. C., 1985. Thermohaline circulation in the arctic mediterranean seas.. Journal of Geophysical Research: Oceans (1978-2012), Volume 90.C3, pp. 4833-4846.

Aagaard-Sørensen, S., Husum, K., Hald, M. & Knies, J., 2010. Paleoceanographic development in the SW Barents Sea during the Late Weichseliane Early Holocene transition.. Quaternary Science Reviews, Volume 29, pp. 3442-3456.

Aagaard-Sørensen, S. et al., 2014. Sub sea surface temperatures in the Polar North Atlantic during the Holocene: Planktic foraminiferal Mg/Ca temperature reconstructions.. The Holocene, Volume 24.1, pp. 93-103.

Aitken, M. J., 1990. Science-based Dating in Archaeology. London: Longman.

Alam, M., Piper, D. & Cooke, H., 1983. Late Quaternary stratigraphy and pale-oceanography of the Grand Banks continental margin, eastern Canada.. Boreas, Volume 12, pp. 253-261.

Alm, T., 1993. Øvre-Æråsvatn-palyonstratigrafphy of a 22,000 to 10,000 BP lacustrine record on Andøya, northern Norway.. Boreas, Volume 22, pp. 171-188.

Andersen, E. S. et al., 1996. Late Quaternary sedimentation and glacial history of the western Svalbard continental margin.. Marine Geology, Volume 133, pp. 123-156.

Andersen, K. K. et al., 2004. High-resolution record of Northern Hemisphere climate extending into the last interglacial periode.. Nature, Volume 431, pp. 147-151.

Andrews, J., 2000. Icebergs and icebergs rafted detritus in the North Atlantic: facts and assumptions.. Oceanography, Volume 13.3, pp. 100-108.

Andrews, J. T. et al., 1994. Late Quaternary (stage 2 and 3) meltwater and Heinrich events Northwest Labrador Sea.. Quaternary Research, Volume 41, pp. 26-34.

Andrews, J. T. et al., 1995. Final stages in the collaps of the Laurentide ice sheet, Hudson Strait, Canada, NWT: 14C AMS Dates, seismic stratigraphy, and magnetic susceptibility logs.. Quaternary Science Reviews, Volume 14, pp. 983-1004.

Armstrong, H. A. & Braiser, M. D., 2005. Microfossils.. 2nd ed. s.l.:Blackwell Publishing.

Ballini, M., Kissel, C., Colin, C. & Richter, T., 2006. Deep-water mass source and dynamic associated with rapid climatic variations during the last glacial stage in the North Atlantic: A multiproxy investigation of the detrital fraction of deep-sea sediments.. Geochemistry, Geophysics, Geosystems, Volume 7.2.

Bandy, O. L., 1960. The geologic significance of coiling ratios in the foraminifer Globigerina pachyderrna (Ehrenberg).. Journal of Palentology, Volume 34.4, pp. 671-681.

Bandy, O. L. & Arnal, R. E., 1957. Distribution of Recent Foraminifera off west coast of Central America.. AAPG Bulletin, Volume 41.9, pp. 2037-2053.

Barnes, R. O. & Goldberg, E. D., 1976. Methane production and consumption in anoxic marine sediments.. Geology, Volume 4, pp. 297-300.

Bauch, D., Carsten, J. & Wefer, G., 1997. Oxygen isotope composition of living Neogloboquadrina pachyderma (sin.) in the Arctic Ocean.. Earth and Planetary Science Letters, Volume 146, pp. 47-58.

Bauch, H. A. et al., 2001. A multiproxy reconstruction of the evolution of dep and surface waters in the subarctic Nordic Sea over the last 30,000 yr.. Quaternary Science Reviews, Volume 20, pp. 659-678.

Bé, A. N. H. & Tolderlund, D. S., 1971. Distribution and ecology of living planktonic foraminifera in surface waters of the Atlantic and Indian Oceans, in Funnel, B. M., and Riedel, W. R. (eds.).. The Micropaleontology of the Oceans, pp. 105-144.

Belanger, P. E. & Streeter, S. S., 1980. Distribution and ecology of benthic foraminifera in the Norwegian-Greenland Sea.. Marine Micropaleontology, Volume 5, pp. 401-428.

Belanger, P. E. & Streeter, S. S., 1980. Distribution and ecology of benthic foraminifera in the Norwegian-Greenland Sea.. Marine Micropaleontology, Volume 5, pp. 401-428.

Benn, D. I. & Evans, D. J. A., 2010. Glaciers and glaciation.. 2nd ed. London: Hodder Anold Publication.

Berger, A., 1978. Long-term variations of caloric insolation resulting from Earth's orbital elements.. Quaternary Research, Volume 9 (2), pp. 139-167.

Berger, A. L. & Loutre, M. F., 1991. Insolation values for the climate of the last 10 million years.. Quaternary Science Reviews, Volume 10, pp. 297-317.

Berger, W. .., 1973. Deep-sea carbonates: Pleistocene dissolution cycles.. J. Foraminiferal Res.,, Volume 3, pp. 187-195.

Berger, W., 1968. Planktonic foraminifera: Selective solution and paleoclimatic interpretation.. Deep Sea Res.,, Volume 1, pp. 31-43.

Berger, W., 1979. Preservation of foraminifera. Foraminiferal Ecology and Paleoecology, SEPM, Short Course, Volume 6, pp. 105-155.

Berger, W. H. & Vincent, E., 1986. Deep-sea carbonates: Reading the carbon-isotope signal.. Geologische Rundschau, Volume 75.1, pp. 249-269.

Berndt, C. et al., 2014. Temporal constraints on hydrate-controlled methane seepage off Svalbard. Science, Volume 343, pp. 284-287.

Beszyczynska-Möller, A., Fahrback, E., Schauer, U. & Hansen, E., 2012. Variability in Atlantic water temperature and transport at the enrance to the Arctic Ocean, 1997-2010.. ICES Journal of Marine Science, Volume 69, pp. 852-863.

Biastoch, A. et al., 2011. Rising Arctic Ocean temperatures cause gas hydrate destabilization and ocean acidification.. Geophysical Research Letters, Volume 38.8 L08602, p. doi:10.1029/2011GL047222..

Birgel, D. & Hass, H. C., 2004. Ocean and Atmospheric variations duringe the last deglaciation in the Fram Strait (Arctic Ocean): a coulped high-resolution organic-geochemical and sedimentological study.. Quaternary Science Reviews, Volume 23, pp. 29-47.

Bischof, J. F. & Darby, D. A., 1997. Mid to late Pleistocene ice drift in the western Arctic Ocean: Evidence for a different circulation in the past.. Science, Volume 277, pp. 74-78.

Blunier, T. & Brook, E. J., 2001. Timing of millennial-scale climate change in Antarctica and Greenland during the last glacial period.. Science, Volume 291 (5501), pp. 109-112.

Boetius, A. et al., 2000. A marine microbial consortium apparently mediating anaerobic oxidation of methane.. Letters to Nature, Volume 407 (6804), pp. 623-626.

Bondevik, S., Mangrud, J., Ronnert, L. & Salvigsen, O., 1995. Post-glacial sea-level history of the Edgeøya and Barentsøya, eastern Svalbard.. Polar Research, Volume 14, pp. 153-180.

Bond, G. et al., 1993. Correlations between climate records from North Atlantic sediments and Greenland ice.. Nature, Volume 365, pp. 143-147.

Bond, G. et al., 1992. Evidence for massive discharges of icebergs into the North Atlantic ocean during the last glacial period.. Nature, Volume 360, pp. 245-249.

Bond, G. & Lotti, R., 1995. Iceberg discharges into the North Atlantic on millennial time scales during the last glaciation.. Science, Volume 267, pp. 1005-1010.

Borowski, W., Paull, C. K. & Ussler III, W., 1996. Marine pore-water sulphate profiles indicate in situ methane flux from underlying gas hydrate.. Geology, Volume 24, pp. 655-658.

Boulton, G. S., 1979. Glacial history of the Spitsbergen archipelago and the problem of a Barents Shelf ice sheet. Boreas, Vol. 8, pp. 31-57.

Bowman, S., 1990. Radiocarbon Dating. London: British Museum.

Bowman, S., 1990. Radiocarbon Dating. Vol 1. California: Uni. of California Press..

Broecker, W. et al., 1992. Origin of the northern Atlantic's Heinrich events.. Climate Dynamics, Volume 6.3-4, pp. 265-273.

Broecker, W. S., 1982. Ocean chemistry during glacial time.. Geochimica et Cosmochimica Acta, Volume 46.10, pp. 1689-1705.

Broecker, W. S., Peteet, D. M. & Rind, D., 1985. Does the ocean-atmosphere system have more than one stable mode of operation?. Nature, Volume 315, pp. 21-26.

Bryn, P. et al., 2005. Explaining the Storegga Slide.. MArine and Petroleum Geology, Volume 22, pp. 11-19.

Bugge, T., 1983. Subamrine slides in the Norwegian sontinental margin with special emphasis on the Storegga area.. IKU Publ., Volume 110, p. 152 pp.

Bungum, H., Lindholm, C. & Faleide, J. I., 2005. Postglacial seismicity offshore mid-Norway with emphasis on spatio-temporal-magnitudal variations.. Mar. Petrol. Geol., Volume 22, pp. 137-148.

Bünz, S. et al., 2012. Activ gas venting through hydrate-bearing sediments on the Vestnesa Rigde, offshore W-Svalbard. Marine Geology, Volume 332-334, pp. 189-197.

Böning, C. W., Bryan, F. O., Holland, W. R. & Döscher, R., 1996. Deeå-Water Formation and Meridional Overturning in a High-Resolution Model of the North Atlantic.. Journal of Physical Oceanography, Volume 26, pp. 1142-1164.

Cann, J. H., Belperio, A. P. & Murray-Wallace, C., 2000. "Late Quaternary paleosealevels and paleoenvironments inferred from foraminifera, northern Spencer Gulf, South Australia.. The Journal of Foraminiferal Research, Volume 30.1, pp. 29-53.

Caralp, M. H., 1989. Abundance of Bulimina exilis and Melonis barleeanum: Relationship to the Quality of Marine Organic Matter.. Geo-Marine Letters, Volume 9.1, pp. 37-43.

Carsten, J. & Wefer, G., 1992. Recent distribution of planktonic foraminifera in the Nansen Basin, Arctic Ocean.. Deep-Sea Research, Volume 39, pp. 507-524.

Chand, S. & Minshull, T. A., 2003. Seismic constraints on the effect of gas hydrates on sediment physical properties and fluid flow: a review.. Geofluids, Volume 3, pp. 275-289.

Chauhan, T., Rasmussen., T. L. & Noormets., R., 2015. Palaeoceanography of the Barents Sea continental margin, north of Nordaustlandet, Svalbard, during the last 74 ka.. Boreas.

Coachman, L. K. & Barnes, C. A., 1963. The movement of Atlantic Water in the Arctic Ocean.. Arctic, [S. I], Volume 16, pp. 8-16.

Consolaro, C. et al., 2015. Carbon isotope (δ13C) excursions suggest time of major methane release during the last 14 kyr in Fram Strait, the deep-water gateway to the Arctic.. Climate of the Past, Volume 11.4, pp. 669-685.

Cook, M. S., Keigwin, L. D., Birgel, D. & Hinrichs, K. U., 2011. Repeated pulses of vertical methane flux recorded in glacial sediments from the southeast Bering Sea.. Paleoceanography, Volume 26, pp. PA2210, doi:1029/2010PA001993.

Corliss, B. H., 1985. Microhabits of benthic foraminifera within deep-sea sediments.. Nature, Volume 314, pp. 435-438.

Corliss, B. H., 1991. Morphology and microhabitat preferences of benthic foraminifera from the northwest Atlantic Ocean.. Marine Micropaleontology, Volume 17, pp. 195-236.

Corliss, B. H. & Chen, C., 1988. Morphotype patterns of Norwegian Sea deep-sea benthic foraminifera and ecological implications.. Geology, Volume 16.8, pp. 716-719.

Craig, H., 1965. The measurement of oxygen isotope paleotemperatures.. In: E. Tongiorgi, ed. Stable isotopes in oceanographic studies and paleotemperatures.. Pisa: s.n.

Darby, D. A. et al., 2002. Arctic ice export events and their potential impact on global climate during the late Pleistocene.. Paleoceanography, Volume 17.2, pp. 1025, 10.1029/2001PA000639.

Darling, K. F., Kucera, M., Kroon, D. & Wade, C. M., 2006. A resolution for the coiling direction paradox in Neogloboquadrina pachyderma.. Paleoceanography, Volume 21, pp. 1-14.

de Garidel-Thoron, T., Beaufort, L., Bassinot, F. & Henry, P., 2004. Evidence for large methane releases leases to the atmosphere from deep-sea gas- hydrate dissociation during the last glacial episode.. National Academy of Sciences Proceedings, Volume 101, p. 9187+9192.

Dickens, G., 2001. On the fate of past gas: What happens to methane released from a bacterially mediated gas hydrate capacitor?. Geochem. Geophy. Geosy., Volume 2, pp. 2000GC000131, doi:10.1029/2000GC000131..

Dickens, G. R., O'Neil, J. R., Rea, D. K. & Owen, R. M., 1995. Dissociation of oceanic methane hydrate as a cause of the carbon isotope excursion at the end of the.. Paleocene Paleoceanogr, Volume 10, pp. 965-971.

Dickson, R. R. & Brown, J., 1994. The production of North Atlantic Deep Water: Sources, rates, and pathways. JOURNAL OF GEOPHYSICAL RESEARCH, Volume 99 C6, pp. 12319-12341.

Dimakis, p. et al., 1998. Cenozoic erosion and the preglacial uplift of the Svalbard-Barents sea Region. Tectonophysics, Vol. 300, pp. 311-327.

Dimakis, P. et al., 2000. Submarine slope stability on high-latitude glaciated Svalbard–Barents Sea margin.. Marine Geology, Volume 162, pp. 30-316.

Dobson, M. & Haynes, J., 1973. Association of foraminifera with hydroids on the deep shelf.. Micropaleontology, pp. 78-90.

Dokken, T. M. & Hald, M., 1996. Rapid climatic shifts during isotope stages 2– 4 in the Polar North Atlantic.. Geology, Volume 24, pp. 599-602.

Dowdeswel, J. A. & Siegert, M. J., 1999. Ice-sheet numerical modelling and marine geophysical measurements of glacier-derived sedimentation on the Eurasian Arctic continental margin.. Geological Society of America Bulletin, Volume 111, pp. 1080-1097.

Dowdeswell, J. A. & Dowdeswell, E. K., 1989. Debris in icebergs and rates of glacimarine sedimentation: observations from Spitsbergen and a simple model.. Journal of Geology, Volume 97, pp. 221-231.

Dowdeswell, J. A. & Elverhøi, A., 2002. The timing of initiation of fast-£owing ice streams during a glacial cycle inferred from glacimarine sedimentation.. Marine Geology, Volume 188, pp. 3-14.

Dowdeswell, J. A. et al., 1997. The Mass Balance of Circum-Arctic Glaciers and Recent Climate Change.. Quaternary Research, Volume 1-14, p. 48.

Dowdeswell, J. A., Whittington, R. J. & Hodgkins, R., 1992. The size, frequencies and freeboard of east Greenland icebergs, observed using ship radar and sextant.. Journal of Geophysicsal research, Volume 97, pp. 3515-3528.

Duplessy, C. J. et al., 1988. Deepwater source variations during the last climatic cycle and their impact on the global deepwater cirkulation.. Paleoceanograph, Volume 3, pp. 343-360.

Ebbesen, H., Hald, M. & Eplet, T., 2007. Late glacial and early Holocene climatic oscillations on the western Svalbard margin, European Arctic.. Quaternary Science Reviews, Volume 26 (15-16), pp. 1999-2011.

Elverhøi, A. et al., 1995. The Growth and Decay of the Late Weichselian Ice Sheet in Western Svalbard and Adjacent Areas Based on Provenance Studies of Marine Sediments.. Quaternary Research, Volume 44, pp. 303-316.

Elverhøi, A. et al., 2002. Submarine mass-wasting on glacially-influenced continental slopes: processes and dynamics.. Geological Society, London, Special Publications, Volume 203 (1), pp. 73-87.

Elverhøi, A. et al., 1993. The Barents Sea Ice Sheet—a model of its growth and decay during the last ice maximum.. Quaternary Science Review, Volume 12, pp. 863-873.

Elverhøi, A., Hooke, R. L. & Solheim, A., 1998. Late Cenozoic erosion and sediment yield from the Svalbard-Barents Sea region: Implications for understanding erosion of glacierized basins.. Quaternary Science Reviews, Volume 19, pp. 209-241.

Elverhøi, A. et al., 1997. On the origin and flow behavior of submarine slides on deep-sea fans along the Norwegian–Barents Sea continental margin.. Geo-Marine Letters, Volume 17, pp. 119-125.

Epstein, S., Buchsbaum, R., Lowenstam, H. A. & Urey, H. C., 1953. Revised carbonate-water isotopic temperature scale.. Geological Society of American Bulletin, Volume 64.11, pp. 1315-1326.

Ericson, D. B., 1959. Coiling Direction Of Globigerina Pachyderma As A Climatic Index.. Science, Volume 130, pp. 219-220.

Ezat, M., Rasmussen, T. L. & Groeneveld, J., 2014. Persistent intermediate water warming during cold stadials in the southeast Nordic seas during the past 65 k.y.. Geology, Volume 42, pp. 663-666, doi:10.1130/G35579.1.

Fahrbach, E. et al., 2001. Direct measurment of volume transport through Fram Strait.. Polar Research, Volume 20.2, pp. 217-224.

Fairbanks, R. G., 1989. A 17,000-year glacio-eustatic sea level record: influence of glacial melting rates on the Younger Dryas event and deep-ocean circulation.. Nature (London), Volume 342, pp. 637-642.

Faleide, J. I. et al., 1996. Late Cenozoic evolution of the western Barents Sea-Svalbard continental margin. Global and Planetary Change, 12, pp. 53-74.

Faugères, J. C. & Stow, D. A., 1993. Bottom-current-controlled sedimentation: a synthesis of the contourite problem.. Sedimentary Geology, Volume 82.1, pp. 287-297.

Faure, G. & Mensing, T. M., 2005. Isotopes, Principles And Applications. Third edition ed. s.l.:John Wiley & Sons, Inc.

Ferré, B., Mienert, J. & Feseker, T., 2012. Ocean temperature variability for the past 60 years in the Norwegian-Svalbard margin influences gas hydrate stability on human time scale.. Journal of Geophysics Research, Volume 117, pp. C10017, doi:10.1029/2012JC008300.

Fillon, R. H., Miller, G. H. & Andrews, J. T., 1981. Terregenous sand in Labrador Sea hemipelagic sediments and paleoglacial events on Baffin Island over the last 100,000 years.. Boreas, Volume 10, pp. 107-124.

Foldvik, A., Aagaard, K. & Tørresen, T., 1988. On the velocity field of the East Greenland Current.. Deep Sea Research Part A. Oceanographic REsearch Papers, Volume 35.8, pp. 1335-1354.

Forman, S. L. et al., 2004. A review of postglacial emergence on Svalbard, Franz Josef Land and Novaya Zemlya, northern Eurasia.. Quaternary Sci. Rev., Volume 23, pp. 1391-1434.

Forman, S. L. et al., 1996. Postglacial emergence of western Franz Josef Land, Russian, and retreat of the barents sea ice sheet.. Quaternary Science Reviews, Volume 15, pp. 77-90.

Gard, G., 1987. Late Quaternary calcareous nannofossil biostratigraphy and sedimentation patterns: Fram Strait, Arctica.. Paleoceanography , pp. 519-529.

Gebhardt, A. C., Geissler, W. H., Matthiessen, J. & Jokat, W., 2014. Changes in current patterns in the Fram Strait at the Pliocene/Pleistocene boundary.. Quaternary Science Reviews, Volume 92, pp. 179-189.

Gibson, T., 1989. Planktonic benthonic foraminifral rations: Modern patterns and Tertiary applicability.. In: Mar. Micropaleontol.. 15: s.n., pp. 29-52.

Gildor, H. & Tziperman, E., 2001. A sea ice climate switch mechanism for the 100-kyr glacial cycles.. Journal of Geophysical Research, Volume 106 (C5), pp. 9117-9136.

Godwin, H., 1962. Half-life of radiocarbon. Nature, 196, p. 944.

Gooday, A. J., 1993. Deep-sea benthic foraminiferal species which exploit phytodetritus: Characteristic features and controls on distribution.. Marine Micropaleontology, Volume 22, pp. 187-205.

Gooday, A. J., 1994. The biology of deep-sea foraminifera: a review of some advances and their applications in paleoceanography.. Palios, Volume 9, pp. 14-31.

Gooday, A. J. & Lambshead, P. J. D., 1989. Influence of seasonally deposited phytodetritus on benthic foraminiferal populations in the bathyal northeast Atlantic: the species response.. The species response." Marine ecology progress series. Oldendorf, Volume 58.1, pp. 53-67.

Gooday, A. J. & Rathburn, A. E., 1999. Temporal variability in living deep-sea benthic foraminifera: a review.. Earth-Science Reviews, Volume 46, pp. 187-212.

Gossman, E. L., 1987. Stable isotopes in modern benthic foraminifera: astudy of vital effect.. Journal of Foraminifera Research, Volume 17.1, pp. 48-61.

Graham, D. W., Corliss, B. H., Bender, M. L. & Keigwin, L. D., 1981. Carbon and oxygen isotopic diseqiulibria of recent deep-sea benthic foraminifera.. Marine Micropaleontology, Volume 6, pp. 483-497.

Graversen, R. G. et al., 2008. Vertical structures of recent Arctic warming.. NAture, Volume 451 (7174), pp. 53-56.

Greinert, J., Bohrmann, G. & Suess, E., 2001. Gas hydrate-associated carbonates and methane-venting at Hydrate Ridge: classification, distribution, and origin of authigenic lithologies.. In: Paull, C.K., Dillon, W.P. (Eds.), Natural Gas Hydrates: Occurrence, rence, Distribution, and Detection. Geophysical Monograph Series. American Geophysical Union, Washington., pp. 99-113.

Grousset, F. E. et al., 1993. Patterns of ice-rafted detrius in the glacial North Atlantic (40°-50°). Paleoceanography , Volume 8.2, pp. 175-192.

Gustafsson, M. & Nordberg, K., 2001. Living (stained) benthic foraminiferal response to primary production and hydrography in the deepest part of the Gullmar Fjord, Swedish west coast, with comparisons to Höglund's 1927 material.. The Journal of Foraminiferal Research, Volume 31.1, pp. 2-11.

Gwiazda, R. H., Hemming, S. R. & Broecker, W. S., 1996. Provenance of icebergs during Heinrich event 3 and the contrast to their sources during other Heinrich episodes.. Paleoceanography, Volume 11.4, pp. 371-378.

Hagen, J. O., Liestøl, O., Roland, E. & Jørgensen, T., 1993. Glacier atlas of Svalbard and Jan Mayen.. Norsk Polarinstitutt, Meddelelser, Volume 129.

Hald, M. & Aspeli, R., 1997. Rapid climatic shifts of the northern Norwegian Sea during the last deglaciation and the Holocene.. Boreas, Volume 26.1, pp. 15-28.

Hald, M., Danielsen, T. K. & Lorentzen, S., 1989. Late Pleistocene-Holocene benthic foraminiferal distribution in the southwestern Barents Sea: Paleoenvironmental implications.. Boreas, Volume 18, pp. 369-399.

Hald, M., Dokken, T. & Hagen, S., 1996. Paleoceanography of the European Arctic margin during the last glaciation.. Geological Society of London Special Publication, Volume 111, pp. 275-287.

Hald, M., Dokken, T. & Mikalsen, G., 2001. Abrupt climatic change during the last interglacial-glacial cycle in the polar North Atlantic.. Marine Geology, Volume 176, pp. 121-137.

Hald, M. et al., 2004. Holocene paleoceanography andglacial history of the West Spitsbergen area, Euro-Arctic margin.. Quaternary Science Reviews, Volume 23, pp. 2075-2088.

Hald, M. & Korsun, S., 1997. Distribution of modern benthic foraminifera from fjords of Svalhard, European Arctic.. Journal of Foraminiferal Research, Volume 27, pp. 101-122.

Hald, M. & Steinsund, P. I., 1992. Distribution of surface sediment benthic foraminifera in the southwestern Barents Sea.. Jormrnol of Foraminiferal Research, Volume 22.4, pp. 347-362.

Hald, M. & Vorren, T. O., 1984. Modern and Holocene foraminifera and sediments on the continental shelf off Troms, North Norway.. Boreas , Volume 13.2, pp. 133-154.

Hald, M. & Vorren, T. O., 1987. Foraminiferal stratigraphy and environment of Late Weichselian deposits on the continental shelf off Troms, Northern Norway.. Marine Micropaleontology, Volume 12, pp. 129-160.

Halfidason, H. et al., 2004. The Storegga Slide: architecture, geometry and slide development.. Marine Geology, pp. 201-234.

Haq, B. U., 1998. Natural gas hydrates: Searching the long-term climatic and slope stability records. The Geological Society, Volume 137, pp. 303-318.

Hebbeln, D. et al., 1994. Moisture supply for northern ice-sheet growth during the Last Glacial Maximum. Nature, Volume 350, pp. 409-411.

Hebbeln, D., Dokken, T., Andersen, E. S. & Hald, M., 1994. Moisture supply for northern ice-sheet growth during the Last Glacial Maximum.. Nature, Volume 350, pp. 409-411.

Hebbeln, D. & Wefer, G., 1991. Effects of ice coverage and ice-rafted material on sedimentation in the Fram Strait.. Nature, Volume 350, pp. 409-411.

Hebbeln, D. & Wefer, G., 1997. Late Quaternary paleoceanography in the Fram Strait.. Paleoceanography, Volume 12.1, pp. 65-78.

Hebbeln, D. & Wefer, G., 1997. Late Quaternary paleoceanography in the Fram Strait.. Paleoceanography, Volume 12.1, pp. 65-78.

Heggeland, R., 1997. Detection of gas migration from a deep source by the use of exploration 3D seismic data. Marine Geology, Volume 137, pp. 41-47.

Heinrich, H., 1988. Origin and Consequences of Cyclic Ice Rafting in the Northeast Atlantic Ocean during the Past 130,000 Years.. Wuaternary Research, Volume 29, pp. 142-152.

Heinrich, R., Kassen, H., Vogelsang, E. & Thiede, J., 1989. Sedimentary facies of glacial-interglacial cycles in the Norwegian Sea during the last 350 ka.. Marine Geology, Volume 86, pp. 283-319.

Hermelin, J. O. R. & Scott, D. B., 1985. Recent benthic foraminifera from the central North Atlantic.. Micropaleontology, pp. 199-220.

Hill, T., Kennett, J. & Spero, H., 2004a. High-resolution records of methane hydrate dissociation: ODP Site 893, Santa Barbara Basin.. Earth and Planetary Science Letters, Volume 223, pp. 127-140.

Hill, T., Kennett, J. & Valentine, D., 2004b. Isotopic evidence for the incorporation of methane-derived carbon into foraminifera from modern methane seeps, Hydrate Ridge, Northeast Pacific.. Geochim. Cosmochim. Acta, Volume 68, pp. 4619-4627.

Hill, T. M., Kennett, J. P. & Spero, H. J., 2003. Foraminifera as indicators of methane-rich environments: A study of modern methane seeps in Santa Barbara Channel, California.. Mar. Micropaleontol., Volume 49, pp. 123-138.

Hill, T. M., Paull, C. K. & Crister, R. B., 2012. Glacial and deglacial seafloor methane emissions from pockmarks on the northern flank of the Storegga Slide complex. Geo-Marine Letters, Volume 32.1, pp. 73-84.

Hinrichs, K.-U. & Boetius, A., 2002. The anaerobic oxidation of methane: New insights in microbial ecology and biogeochemistry.. In: G. B. D. a. H. D. Wefer, ed. Ocean Margin Systems. Berlin, Heidelberg: Springer Verlag, pp. 457-577.

Hisdal, V., 1998. Svalbard Nature and History., Oslo: Polarhåndbok No. 12, Norsk Polarinstitutt, 123 pp.

Hjelstuen, B., Elverhøi, A. & Falaide, J., 1996. Cenozoic erosion and sediment yield in the drainage area of the Storfjorden Fan.. Global and Planetary Change, Volume 12, pp. 95-117.

Hjelstuen, B. et al., 2004. Late Quaternary seismic stratigraphy and geological development of the south Vøring margin, Norwegian Sea.. Quaternary Science Reviews, pp. 1847-1865.

Hoefs, J., 1997. Stable Isotope Geochemistry, 4th ed.. Heidelberg: Springer-Verlag.

Holtedahl, H. & Bjerkli, K., 1982. Late Quaternary sediments and statigraphy on the continental shelf off Møre-Trøndelag, W. Norway.. Marine Geology, Volume 45, pp. 179-226.

Hovland, M. et al., 1987. Methane-related carbonate cements in pockmark of the North-Sea.. Journal of Sedimentarty Petrology, Volume 57 (5), pp. 881-892.

Howe, J. A., Shimmield, T. M. & Harland, R., 2008. Late Quaternary contourites and glaciomarine sedimentation in the Fram Strait.. Sedimentology, Volume 55, pp. 179-200.

Hunt, A. S. & Corliss, B. H., 1993. Distribution and microhabitats of living (stained) benthic foraminifera from the Canadian Arctic Archipelago.. Marine Micropaleontology, Volume 20, pp. 321-345.

Hustoft, S., Bunz, S., Mienert, J. & Chand, S., 2009. Gas hydrate reservoir and active methane-venting province in sediments on < 20 Ma young oceanic crust in the Fram Strait, offshore NW-Svalbard.. Earth Planet. Sc. Lett., Volume 284, pp. 12-24.

Husum, K. & Hald, M., 2004a. A continuous marine record 8000-1600 cal. yr BP from the Malangenfjord, north Norway: foraminiferal and isotopic evidence.. he Holocene, Volume 14.6, pp. 877-887.

Husum, K. & Hald, M., 2004b. Modern foraminiferal distribution in the subarctic Malangen fjord and adjoining shelf, Northern Norway.. Journal of Foraminiferal Research, Volume 34.1, pp. 34-48.

Hutson, W. H., 1980. The Agulhas Current during the Late Pleistocene: Analysis of Modern Faunal Analogs.. Science, Volume 207.4426, pp. 64-66.

Ingólfsson, Ó., 2004. Outline of the geography and geology of Svalbard. Volume 2005: Longyearbyen, UNIS, UNIS course.

IPCC, I. P. o. C. C., 2007. Climate Change 2007: The Physical Science Basis. Contribution of Working Group I to the Fourth Assessment Report of the Intergovernmental Panel of Climate Change. edited by S. Solomon et al., Cambridge Univ. Press, Cambridge, U. K.: s.n.

Iversen, N. & Jørgersen, B. B., 1986. Anaerobic methane oxidation rates at the sulfate-methane transition in marine sediments from Kattegat and Skagerrak (Denmark), Limnol.. Oceanogr., Volume 30, pp. 944-955.

Jakobsson, M. et al., 2012. The International Bathymetric Chart of the Arctic Ocean. GEOPHYSICAL RESEARCH LETTERS, Volume 39.

Jansen, E., 1989. The use of stable oxygen and carbon isotope stratigrafy as a dating tool.. Quaternary International, Volume 1, pp. 151-166.

Jansen, E. et al., 1983. Late Weichselian paloceanography of the southeastern Norwegian Sea.. Norsk Geologiske Tiddskrift, Volume 63, pp. 117-146.

Jennings, A. E. & Helgadottir, G., 1994. Foraminiferal assemblages from the fjords and shelf of eastern Greenland.. The Journal of Foraminiferal Research, Volume 24.2, pp. 123-144.

Jennings, A. E., Weiner, N. J., Helgadottir, G. & Andrews, J. T., 2004. Modern froaminiferal faunas of the southwestern to northern Iceland shelf: Oceanographic and environmental controls.. Journal of Foraminiferal Research, Volume 34.3, pp. 180-207.

Jessen, S. P., 2015. Ice rafting, Ocean circulation and Glacial activity on the western Svalbard margin 0-74 000 years BP., Tromsø: Department of Science and Techology, Department of Geology.

Jessen, S. P. & Rasmussen, T. L., 2015. Sortable silt cycles in Svalbard slope sediments 74–0 ka.. Journal of Quaternary Science (in press), p. DOI: 10.1002/jqs.2807.

Jessen, S. P., Rasmussen, T. L., Nielsen, T. & Solheim, A., 2010. A new Late Weichselian and Holocene marine chronology for western Svalbard slope 30,000-0cal years BP.. Quaternary Science Reviews, Volume 29, pp. 1301-1312.

Johannesen, O. M., 1986. Brief overview of the physical oceanography.. Springer, pp. 103-128.

Johannessen, T., Jansen, E., Flatøy, A. & Ravelo, A. C., 1994. The relationship between surface water masses, oceanographic fronts and paleoclimatic proxies in surface sediments of the Greenland, Iceland, Norwegian Seas.. In: E. e. a. Zahn, ed. Carbon Cycling in the Glacial Ocean: Contraints on the Ocean's Role in Global Change.. Berlin: Springer, pp. 61-85.

Jones, G. A. & Keigwin, L. D., 1988. Evidence from Fram Strait (78°N) for early deglaciation.. Nature, Volume 336, pp. 56-59.

Judd, A. G. & Hovland, M., 2007. Seabed Fluid Flow; the impact on Geology, Biology and the Marine Environment.. s.l.:Cambridge University Press..

Jung, W. & Vogt, P., 2004. Effect of bottom water warming and sea level rise on Holocene hydrate dissociation and mass wasting along the Norwegian-Barents Continental Margin.. Journal of Geophysical Research , Volume 109 (B6), p. B06104 doi:10.1029/2003JB002738..

Kaiho, K., 1994. Benthic foraminiferal dissolved-oxygen index and dissolved-oxygen levels in the modern ocean.. Geology, Volume 22, pp. 719-722.

Katz, M. E. et al., 2010. Traditional and emerging geochemical proxies in foraminifera.. Journal of Foraminiferal, Volume 40, pp. 165-192.

Keigwin, L. D., 2002. Late Pleistocene-Holocene paleoceanography and ventilation of the Gulf of California. Journal of Oceanography , Volume 58, pp. 421-432.

Kennett, J., Cannariato, K. G., Hendy, I. L. & Behl, R. J., 2003. Methane hydrates in Quaternary climate changes: the clathrate gun hypothesis.. Washington, DC: American Geophysical Union.

Kennett, J. P., Cannariato, K. G., Hendy, I. L. & Behl, R. J., 2000. Carbon Isotopic evidence for methane hydrate instability during Qauternary interstadial.. Science, Volume 288, pp. 128-133.

Kim, G. Y. et al., 2011. Evidence of gas hydrate from downhole logging data in the Ulleung Basin, East Sea.. Mar. Petrol. Geol., Volume 28, pp. 1979-1985.

King, E. L., Haflidason, H., Serjup, H. P. & Løvlie, R., 1998. Glacigenic debris flows on the North Sea Trough Mouth Fan during ice stream maxima.. Marine Geology, Volume 152, pp. 217-246.

Kissel, C. et al., 1997. Changes in the strength of the Iceland–Scotland Overflow Water in the last 200,000 years: Evidence from magnetic anisotropy analysis of core SU90-33.. Earth and Planetary Science Letters, Volume 152, pp. 25-36.

Kleiber, H. P., Knies, J. & Niessen, F., 2000. The Late Weichselian glaciation of the Franz Victoria Through, northern Barents Sea: ice sheet extent and timing.. Marine Geology, Volume 168, pp. 25-44.

Klitgaard Kristensen, D. & Sejrup, H. P., 1996. Modern benthic foraminiferal biofacies across the Northern North Sea.. Sarsia, Volume 81, pp. 97-106.

Klitgaard-Kristensen, D., Sejrup, H. P. & Haflidason, H., 2001. The last 18 kyr fluctuations in Norwegian Sea surface conditions and implications for the magnitude of climatic change: evidence from the North Sea.. Paleoceanography , Volume 16.5, pp. 455-467.

Knies, J. et al., 2001. Marine ice rafted debris records constrain maximum extent of Saalian and Weichselian ice-sheets along the northern Eurasian margin.. Global and Planetary Changes, Volume 31, pp. 45-64.

Knies, J. & Stein, R., 1998. New aspects of organic carbon deposition and its paleoceanographic implications along the Northern Barents Sea Margin during the last 30,000 years.. Paleoceanography, Volume 13.4, pp. 384-394.

Knies, J., Vogt, C. & Stein R, 1999. Late Quaternary growth and decay of the Svalbard/Barents Sea Ice Sheet and paleoceanographic evolution in the adjacent Arctic Ocean.. Geo-Marine Letters, Volume 18, pp. 195-202.

Knies, J., Vogt, C. & Stein, R., 1999. Late Quaternary growth and decay of the Svalbard/Barents Sea ice sheet and paleoceanographic evolution in the adjacent Arctic Ocean.. Geo-Marine Letters, Volume 18, pp. 195-202.

Knudsen, K. L., 1998. Foraminiferer i 'kvatær stratigrafi: Laboratorie- og fremstillingsteknik samt udvalgte eksempler. Geologisk Tidsskrify, Volume 3, pp. 1-25.

Koç-Karpuz, N. & Jansen, E., 1992. A high-resolution diatom record of the last deglaciation from the SE Norwegian Sea; documentation of rapid climatic changes.. Paleoceanography, Volume 7.4, pp. 499-520.

Koç, N., Jansen, E., Hald, M. & Labeyrie, L., 1996. Late-glacial-Holocene sea surface temperatures and gradients between the North Atlantic and the Norwegian Sea: implications for the Nordic heat pump.. Geological Society of London Special Publication, Volume 111, pp. 177-185.

Koç, N., Jansen, E. & Halflidason, H., 1993. Paleoceanographic reconstruction of surface water conditions in the Greenland, Iceland and Norwegian Seas through the last 14 ka based on diatoms.. Quaternary Science Reviews, Volume 12, pp. 115-140.

Koç, N. et al., 2002. Late glacial palaeoceanography of Hinlopen Strait, northern Svalbard. Polar Research, Volume 21, pp. 307-304.

Kohfeld, K. E., Fairbanks, R. G., Smith, S. L. & Walsh, I. D., 1996. Neogloquadrina pachyderma (sinistral coiling) as paleoceanographic tracers in polar oceans: Evidence from Northeast Water Polynya plankton tows, sediment traps, and surface sediment samples.. Paleoceanography, Volume 11, pp. 679-700.

Korsun, S. & Hald, M., 1998. Modern benthic foraminifera off Novaya Zemlya tidewater glacier, Russian Arctic.. Arctic and Alpine Research, Volume 30.1, pp. 61-77.

Korsun, S. & Hald, M., 2000. Seasonal dynamics of benthic foraminifera in a glacially fed fjord of Svalbard, Eurpean Arctic.. Journal of Foraminiferal Research, Volume 30.4, pp. 251-271.

Kozdon, R. et al., 2009. Intratest oxygen isotope variability in the planktonic foraminifer N. pachyderma: Real vs. apparent vital effects by ion microprobe.. Chemical Geology, Volume 258, pp. 327-337.

Krey, V. et al., 2009. Gas hydrates: Entrance to a methane age or climate threat?. eNVIRONMENTAL rESEARCH lETTERS, Volume 4.3, p. 034007.

Kuijpers, A. et al., 2001. Late Quaternary slope instability on the Faeroe margin: mass flow features and timing on events.. Geo-Mar Letters , Volume 20, pp. 149-159.

Kulm, L. D., 1986. Oregon subduction zone: venting, fauna, and carbonates.. Science, Volume 231 (4738), pp. 561-566.

Kulm, L. D. & Suess, E., 1990. Relationship between carbonate deposits and fluid venting: Oregon accretionary prism.. J. Geophys. Res., Volume 95, pp. 8899-8915.

Kvenvolden, K., 1988. Methane hydrates-a major reserve of carbon in the shallow geosphere?. Chemical Geology, Volume 71, pp. 41-51.

Kvenvolden, K. A., 1993. Gas Hydrates-Geological perspective and global change.. Reviews of Geophysics, Volume 31.2, pp. 173-187.

Kvenvolden, K. A., 1998. A primer on the geological occurrence of gas hydrate.. Geological Society, London, Special Publications, Volume 137.1, pp. 9-30.

Kvenvolden, K. A., 2000. Natural gas hydrate; Introduction and history of discovery.. Coastal System and Continental Margins, Natural Gas Hydrate in Oceanic and Permafrost Environments. Kluwer Academics Press, London., pp. 9-16.

Kvenvolden, K. A. & McMenamin, M. A., 1980. Hydrates of natural gas: a review of their geological occurrenves. s.l.:Geological Survey.

Laberg, J. S. & Vorren, T. O., 1995. Late Weichselian submarine debris flow deposits on the Bear Island Trough Mouth Fan.. Marine Geology , Volume 127, pp. 45-72.

Lambeck, K., Estat, T. M. & Potter, E. K., 2002. Links between climate and sea levels for the past three million years.. Nature, Volume 419 (6903), pp. 199-206.

Landvik, J. et al., 1992. Weichselian stratigraphy and plaeoenvironments at Bellsund, western Svalbard.. Boreas, Volume 21, pp. 335-358.

Landvik, J. Y. et al., 1998. The Last Glacial Maximum of Svalbard and the Barents Sea Area: Ice Sheet Extent and Configuration. Quaternary Science Reviews, Vol.17, pp. 43-75.

Landvik, J. Y. et al., 1998. The last glacial maximum of Svalbard and the Barents Sea Area: ice sheet extent and configuration.. Quaternary Science Reviews, Volume 17, pp. 43-75.

Landvik, J. Y. et al., 2005. Rethinking Late Weichselian ice-sheet dynamics in coastal NW Svalbard. Boreas, Volume 34, pp. 7-24.

Landvik, J. Y., Mangerud, J. & Salvigsen, O., 1988. Glacial history and permafrost in the Svalbard area. CONFERENCE PAPER.

Langehaug, H. R. & Falck, E., 2012. Changes in the properties and distribution of the intermediate and deep waters in the Fram Strait.. Progress in Oceanography, Volume 96, pp. 57-67.

Larsen, H. C. et al., 1994. Seven million years of glaciation in Greenland. Science, 264, pp. 952-955.

Laskar, J. et al., 2004. A long-term numerical solution for the insolation quantities of the Earth.. Astronomy & Astrophysics, Volume 428, pp. 261-285. doi:10.1051/0004-6361:20041335..

Lehman, S., 1993. Ice sheets, wayward winds and sea change.. Nature, Volume 365, pp. 108-110.

Lehman, S. J. & Forman, S. L., 1992. Late Weichselian Glacier Retreat in Kongsfjorden, West Spitsbergen, Svalbard.. Quaternary Research, Volume 37, pp. 139-154.

Lekens, W. A. H. et al., 2005. Laminated sediments preceding Heinrich event 1 in the Northern North Sea and Southern Norwegian Sea: Origin, processes and regional linkage.. Marine Geology, Volume 216, pp. 27-50.

Lide, D. R. & Frederikse, H. P. R., 1995. Handbook of chemistry and Physics, 76th ed.. Florida: CRC Press.

Linick, T. W., Damon, P. E., Donahue, D. J. & Jull, A. J. T., 1989. Accelerator Mass Spectrometry: The new revolution in radiocarbon dating. Quaternary Internationa. Vol. 1, pp. 1-6.

Linke, P. & Lutze, G. F., 1993. Microhabitat preferences of benthic foraminifera a static concept or a dynamic adaptation to optimize food acquisition?. Marine Micropaleontology, Volume 20, pp. 215-234.

Lloyd, J., Kroon, D., Laban, C. & Boulton, G., 1996. Deglaciation history and paleoceanography of the western Spitsbergen margin since the last glacial maximum.. Geological Society of London Special Publication, Volume 111, pp. 289-301.

Loeng, H., 1980. Physical oceanographic investigations in central parts of the Barents Sea, Fisken Hay.

Loeng, H., 1991. Features of the physical oceanographic conditions of the Barents Sea.. Polar Research, Volume 5-18, p. 10.

Loeng, H., 1991. Features of the physical oceanographic conditions of the Barents Sea.. Polar Research, Volume 10 (1), pp. 5-18.

Lowe, J. J. & Walker, M., 1997. Quaternary Environments. 2nd edition.. s.l.:Addison Wesley Longman Limited 1997.

Lubinski, D. J., Polyak, L. & Forman, S. L., 2001. Freshwater and Atlantic water inflows to deep northern Barents and Kara Sea since 13 14C ka: foraminifera and stable isotopes.. Quaternary Science Reviews, Volume 20, pp. 1851-1879.

Lubinski, D. et al., 1996. The last deglaciation of the Franz Victoria Trough, northern Barents Sea.. Boreas, Volume 25, pp. 98-100.

Mackensen, A. & Hald, M., 1988. Cassidulina teretis Tappan and C. laevigata d'Orbigny; their modern and late Quaternary distribution in northern seas.. The Journal of Foraminiferal Research, Volume 18.1, pp. 16-24.

Mackensen, A., Schmiedl, G., Harloff, J. & Giese, M., 1995. Deep-sea foraminifera in the South Atlantic Ocean: Ecology and assemblage generation.. Micropaleontology, pp. 342-358.

Mackensen, A., Serjup, H. P. & Jansen, E., 1985. The distribution of living benthic foraminifera on the continental slope and rise off southwest Norway.. Marine Micropaleontolog, Volume 9, pp. 275-306.

Mackensen, A., Serjup, H. P. & Jansen, E., 1985. The distribution of living benthic foraminifera on the continental slope and rise off Southwest Norway.. Marine Micropaleontology, Volume 9, pp. 275-306.

Mackensen, A., Wollenburg, J. & Licari, L., 2006. Low δ13C in tests of live epibenthonic and endobenthonic foraminifera at a site of active methane seepage.. Paleoceanography, pp. PA2022, doi:10.1029/2005PA001196.

Malmgren, B. A., 1983. Ranking of dissolution susceptibility of planktonic foraminiferaa t high latitudes of the South A tlantic Ocean.. Mar. Micropaleontol., Volume 8, pp. 193-191.

Mangerud, J., 1991. The last interglacial/glacial cycle in northern Europe.. In: L. C. K. S. a. E. J. Cushing, ed. Quaternary landscape. Minneapolis: Univ. Minnesota Press, pp. 39-75.

Mangerud, J. et al., 1992. The last glacial maximum on Spitsbergen, Svalbard.. Quaternary Research, Volume 38, pp. 1-31.

Mangerud, J. et al., 1998. Fluctuations of the Svalbard-Barents Sea Ice Sheet during the last 150 000 years.. Quaternay Science Review, Volume 17, pp. 11-42.

Mangerud, J., Jansen, E. & Landvik, J. Y., 1996. Late Cenozoic history of the Scandinavian and Barents Sea ice. Global and Planetary Change 12, pp. 11-26.

Mangerud, J. & Landvik, J. Y., 2007. Younger Dryas cirque glaciers in western Spitsbergen: smaller than during the Little Ice Age.. Boreas-International Journal of Quaternary Research, Volume 36, pp. 278-285.

Mangerud, J. & Svendsen, J. I., 1990. Deglaciation chronology inferred from marine sediments in a proglacial lake basin, western Spitsbergen, Svalbard.. Boreas, Volume 19, pp. 263-272.

Mangerud, J. & Svendsen, J. I., 1992. The last Intergalcial-Glacial period on Spitsbergen, Svalbard.. Quaternary Science Reviews, Volume 11, pp. 633-664.

Manley, T. O., 1995. Branching of Atlantic Water within the Greenland-Spitsberge Passage: An estimate of recirculation.. JOURNAL OF GEOPHYSICAL RESEARCH (1978-2012), Volume 100.C10, pp. 20627-20634.

Martin, J. B. et al., 2004. Relationships between the stable isotopic signatures of living and fossil foraminifera in Monterey Bay, California.. Geochemistry, Geophysics, Geosystems, Volume 5.4, pp. Q04004, doi:10.1029/2003GC000629..

Martin, R. A., Nesbitt, E. A. & Campbell, K. A., 2007. Carbon stable isotopic composition of benthic foraminifera from Pliocene cold methane seeps, Cascadia accretionary margin.. Palaeogeogr. Palaeocl. Palaeoecol., Volume 246, pp. 260-277.

McCabe, A., Clark, P. & Clark, J., 2005. AMS14C dating of deglacial events in the Irish Sea Basin and other sectors of the BritisheIrish ice sheet.. Quaternary Science Reviews, Volume 24, pp. 1673-1690.

McCorkle, D. C. & Keigwin, L. D., 1990. The influence of microhabitats on the carbon isotopic composition of deep sea benthic foraminifera.. Paleoceanography, Volume 5, pp. 161-186.

McCrea, J. M., 1950. On the isotopic chemistry of carbonates and a a apleotemperature scale.. The Journal of Chemical Physics, Volume 18.6, pp. 849-857.

McIver, R. D., 1982. Role of naturally occurring gas hydrates in sediment transport.. American Association of Petroleum Geologist Bulletin, Volume 66 (6), pp. 789-792.

McManus, J. F. et al., 2004. Collapse and rapid resumption of Atlantic meridional circulation linked to deglacial climate changes.. Nature, Volume 428, pp. 834-837.

Mienert, J., Posewang, J. & Lukas, D., 2001. Changes in the Hydrate Stability Zone on the Norwegian Margin and their consequences for methane and carbon releases into the Oceanosphere.. In: P. R. W. S. W. T. J. Schaefer, ed. The Northern North Atlantic: A Changing Environment.. Berlin: Springer, pp. 259-280.

Mienert, J. et al., 2005. Ocean warming and gas hydrate stability on the mid-Norwegian margin at the Storegga Slide.. Marine and Petroleum Geology, Volume 22, pp. 233-244.

Migeon, S., Weber, O., Faugeres, J. C. & Saint-Paul, J., 1999. SCOPIX: A new x-ray imaging system for core analysis. Geo-Marine Letters, Volume 18, pp. 251-255.

Miller, A. A., Scott, D. B. & Medioli, F. S., 1982. Elphidium excavatum (Terquem); ecophenotypic versus subspecific variation.. The Journal of Foraminiferal Research, Volume 12.2, pp. 116-144.

Millo, C., Sarnthein, M., Erlenkeuser, H. & Frederichs, T., 2005. Methane-driven late Pleistocene δ13C minima and overflow reversals in the southwestern Greenland Sea.. Geol., Volume 33, pp. 873-876.

Moros, M. et al., 1997. Physical properties of Reykjanes Ridge sediments and their linkage to high-resolution Greenland Ice Sheet Project 2 ice core data.. Paleoceanography , Volume 12.5, pp. 687-695.

Moros, M. et al., 2002. Were glacial iceberg surges in the North Atlantic triggered by climatic warming?. Marine Geology, Volume 192, pp. 393-417.

Morris, T. H., 1988. Stable isotope stratigraphy of the Arctic Ocean: Fram Strait to central Arctic.. Palaeogeography, palaeoclimatology, palaeoecology, Volume 64.3, pp. 201-219.

Mosby, H., 1938. Svalbard Waters.. Geofysiske Publikasjoner, Volume 12, pp. 1-86.

Mudie, P. J. & Aksu, A. E., 1984. Palaeoclimate of Baffin Bay from 300,000-year record of foraminifera, dinoflagellates abd pollen.. Nature, Volume 312, pp. 630-631.

Mudie, P. J., Keen, L. A., Hardy, I. A. & Vilks, G., 1984. Multivariate analysis and quantitative paleoecology of benthiv foraminifera in surface and late Quaternary shelf sediments, Northern Canada.. Marine Micropaleontology, Volume 8, pp. 283-313.

Murray, J. W., 1984. Paleogene and Neogene benthic foraminifers from Rockall Plateau.. Initial Reports of the Deep Sea Drilling Project, Volume 81, pp. 503-534.

Myhre, A. M., Thiede, J. & Firth, J. V., 1995. Proceedings of the Ocean Drilling Program. Initial Reports, Vol, 151.

Müller, J., Massé, G., Stein, R. & Belt, S. T., 2009. Variability of sea-ice conditions in the Fram Strait over the past 30,000 years.. Nature Geoscience, Volume 2.11, pp. 772-776.

Nansen, F., 1902. Oceanography of the North Polar Basin. The Norwegian North Polar Expedition 1893-96.. Scientific Results, Volume 2, p. 427.

Niemann, H. et al., 2006. Novel microbial communities of the Haakon Mosby mud volcano and their role as a methane sink.. Nature, Volume 443, pp. 854-858.

Niewöhner, C. et al., 1998. Deep sulfate reduction completely mediated by anaerobic methane oxidation in sediments of the upwelling area off Namibia.. Geochim. Cosmochim. Ac., Volume 62, pp. 455-464.

Nisbet, E. G., 2002. Have sudden large release of methane from geological reservoir occured since the Last Glacial Maximum, and could such release occur again?. Philisophical Transactions of the Royal Society of London, Volume 360, pp. 581-607.

Nørgaard-Pedersen, N. et al., 2003. Arctic Ocean during the Last Glacial Maximum: Atlantic and polar domains of surface water mass distribution and ice cover.. Paleoceanography, Volume 18.3.

Nørgaard-Pedersen, N., Spielhagen, R. F., Thiede, J. & Kassens, H., 1998. Central Arctic surface ocean environment during the past 80,000 years.. Paleoceanography, Volume 13.2, pp. 193-204.

Oppo, D. W. & Lehman, S. J., 1995. Suborbital timescale variability of the North Atlantic Deep Water during the past 200,000 years.. Paleoceanography, Volume 10.5, pp. 901-910.

Osterman, L. E. & Nelson, A. R., 1989. Latest Quaternary and Holocene paleoceanography of the eastern Baffin Island continental shelf, Canada: benthic foraminiferal evidence.. Canadian Journal of Earth Sciences, Volume 26.11, pp. 2236-2248.

Ottesen, D. & Dowdeswell, J. A., 2009. An inter–ice-stream glaciated margin: Submarine landforms and a geomorphic model based on marine-geophysical data from Svalbard. Geological Society of America Bulletin, Volume 121, pp. 1647-1665.

Ottesen, D., Dowdeswell, J. A., Landvik, J. Y. & Mienert, J., 2007. Dynamics of the Late Weichselian ice sheet on Svalbard inferred from high-resolution sea-floor morphology. Boreas-International Journal of Quaternary Research, Volume 36, pp. 286-306.

Panieri, G. et al., 2014. Late Holocene foraminifera of Blake Ridge diapir: Assemblage variation and stable-isotope record in gas-hydrate bearing sediments.. Mar. Geol., Volume 353, pp. 99-107.

Panieri, G. et al., 2012. Tracing seafloor methane emissions with benthonic foraminifera: Results from the Ana submarine landslide (Eivissa Channel, Western Mediterranean Sea).. Mar. Geol., Volume 291, pp. 91-112.

Panieri, G. et al., 2009. Methane seepages recorded in benthonic foraminifera from Miocene seep carbonates, Northern Apennines (Italy).. Palaeogeogr. Palaeocl. Palaeoecol., Volume 284, pp. 271-282.

Paquette, R. Q., Bourke, R. H., Newton, J. F. & Perdue, W. F., 1985. The East Greenland Polar Front in Autumn.. Journal of Geophysical Research, Volume 90.C3, pp. 4866-4882.

Paull, C., Ussler III, K. & Borowski, W., 1994. Sources of Biogenic Methane to Form Marine Gas Hydrates In Situ Production or Upward Migration? a.. Annals of the New York Academy of Sciences , Volume 715.1, pp. 392-409.

Peltier, W. & Fairbanks, R., 2006. Global glacial ice volume and Last Glacial Maximum duration from an extended Barbados sea level record.. Quaternary Science Reviews, Volume 25, pp. 3322-3337.

Pfirman, S. L., Bauch, D. & Gammelsrød, T., 1994. The Northern Barents Sea: Water mass distribution and modification.. Geophysical Monograph, Volume 85.

Pflaumann, U., Duprat, J., Pujol, C. & Labeyrie, L. D., 1996. SIMMAX: A modern analog technique to deduce Atlantic sea surface temperatures from planktonic foraminifera in deep-sea sediments.. Paleoceanography, Volume 11.1, pp. 15-35.

Pflaumann, U. et al., 2003. Glacial North Atlantic: Sea-surface conditions reconstructed by GLAMAP 2000.. Paleoceanography, Volume 18.3, pp. 1065, doi:10.1029/2002PA000774.

Pirrung, M. et al., 2002. Magnetic susceptibility and ice-rafted debris in surface sediments of the Nordic Seas: implications for Isotope Stage 3 oscillations.. Geo-Mar Lett, Volume 22, pp. 1-11.

Plaza-Faverola, A., Bünz, S. & Mienert, J., 2011. Repeated fluid expulsion through sub-seabed chimneys offshore Norway in response to glacial cycles.. Earth Planet. Sc. Lett., Volume 305, pp. 297-308.

Polyak, L., Gataullin, V., Okuneva, O. & Stelle, V., 2000. New constraints on the limits of the Barents-Kara ice sheet during the Last Glacial Maximum based on borehole stratigraphy from the Pechora Sea.. Geology, Volume 28.7, pp. 611-614.

Polyak, L. et al., 2002. Benthic foraminiferal assemblages from the southern Kara Sea, a river-influenced arctic marine environment.. Journal of Foraminiferal Research, Volume 32.3, pp. 252-273.

Polyak, L. et al., 2002. Benthic foraminiferal assemblages from the southern Kara Sea, a river-influenced Arctic marine environment.. The Journal of Foraminiferal Research, Volume 32.2, pp. 252-273.

Polyak, L., Lehman, S., Gataullin, V. & Jull, A., 1995. Two-step deglaciation of the southeastern Barents Sea.. Geology, Volume 23, pp. 267-571.

Polyak, L. & Mikhailov, V., 1996. Post-glacial environments of the southeastern Barents Sea: foraminiferal evidence.. Geological Society, London, Special Publications, Volume 111.1, pp. 323-337.

Polyak, L. & Solheim, A., 1994. Late- and postglacial environments in the northern Barents Sea west of Franz Josef Land.. Polar Research, Volume 13.2, pp. 197-207.

Poole, D., 1994. Miocene to Quaternary paleoenvironments and uplift history on the mid Norwegian shelf.. Marine Geology, Volume 115, pp. 173-205.

Quadfasel, D., Gascard, J. C. & Koltermann, K. P., 1978. Large-Scale Oceanography in Fram Strait During the 1984 Marginal Ice Zone Experiment.. JOURNAL OF GEOPHYSICAL RESEARCH., Volume 92.C7, pp. 6719-6728.

Quadfasel, D., Gascard, J. C. & Koltermann, K. P., 1987. Large-Scale Oceanography in Fram Strait During the 1984 Marginal Ice Zone Experiment.. Journal of Geophysical Research, Volume 92.C7, pp. 6719-6728.

Quadfasel, D., Rudels, B. & Kurz, K., 1988. Outflow of dense water from a Svalbard fjord into the Fram Strait.. Deep Sea Research, Volume 35.7, pp. 1143-1150.

Quinn, R., Bull, J. M. & Dix, J. K., 1998. Optimal processing of marine high-resolution seismic reflection (Chirp) data.. Marine Geophysical Researches., Volume 20.1, pp. 13-20.

Rajan, A., Mienert, J. & Bünz, S., 2012. Acoustic evidence for a gas migration and release system in Arctic glaciated continental margins offshore NW-Svalbard.. Marine and Petroleum Geology, Volume 32, p. 3649.

Rasmussen, T. L. et al., 2002. The Faroe–Shetland Gateway: Late Quaternary water mass exchange between the Nordic seas and the northeastern Atlantic.. Marine Geology, Volume 188.1, pp. 165-192.

Rasmussen, T. L. & Forwick, M., 2012. Cruise Report-GEO3144/8144-Marine Geology and Geophysics Cruise: Past and present polar marine-geological processes and climate: from fjords to the deep sea-West Svalbard slope, Vestnesa Ridge, the Fram Strait, and Spitsbergen fjords-on R/V Helmer Hansen, s.l.: s.n.

Rasmussen, T. L., Forwick, M. & Mackensen, A., 2013. Reprint of: Reconstruction of inflow of Atlantic Water to Isfjorden, Svalbard during the Holocene: Correlation to climate and seasonality.. Marine Micropaleontology, Volume 99, pp. 18-28.

Rasmussen, T. L., Nielsen, T., Zamelczyk, K. & Sztybor, K., 2014. Cruise report. CAGE-CO2 Cruise and GEO3144 Teaching Cruise to the western Svalbard margin and the Barents Sea. Vestnesa Ridge, West Svalbard slope, Storfjorden Trough, Storfjorden and the Barents Sea-on R/V Helmer Hanssen, July 21 th -July 29th 2014, Tromsø: Department of geology, UIT, Arctic University of Norway.

Rasmussen, T. L., Thomasen, E., van Weering, T. C. E. & Labeyrie, L., 1996a. Rapid changes in surface and deep water conditions at the Faroe margin during the last 58,000 years.. Paleoceanography, Volume 11, pp. 767-771.

Rasmussen, T. L. & Thomsen, E., 2013. Pink marine sediments reveal rapid ice melt and Arctic meltwater discharge during Dansgaard–Oeschger warmings.. Nature communications, Volume 4.

Rasmussen, T. L. & Thomsen, E., 2015. Palaeoceanographic development in Storfjorden, Svalbard, during the deglaciation and Holocene: evidence from benthic foraminiferal records.. Boreas, Volume 44.1, pp. 24-44.

Rasmussen, T. L., Thomsen, E., Labeyrie, L. & van Weering, T. C. E., 1996b. Circulation changes in the Faeroe-Shetland Channel correlating with cold events during the last glacial period (58-10ka). Geology, Volume 24, pp. 937-940.

Rasmussen, T. L. et al., 2007. Paleoceanographic evolution of the SW Svalbard margin (76°N) since 20,000 14C yr BP.. Quaternary Research, Volume 67, pp. 100-114.

Rasmussen, T. L., Thomsen, E. & van Weering, T. C. E., 1998. Cyclic changes in sedimentaion on the Faroe Drift 53-9 kyr BP related to climate variations. In:Stoker, M., Evans, D., Cramp, R. (eds). Geological Processes on Continental Margins: Sedimentation, Mass-VWasting and Stability. Geological Society Special Publications., Volume 129, pp. 255-267.

Rathbum, A. E. & Corliss, B. H., 1994. The ecology of living (stained) deep-sea benthic foraminifera from the Sulu Sea.. Paleoceanography, Volume 9.1, pp. 87-150.

Rathburn, A. E., Levin, L. A., Held, Z. & Lohmann, K. C., 2000. Benthic foraminifera associated with cold methane seeps on the northern California margin: Ecology and stable isotopic compostion.. Mar. Micropaleontol., Volume 38, pp. 247-266.

Rathburn, A. E. et al., 2003. Relationships between the distribution and stable isotopic composition of living benthonic foraminifera and cold methane seep biogeochemistry in Monterey Bay: California.. Geochem. Geophy. Geosy., Volume 4, p. 1106.

Rathmann, S. & Kuhnert, H., 2008. Carbonate ion effect on Mg/Ca, Sr/Ca and stable isotopes on the benthic foraminifera Oridorsalis umbonatus off Namibia.. Marine Micropaleontology , Volume 66, pp. 120-133.

Rebesco, M. et al., 2013. Quaternary contourite drifts of the Western Spitsbergen margin.. Deep Sea Research Part I: Oceanographic Research Papers, Volume 79, pp. 156-168.

Reeburgh, W. S., 2007. Oceanic methane biogeochemistry.. Chem. Rev., Volume 107, pp. 486-513.

Reimer, P. J. et al., 2013. Intcall113 and MARINE13 radiocarbon age calibration curves 0-50000 years calBP. Radiocarbon, Volume 55 (4), p. DOI:10.2458/azy_js_rc.55.16947.

Reimer, P. J. et al., 2002. Preliminary Report of the first workshop of the IntCal04 Radiocarbon Calibration/Comparison Working Group.. Radiocarbon, Volume 44, pp. 653-661.

Richter, T. O. et al., 2006. The Avaatech XRF Core Scanner: technical description and applications to NE Atlantic sediments. In R. G. Rothwell (Ed.), New techniques in sediment core analysis. Geological Society, Volume 267, pp. 39-50.

Robinson, S. G., Maslin, M. A. & McCave, I. N., 1995. Magnetic susceptibility variations in Upper Pleistocene deep-sea sediments of the NE Atlantic: Implications for ice rafting and paleocirculation at the last glacial maximum.. Paleoceanography, Volume 10, pp. 221-250.

Robinson, S. G., Sahota, J. T. S. & Oldfield, F., 2000. Early diagenesis in North Atlantic abyssal plain sediments characterized by rock-magnetic and geochemical indices.. Marine Geology, Volume 163, pp. 77-107.

Ruddiman, W. F., 1977. Late Quaternary deposition of ice-rafted sand in sub-polar North Altantic (40-60 N).. Geological Society of America, Bulletins, Volume 88, pp. 1813-1827.

Ruddiman, W. F. & McIntyre, A., 1976. Northeast Atlantic paleoclimate changes over the past 60,000 years.. Geo. Soc. Am. Mem, Volume 145, pp. 11-146.

Rudels, B. et al., 2005. The interaction between waters from the Arctic Ocean and the Nordic Seas north of Fram Strait and along the East Greenland Current: results from the Arctic Ocean-02 Oden expedition.. Journal of Marine Systems, Volume 55, pp. 1-30.

Rudels, B., Jones, E. P., Anderson, L. G. & Kattner, G., 1994. On the Intermediate Depth Waters of the Arctic Ocean.. The polar ocean and their role in shaping the global environment, Geophys . Mongr., Volume 85, pp. 33-46.

Rudels, B. et al., 2000. Water mass distribution in Fram Strait and over the Yermak Plateau in summer 1997.. Ann. Geophysicae, Volume 18, pp. 687-705.

Rudiman, W. F. & McIntyre, A., 1981. The North Alantic Ocean during the last deglaciation.. Palaeogeography, Palaeoclimatology, Palaeoecology, Volume 35, pp. 145-214.

Ruppel, C., 2011. Methane hydrates and contemporary climate change.. Nat. Educ. Knowl., Volume 3 (10), p. 29.

Rytter, F., Knudsen, K. L., Seidenkrantz, M. S. & Eiríksson, J., 2002. Modern distribution of benthic foraminifera on the North Icelandic shelf and slope.. The Journal of Foraminiferal Research, Volume 32.3, pp. 217-244.

Sarntheim, M., Pflaumann, U. & Weinelt, M., 2003. Past extent of sea ice in the northern North Atlantic inferred from foraminiferal paleopaleotemperature estimates.. Paleoceanography, Volume 18.2, pp. 1047, doi:10.1029/2002PA000771.

Scahuer, U., 1995. The release of brine-enriched shelf water from Storfjord into the Norwegian Sea.. Journal of Geophysical Research, Volume 100.C8, pp. 16,015-16,028.

Schiebel, R. & Hemleben, C., 2005. Modern planktic foraminifera.. Paläontologische Zeitschrift, Volume 79.1, pp. 135-148.

Schmidt, D. N. et al., 2004. Size distribution of Holocene planktic foraminifer assemblages: biogeography, ecology and adaptation.. Marine Micropaleontology, Volume 50, pp. 319-338.

Schmiedl, G., Mackensen, A. & Müller, P. J., 1997. Recent benthic foraminifera from the eastern South Atlantic Ocean: Dependence on food supply and water masses.. Marine micropaleontology, Volume 32, pp. 249-287.

Schoning, K., 2002. Palaeohydrography and marine conditions in the south-western part of the Vänern basin during the Younger Dryas and Early Preboreal.. GFF , Volume 124.1, pp. 1-10.

Scott, D. B. et al., 1989b. Biostratigraphy and late Cenozoic paleoceanography of the Arctic Ocean: Foraminiferal, lithostratigraphic and isotopoic evidence.. Geol. Soc. Am. Bull., Volume 101, pp. 260-277.

Scott, D. B. et al., 1989a. Lithostratigraphy, biostratigraphy, and stable isotope stratigraphy of cores from OPD leg 105 site survey, Labrador Sea and Baffin Bay.. Poc. Ocean Drill. Program Sci. Results., Volume 105, pp. 561-582.

Scott, D. & Vilks, G., 1991. Benthonic foraminifera in the surface sediments of the deep-sea Artic Ocean.. J. Foraminiferal. Res., Volume 21, pp. 20-38.

Seidenkrantz, M. S., 1995. Cassidulina teretis Tappan and Cassidulina neoteretis new species (Foraminifera): stratigraphic markers for deep sea and outer shelf areas.. Journal of Micropalaeontology, Volume 14.2, pp. 145-157.

Sejrup, H. P., Birks, H. J. B., Klitgaard Kristensen, D. & Madsen, H., 2004. Benthonic foraminiferal distributions and quantitative transfer functions for the northwest European continental margin.. Marine Micropaleontology, Volume 53, pp. 197-226.

Sejrup, H. P. et al., 1981. Benthonic foraminifera in surface samples from the Norwegian Continental Margin between 62°N and 65°N.. Journal of Foraminiferal Research, Volume 11.4, pp. 277-295.

Sen Gupta, B. K., Platon, E., Bernhard, J. M. & Ahron, P., 1997. Foraminiferal colonization of hydrocarbon-seep bacterial mats and underlying sediment, Gulf of Mexico Slope.. J. Foramin. Res., Volume 27.4, pp. 292-300.

Shackelton, N. J., 1977. Tropical rainforest history and the equatorial Pacific carbonate dissolution cycles.. Anderson, N R and Malahoff, A, eds, The fate of fossil fuel CO2 in the oceans: New York, Plenum Press, pp. 401-428.

Shackleton, N. J., 1987. The carbon isotope record of the Cenozoic" history of organic carbon burial and of oxygen in the ocean and atmosphere.. Geological Society, London, Special Publications, Volume 26.1, pp. 423-434.

Shackleton, N. J., Imbrie, J. & Hall, M. A., 1983. Oxygen and carbon isotope record of East Pacific core V19-30: implications for the formation of deep water in the late Pleistocene.. Earth and Planetary Science Letters, Volume 65, pp. 233-244.

Shackleton, N. J. & Pisias, N. G., 1985. Atmospheric carbon dioxide, orbital forcing, and climate.. Geophysical Monograph Series, Volume 32, pp. 303-317.

Shackleton, N. J. & Vincent, E., 1978. Oxygen and carbon isotope studies in recent foraminifera from the southwest Indian Ocean.. Marine Micropaleontology, Volume 3.1, pp. 1-13.

Shakhova, N. et al., 2010. Extensive methane venting to the atmosphere from sediments of the East Siberian Shelf.. Science, Volume 327, pp. 1246-1250.

Siegert, M. J. & Dowdeswell, J. A., 2002. Late Weichselian iceberg, surface-melt and sediment production from the Eurasian Ice Sheet: results from numerical ice-sheet modeling.. Marine Geology, Volume 1988, pp. 109-127.

Simstich, J., Sarnthein, M. & Erlenkeuser, H., 2003. Paired N18O signals of Neogloboquadrina pachyderma (s) and Turborotalita quinqueloba show thermal strati¢cation structure in Nordic Seas. Marine Micropaleontology, Volume 48, pp. 107-125.

Sloan, E. D. J., 1998. Physical/chemical properties of gas hydrates and application to world margin stability and climatic change.. Geological Society, London, Special Publications, Volume 137, pp. 31-50.

Ślubowska, M. A., Koç, N., Rasmussen, T. L. & Klitgaard-Kristensen, D., 2005. Changes in the flow of Atlantic water into the Arctic Ocean since the last deglaciation: Evidence from the northern Svalbard continental margin, 80°N.. Paleoceanography, Volume 20, pp. PA4014, doi:10.1029/2005PA001141.

Ślubowska-Woldengen, M. et al., 2007. Advection of Atlantic Water to the western and northern Svalbard shelf.. Quaternary Science Reviews, Volume 463-478, p. 26.

Smetacek, V., 1999. Diatoms and the ocean carbon cycle.. Protist , Volume 150.1, pp. 25-32.

Smith, A. J., Mienert, J., Bünz, S. & Greinert, J., 2014. Thermogenic methane injection via bubble transport into the upper Arctic Ocean from the hydrate-charged Vestnesa Ridge, Svalbard.. Geochemistry, Geophysics, Geosystems, Volume 15.5, pp. 1945–1959, doi:10.1002/2013GC005179..

Smith, L. M. et al., 2001. Light δ13C events during deglaciation of the East Greenland continental shelf attributed to methane release from gas hydrates.. Geophysics Research Letters, Volume 28, pp. 2217-2220.

Smith, V. O., 1995. Primary productivity and new production in the Northeast Water (Greenland) Polynya during summer 1992.. Journal of Geophysical Research, Volume 100 (C3), pp. 4341-4356.

Snyder, G. T. et al., 2007. Pore sediments above the methane-charged system on Umitaka Spu, Japan Sea.. Deep-Sea Res. PartII, Volume 54, pp. 1216-1239.

Solheim, A. & Elverhøi, A., 1985. A pockmark field in the central Barents Sea; gas from petrogenic source?. Polar Research, Volume 3, pp. 11-19.

Spielhagen, R. F. & Erlenkeuser, H., 1994. Stable oxygen and carbon isotopes in planktic foraminifers from Arctic Ocean surface sediments: Reflection of the low salinity surface water layer.. Marine geology, Volume 119, pp. 227-250.

Stabell, B., 1986. A diatom maximum horizon in upper quaternary deposits.. Geologische Rundschau, Volume 75, pp. 174-184.

Stein, R. et al., 1994a. The last deglaciation event in the eastern central Arctic Ocean.. Science, Volume 264, pp. 692-696.

Stein, R., Schubert, C., Vogt, C. & Flüttereer, D., 1994b. Stable isotope stratigraphy, sedimentatiorates and paleosalinity in the latest Plestocene to Holocene Central Arctic Ocean.. Marine Geology, Volume 119, pp. 333-355.

Steinsund, P. I. et al., 1994. Benthic foraminifera in surface sediments of the Barents and Kara seas: modern and late Quaternary applications.. s.l.:University of Tromsø.

Stoner, J. S., Channell, J. E. T. & Hillaire-Marcel, C., 1996. The magnetic signature of rapidly deposited detrital layers from the deep Labrador Sea: relationship to North Atlantic Heinrich layers.. Paleoceanography, Volume 11, pp. 30-325.

Stott, L. et al., 2002. Does the oxidation of methane leave an isotopic fingerprint in the geologic record?. Geochem. Geophys. Geosyst., Volume 3:2, p. doi:10.1029/2001GC000196.

Stuvier, M. & Reimer, P. J., 1993. Radiocarbon. Volume 35, pp. 215-230.

Sun, X., Corliss, B. H., Brown, C. W. & Showers, W. J., 2006. The effect of primary productivity and seasonality on the distribution of deep-sea benthic foraminifera in the North Atlantic.. Deep-Sea Research, Volume i 53, pp. 28-47.

Svendsen, J. et al., 1999. Maximum extent of the Eurasian ice sheets in the Barents and KaraSea region during the Weichselian.. Boreas, Volume 28, pp. 234-242.

Svendsen, J. I. et al., 2004a. Late Quaternary ice sheet history of northern Eurasia.. Quaternary Science Reviews, Volume 23, pp. 1229-1271.

Svendsen, J. I., Elerhøi, A. & Mangerud, J., 1996. The retreat of the Barents Sea Ice Sheet on the western Svalbard margin.. Boreas, Volume 25, pp. 244-256.

Svendsen, J. I., Gataullin, V., Mangerud, J. & Polyak, L., 2004b. The glacial History of the Barents and Kara Sea Region.. Developments in Quaternary Sciences, Volume 2, pp. 369-378.

Svendsen, J. I. & Mangerud, J., 1992. Paleoclimatic inferences from glacial fluctuations on Svalbard during the last 20 000 years.. Climatic Dynamics, Volume 6, pp. 213-220.

Svendsen, J. I., Mangerud, J., Elverhøi, A. & Solheim, A., 1992. The Late Weicselian glacial maximum on western Spitsbergen iferred from offshore sediment core.. Marine Geology, Volume 104, p. 1992.

Svensson., A. et al., 2008. A 60 000 year Greenland stratigraphic ice core chronology. Climate of the Past, Volume 4.1, pp. 47-57.

Swift, J. H., 1986. "The arctic waters." The Nordic Seas.. Springer New York, pp. 129-154.

Swift, J. H. & Aaagard, K., 1981. Seasonal transitions and water mass formation in the Iceland and Greenland seas.. Deep-Sea Research, Volume 28A, pp. 1107-1129.

Sættem, J., Poole, D. A. R., Serjrup, H. P. & Ellingsen, K. L., 1992. Glacial geology of outer Bjørnøyarenna, southwestern Barents Sea. Marine Geology, Vil. 103, pp. 15-51.

Torres, M. E., Martin, R. A., Klinkhammer, G. P. & Nesbitt, E., 2010. Post depositional alteration of foraminiferal shells in cold seep settings: New insights from flow-through time-resolved analysis of biogenic and inorganic seep carbonates.. Earth Planet. Sc. Lett., Volume 299, pp. 10-22.

Torres, M. E. et al., 2003. Is methane venting at the seafloor recorded by δ13C of benthonic foraminifera shells?. Paleoceanography, Volume 18, pp. 1062, doi:10.1029/2002PA000824.

Treude, T. et al., 2003. Anaerobic oxidation of methane above gas hydrates at Hydrate Ridge, NE Pacific Ocean.. Mar. Ecol.-Prog. Ser., Volume 264, pp. 1-14.

Treude, T. et al., 2005. Anaerobic oxidation of methane and sulfate reduction along the Chilean continental margin.. Geochim. Cosmochim. Ac., Volume 69, pp. 2767-2779.

Urey, H. C., 1947. The thermodynamic properties of isotopic substances.. Journal of the Chemical Society, pp. 562-581.

Vanneste, M., 2000. Gas hydrate stability and destabilisation processes in marine and lacustrine sediments: results from theoretical analysis and multi-frequency seismic investigations., s.l.: PhD Thesis, University of Ghent, Belgium.

Vidal, L. et al., 1997. Evidemce for changes in the North Atlantic Deep Water linked to meltwater surges during the Heinrich Events.. Earth and Planetary Science Letters, Volume 146, pp. 13-27.

Vilks, G., 1969. Recent foraminifera in the Canadian Arctic.. Micropaleontology, pp. 35-60.

Vilks, G., 1970. Circulation of surface waters in parts of the Canadia Arctic Archipelagao based on foraminiferal evidence.. J. Arct. Inst. North Am., Volume 23, pp. 100-111.

Vilks, G., 1975. Comparison of Globorotalia pachyderma (Ehrenberg) in the water column and sediments of the Canadian Arctic.. J. Foraminiferal Res., Volume 5, pp. 313-325.

Vilks, G., 1981. Late Glacial-Postglacial Foraminiferal Boundary in Sediments of Eastern Canada, Denmark and Norway.. Geoscience Canada, Volume 8, pp. 48-56.

Vilks, G., 1989. Ecology of recent foraminifera of the Candaian Continental Shelf of the Arctic Ocean.. In: Y. Herman, ed. The Arctic Seas. New York: Van Nostrand Reinhold, pp. 497-569.

Vilks, G. et al., 1989. Late Quaternary paleoceanography and sedimentary environments in Hudson Strait.. Géographie physique et Quaternaire, Volume 43.2, pp. 161-178.

Vinje, T. A., 1975. Sea ice conditions in the European sector of the marginal seas of the Arctic, 1966–1975.. Norsk Polarinstitutt Årbok, pp. 163-174.

Vinje, T. E., 1985. Sea ice distribution 1971-1980.. Norsk Polarinstitutt, pp. 12-20.

Voelker et al, 2002. Global distribution of centennial-scale records for Marine Isotope Stage (MIS) 3: a database.. Quaternary Science Reviews, Volume 21, pp. 1185-1212.

Vogt, C., Knies, J., Spielhagen, R. F. & Stein, R., 2001. Detailed mineralogical evidence for two nearly identical glacial/deglacial and Atlantic Water advection to the Arctic Ocean during the last 90,000 years.. Global and Planetary Change, Volume 31, pp. 23-44.

Vogt, P. & Jung, W.-Y., 2002. Holocene mass wasting on upper non-Polar continental slopes-due to post-glacial ocean warming and hydrate dissociation?. Geophysical Research Letters., Volume 29 (9).

Vogt, P. R. et al., 1994. Methane-generated (?) pockmarks on young, thickly sedimented oceanic crust in the Arctic; Vestnesa Ridge, Fram Strait.. Geology, Volume 22, pp. 255-258.

Vogt, P. R., Gardner, J. & Craner, K., 1999. The Norwegian-Barents-Svalbard (NBS) continental margin: introducing a natural laboratory of mass wasting, hydrates and ascent of sediment, pore water and methane.. Geo-Marine Letters, Volume 19, pp. 2-21.

Volkmann, R. & Mensch, M., 2001. Stable isotope composition (δ18O, δ13C) of living planktic foraminifers in the outer Laptev Sea and the Fram Strait.. Mar. Micropaleontol., Volume 42, pp. 163-188.

Vorren, T. & Kristoffersen, Y., 1986. Late Quaternary glaciation in the southwestern Barents Sea.. Boreas, Volume 15, pp. 51-60.

Vorren, T. O. & Laberg, J. S., 1997. Trough Mouth Fans-Paleoclimate and ice-sheet monitors.. Quaternary Science Reviews, Volume 16, pp. 865-881.

Vorren, T. O. & Lysså, A., 1997. Seismic facies and architecture of ice-contact submarine fans in high-relief fjords, Troms, Northern Norway. Boreas, Volume 26,4, pp. 309-328.

Waelbroeck, C. et al., 1998. Improving past sea surface temperature estimates based on planktonic fossil fauna.. Paleoceanography, Volume 13.3, pp. 272-283.

Walther, J. V., 2009. Essentials of Geochemistry. 2nd ed. Sudbury, Massachusetts: Jones and Bartlett Publishers.

Wang, P. & Chappell, J., 2001. Foraminifera as Holocene environmental indicators in the South Alligator River, Northern Australia.. Quaternary International, Volume 83-85, pp. 47-62.

Weber, M. E., Niessen, F., Kuhn, G. & Wiedick, M., 1997. Calibration and application of marine sedimentary physical properties using a multi-sensor core logger.. Marine Geology 136 (1), pp. 151-172.

Wefer, G., Heinze, P.-M. & Berger, W. H., 1994. Clues to ancient methane release.. Nature, Volume 369, p. 282.

Westbrook, G. K. et al., 2009. Escape of methane gas from the seabed along the West Spitsbergen continental margin. Geophysical REsearch, Volume 36, p. L15608.

Williamson, M. A., Keen, C. E. & Mudie, P. J., 1984. Foraminiferal distribution on the continental margin off Nova Scotia.. Marine Micropaleontology, Volume 9.3, pp. 219-239.

Wilson, L. J., Hald, M. & Godtliebsen, F., 2011. Foraminiferal faunal evidence of twentieth-century Barents Sea warming.. The Holocene, Volume 21.4, pp. 527-537.

Wollenburg, J. E., Kuhnt, W. & Mackensen, A., 2001. Changes in Arctic Ocean paleoproductivity and hydrography during the last 145 kyr: The benthonic foraminiferal record.. Paleoceanography, Volume 16, pp. 65-77.

Wollenburg, J. E. & Mackensen, A., 1998. On the vertical distribution of living (Rose Bengal stained) benthic foraminifers in the Arctic Ocean.. Journal of Foraminiferal Research, Volume 28.4, pp. 268-285.

Wollenburg, J., Knies, J. & Mackensen, A., 2004. High-resolution paleoproductivity fluctuations during the last 24 kyr as indicated by benthic foraminifera in the marginal Arctic Ocean.. Palaeogeography, Palaeoclimatology, Palaeoecology, Volume 204, pp. 209-238.

Zamelczyk, K. et al., 2014. Surface water conditions and calcium carbonate preservation in the Fram Strait during marine isotope stage 2, 28.8–15.4 kyr.. Paleoceanography, Volume 29.1, pp. 1-12.

Zeebe, R. E., 1999. An explanation of the effect of seawater carbonate concentration on foraminiferal oxygen isotopes.. Geochemica et Cosmochimica Acta, Volume 63.13, pp. 2001-2007.